



Structural Dynamic Response Analysis on Marine Vessels with Time-Varying Mass Property and Large-scale Discontinuous Hull Structures

Yerong Zhang

Marine, Offshore and Subsea Technology Group

School of Engineering

Newcastle University

For the degree of
Doctor of Philosophy

Date of submission: 29/05/2024

Abstract

For some types of special-purpose marine vessels, such as dredgers, the variability of mass in onboard stemming from their operational dynamics causes a distinctive challenge. This variability can swiftly induce unforeseen loads within short time periods during their unloading working conditions, leading to unexpected structural responses and potential fatigue damage. Specifically, in the case of dredgers, the additional loads arising from variations in mass during specialized operations raise significant concerns. What adds to the complexity is that these challenges often escape effective consideration during the design phase. This dynamic interplay of mass variation, occurring within short time intervals, has the potential to compromise structural integrity of the vessel and underscores the need for a more accuracy approach to design and structural analysis in the realm of specialized marine technology.

This thesis stands as a pioneering endeavour, proposing a innovate mathematical and numerical model for structural dynamic analysis of variable cross-section hull girder with time-varying mass characteristics subjected to complex operational and sea environmental loads. At its core, the proposed model leverages the modified Euler-Bernoulli beam theory to accommodate variable mass functions and employs a semi-analytical approach for the vibration characteristics analysis in the variable cross-section beam. The loads acting on the hull girder are composed of hydrodynamic loads, engine excitation loads, and propeller excitation loads respectively defined in the dynamic model. Furthermore, an improved Kane's dynamic equation is established and integrated into the mathematical and numerical model, tailored for time-varying mass systems, serving as the primary dynamic module solver. Dynamic results calculated by the proposed mathematical and numerical model can be transferred into three-dimensional finite element model of the target vessel for the further structural analysis in ANSYS to obtain strength and fatigue assessments.

A customized programme, written in FORTRAN language, is developed based on the proposed mathematical and numerical model. In addition, some verification results and user-defined case studies are given in this thesis. The semi-analytical approach for vibration analysis of various cross-section Euler-Bernoulli beam has been verified with FEA results. The varying wet surface and trim characteristics of the ship hull within a short period are also taken into consideration via dividing wet surface into 10 shifting waterlines and load cases under variable mass working conditions. Hydrodynamic results pre-calculated by

SESAM are inputted and read by the program for further calculations. Finally, dynamic results including displacement and angular responses of each predefined rigid cross-section in the hull girder are calculated by the programme, which have been used for further FEA to achieve detailed structural assessments.

Dynamic response results, including displacement and angular responses of each predefined rigid cross-section in the hull girder, are calculated by the customized program, which has been used for further FEA analysis to achieve detailed stress and deformation structural assessments. The key findings of this research highlight the significant impact of mass variability on the dynamic responses of marine vessels. Structure was found to be more sensitive to oblique wave impacts, necessitating careful design considerations. The study also verified the accuracy of the semi-analytical approach by comparing it with FEA results, demonstrating its efficacy for vibration analysis of variable cross-section beams. Furthermore, the integration of pre-calculated hydrodynamic analysis results from SESAM into the customized program facilitated a comprehensive evaluation of the vessel's dynamic behaviour under variable mass conditions. These advancements contribute to a more precise and efficient method for assessing and ensuring the structural integrity of special-purpose marine vessels during their design and operational phases.

The proposed mathematical and numerical model can be used in the design stage for marine vessels who have time-varying mass features to evaluate their special structural responses during loading or unloading operations.

Keywords: Structural dynamics, marine vessel, time-varying mass model, hull girder, variable cross-section, dynamic analysis, FEA

Acknowledgement

I would like to express my deepest gratitude and appreciation to all those who have contributed to the completion of my Ph.D. study.

First and foremost, I am profoundly thankful to my supervisor, Professor Zhiqiang Hu, whose guidance, supports, and encouragements have been invaluable throughout this research journey. His expertise and commitments to academic excellences have shaped my scholarly endeavours and personal growth significantly.

I extend my sincere thanks to my second supervisor, Dr Yongchang Pu, for their insightful feedback, constructive criticisms, and unwavering supports. His expertise and dedications have played a pivotal role in shaping the quality and rigor of my Ph.D. research.

I am indebted to Newcastle University for providing a conducive academic environment and resources essential for undertaking this research. The school of engineering has been a source of inspiration and collaboration, fostering an atmosphere of intellectual curiosity and academic excellence.

My heartfelt appreciation goes to my colleagues and fellow researchers for their camaraderie, stimulating discussions, and shared passion for advancing knowledge in our field. The collaborative spirit within marine technology group has significantly enriched my research experience.

To my friends and families, your unwavering supports, understandings, and encouragements have been my pillars of strength. Your belief in my abilities has been a constant motivation.

Much appreciated to everyone who has been a part of this transformative experience.

Table of contents

Abstract	I
Acknowledgement	III
Table of contents.....	IV
Lists of figures	VIII
List of tables.....	XVII
Lists of abbreviations.....	XVIII
Nomenclature.....	XIX
List of publications	XXII
Chapter 1. Introduction	1
1.1. Background of dredgers.....	1
1.2. Natural features of dredgers	3
1.2.1. Time-varying mass characteristics	3
1.2.2. Discontinuous structure characteristics	5
1.2.3. Complex loads.....	5
1.3. Overview of doctoral programme.....	6
1.3.1. Motivation	6
1.3.2. The research background and significance	7
1.3.3. Aim and objectives.....	8
1.3.4. Overview of novelties	9
1.3.5. Outline of the thesis.....	10
Chapter 2. Literature review	13
2.1. Literature reviews on dredgers	13
2.1.1. Structural research reviews of dredgers	13
2.1.2. Studies of excitation loads on dredgers.....	18

2.2. Literature reviews on dynamic analysis of marine structures	22
2.3. Literature reviews of hydrodynamic analysis in marine vessels	26
2.3.1. Classical hydrodynamic analysis methods in marine field	26
2.3.2. Hydrostatic and hydrodynamic analysis of special marine vessels.....	29
2.4. Literature reviews of time-varying structures	31
2.4.1. Time-varying structure studies.....	31
2.4.2. Numerical algorithms of dynamic analysis of linear mass-varying structures	34
2.5. Literature reviews of strength and fatigue analysis in marine vessels	37
2.5.1. Global strength analysis of specific marine vessels.....	38
2.5.2. Detailed fatigue analysis of specific marine vessels	40
2.6. Summary of Chapter 2.....	41
Chapter 3. Methodology	43
3.1. Fundamentals of proposed mathematical and numerical model	43
3.2. Modified Euler-Bernoulli beam theory with time-varying mass function	47
3.3. Semi-analytical of vibration analysis of variable cross-section beam.....	50
3.3.1. Modelling assumptions and simplification	51
3.3.2. Relationship of continuity and transfer matrix for lateral beam equation.....	52
3.3.3. Boundary conditions and non-linear eigen equation for lateral beam equation	56
3.3.4. Relationship of continuity and transfer matrix for axial beam equation... ..	58
3.3.5. Boundary conditions and non-linear eigen equation for axial beam equation	60
3.4. Hydrodynamic load calculation for draft-varying conditions	60
3.4.1. Coordinate Definition.....	61
3.4.2. Linear potential flow theory.....	61
3.4.3. First order hydrodynamic loads calculation method.....	66

3.4.4. Radiation force	67
3.4.5. Static restoring force	67
3.4.6. Pre-calculation in SESAM based on boundary element method	68
3.5. Other excitation loads	70
3.5.1 Excitation loads from propeller	70
3.5.2 Excitation loads from diesel engine	70
3.6. Numerical solver for dynamic analysis of proposed mathematical model by improved Kane's dynamic equation	71
3.6.1 Basic dynamic equation of variable mass points system	72
3.6.2. Generalized forces	73
3.6.3. Dynamical equations	75
3.6.4. Matrix form of dynamical equations	81
3.7. Determinations in improved Kane's dynamic equation for marine structures ...	89
3.8. The Runge-Kutta time integration method	90
3.9. Multiple point constraints technology in FEA	92
3.10. Outline of proposed mathematical and numerical model	94
3.10.1. Outline of TVM_HullGirder program	95
3.10.2. Application of TVM_HullGirder program in FEA	96
3.11. Summary of Chapter 3	97
Chapter 4. Case studies and discussions	98
4.1. Verifications of the semi-analytical approach	98
4.1.1. Vibration analysis results of the cantilever Euler-Bernoulli beam in axial direction	98
4.1.2. Vibration analysis results of the cantilever Euler-Bernoulli beam in transverse	102
4.2. Model descriptions and case settings	106
4.3. Pre-calculation results by SESAM	115

4.3.1. Added mass	117
4.3.2. Damping coefficients	120
4.3.3. RAOs	122
4.4. Vibration natural frequency due to mass-variation	129
4.5. TVM_HullGirder simulation results during unloading conditions	136
4.5.1. Motion responses of the hull girder.....	137
4.5.2. Structural vibration responses	144
4.6. Results by FE analysis	161
4.6.1. FE Model settings in ANSYS	162
4.6.2. FEA results in ANSYS by MPC	164
4.6.3. Verifications by qualitative analysis	175
4.7. Summary of Chapter 4.....	177
Chapter 5. Conclusions and future works	178
5.1. Proposed math and numerical model.....	178
5.2. Novelty and impact of the work	179
5.3. Future works	181
List of references.....	184
Appendices.....	200
Appendix A. Bisection method codes for solving non-linear equation.....	200
Appendix B. Transfer matrix method codes for solving natural frequency	202
Appendix C. Orthonormal basis solution codes	208

Lists of figures

Figure 1. Drawing of one of newest dredger commissioned (Vidal, 2001).	2
Figure 2. Rainbowing clean sand for land reclamation (N. Bray & Cohen, 2004).	2
Figure 3. The dumping process of TSHDs at the disposal site (Dragados, 2017).....	3
Figure 4. The typical working cycle of TSHDs (Mourik & Osnabrugge, 2014).	4
Figure 5. A schematic view of the change in draught of a TSHD in service (Basic et al., 2017).....	4
Figure 6. The typical cross-section at midship of TSHDs (DE JONG, 2010).	5
Figure 7. Hybrid driving system of TSHDs (Vlasblom W, 2007).	6
Figure 8. The outline of this thesis.	11
Figure 9. Ship ratio of TSHDs in year of construction (Vlasblom, 2003).	14
Figure 10. Payload-draught relation of TSHDs (Vlasblom, 2003).....	15
Figure 11. Planform of a typical TSHD (Walton, 1902).	16
Figure 12. A diesel engine directly drives propeller (Shi, 2013).	18
Figure 13. Diesel engine directly drives dredge pump (Shi, 2013).....	18
Figure 14. Diesel directly drives propeller and electrically drives dredge pump (Shi, 2013).....	19
Figure 15. Outline of the latest drive line in a hopper dredger (Petit & Loccufier, 2009).	19
Figure 16. Reduced model of the mass-elastic system (Petit & Loccufier, 2009).	20
Figure 17. Side-by-side configuration of the dredging ship and the mud barge (Song Chang, 2017).	31
Figure 18. Classical hull girder with variable cross-sections.	43
Figure 19. The outline of proposed math model.	44
Figure 20. Hull girder model subjected to complex excitation loads with variable mass systems.....	46

Figure 21. Results transferred from calculation programme into FEM by MPC technology.	46
Figure 22. Force diagram of classical Euler-Bernoulli beam element.	47
Figure 23. Time-varying mass beam with variable mode shape in time domain.	50
Figure 24. N segments of variable cross-section beam.	51
Figure 25. Coordinate systems defined in hydrodynamic calculation.	61
Figure 26. Transformation from wave spectrum to wave time-series (Faltinsen, 1993).	65
Figure 27. Sampling method in frequency-domain.	65
Figure 28. Source point on wetted interface of ship hull structure.	69
Figure 29. Schematic diagram of the motion vector relationship of the mass point. .	76
Figure 30. Outline and application of proposed model.	95
Figure 31. The outline of TVM_HullGirder program.	96
Figure 32. Dynamic response information transferred into FEM by MPC in selected cross-section.	97
Figure 33. The geometric model of the cantilever Euler-Bernoulli beam in ABAQUS.	99
Figure 34. Natural frequency results in axial calculated by ABAQUS and the semi-analytical approach.	101
Figure 35. Difference percentage in axial of ABAQUS and the semi-analytical approach.	101
Figure 36. Geometric model of the cantilever Euler-Bernoulli beam in ABAQUS.	103
Figure 37. Natural frequency results in transverse calculated by ABAQUS and the semi-analytical approach.	104
Figure 38. Difference percentage in transverse of ABAQUS and the semi-analytical approach.	104
Figure 39. Mode shape generated by the semi-analytical approach.	105
Figure 40. Basic structural diagram of a TSHD from the side view.	107

Figure 41. Basic structural diagram of a TSHD from the top view.....	107
Figure 42. Hull lines plan of a TSHD.....	107
Figure 43. Hull girder model with defined variable-mass beam elements in the middle.	108
Figure 44. Example of cross-sectional parameters calculation in ANSYS/Spaceclaim.	110
Figure 45. Panel model in SESAM.	111
Figure 46. Weight distribution along with ship frame in ten load cases.	112
Figure 47. Variation in TSHD draft line.....	115
Figure 48. Variable draft line at the bow and stern of the TSHD.....	115
Figure 49. Approximation of the objective ship hull by 2408 quadrilateral elements.	116
Figure 50. The panel model in fully weighted load case 01.....	116
Figure 51. The panel model for fully lighted load case 10.....	116
Figure 52. Added mass in surge with 10 load cases.....	117
Figure 53. Added mass in sway with 10 load cases.	117
Figure 54. Added mass in heave with 10 load cases.	118
Figure 55. Added mass in roll with 10 load cases.	118
Figure 56. Added mass in pitch with 10 load cases.....	119
Figure 57. Added mass in yaw with 10 load cases.....	119
Figure 58. Damping coefficients in surge with 10 load cases.	120
Figure 59. Damping coefficients in sway with 10 load cases.	120
Figure 60. Damping coefficients in heave with 10 load cases.	121
Figure 61. Damping coefficients in roll with 10 load cases.	121
Figure 62. Damping coefficients in pitch with 10 load cases.....	122
Figure 63. Damping coefficients in yaw with 10 load cases.....	122
Figure 64. RAOs in surge with 10 load cases in 0-degree wave.	123

Figure 65. RAOs in heave with 10 load cases in 0-degree wave. 123

Figure 66. RAOs in pitch with 10 load cases in 0-degree wave..... 124

Figure 67. RAOs in surge with 10 load cases in 45-degree wave. 124

Figure 68. RAOs in sway with 10 load cases in 45-degree wave. 125

Figure 69. RAOs in heave with 10 load cases in 45-degree wave. 125

Figure 70. RAOs in roll with 10 load cases in 45-degree wave. 126

Figure 71. RAOs in pitch with 10 load cases in 45-degree wave..... 126

Figure 72. RAOs in yaw with 10 load cases in 45-degree wave. 127

Figure 73. Dredger in load case 03 (left) and load case 04 (right). 127

Figure 74. The first-order natural frequency results with four different simulation cases involving three various added mass calculation methods (Wet) and the case without consideration of added mass (Dry) in Y direction. 130

Figure 75. The first-order natural frequency results with four different simulation cases involving three various added mass calculation methods (Wet) and the case without consideration of added mass (Dry) in Z direction. 130

Figure 76. The first-order natural frequency results with three various added mass calculation methods (Wet) in Y direction..... 132

Figure 77. The first-order natural frequency results with three various added mass calculation methods (Wet) in Z direction. 132

Figure 78. The second-order natural frequency results with four different simulation cases involving three various added mass calculation methods (Wet) and the case without consideration of added mass (Dry) in Y direction. 134

Figure 79. The second-order natural frequency results with four different simulation cases involving three various added mass calculation methods (Wet) and the case without consideration of added mass (Dry) in Z direction. 134

Figure 80. The second-order natural frequency results with three various added mass calculation methods (Wet) in Y direction..... 135

Figure 81. The second-order natural frequency results with three various added mass calculation methods (Wet) in Z direction. 135

Figure 82. Descriptions for outputted results from the hull girder model.....	136
Figure 83. Oscillation results of hull girder in heave with various dynamic model and mass change settings.....	137
Figure 84. Acceleration of hull girder in heave as a rigid-flexible coupled body with variable mass (8211) and invariant-mass (7211) working conditions.....	139
Figure 85. Acceleration of hull girder in heave as a rigid body with variable mass (6211) and invariant-mass (5011) working conditions.	139
Figure 86. Acceleration of hull girder in pitch as a rigid-flexible coupled body with variable mass (8211) and invariant-mass (7211) working conditions.....	139
Figure 87. Acceleration of hull girder in pitch as a rigid body with variable mass (6211) and invariant-mass (5011) working conditions.	140
Figure 88. Oscillation results of the hull girder in heave in 0-degree and 45-degree wave direction during unloading operations.	141
Figure 89. Angular results of the hull girder in pitch in 0-degree and 45-degree wave direction during unloading operations.....	142
Figure 90. Oscillation results of the hull girder in heave in 0-degree and 45-degree wave direction during invariant-mass working conditions.....	143
Figure 91. Angular results of the hull girder in pitch in 0-degree and 45-degree wave direction during invariant-mass working conditions.....	143
Figure 92. Acceleration results of the hull girder in heave under 0-degree and 45-degree wave sea condition respectively.....	144
Figure 93. Angular acceleration results of the hull girder in pitch under 0-degree and 45-degree wave sea condition respectively.	144
Figure 94. Displacement results of invariant-mass beam element 01 - 06 in Z direction under unloading working conditions.	145
Figure 95. Displacement results of time-varying mass beam element 07 - 14 in Z direction under unloading working conditions.....	146
Figure 96. Displacement results of invariant-mass beam element 15 - 20 in Z direction under unloading working conditions.	146

Figure 97. Displacement results of beam element 01 in Z direction with variable mass (8211) and invariant mass (7211) working conditions respectively..... 147

Figure 98. Displacement results of beam element 06 in Z direction with variable mass (8211) and invariant mass (7211) working conditions respectively..... 147

Figure 99. Displacement results of beam element 10 in Z direction with variable mass (8211) and invariant mass (7211) working conditions respectively..... 148

Figure 100. Displacement results of beam element 16 in Z direction with variable mass (8211) and invariant mass (7211) working conditions respectively..... 148

Figure 101. Displacement results of beam element 20 in Z direction with variable mass (8211) and invariant mass (7211) working conditions respectively..... 149

Figure 102. Angular results of invariant-mass beam element 01 - 06 about Y axis under unloading working conditions. 150

Figure 103. Angular results of time-varying mass beam element 07 - 14 about Y axis under unloading working conditions. 150

Figure 104. Angular results of invariant-mass beam element 15 - 20 about Y axis under unloading working conditions. 151

Figure 105. Angular results of beam element 01 about Y axis with variable mass (8211) and invariant mass (7211) working conditions respectively. 151

Figure 106. Angular results of beam element 06 about Y axis with variable mass (8211) and invariant mass (7211) working conditions respectively. 152

Figure 107. Angular results of beam element 10 about Y axis with variable mass (8211) and invariant mass (7211) working conditions respectively. 152

Figure 108. Angular results of beam element 16 about Y axis with variable mass (8211) and invariant mass (7211) working conditions respectively. 153

Figure 109. Angular results of beam element 20 about Y axis with variable mass (8211) and invariant mass (7211) working conditions respectively. 153

Figure 110. Displacement results of the beam element 01 in Z direction with 0-degree and 45-degree sea wave conditions respectively..... 155

Figure 111. Displacement results of the beam element 06 in Z direction with 0-degree and 45-degree sea wave conditions respectively.....	155
Figure 112. Displacement results of the beam element 10 in Z direction with 0-degree and 45-degree sea wave conditions respectively.....	156
Figure 113. Displacement results of the beam element 16 in Z direction with 0-degree and 45-degree sea wave conditions respectively.....	156
Figure 114. Displacement results of the beam element 20 in Z direction with 0-degree and 45-degree sea wave conditions respectively.....	157
Figure 115. Angular results of the beam element 01 in Z direction with 0-degree and 45-degree sea wave conditions respectively.....	158
Figure 116. Angular results of the beam element 06 in Z direction with 0-degree and 45-degree sea wave conditions respectively.....	159
Figure 117. Angular results of the beam element 10 in Z direction with 0-degree and 45-degree sea wave conditions respectively.....	159
Figure 118. Angular results of the beam element 16 in Z direction with 0-degree and 45-degree sea wave conditions respectively.....	160
Figure 119. Angular results of the beam element 20 in Z direction with 0-degree and 45-degree sea wave conditions respectively.....	160
Figure 120. Geometric model of middle sections in ANSYS from main view.....	162
Figure 121. Geometric model of middle sections in ANSYS from top view.....	162
Figure 122. Finite element model of middle sections in ANSYS.....	163
Figure 123. MPC settings in six cross sections of middle parts.....	163
Figure 124. MPC setting at A surface corresponds to beam element 07.....	164
Figure 125. MPC setting at C surface corresponds to beam element 09.....	164
Figure 126. Maximum von-Mises stress during the simulation time with different case settings.....	165
Figure 127. Maximum principal stress during the simulation time with different case settings.....	165

Figure 128. Maximum stress intensity during the simulation time with different case settings.....	166
Figure 129. Maximum equivalent strain during the simulation time with different case settings.....	167
Figure 130. Maximum principal elastic strain during the simulation time with different case settings.	167
Figure 131. Maximum elastic strain intensity during the simulation time with different case settings.	168
Figure 132. Maximum total deformation during the simulation time with different case settings.....	169
Figure 133. Maximum equivalent von-Mises stress in 0-degree wave - 8211.....	170
Figure 134. Maximum equivalent von-Mises stress in 0-degree wave - 7211.....	170
Figure 135. Maximum equivalent von-Mises stress in 45-degree wave - 8211.....	170
Figure 136. Maximum equivalent von-Mises stress in 45-degree wave - 7211.....	171
Figure 137. Selected von-Mises stress points on the cross-section of beam element 07 in 0-degree wave -8211.	172
Figure 138. Selected von-Mises stress points on the cross-section of beam element 07 in 0-degree wave -7211.	172
Figure 139. Selected von-Mises stress points on the cross-section of beam element 07 in 45-degree wave -8211.	173
Figure 140. Selected von-Mises stress points on the cross-section of beam element 07 in 45-degree wave -7211.	173
Figure 141. Column distribution diagram in engine room of the TSHD.	175
Figure 142. Velocity spectrum (left) and virtual value (right) of engine room column 1.	176
Figure 143. Velocity spectrum (left) and virtual value (right) of engine room column 2.	176
Figure 144. Velocity spectrum (left) and virtual value (right) of engine room column 7.	176

List of tables

Table 1. The Euler-Bernoulli beam parameters for vibration analysis in axial direction.	99
Table 2. Natural frequency analysis results of the cantilever Euler-Bernoulli beam in axial direction outputted from ABAQUS software and the semi-analytical approach.....	100
Table 3. The Euler-Bernoulli beam parameters for vibration analysis in transverse direction.....	102
Table 4. Natural frequency analysis results of the cantilever Euler-Bernoulli beam in transverse direction outputted from ABAQUS software and the semi-analytical approach.....	103
Table 5. The main scantlings of the dredging ship.....	106
Table 6. Structural property data as input.....	109
Table 7. Main parameters in each beam element.	110
Table 8. Hydro parameters in ten load cases.	112
Table 9. Simulation parameters as input.	113
Table 10. Sea environmental data as input.....	113
Table 11. Definitions for users as input.....	114

Lists of abbreviations

CFD	Computational Fluid Dynamics
COB	Centre of Buoyancy
COG	Centre of Gravity
FEA	Finite Element Analysis
FEM	Finite Element Model
FLNG	Floating Liquefied Natural Gas
FPSO	Floating Production Storage and Offloading
MPC	Multiple Point Constraints
RAO	Response Amplitude Operator
TSHD	Trailing Suction Hopper Dredger
TVM	Time-Varying Mass

Nomenclature

A	Cross-sectional area of the beam
A_1	System vector
A_2	System vector
A_1^T	Transposition of the system vector
\vec{a}^B	Acceleration of the local coordinate system in global coordinate system
\vec{a}^k	Acceleration of the k^{th} mass point with respect to global coordinate system
$\vec{a}_{k/B}$	Acceleration of the k^{th} mass point with respect to local coordinate system
\vec{b}	Modal integral
C	Generalized damping matrix
C_t^1	Ordinary differential equation solution coefficient at time t
C_t^2	Ordinary differential equation solution coefficient at time t
C_t^3	Ordinary differential equation solution coefficient at time t
C_t^4	Ordinary differential equation solution coefficient at time t
\vec{d}^k	Deflection of the k^{th} mass point
D_r	Modal integral
d_{rj}	Modal integral
δ_{ri}	Kronecker delta
$\frac{\partial^2 \phi}{\partial t^2}$	Deflection acceleration of the beam
E_1	Generalized mass matrix
EI	Cross-sectional stiffness of the beam
η	Modal coordinate vector
$\dot{\eta}$	First time derivation of modal coordinate vector
$\ddot{\eta}$	Second time derivation of modal coordinate vector

η_i	Modal coordinate vector for i^{th} mode
$\dot{\eta}_i$	First time derivation of modal coordinate vector for i^{th} mode
$\ddot{\eta}_i$	Second time derivation of modal coordinate vector for i^{th} mode
\vec{f}_{ext}^B	Total external force vector acted on the body
\vec{F}^k	External force vector acted on the k^{th} mass point
F_r	r^{th} generalized active force in Kane's method
F_r^*	r^{th} generalized inertia force due to the time rate of change of velocity in Kane's method
F_r^{**}	r^{th} generalized inertia force due to the time rate of change of mass in Kane's method
\vec{g}	Modal integral
\vec{H}	Angular momentum of the body
\hat{I}	Inertia tensor of the body
K	Generalized stiffness matrix
k^g	Geometric stiffness
λ_t	Ordinary differential equation coefficient at time t
M	Generalized mass matrix
M_1	Kane's system matrix
m_t^B	Total mass of the body at time t
m_{gen}	Generalized mass
m^k	Mass of the k^{th} mass point
N_i	Modal integral
$\vec{\omega}^B$	Angular velocity of the local coordinate system with respect to global coordinate system
$\vec{\omega}_r^B$	Partial derivation of angular velocity of the local coordinate system in global coordinate system for the r^{th} generalized speed

Ω_i	Natural frequency at i^{th} mode
\vec{p}^k	Undeformed position vector of the k^{th} mass point
$\phi_t(x)$	Mode shape of the beam at time t
$\phi(x, t)$	Deflection function of the beam
\tilde{r}_c	Average moment arm of all mass points
$\rho(t)$	Mass density function of the beam with respect to time
\vec{S}	Modal integral
\tilde{S}	Skew-symmetric matrix of vector \vec{S}
\vec{t}_{ext}^B	Total external torque vector acted on the body
U	Identity matrix
\vec{v}^B	Velocity of the local coordinate system with respect to the global coordinate system
$\vec{v}_{k/B}$	Velocity of the k^{th} mass point with respect to the local coordinate system
\vec{v}_e^k	Mass loss velocity of the k^{th} mass point
\vec{v}_r^B	Partial derivation of velocity of the local coordinate system with respect to global coordinate system for the r^{th} generalized speed
\vec{v}_r^k	Partial derivation of velocity of the k^{th} mass point with respect to global coordinate system for the r^{th} generalized speed
X_1	Kane's system vector
Y_1	Kane's system vector
Z_1	Kane's system vector
ξ	Modal damping coefficient

List of publications

Journal publication:

Zhang, Y., Pu, Y. and Hu, Z., 2023. A mathematical and numerical model for variable cross-section hull girder with time-varying mass systems applied in marine vessels. (submitted to Marine Structures, revision)

Conference publications:

Zhang, Y. and Hu, Z., 2023. A mathematical model for variable cross-section hull girder with time-varying mass characteristics. In *Advances in the Analysis and Design of Marine Structures* (pp. 309-317). CRC Press.

Zhang, Y. and Hu, Z., 2023. Hydrodynamic and vibration analysis of specific offshore engineering vessels with time-varying wet surface and longitudinal inclination characteristics. International Conference on Collision and Grounding of Ships and Offshore Structures (ICCGS 2023)

Chapter 1. Introduction

This chapter provides the background of dredgers, especially Trailing Suction Hopper Dredgers (TSHDs), focusing on their specific working conditions, structural characteristics, and current challenges of design and structural analysis. The proposed mathematical and numerical model, a central aspect of this Ph.D. research, is introduced to underline its novelty and potential contributions to the marine engineering industry.

1.1. Background of dredgers

Advancements in sciences and technology have given rise to a growing variety of specialized vessels designed for specific oceanic operations, for instance, pipe layer, and dredger etc. These kinds of vessels are designed by cutting-edge technology (Andrun et al., 2020), which are playing a significantly important role in the field of marine and offshore engineering. Presently, dredging industry is playing a distinctly essential role in the field of coastal and offshore engineering. In general, dredgers can be broadly classified into two main types: (i) mechanical dredgers; (ii) hydraulic dredgers (Yell & Riddell, 1995). One of hydraulic dredgers is called Trailing Suction Hopper Dredgers (TSHDs) which has become an essentially specific ship in the dredging industry (R. N. Bray et al., 1997).

TSHD is a kind of dredgers that has a full sailing capacity used to maintain navigable waterways, deepen the maritime canals (Figure 1) and construct new land (Figure 2). This is made possible by large powerful pumps and engines able to suck sand, clay, silt and gravel (R. N. Bray et al., 1997). Its hull and exterior resemble typical self-propelled transport vessels. In addition to featuring standard navigation machinery and various facilities, it is equipped with a set of dredging equipment for dredging suction and a mud chamber for loading slurry, as well as equipment for discharging cargoes through the hopper doors at the bottom (Figure 3).

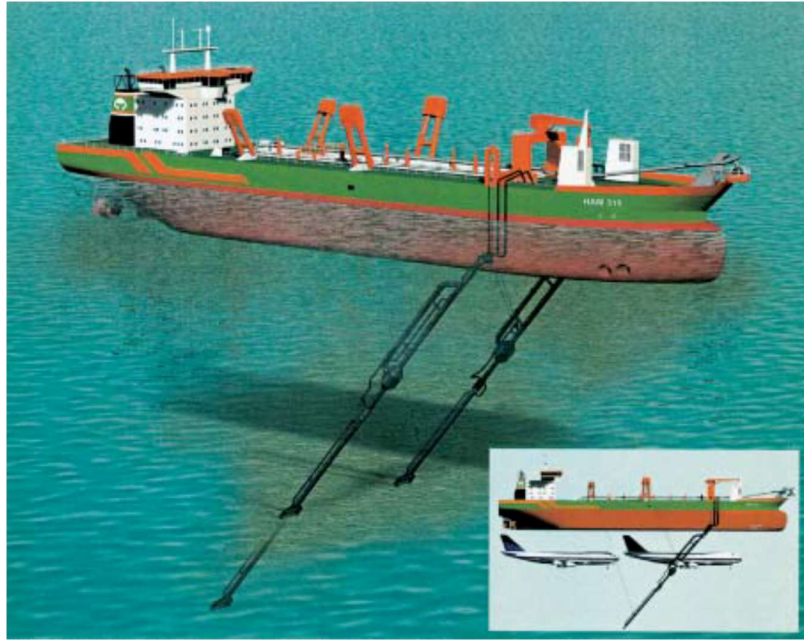


Figure 1. Drawing of one of newest dredger commissioned (Vidal, 2001).



Figure 2. Rainbowing clean sand for land reclamation (N. Bray & Cohen, 2004).

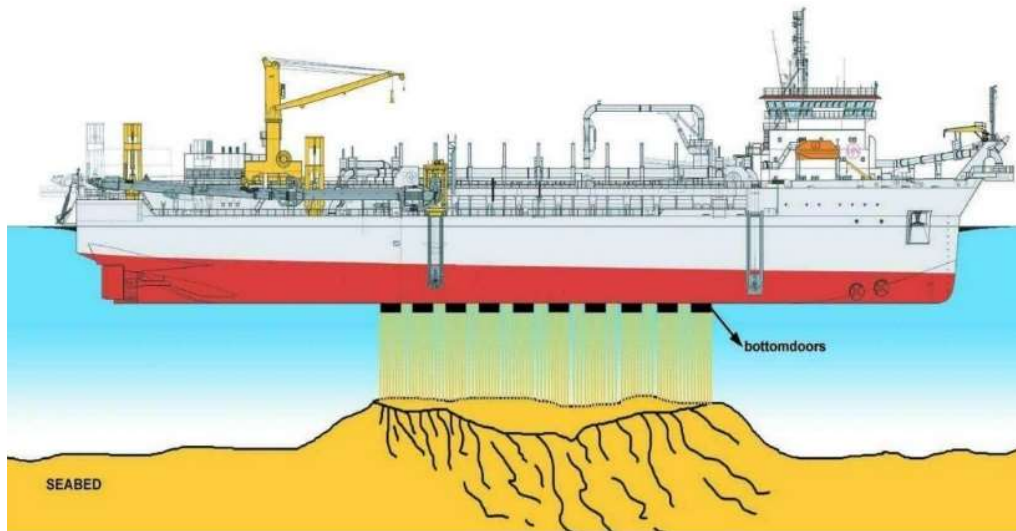


Figure 3. The dumping process of TSHDs at the disposal site (Dragados, 2017).

1.2. Natural features of dredgers

In order to achieve their special engineering purposes, however, TSHDs have some particular structural designs and characteristics in operations that are different from general ships.

1.2.1. Time-varying mass characteristics

The main working feature of TSHDs is to excavate a large number of materials from the seabed and then transport them to a designated area for unloading. Therefore, the working cycle of TSHDs can be briefly separated by four main working operations, which are sailing empty, dredging, sailing loaded and discharging respectively (Figure 4).

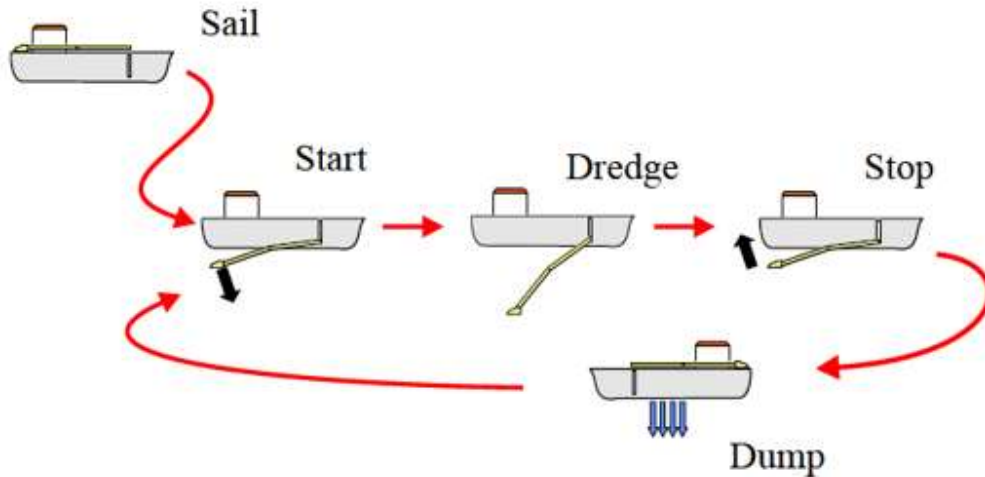


Figure 4. The typical working cycle of TSHDs (Mourik & Osnabrugge, 2014).

Moreover, according to the study of DE JONG (2010), it shows that “frequency of loading and discharging is up to four times per day and the freeboard can be increased from the dredger load line to the summer load line within eight minutes under normal operation of the dumping system.” It means that TSHDs have obvious characteristics of variable mass due to loading or unloading working conditions. Not only is the frequency of such changes in a day very high, but the short-term dumping periods lead to an increase in the rate of mass change for this vessel (Figure 5).

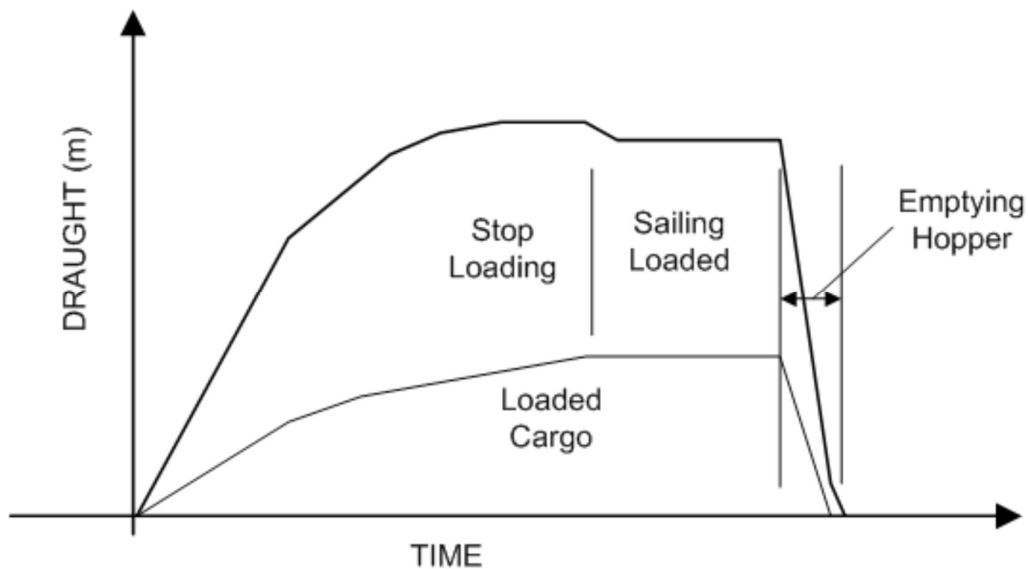


Figure 5. A schematic view of the change in draught of a TSHD in service (Basic et al., 2017).

During the rapid shift operation time, the weight and displacement of a dredger can be reduced as quick as several minutes, which leads to substantial variations in vessel's mass and makes it a typical mass-variation system.

1.2.2. Discontinuous structure characteristics

With the purpose of loading and unloading, the middle structures of TSHDs had to be designed into a large number of discontinuous structures (Figure 6). That is to say, numerous discontinuous structures must exist on TSHDs rather than that of general ships, which potentially causes the stiffness of such this kind of ships to be seriously insufficient.

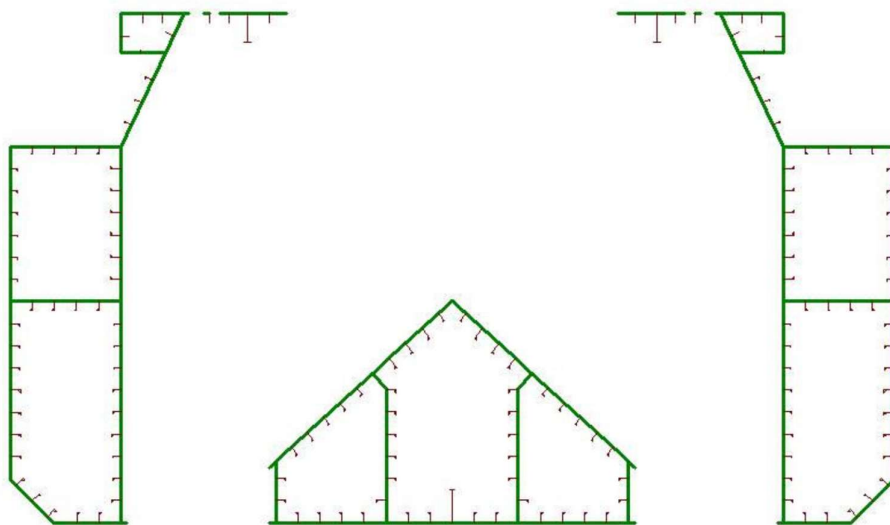


Figure 6. The typical cross-section at midship of TSHDs (DE JONG, 2010).

1.2.3. Complex loads

Due to the invention of the centrifugal pump, high-performance coupling and clutch as well as gearbox, this makes new types of TSHDs can be driven by a hybrid system technically feasible (Figure 7). This hybrid system powered by main diesel engines is composed of dredging pumps, propellers and generators with some linking components such as couplings and clutches etc. Consequently, this hybrid system arranges some devices that can generate the main excitation source at the stern of the ship, and they are connected with each other instead of separately to generate excitation force. In other words, such a specially driving system as a source of ship's own excitation is necessary for detailed study as well as other external loads such as hydrodynamic loads with time-

varying wet surface and mass changing in the ocean environment during operational conditions.

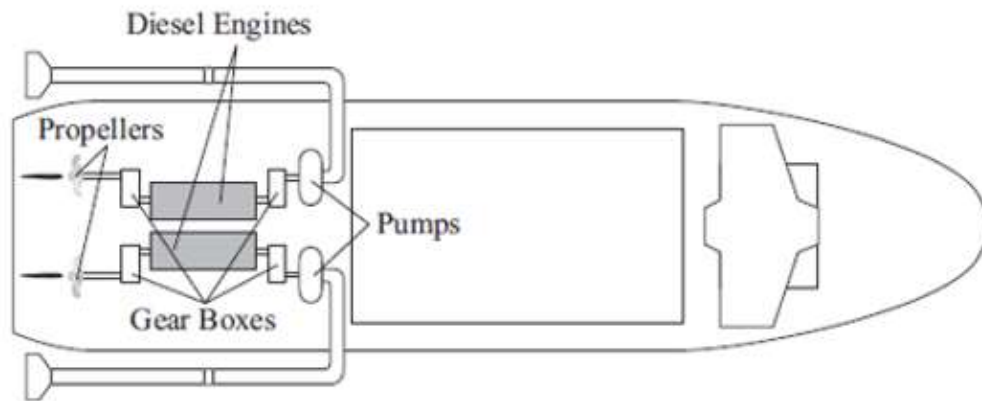


Figure 7. Hybrid driving system of TSHDs (Vlasblom W, 2007).

In short, the main characteristics of TSHDs are the changes of structural mass properties during working conditions, and a series of structural discontinuities lead to a significant reduction in structural stiffness properties, as well as complex loads generated by special equipment on the ship and ocean environment. Consequently, some main challenges of TSHDs in this project could be summarized due to their natural characteristics as:

- Time-varying mass system with frequently changing of its natural properties during working conditions.
- Many discontinuous structures.
- Various complex loads due to engineering mechanical vibrations, hydrodynamic loads with time-varying wet surface and mass changing.

1.3. Overview of doctoral programme

1.3.1. Motivation

In view of unique engineering purposes of TSHDs, the structural design of these vessels with time-varying mass characteristics often involves inherent structural discontinuities. This structural design potentially has low stiffness characteristics along ship hull length due to a large opening on the deck and several openings at the bottom of ship hull. When coupled with these characteristics and complex operating loads, the dynamic

effects stemming from time-varying mass become significant potentially. To addressing this challenge is unavoidable during the design and development phases, especially considering the rapid changes in mass during unloading operations.

However, there is a noticeable scarcity of research that has specifically addressed the structural dynamics for these unique offshore structures who have time-varying mass system and many discontinuous structures subjected to complex loads. Furthermore, currently available commercial software or calculation programmes lack the capability to perform dynamic analysis for marine structures with variable mass characteristics. Given this scenario, the development of variable-mass marine structures necessitating the establishment of a flexible structural dynamics model that not only accounts for the influence of time-varying mass and structural discontinuity, but also accommodates the complex sea environmental and operational loads acted on the marine structures. Therefore, it becomes imperative to develop mathematical models and numerical programme tailored to these variable-mass marine structures. These tools can serve as indispensable analytical resources for structural designers during the preliminary research and design phases.

1.3.2. The research background and significance

The study of dynamic analysis in marine structures under varying mass conditions is crucial for marine engineering and naval architecture. Here is a concise overview of the research background and significance:

(1) Static and time-varying dynamic loading condition

While static loading conditions refers to loads that are applied slowly and remain constant or nearly constant over time provide a foundation for understanding the basic structural requirements of a marine vessel, time-varying dynamic loading conditions involves loads that change over time in magnitude, direction, and location are essential for capturing the complexities of real-world operations for marine vessels. These dynamic loads are influenced by the movement of marine vessels and the surrounding environment. Accounting for time-varying dynamic loads of marine structures ensures comprehensive design, enhancing the marine structural safety, durability, and performance in the dynamic marine environment.

(2) Challenges of variable mass system in marine structures

Some specific engineering vessels experience dynamic challenges due to changing mass during loading and unloading operations such as TSHDs. Understanding these challenges and developing relevant analysis tools are essential for structural integrity and operational safety in marine engineering field.

(3) Development challenges of innovative modelling approach

This research employs advanced mathematical models based on innovative methodologies to simulate and analyse dynamic responses of specific marine vessels under time-varying mass conditions coupled with complex loads, providing accurate predictions of structural behaviour not only applied in such TSHDs, but also other types of marine vessels who have same operational characteristics.

(4) Design and safety implications:

Outcomes will inform improved design practices, operational guidelines, and safety protocols for marine structures who have variable-mass system and coupled operational loads, enhancing overall safety and efficiency.

(5) Contributions to marine engineering:

This study advances understanding in marine engineering, addressing gaps in the knowledge and paving the way for more robust methodologies in the analysis and design of vessels facing variable mass conditions subjected to complex operating loads.

In summary, this research on dynamic analysis in structures of marine vessels such TSHDs or other vessels who have similar characteristics under time-varying mass conditions contributes significantly to safety, efficiency, and reliability in loading or unloading operations coupled with external and internal operating loads. An innovative mathematical and numerical model is proposed, and a programme is developed in this study, which is at the forefront of advancements in structural dynamics of marine vessels.

1.3.3. Aim and objectives

(1) Aim

The aim of this project is to propose an innovative approach for estimating dynamic structural response on time-varying mass system subjected to various complex loads including hydrodynamic loads with time-varying wet surface, and other excitation

loads when its natural properties are frequently changing. With the proposed approach, structural dynamic responses can be analysed in a better accuracy, which can be transferred into FEM for further structural strength and fatigue assessments. The proposed approach will be conveniently applied for guiding the real offshore engineering practices.

(2) Objectives

In this project, the biggest challenge and the most innovative point is to propose a mathematical and numerical model that meets the main aim based on the existing finite element technology. Through programming language FORTRAN and code editor Microsoft Visual Studio, the proposed novel mathematical model would be built into a flexible and accurate calculation program that can meet engineering applications and other analysis. The followings are objectives of this study:

- Propose a mathematical model that combines complex loads including hydrodynamic loads, excitation loads such as excitation load generated by diesel engine and propellers during the motion with time-varying mass operations.
- Build a programme to link the proposed mathematical model with global structural analysis in finite element software ANSYS to fulfil the dynamic structural analysis and other structural strength assessments.
- Investigate the dynamic responses based on finite element technology with the proposed mathematical and numerical model coupled with various complex loads and time-varying mass system.
- Summarize the dynamic analysis results and provide useful recommendations for further engineering field.

1.3.4. Overview of novelties

From introducing groundbreaking methodologies that redefine traditional approaches to unveiling innovative findings that push the boundaries of existing knowledge, the novelties of this research can be summarized as follows:

- An innovative mathematical and numerical model for dynamic analysis of specific marine vessels during time-varying mass working conditions are proposed.

- The proposed model has been compiled as a time-history dynamic analysis programme by FORTRAN language - TVM_HullGirder programme.
- The programme can calculate and output motion responses of the marine vessel and local structure dynamic responses and other variable values in time domain.
- Results calculated by the programme could be transferred to detailed FEM by MPC technology for further structural analysis and assessment.
- Through post-processing analysis of structural FEA, design flaws or other deficiencies of the structure can be evaluated to meet the needs of engineers.

1.3.5. Outline of the thesis

In this thesis, a mathematical and numerical model is proposed to investigate the dynamic analysis of marine structures featuring time-varying mass systems. Figure 8 shows the brief outline of this thesis. The general scope of each chapter is arranged as below:

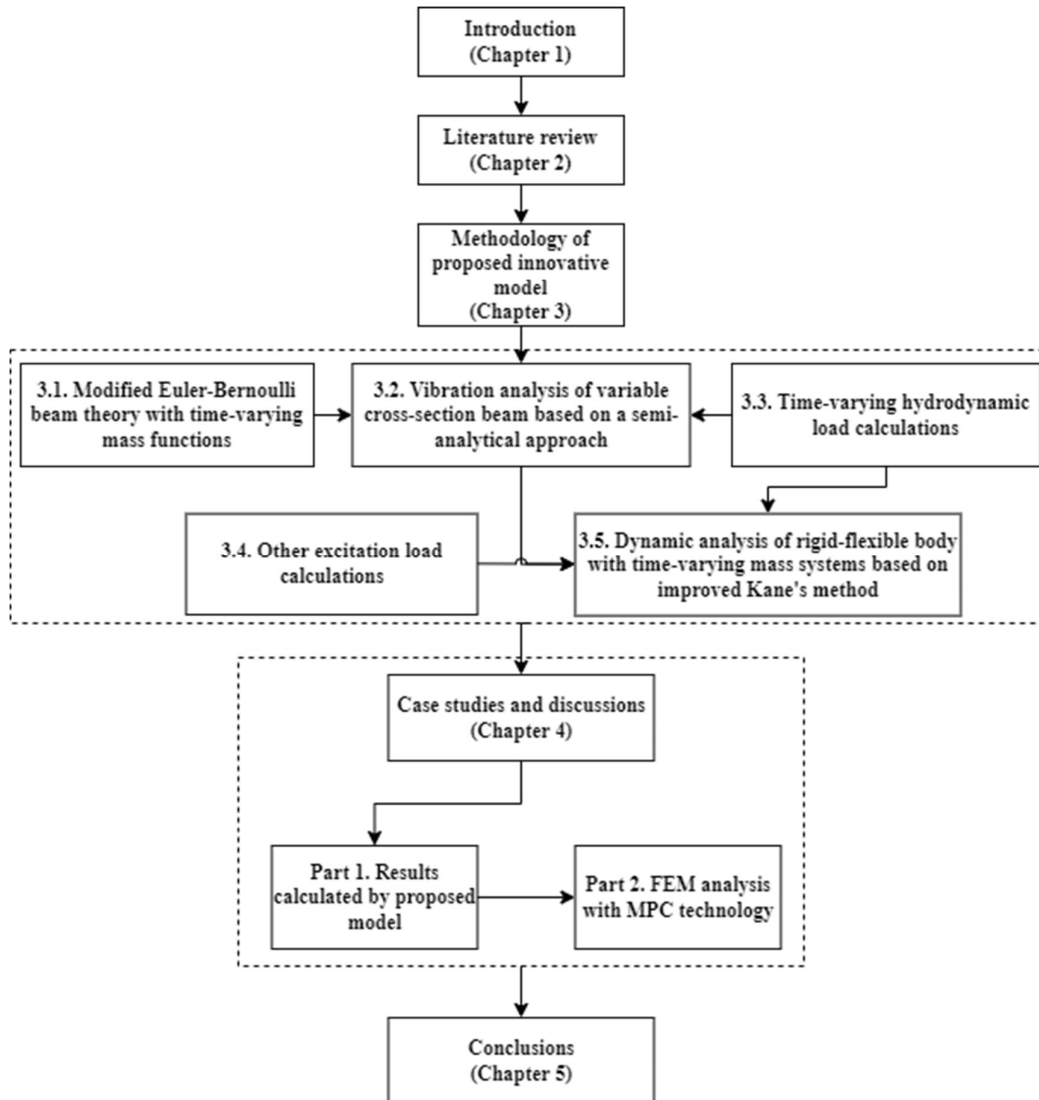


Figure 8. The outline of this thesis.

Chapter 2: A literature review of dredgers is made in this chapter. Moreover, this chapter compiles relevant literatures about dynamic analysis of marine vessels and time-varying dynamic structures. Furthermore, an extensive review of literatures related to hydrodynamics analysis and other excitation loads in marine structures is presented.

Chapter 3: The theoretical foundations and methodologies of the proposed innovative mathematical and numerical model are detailed in this chapter. These primarily encompass the modified Euler-Bernoulli beam theory with time-varying mass function, semi-analytical approach of vibration characteristic analysis of variable cross-section beam, time-varying hydrodynamic calculation method, other excitation load calculation

methods, and the improved Kane's dynamic equations with time-varying mass system as main dynamic analysis approach.

Chapter 4: Semi-analytical approach of vibration characteristic analysis on variable cross-section beam has been verified in this chapter by comparing with FEA results. Pre-calculation results of user-defined case study during unloading operations have been shown in this chapter, which includes vibration analysis results and hydrodynamic analysis results respectively. Moreover, motion responses and structural dynamic responses of the hull girder are outputted by self-developed programme, which are transferred into FEM by MPC technology in ANSYS for further strength assessments. FEA results of real-scale three-dimensional model of the vessel based on calculation outputs from self-developed programme are shown in final part in this chapter.

Chapter 5: This chapter concludes the present works. Some novel summarises of this research and contribution to marine structure safety are concluded. Finally, the directions and possibilities of future research are discussed.

Chapter 2. Literature review

This chapter summarizes some recent literature reviews about structure and excitation loads research in dredgers, dynamic analysis, hydrodynamics and structural analysis of marine structures, which provides a valuable reference for the study of this project.

2.1. Literature reviews on dredgers

Dredging techniques are defined as soil or rock erosion, transport, and sedimentation processes, which are carried out through human intervention and specially designed machines. The dredging industry has evolved from localized activities to maintain the navigable waterways as a global industry that includes maintenance dredging, coastal and port construction, land reclamation, and offshore structures by leveraging increasingly complex and powerful dredgers.

Among all types of dredgers, the Trailing Suction Hopper Dredger (TSHD) stands out as one of the leading vessel types in the dredging industry, with vast prospects and considerable development potential. In this part, the existing literatures on the structural analysis and complex loads of TSHDs will be summarized in this section.

2.1.1. Structural research reviews of dredgers

The TSHD is the advanced vessel type in the dredging industry, however, its complex structure poses various challenges that require in-depth research. Due to the need for multiple structural openings, such as at the bottom, sides, and deck, to fulfil specific operational purposes, the TSHD exhibits discontinuities in its longitudinal structural components. This condition results in distinct characteristics in terms of structural strength, overall deformation, and global vibration properties compared to conventional vessels. Therefore, it is imperative to conduct a comprehensive structural analysis of the TSHD.

TSHDs are essential in dredging operations due to their self-propelled, self-loading, self-dredging, and self-unloading capabilities (Zhou et al., 2024). These vessels are widely utilized in large-scale dredging projects globally. Moreover, the book of Eisma (2005) has illustrated that with the exception of the TSHD, all dredgers are unsuitable for working under offshore conditions, besides they are special designed for it.

From the view of geometric design, professor Vlasblom (2003) introduced specific ship ratio of TSHDs (L/B, B/H and B/T ratio's, L=length, B=width, H=depth and T=draught) concerning market requirements over time (Figure 9).

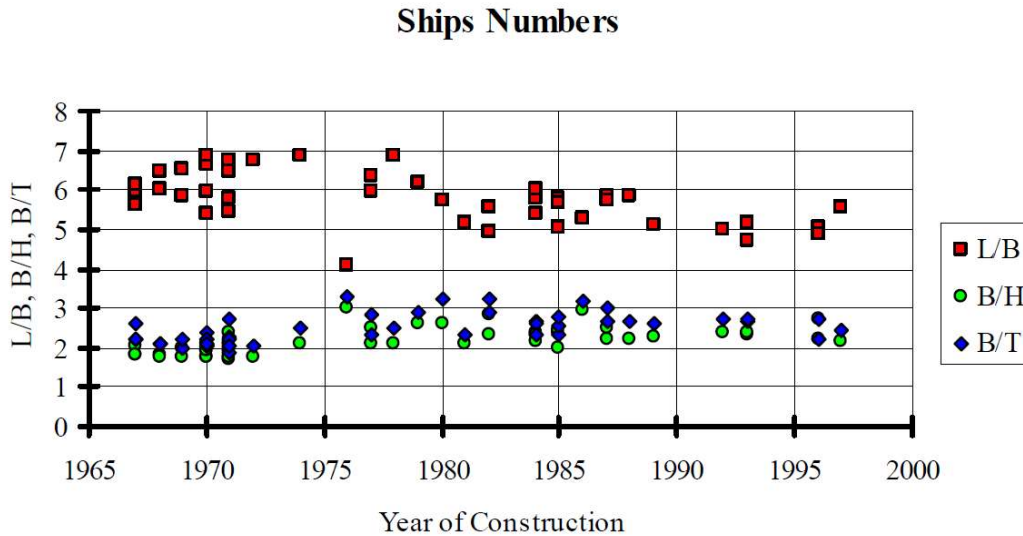


Figure 9. Ship ratio of TSHDs in year of construction (Vlasblom, 2003).

Ship proportions critically influence both performance and structural design. A high width-to-draught (B/T) ratio offers initial stability but may lead to pronounced ship motions and increased resistance. Conversely, a high length-to-width (L/B) ratio supports streamlined and cost-effective construction with lower resistance. Smaller width-to-height (B/H) and larger L/B ratios generally lead to reduced building costs. However, considerations for draught (T) costs should align with enhanced usability to justify any additional expenses. This study highlights the need for a balanced approach to optimize performance, structural robustness, and cost-efficiency. Integrating advanced simulation and real-time data can further refine these design principles, ensuring TSHDs remain efficient and adaptable.

For specialized tasks like harbour maintenance, the ship's data and production capacity are usually well-defined. However, for international dredging contractors, predicting future needs, especially regarding average cycles and production capacity, is complex. Their primary focus is cost-effective dredging to outperform competitors, driving a preference for larger dredgers. The main constraint in building larger vessels is the draught, as increased draught reduces ship usability. Contractors, considering expected

work and initial dredging depth, must balance ship availability with draught constraints (Figure 10).

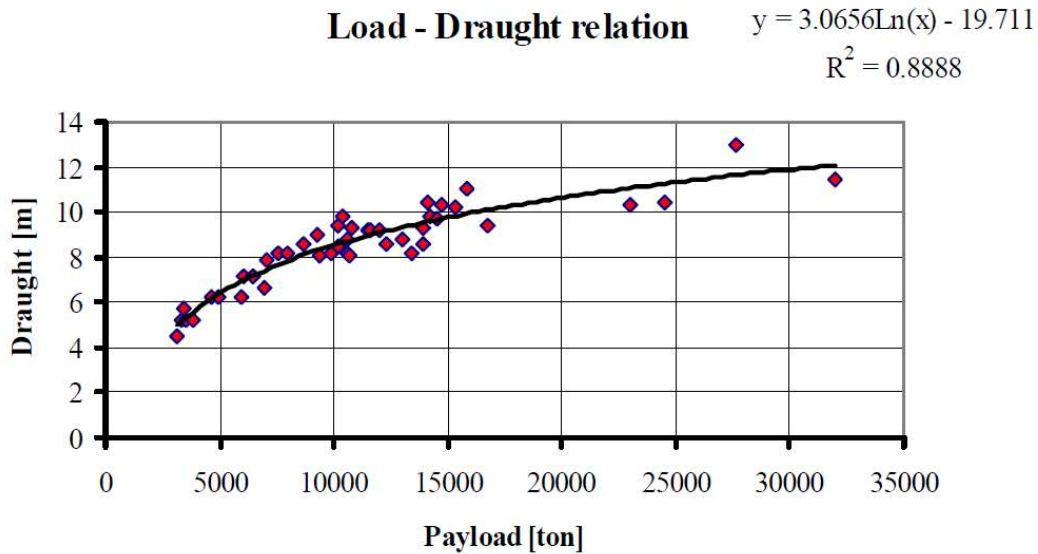


Figure 10. Payload-draught relation of TSHDs (Vlasblom, 2003).

On the other hand, this type of dredger, loading is carried out with the ship moving slowly forward, and unloading is usually carried out by means of a bottom-discharge arrangement, or by pump discharge, in the latter case usually by pumping to the shore. It means TSHDs have a large hatch opening at the deck and discontinuous openings at the bottom construction for their nature of working. The implication is that it has severe structural discontinuities in this kind of ships. Nowadays, classification society rules and structural analysis methods provide a means of determining the dimension and thickness of each part of the ship's structure. When these resources and methods are properly applied, the designer may reasonably define these so as to provide sufficient strength for the hull structure. Equally important, however, is structural continuity.

Taggart (1980) has argued that "structure has continuity when it is capable of transferring the loads in the structure without creating abrupt changes in stress levels." This means that for ships with discontinuous structural features, the structure is prone to cause abrupt changes in stress levels when transmitting loads.

In this study, as far as dredgers are concerned, which fall into various categories such as suction, grab, or bucket type. Additionally, these might be with or without their own hopper. Where the dredgers carry their own spoil, this is carried in a hopper situated

amidships and generally requiring buoyancy tanks at the sides, port and starboard, for the length of the hopper (Walton, 1902). This can be illustrated in Figure 11.

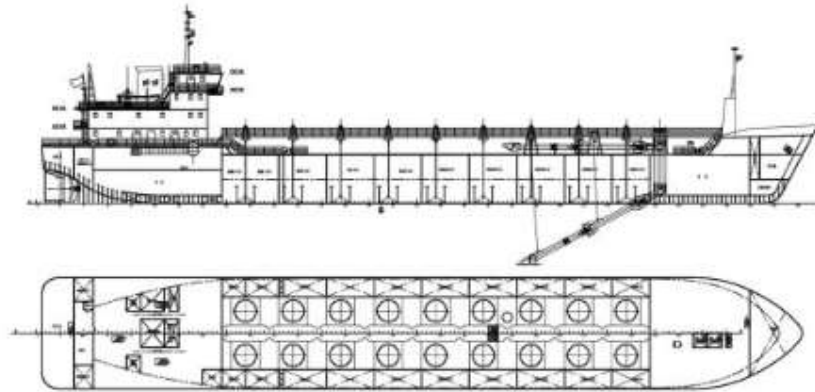


Figure 11. Planform of a typical TSHD (Walton, 1902).

As shown in the above figure, it easily can be found that there are several discontinuous openings in the bottom of the dredgers' hopper due to the nature of their activity.

Moreover, in the introduction of Taggart (1980) it is notable by him that the structural arrangements of self-unloaders are highly specialized, there being usually not tight transverse bulkheads and the double bottom being unusually shallow. Large ballast tanks are formed by the sloping hopper plating and the side shell. The implication is that for the TSHDs, it also has highly similar structural features. This special design not only increases the space for cargoes with shallow double bottom, but also arranges the fuel tanks, freshwater tanks and buoyancy tanks at both sides, and the hopper in the middle can be used as the ballast tank to improve the stability of the ship during navigation. Meanwhile, it was shown by Walton (1902) that the ratio of length of hopper space to ships' length is usually small being between 0.2 and 0.35. However, with the development of technology today, this ratio is usually larger than 0.35 for TSHDs. It means that this kind of ships should pay more attention to analyse the longitudinal and torsional strength since it has a longer hopper space with discontinuous openings at the bottom.

For such ships, the hopper can usually carry 5,000 to 25,000 tons of spoils according to the textbook of Vlasblom (2003), and these spoils are distributed over the hopper amidships, the weights at the ends of the ship being comparatively small. In such cases, the sagging bending moment in still water can be considerable. Moreover, it was

claimed by Walton (1902) that in contrast with dredgers, perhaps in no other ship has the block coefficient so important an influence on strength. However, in author's study, the block coefficient is determined as 0.88, which could easily be double the bending moment in light of the book of Walton (1902).

Some studies have investigated the motion response of TSHDs under swell conditions, highlighting the importance of accounting for environmental factors in their design and operation. Peng et al. (2023a) emphasize that understanding how TSHDs respond to swells is crucial for ensuring their stability and operational efficiency. This research underscores the need for comprehensive environmental assessments in the design phase to mitigate adverse effects on vessel performance and safety.

Additionally, optimization algorithms have proven effective in enhancing ship structures, including the midsection of TSHDs. Vuijk (2020) demonstrates that these algorithms can provide significant improvements by advising on the structural design process. By optimizing the midsection, these methods can lead to more robust and efficient designs, reducing stress concentrations and improving overall vessel integrity. This approach not only refines the structural performance of TSHDs but also supports cost-effective construction and maintenance strategies. Integrating optimization algorithms into the design process can thus play a pivotal role in advancing TSHD technology, ensuring these vessels meet the demanding requirements of modern dredging operations.

In additions, the paper of Vujasinović et al. (2012) aims to present the structural analysis conducted on a 14,000 m³ Trailing Suction Hopper Dredger. The calculations were executed to explore stress and buckling behaviour within the hopper region, with a specific focus on assessing stress concentration around the rounded corners of large openings. The objective was to attain optimized structural dimensions, particularly concerning the primary structure and significant openings. The rational structural design approach has successfully led to a reduction in structural weight.

To investigate the significance of the discharge process dynamics on actual ship stability, unsteady numerical simulations were performed with the Discrete Element Method (DEM) for symmetrical hopper opening during cargo discharge procedure, without the hull opening failure modes examined. Numerical simulations indicate that

the dynamics of the cargo during its discharging should not be ignored due to its effect on the transverse stability of the ship (Basic et al., 2017).

In conclusion, the reviewed literature underscores the necessity for comprehensive structural analysis and innovative design approaches to address the unique challenges posed by TSHDs. Ensuring structural integrity and optimizing performance require a deep understanding of the factors influencing stress, strain, and overall deformation, as evidenced by the discussed studies.

2.1.2. Studies of excitation loads on dredgers

During its operational lifespan, a vessel is subjected to various excitations, including hydrodynamic loads, excitation loads generated by main engine and propeller etc. For TSHDs, the excitations become even more intricate. In addition to the typical loads encountered by conventional ships, TSHDs face the added challenge of mass variations during operations. These sustained excitations over prolonged periods can result in structural damage to the vessel, posing risks to the well-being of onboard personnel and significantly impacting navigational safety.

The paper of Shi (2013) has introduced that there are few types of layouts of the drive line of a hopper dredger, (1) propeller and dredge pump directly driven by diesel engines separately (Figure 12 and Figure 13), (2) Diesel directly drives propeller and electrically drives dredge pump (Figure 14).

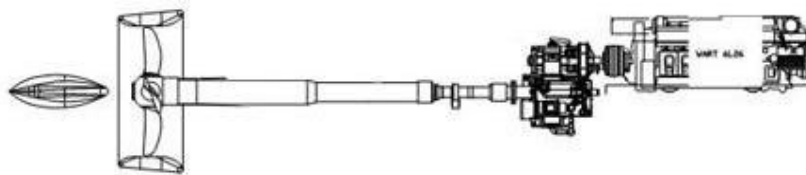


Figure 12. A diesel engine directly drives propeller (Shi, 2013).

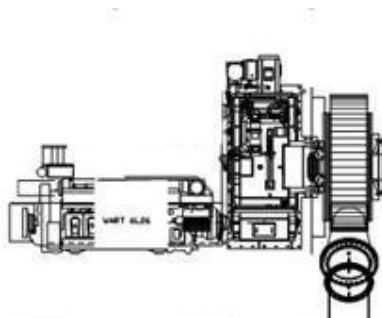


Figure 13. Diesel engine directly drives dredge pump (Shi, 2013).

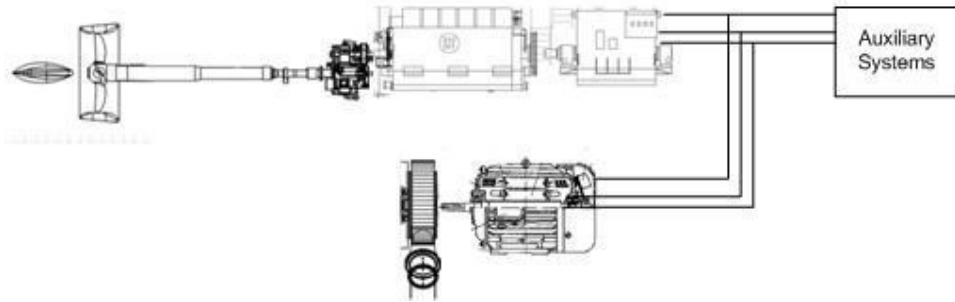


Figure 14. Diesel directly drives propeller and electrically drives dredge pump (Shi, 2013).

Another paper from Petit and Locuffier (2009) has presented the newest layout of driving line of TSHDs currently (Figure 15).

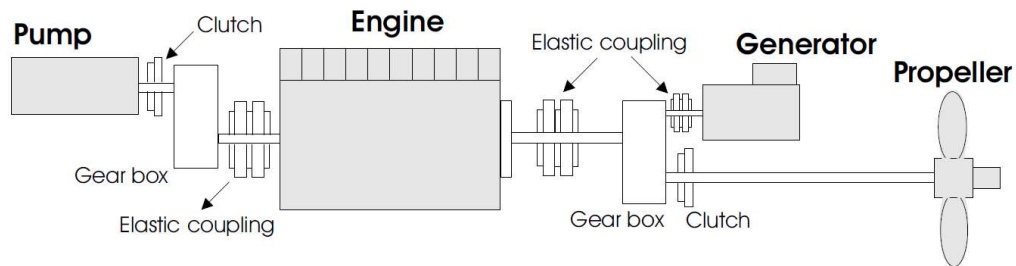


Figure 15. Outline of the latest drive line in a hopper dredger (Petit & Locuffier, 2009).

This paper studies torsional vibrations on a hopper dredger due to transient conditions by a reduced model of the mass-elastic system (Figure 16). The different transient loads are described in detail for the specific case of a TSHD. Transient loads involve among others starting/stopping the engine, engaging/disengaging clutches, altering the vessel's speed and changing the pitch of the propeller. The various factors contributing to this transient load and their influence are elucidated without the need for a complex simulation model.

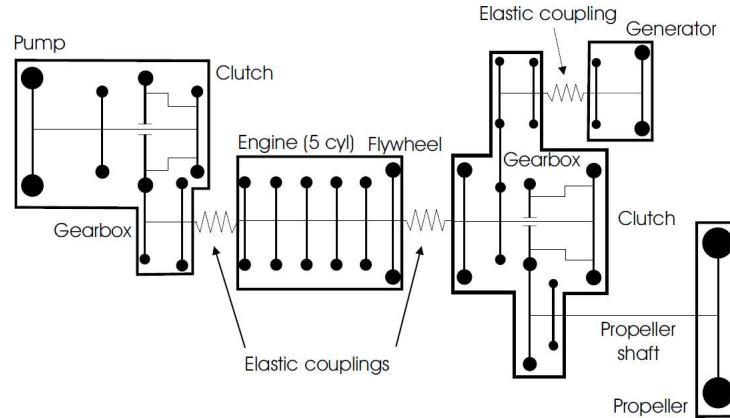


Figure 16. Reduced model of the mass-elastic system (Petit & Loccufier, 2009).

While the study provides valuable insights into the torsional vibrations of TSHDs under transient conditions, it would benefit from a more comprehensive approach that includes complex simulation models to capture the intricate dynamics accurately. Simplified models, although useful for initial analysis, might overlook critical interactions and nonlinear effects that could significantly impact the vessel's performance and safety. Moreover, the paper does not sufficiently address the long-term effects of these transient loads on the structural integrity and fatigue life of the vessel. A detailed fatigue analysis would be necessary to understand the cumulative damage and its implications for maintenance and operational planning.

TSHDs are generally equipped with diesel engines as single power source. The integration of hybrid propulsion systems in TSHDs represents a significant advancement towards sustainable and efficient marine operations. Zhan et al. (2015) explored optimal retrofitting of a hybrid propulsion system using NSGA-ii algorithm for trailing suction hopper dredger. The nondominated sorting genetic algorithm II (NSGA-II) is adopted to optimize the hybrid propulsion system design, showing promising potential for improving efficiency and reducing emissions. This study highlights the importance of adopting advanced optimization algorithms to enhance the performance and environmental footprint of marine vessels. However, while the use of NSGA-II provides a robust framework for optimization, it is crucial to validate the theoretical models with real-world data to ensure the practical applicability of the proposed hybrid systems. In additions, the detailed research of dredge pumps has studied by the paper of Musriyadi and Naifah (2020), which describes about drawing process and computerized simulation at Ansys Software for pump performance with

three different fluid types and five variations of impeller rotation. This study is instrumental in understanding the performance dynamics of dredge pumps under various operational conditions, which is critical for the efficient design and operation of TSHDs. The use of Ansys for simulation offers a precise and comprehensive analysis of pump performance, yet it is essential to conduct experimental validation to corroborate the simulation results. Nonetheless, the reliance on simulation data alone might not capture all real-world variables, such as wear and tear, maintenance challenges, and unexpected operational stresses. Therefore, combining simulation with empirical testing would offer a more comprehensive evaluation of the pump's performance and reliability.

On the other hand, Sheehan et al. (2010) present the annual profits or losses for each scenario for a range of topsoil production quantities and integrated into the current dredging regime at the Port of Waterford. The real-time prediction of drag-head motion induced by trailing suction hopper dredger motion is important to enable high operating efficiency and crucial to proper design of wave compensation device of drag-head. The real-time prediction of drag-head motion induced by trailing suction hopper dredger motion is important to enable high operating efficiency and crucial to proper design of wave compensation device of drag-head. Zhanglan et al. (2014) study the numerical prediction of drag-head motion of trailing suction hopper dredger in time domain. A numerical method to predict the drag-head motion excited by the dynamic response of trailing suction hopper dredger to disturbance is introduced.

With the continuous development of the dredging business to overseas markets, dredging ships are faced with a more and more complex hydrodynamic environment. Focused on the TSHDs, Zhu et al. (2023b) study the motion response characteristics of the TSHD under the influence of swell. Other influential works in this part include paper of Bisschop et al. (2010), Wit et al. (2014) and Li et al. (2021).

In recent years, although some progress has been made in the optimization design of the structural dynamic response of TSHDs, there are still many issues that need to be addressed. These include:

- (1) Current research on TSHDs often focuses on individual consideration of the hull or specific structural components. There is a limited amount of coupled research on various loads. In practical situations, the coupling of complex loads cannot be ignored.

(2) Regarding the optimization design of the overall ship structure, most optimizations are targeted at small-scale models. Finite element models are not large, or simplified models such as hull girder hybrid models or local models are used. Beam or local detailed models are not comprehensive for the analysis of the entire ship structure. Traditional optimization methods are also challenging to apply to large and complex whole ship structures (finite element models with at least tens of thousands of nodes). Therefore, for the optimization design of large and complex whole ship structures, appropriate sensitivity analysis methods and optimization algorithms need to be selected. A rational optimization model needs to be established, and new optimization methods should be applied for solutions.

(3) The excitation loads of TSHDs are highly complex. In addition to the conventional excitations present in typical vessels, such as propeller, hydrodynamic loads, and engine loads, working conditions also involve rapidly changing mass situations. The issues and analysis situations involved in dynamic response are extremely complex.

(4) The dynamic optimization design of the whole ship structure is limited to the optimization design of vibration characteristics. The constraint conditions generally only consider strength and low-order natural frequency constraints. There is limited research on the dynamic response optimization design of the entire ship structure. The model for the dynamic response optimization of the whole ship structure of self-propelled hopper dredgers will become more complex. The optimization solution will also become more challenging, considering constraints such as stress, displacement, natural frequencies, dynamic response, etc. Compared to the optimization design of dynamic characteristics, it is much more intricate. However, dynamic response is a crucial mechanical performance indicator that plays a vital role in the safe operation of the entire ship structure. Therefore, it is imperative to conduct dynamic response optimization design for the whole ship structure.

2.2. Literature reviews on dynamic analysis of marine structures

The research focused structural dynamics in the marine and offshore field primarily encompasses structural vibration analysis, excitation load calculations, dynamic responses etc. Structural vibration analysis being the most fundamental and crucial issue in dynamic research. In general, three methods are commonly employed to compute the vibration analysis of the variable cross-section hull girder: (i). Empirical

formula estimation method; (ii). Finite element method; and (iii). Transfer matrix method.

The empirical formula estimation method primarily proposes approximate estimation formulas to assess the lower-order frequencies of hull girder vibrations (Weng, 1978; D. Y. Zhao, 1979), thus mitigating the risk of encountering low-order resonance (Kumai, 1967; Yin et al., 2014). The use of empirical formulas for estimating lower-order frequencies is a well-established practice in naval architecture. These formulas, derived from extensive empirical data, offer a straightforward method for evaluating vibrational characteristics without the need for complex computations. However, one of the primary limitations of this approach is its reliance on historical data, which may not always accurately reflect the nuances of modern ship designs and materials. As a result, while empirical formulas provide valuable initial insights, they should be supplemented with more detailed numerical analyses as the design progresses.

The finite element method involves the discretization of the hull structure into discrete elements, with each element regarded as a continuous structure. By establishing stiffness and mass matrix for each of these elements, they are subsequently aggregated to construct the comprehensive stiffness matrix and overall mass matrix for the entire structure (Hakala, 1986; Yucel & Arpaci, 2010). This systematic approach facilitates the derivation of a multi-degree-of-freedom vibration equation for the hull girder, whose solution provides the natural frequency and corresponding vibration mode (Avi et al., 2021; Muis Alie et al., 2016). While the finite element method offers unparalleled precision and flexibility, it is not without its challenges. One of the primary drawbacks is the computational intensity required for detailed FEM analyses. High-fidelity models can be resource-intensive, necessitating significant computational power and time. This can be a limiting factor, especially in the preliminary stages of design when quick assessments are needed. Additionally, the accuracy of FEM analyses depends heavily on the quality of the input data and the expertise of the analyst. Inaccurate material properties, boundary conditions, or simplifications in the model can lead to erroneous results. Therefore, it is essential to combine FEM with empirical data and validation experiments to ensure the reliability of the outcomes.

The transfer matrix method (TMM) is a powerful tool in structural vibration analysis, particularly beneficial for complex structures such as ship hulls. This method's primary

advantage lies in its ability to break down a complicated system into smaller, manageable segments, making the analysis more tractable (Attar, 2012; Cui et al., 2012). By using matrices to relate the motion and forces at one end of the structure to those at the other, TMM provides a systematic approach to understanding how vibrations propagate through the structure (Han et al., 2012).

One significant benefit of TMM is its efficiency in handling large and complex systems. Unlike finite element methods that can become computationally intensive, TMM allows for a more straightforward representation and solution of the system's dynamic equations (Boiangiu et al., 2016). This efficiency is particularly useful in the preliminary stages of design, where quick assessments of vibrational characteristics are essential.

Feyzollahzadeh and Bamdad (2020) and J. W. Lee and Lee (2016) highlight that TMM is highly effective in modelling the dynamic behaviour of multi-span structures, which are common in marine vessels. This method can accurately predict the natural frequencies and mode shapes of the structure, which are critical for ensuring the vessel's structural integrity and operational safety.

While the transfer matrix method offers several advantages, it is not without its limitations. One of the primary challenges is that TMM can sometimes oversimplify the representation of complex structures, potentially overlooking critical local effects and interactions. For instance, in a ship hull, localized structural details and discontinuities might not be adequately captured, leading to less accurate predictions of stress concentrations and failure modes. Moreover, TMM requires a precise definition of boundary conditions and connections between elements. Any inaccuracies in these definitions can propagate through the analysis, resulting in erroneous predictions. Therefore, engineers must exercise caution and validate the TMM results against experimental data or more detailed simulations when possible. Another limitation is that while TMM is efficient for linear systems, its application to non-linear dynamic problems is less straightforward. Many real-world structural problems involve non-linearities, such as material behaviour and large deformations, which TMM might not handle effectively without significant modifications.

Despite these limitations, the transfer matrix method remains a valuable tool in the engineer's toolkit. Its ability to provide quick and reasonably accurate insights into the

dynamic behaviour of complex structures makes it particularly useful in the early design stages. However, it should ideally be used in conjunction with other methods, such as finite element analysis and experimental validation, to ensure comprehensive and reliable structural assessments.

In short, the transfer matrix method enables the vibration analysis of multi-degree-of-freedom systems, including multiple interconnected substructures. In contrast to traditional empirical approaches, it offers more precise modal data and frequency responses, making it suitable for analysing complex structures. However, it differs from the finite element method in that it does not require overly complex numerical models, extensive computational resources, or specialized finite element modelling expertise. This makes it a valuable tool for initial design and quick estimations, delivering accurate vibration analysis results without the need for intricate computational procedures.

On the other hand, the investigation of hull vibration has assumed growing significance, primarily attributed to the continuous trend of marine structures undergoing elongation and expansion (Thekinen & Datta, 2019). For modelling the ship's structures, the concept of hull-girder can be adopted (Lewis, 1988). In the domain of one-dimensional beam modelling research, pioneering efforts were initiated by Schlick (1884), who treated the ship's hull as a Bernoulli-Euler beam with free-free boundary condition, thereby determining the ship's first-order natural frequency in the vertical direction. Besides, as the ship transversal dimensions are not negligible when compared to the longitudinal ones, the hull-girder may be classified as a short beam (Weaver Jr et al., 1991). Due to the large dimensions of the ship (length, breadth, etc.), the stresses suffered by the structure may propagate by the scantlings, which demands the use of thin-walled shear flow theory when the 1D model is to be used. The research of Ohtaka et al. (1964) employed a one-dimensional beam model to compute the natural frequencies of the ship's vertical vibrations. Jensen (1983) provided a comprehensive consolidation of beam models for ship vibration analysis. When calculating the higher-order vibration natural frequencies of the ship's hull using a one-dimensional beam model, it is necessary to make corrections. Currently, two main methods, the reduction coefficient method and the shear lag coefficient method, are employed for this purpose. The reduction coefficient method involves multiplying the sectional moment of inertia by the corresponding reduction coefficient when calculating the higher-order vibration

natural frequencies of the ship's hull beam. Cowper (1966) provided a correction to the Timoshenko beam theory, deriving a formula for calculating shear coefficients and presenting specific expressions for common beam section shear coefficients.

Furthermore, Ozsoysal (2004) summarized the research achievements in the field of ship vibration from 2000 to 2003. Previous investigations on the vibration characteristics of the variable cross-section beam have been limited and frequently focused on specific cross-sectional variations. Gupta (1985) utilized the finite element method to calculate natural frequencies of the variable cross-section beam. Naguleswaran (1994) presented an approximate formula for calculating the natural frequencies of rectangular cross-section beams when the side lengths are a quadratic function of the axial length. Laura et al. (1996) proposed an approximation for the natural frequencies of rectangular cross-section beams based on the Euler-Bernoulli beam model, but this method required a constant beam width and bilinear variation of thickness along the axial direction. Other studies (Q. Mao, 2011; Q. Mao & Pietrzko, 2010) employed the Adomian decomposition method (ADM) to investigate the lateral vibration of step beams. However, there has been limited research on rapidly computing the vibration characteristics of the arbitrary variable cross-section beam. It is evident that early research on the vibration characteristics of variable cross-section beam was often restricted to specific cases, with finite element analysis being the primary method. In addition, finite element method has some limitations including complicated modelling works and time-consuming computations.

2.3. Literature reviews of hydrodynamic analysis in marine vessels

Though the ship behaves as an elastic body in a seaway and ship structural dynamics have been treated as separate subjects over the years. The rapid increase in the size of ships constructed during the 1960s has led to the realization that the wave induced ship hull vibration can give rise to significant stresses in the hull. This section concludes that general hydrodynamic calculation methods and applications in specific marine vessels.

2.3.1. Classical hydrodynamic analysis methods in marine field

The rapid increase in the size of ships constructed during the 1960s has led to the realization that the wave induced ship hull vibration can give rise to significant stresses in the hull (Jung et al., 2003). In recent times, there has been a considerable amount of

research on the hydrodynamics of ship structures. For example, the study of Troesch (1984) conducted a comprehensive study on wave-induced hull vibrations, both through theoretical analysis and experimental investigations. However, the springing mode shape was notably simplified, adopting a piece-wise rigid-body mode. The outcomes of this research included the derivation of normalized springing response spectra for various Froude numbers, specifically focusing on the Great Lakes bulk carrier model.

Jung et al. (2003) outlines the construction of an analytical model designed for assessing the hull girder response of ships under the influence of waves, with a specific focus on incorporating torsional effects. The analysis re-evaluates springing effects on the hull girder, taking into account non-linear wave excitations and torsional vibrations. The stress distribution on the hull girder is computed using the Timoshenko beam model, and the solution is derived through the application of the superposition method.

Jensen (1996) conducted an extensive investigation into the statistical properties of wave-induced bending moments and shear forces in non-prismatic Timoshenko hull vibrations within stochastic seaways, covering both short-term and long-term analyses. This study employed quadratic strip theory for analysis.

Newman (1993, 1994) explored the bending behaviours of diverse structures such as slender barges, vertical columns, hinged barges, and wave effects in a channel. The study involved establishing a 2D boundary value problem in radiation-diffraction, considering both rigid-body and flexural radiation potentials. Despite the comprehensive nature of the investigation, the structures maintained a uniform configuration.

Wu and Moan (2005) conducted an analytical and experimental investigation into similar phenomena, incorporating dynamic effects such as slamming. The study aimed to comprehensively understand the intricate interactions involved.

Kim et al. (2009) conducted a numerical exploration of springing coupled with rigid body modes, employing a fully coupled CFD-FEM analysis and the higher-order Rankine-panel method. Notably, this computationally intensive analysis was confined to the time domain.

Zhu et al. (2011) took an experimental route to analyse bending and torsional hull vibrations using a backbone model. However, this approach, while insightful, is both

resource-intensive and time-consuming, bypassing certain mathematical rigor in the process.

On the other hand, in the field of hydrodynamics, there has been extensive research on both linear and nonlinear aspects. For instance, two papers authored by Singh and Sen (2007b, 2007a) provide comprehensive summaries of several representative linear and nonlinear hydrodynamic analysis methods employed for predicting the motion of floating structures. Sen (2002) utilized a Force-Kelvin (F-K) nonlinear time-domain computational model to predict both the linear and nonlinear motion responses of the Wigley ship at various speeds. The study also investigated the nonlinear motion response characteristics of sway and yaw under different speeds and wave steepness conditions. Qiu et al. (2001) and Fonseca and Soares (2002) applied this theory to predict nonlinear wave pressure and load responses.

In recent years, there has been a growing trend in using the boundary element method to calculate hydrodynamic loads on marine structures. The paper of Lin and Yue (1991), based on the theory of free surface nonlinearity, established boundary integral equations satisfied by the distribution of source density on an instantaneous free surface using the three-dimensional time domain Green's function method. They conducted numerical predictions for the large-amplitude motions of surface-piercing bodies such as spheres and the Wigley ship. The research of Yang and Ertekin (1992) studied nonlinear wave diffraction problems using the constant panel method. Lee et al. (1995) and Ning and Teng (2007) applied high-order boundary element methods to simulate fully nonlinear numerical wave propagation problems. The fully nonlinear time domain theory takes into account various nonlinear factors and is closer to real-world conditions. However, this theory requires tracking the instantaneous free surface at each moment, determining the intersection between the instantaneous free surface and the instantaneous body surface, and remeshing the grid and solving linear algebraic equations, which significantly increases computational and storage requirements.

Linear theories addressing the computation of springing excitation and motion coefficients are typically characterized by strip or slender-body approximations. Strip theories often employ a combination of rational and intuitive approaches, with notable examples found in the works of Belgova (1962), Goodman (1971), Van Gunsteren (1974), and Hoffman and van Hoof (1976). Slender-body theory, on the other hand,

leverages matched asymptotic expansions, as exemplified by the works of Bishop et al. (1977), Maeda (1980), Beck and Troesch (1980), and Skjoldal and Faltinsen (1980). Chen and Chiou (1981) offer a systematic comparison of several prevalent strip and slender-body theories. The nonlinear aspect of the problem is further compounded by the intricate conditions imposed by the complex free surface and hull boundaries. Investigations into the nonlinear effects of ship springing in the presence of long waves have been undertaken by researchers such as Jensen and Pedersen (1981) and various Japanese scholars.

In fact, the periodic deflection of the main hulls of large tankers could be visually observed. With increase in size or speed of the ship and increase in flexibility due to geometrical considerations (open containership, shallow-draft ship), or with the application of high strength steel in ship construction, a phenomenon of hull flexural vibration, known as springing, may be observed. An example of full-scale springing stresses in Great Lakes bulk carriers was shown by Stiansen et al (1977).

Moreover, all theoretical ship hydrostatic particulars are pre-calculated in advance for all possible loading conditions, containing three degrees of freedom for a quasi-static ship condition of the draught, the angle of trim and the heel angle (Basic et al., 2017).

2.3.2. Hydrostatic and hydrodynamic analysis of special marine vessels

According to the study of Jiang et al. (2011), in the case of cutter-suction, whose slotting is at the bow and stern, the amplitude of longitudinal motion is larger than that of transverse motion. It was proved by comparing calculative RAO results between a cutter-suction dredger and a similar ship without the slotting at its bow and stern. It means that the green water is more likely to get on the deck and the propeller out of water, which will significantly reduce the safety and reliability of some equipment and structural components. Meanwhile, Kim et al. (2011) have summarized that, for large vessels, green water loading in sagging conditions has a more serious negative influence on the wave induced vertical bending moments than hogging conditions on bow deck. However, in author's study, the objective dredger's influence on its motion response should be considered differently, as its slotting is at the middle-bottom part, and the green water loading will happen on the stern deck in most situations, where the dredger is overloaded sailing at rough sea state. Thus, it is necessary to re-analyse these conclusions by using similar methodology in WASIM for this kind of dredgers.

In addition, the hydrodynamic effects on dredgers in restricted or shallow waterways should be considered carefully because of their unique working conditions. Recent research proposed that calculating hydrodynamic interaction in restricted waterways with a numerical method could be used to improve safety factor of vessels' operation (C.-K. Lee, 2012). Furthermore, Li, et al (2003) argued that the prediction for the motion performance of large FPSOs in shallow water should use the linear three-dimension potential theory and time domain simulations. Thus, these two papers could provide numerical methods to get results, which can be compared to simulate results in SESAM for the performance analysis of dredgers in restricted and shallow waterways.

In recent years, an innovative dredging approach has been proposed and practiced, which is the side-by-side configuration of the dredging ship and the mud barge during the dredger's side cast dredging operation. Zhao, et al (2018) pointed out that the hydrodynamic interactions would have a significant impact on the ships' motion when they get close to each other. Meanwhile, they also found that those interactions are sensitive to wave directions for shielding effects. Similarly, another paper of Zhao, et al. (2018) also focused on hydrodynamic interactions of side-by-side floating bodies. They asserted that roll motions, sloshing and free surface motions are sensitive to excitation frequencies and damping levels for FLNG-side-by-side offloading. Moreover, in light of Zhao, et al. (2012), the low-frequent motion responses of two vessels could be affected by the hydrodynamic interactions, which can also affect the loads among connection systems. These studies show that the hydrodynamic interaction of the side-by-side configuration between two floating bodies is worth exploring, especially for dredgers' offloading. It is notable that the dredger is moving at a low speed (< 3 knots) during sidecast dredging operation, which is different from FLNG or FPSO that is moored. In addition, Zhao, et al. (2013) and Zhao, et al. (2014) proposed a hydrodynamic analysis of FLNG systems in offloading operation where the carrier connects to the stern of the FLNG, and a prediction of hydrodynamic performance of an FLNG system in offloading operation, respectively. Therefore, due to the complexity and difference of offloading conditions between dredgers and FLNGs or FPSOs, the hydrodynamic interactions on this up-to-date productive technology need to be analysed, so as to improve productivity greatly.



Figure 17. Side-by-side configuration of the dredging ship and the mud barge (Song Chang, 2017).

2.4. Literature reviews of time-varying structures

With the increasing size of dredgers, their structural stiffness decreases, and flexibility increases, making the coupling effect of flexibility and rigidity more pronounced. This issue cannot be avoided during the design and development phase. Additionally, dredgers experience rapid changes in mass during unloading condition, and as a consequence of the declining structural stiffness, additional dynamic loads induced by time-varying mass become more significant. Given this section, in the development process of dredgers, establishing a flexible structural dynamic model that simultaneously considers the effects of time-varying mass and rigid-flexible coupled body is of paramount importance.

2.4.1. Time-varying structure studies

At present, there have been numerous research outcomes related to rigid body dynamics with time-varying mass. The body of research on rigid body dynamics with time-varying mass has significantly expanded over the years. The contributions by Bestaoui (2010), along with the studies by Waishek et al. (2009), Waishek et al. (2010), Pourtakdoust and Assadian (2004), and Majji et al. (2010), have laid a robust foundation in understanding and modelling the complexities associated with these systems. These studies collectively underscore the importance of considering mass variations in the dynamic analysis of rigid bodies, which is particularly relevant in applications such as aerospace engineering and marine structures.

The work of Strzałko and Grabski (1995) and Henson (2008) provides crucial insights into time-varying single-degree-of-freedom systems and beam structures. Their focus on these areas highlights the critical need for simplified models to understand the fundamental behaviours of more complex systems. These simplified models are invaluable in offering initial insights and guiding more detailed, multi-degree-of-freedom analyses. However, it is essential to note that while these models are insightful, they may not capture all the intricacies of real-world applications, which often involve multi-degree-of-freedom systems and more complex interactions.

Furthermore, the application of boundary element methods (BEM) in the modelling and simulation of time-varying mass systems, as demonstrated by Grant et al. (2009), H. Holl & Irschik (1996), and H. J. Holl et al. (1999), represents a significant methodological advancement. BEM offers an efficient computational approach, particularly beneficial for problems involving infinite or semi-infinite domains, such as those encountered in marine and aerospace engineering. However, while BEM is powerful, it also presents challenges, particularly in handling non-linearities and complex boundary conditions, which are often present in practical engineering problems.

The research on rigid body dynamics with time-varying mass has made substantial progress, offering valuable theoretical and methodological contributions. However, to advance this field further, it is crucial to focus on multi-degree-of-freedom systems, address the limitations of boundary element methods, and prioritize experimental validation. These steps will ensure that the theoretical advancements translate effectively into practical engineering solutions, enhancing the design and analysis of systems with time-varying mass properties.

Nikkhoo et al. (2007) conducted research on the dynamic behaviour and control of beam structures with moving concentrated masses. Similarly, the paper of Bilello et al. (2004) carried out experimental studies on small-sized beam models with moving concentrated masses. Two papers of Van Horssen et al. (2010; 2011) established the control equations for a linear time-varying mass single-degree-of-freedom damped system and investigated its free and forced vibrations. For free vibrations, they provided the minimum damping ratio required to maintain the system's indefiniteness. They also studied the forced vibration response and stability of the system under periodic impacts

and harmonic loadings. The study of Nhleko (2009), based on the previous work by Li (2000), conducted a more detailed subdivision of the response parameter range for systems with time-varying mass parameters. This study examined the response patterns of single-degree-of-freedom systems with time-varying mass parameters and the system's stability under rapid mass changes within different parameter ranges. Additionally, it elucidated the additional damping characteristics caused by time-varying mass and validated the summarized vibration response patterns using numerical examples. McGhee (2004) explored the approximation of deformation in flexible structures with time-varying mass using canonical modal series.

Moreover, the mass-variation influence on engineering structure has been broadly employed in aerospace field. The study of Joshi (1995) investigated the variations in mode shapes and mode frequencies of time-varying mass flexible rocket structures under axial thrust with acceleration loads. In this study, it initially established differential equations for the lateral vibration control of variable cross-section beams subjected to time-varying axial loads. Then it discretized the structure into a series of small segments, each satisfying the requirements of approximately constant axial loads and cross-sectional parameters. This led to the derivation of control differential equations for each small segment. Finally, they solved the simultaneous equation system formed by the mode functions of each small segment and boundary conditions. This paper also presented numerical simulation examples for a variable cross-section rocket structure under constant thrust conditions.

However, the article by Meirovitch (1970) first established the dynamic equations of the rocket structure with time-varying mass for the flow of internal objects. These include six ordinary differential equations that express the motion of a rigid body and three ordinary differential equations that express the elastic deformation. These equations are nonlinear and with time-varying coefficients. The article also introduces the analysis of dynamic characteristics of structures with time-varying mass. This played a great guiding role in the first phase of the project.

Moreover, the study of Banerjee (2000) established a rocket structural system of solid propellant with time-varying mass. This model considers that the mass of some structures gradually decreases during the flight of the rocket. And the Kane's equation developed by the research of Kane (1961) and Kane et al. (1983) is used to establish

the dynamic equation of the model in this study. This article also proposes to continuously update the modal information for the solution of the dynamic equations by continuously solving the characteristic equations or calculating the modal shape only at some discrete time freezing points. This suggestion provided effective help for the research of this project. The study of Banerjee (2000) also rewritten the dynamic equations into matrix form. In other words, in this project, the following research work which is the secondary development of ANSYS modal analysis will be largely similar to it.

Furthermore, Huang and Zeiler (2006) employed the Lagrange's equation to formulate dynamic equations for time-varying mass flexible rocket structures. Tobbe et al (2009) conducted dynamic modelling and numerical simulations of flexible structures with time-varying mass parameters using the ARTEMIS software relied upon by the Ares I rocket structure. In their research, they initially derived dynamic equations for time-varying mass flexible structures based on the Boltzmann-Hamel equation (P. A. Tobbe, 1995). Nevertheless, they did not consider the influence of mode shape rates of change with respect to time, which resulted from mass variations, and instead accounted for the effects of time-varying mass by continuously updating the mass matrix and mode shape matrix during the dynamic equation solving process. The study also treated various sections of the rocket structure as substructures, combined with multi-threaded parallel computing techniques to enhance real-time simulation computational efficiency. Finally, numerical simulations were conducted for a time-varying mass flexible beam structure, and the results were compared with calculations from NASTRAN and TREETOPS software.

In summary, the extensive research on time-varying mass structures has provided significant theoretical and methodological advancements. Foundational studies have underscored the importance of accounting for mass variations in dynamic models, leading to more accurate predictions and robust designs. These steps will enhance the design and analysis of systems with time-varying mass properties, translating theoretical progress into real-world marine engineering solutions.

2.4.2. Numerical algorithms of dynamic analysis of linear mass-varying structures

Up to now, several studies have developed a variety of numerical algorithms for the calculation of the dynamic response of linear time-varying structures. The research of

Holl et al. (1998) developed a semi-analytical dynamic response calculation method for transient response analysis of linear time-varying systems with non-classical damping based on the modal method. In this method, the transient response is decomposed into two parts: the transient response corresponding to the external load and the transient response corresponding to the load caused by time-varying parameters. Consequently, the equations of motion in this system are correspondingly decomposed into two sets of equations. This algorithm may be used as a guide or directly applied in the future research of this project, because this method can largely conform to many practical situations of TSHDs, such as the external load considered by this method and the load caused by time-varying parameters.

Moreover, a transient response analysis method for linear multi-degree-of-freedom systems with time-varying damping and stiffness systems has been proposed by the study of Kucharski (2000). This method uses the state variable method to establish the system dynamics equations, which decomposes the system state transition matrix into time-invariant parts and time-varying parts. Furthermore, it gives an efficient estimation method for the state transition matrix. At this stage of the project, the multi-degree-of-freedom system with time-varying mass parameters needs to be studied, which is very similar to the study. In addition, only the hopper section of the TSHD vessel in this project has the time-varying mass characteristic, and the rest remains the time-invariant characteristic. In other words, the research method has a strong reference significance for this project. Fortunately, the article of Bartels (2003) developed a method for calculating the dynamic response of structural dynamic equations based on the state transition matrix on the basis of Kucharski's study (2000). This method can be used to analyse the transient response of any linear time-varying parameters system and nonlinear systems. It means this provides a great reference value for the transient response analysis of the nonlinear system of this project in the future.

In addition, the precision direct integration method that is widely used in the transient response analysis of linear time-invariant structures has also been extended to the transient response analysis of linear time-varying structures by many researchers. The study of Liu et al. (2014) has proposed an improved precision direct integration method for solving the dynamic response of linear time-varying systems with time-varying polynomial function coefficient matrix by introducing new variables and extending latitude. Moreover, an improved precise integration method for transient response

analysis of linear time-varying structures has been proposed by the research of Yue et al. (2016) based on Magnus expansion method and precision direct integration method. Compared with the Newmark algorithm in linear time-varying structure, this improved method based on Magnus has higher calculation accuracy. Furthermore, some other literatures have also done a similar study of the precision direct integration method in time-varying structural dynamic systems. This is supported by the article of Zhou and Jiang (2005), two papers of PENG and WU (2009; 2009), Tan and Zhong (2006), Fu et al. (2012).

Besides, time-domain finite-element algorithm, which is widely used in the transient response analysis of linear time-invariant structures, has also been extended to the transient response analysis of linear time-varying structures by many researchers. The papers of Penny and Howard (1980) and Yu et al. (1997) have developed a time-finite element algorithm for the transient response analysis of linear single-degree-of-freedom and multi-degree-of-freedom systems with time-varying parameters respectively based on the Hamilton principle of constant mass systems. These methods use the Hermitian difference to approximate the mass, damping and stiffness matrices at each time step. Their research results show that the method has high calculation accuracy. On the other hand, some papers have proposed a space-time finite element method for transient response analysis of linear systems with moving inertial loads (Bajer & Dyniewicz, 2008, 2009, 2012; Dyniewicz, 2012).

The above research results show that in the study of linear time-varying structural dynamic response algorithms, in addition to methods from the papers of Holl et al. (1998), Kucharski (2000) and Bartels (2003), there are also the precision direct integration method that is widely used in time-invariant structural dynamics, as well as the time-domain finite-element algorithm and space-time finite element method. However, not all methods are efficient and accurate in engineering applications. And so far, no time-varying dynamic response algorithm has been proposed in the field of ships. Therefore, developing a linear time-varying structure dynamic response algorithm applied in the field of ships will be the main challenge in this project.

While applying the linear time-dependent structural time finite element algorithms developed based on the Hamiltonian principle for constant mass systems to compute the dynamic response of time-varying mass structures, it observed that the results

obtained from these algorithms are not always accurate. It is evident from these computations that these time finite element algorithms are suitable for linear time-varying structures where mass release or absorption relative to the inertial reference frame has zero velocity. Further investigation revealed that the main reason for this phenomenon is that the Hamiltonian principle for constant mass systems is only applicable to variable mass systems with mass release or absorption having zero velocity relative to the inertial coordinate system. Numerical algorithms based on the variational principles of mechanics inherit the applicability range of the variational principles of mechanics. Additionally, the number of unknowns in the linear system of equations that needs to be solved at each time step in these linear time-varying structural time finite element algorithms is at least twice the number of system degrees of freedom. When practical engineering requirements necessitate the computation of large and complex time-varying structural dynamic responses with smaller time steps, these linear time-varying structural time finite element algorithms become computationally expensive.

In summary, the extensive research on time-varying mass structures has significantly advanced the theoretical and methodological frameworks essential for marine vessel analysis in this study. Foundational studies in rigid body dynamics with time-varying mass have laid a robust groundwork, emphasizing the necessity of incorporating mass variations to predict structural behaviour accurately. Simplified models provide valuable initial insights but must evolve to encompass multi-degree-of-freedom systems to address the complexities inherent in marine structures.

In the context of marine vessels, this research fills critical gaps by enhancing the accuracy of dynamic response predictions, especially for specialized vessels like TSHDs that experience significant mass variations. By integrating these advanced methodologies, the thesis proposes a comprehensive framework for the dynamic analysis of marine vessels, ensuring more robust design and operational strategies. This work helps bridge the gap between theoretical advancements and practical engineering solutions, contributing to safer and more efficient marine vessel operations.

2.5. Literature reviews of strength and fatigue analysis in marine vessels

This review explores the structural integrity and fatigue analysis of specific marine vessels. It encompasses studies on structural responses to diverse loading conditions,

materials in vessel construction, and methodologies for assessing fatigue life. These insights contribute to ongoing efforts in improving design, maintenance, and overall safety, crucial for dredging vessel operation across diverse marine applications accordingly.

2.5.1. Global strength analysis of specific marine vessels

With the purpose of exploring the hull girder of dredgers, firstly, a number of studies have shown that the simple beam theory cannot be addressed to analyse the hull girder response, especially for ships with large deck openings (Payer et al., 1994; Valsgard et al., 1995). Similarly, Rörup, et al. (2017) compared this approach with global FE model and suggested that it is necessary for the model with large deck openings to apply warping force on the boundary condition in order to get more accurate results. That is to say, these conclusions not only have an impact on the hull girder of containers with large deck openings but may also on dredgers with large deck openings and several bottom holes. Secondly, although Paik, et al. (2001) argued that if the magnitude of torsion is not predominant, the torsion would not be very sensitive to the load component of the ultimate vertical bending moment of container hulls. As we know, the object of this paper has large openings on the deck, which is different from dredgers with large openings both on the deck and bottom. That means the conclusions might be changed by analysis of dredgers. Moreover, in light of the paper of Chen (2016), who proposed following important conclusions of reliability assessment of FPSOs' hull girder: first of all, the hull girder reliability will be decreased as the return period of the extreme value of vertical wave-induced bending moment increases. Secondly, the hull girder of this kind of ship is sensitive to specific wave states. Finally, the environmental severity factor has a significant impact on the reliability of hull girder. These two papers summarized some important results of hull girder of a container and FPSOs respectively, which could be based on the analysis of dredgers' hull girder.

Furthermore, Sun and Bai (2003) suggested that a modified Smith method to calculate ultimate value of the longitudinal bending moment at the amidships section for hull girders' and according to Gaspar, et al. (2016), the direct calculation method provides more accurate prediction for the reliability of actual hull girders under sagging conditions, because current design formulation underestimates the effects of nonlinear.

Therefore, these conclusions could be used to analyse the hull girder of dredgers in global FEA as fundamental methods.

In light of the study of Saad-Eldeen, et al. (2016), the effects of different dent shapes for highly damaged plates were summarized to cope with various damage conditions. Moreover, he also concluded that when the plate slenderness ratio is less than 2.63, the dent shape is beneficial to the behaviour of the structure and the effect of deeper dent is missing in the ultimate strength. In other words, it means that the maintenance cycle will be extended for highly damaged plates, which will reduce costs to a great extent. Moreover, Underwood et al. (2015) claimed that all potential failure modes of the structure should be considered for the ultimate strength assessment of damage stiffened steel structures in order to accurately assess the true residual strength of the structure when it happens. It is inevitable for dredgers to collide or have accidents during running and maintaining periods. The implication is that all potential modes should be applied to structural components of dredgers, especially for specific sections, such as the panels around hopper doors and dredging pumps room. Furthermore, the bottom plates and the lower parts over side shells of the ship are mainly resulted from the uniaxial and biaxial compressive or tensile loads with hydrostatic water pressure, which has been researched for many years by Crisfield (1975) and Paik et al. (2000). Some ideas could be borrowed from their research for studying non-continuous bottom of specific vessels, like dredgers. It is important to investigate the ultimate limit state of the bottom structure for specific ships. Meanwhile, Xu, et al. (2017) proposed some useful formulas to identify the difference of constrained condition on the ultimate strength under simulated loads. And they also suggested to use different formulas to forecast the ultimate strength of stiffened plates for different positions of ship. It means that these different formulas should be used to special positions of dredgers like hopper doors.

Besides, it is necessary to analyse some panels which already have cut-outs. This is supported by Mohtaram, et al. (2012), Kumar, et al. (2007), Kumar, et al. (2009a) and another study of Kumar, et al. (2009b). He analysed ultimate limit state of rectangular plates with groove-shaped cutouts, square plate with rectangular openings, stiffened plates with a square opening and stiffened panel with circular opening, respectively. Meanwhile, Yu and Lee (2012) argued that the ultimate strength of plate with transverse opening has not been affected by opening position ratio. Nevertheless, the plate slenderness parameter plays a role on the ultimate strength of plate with longitudinal

opening when it less than 1.77. Furthermore, Yu, et al. (2015) asserted that the nonlinear finite element method could be used to analyse the ultimate strength of stiffened panel with various opening locations and fit design formulas for them on the basis of experimental data. Although it is inconvenient to collect experimental data, some FEA software could simulate the data like ANSYS. In the paper of Saad-Eldeen, et al. (2014), an expression was developed to estimate the ultimate strength of the plate with a large opening.

In summary, the comprehensive studies on the global strength analysis of marine vessels, specifically focusing on dredgers, reveal critical insights into their structural behaviour under various conditions. Traditional beam theory often falls short in accurately predicting the responses of hull girders, particularly those with significant structural discontinuities like large deck and bottom openings. The research underscores the necessity of using advanced methods, such as global finite element analysis and modified Smith methods, to achieve more precise assessments. The studies also highlight the importance of considering potential damage and ultimate strength in design, emphasizing the role of detailed FEA in evaluating non-continuous structures and cut-outs. By integrating these advanced analytical methods, this thesis addresses existing gaps in the structural analysis of marine vessels, particularly TSHDs, ensuring more robust design and operational strategies to enhance their reliability and safety.

2.5.2. Detailed fatigue analysis of specific marine vessels

For fatigue analysis, according to Ringsberg, et al. (2015), the amidships hatch corners, amidships engine room and the bilge regions are critical regions for a container ship, which is proved by using SESAM software, and they also did linear and nonlinear analysis as well as the assessment of the partial fatigue damage for those parts. It means that some critical regions could be found by using SESAM under a specific state sea for detailed fatigue analysis of models firstly, and there is no exception for dredgers with openings in the deck and bottom. Li, et al. (2012) mentioned that a traditional method should be questioned when being applied to the ship with large deck openings. As it would cause low torsion rigidity of the structure, which influences the assessment of ship structural fatigue damage. Meanwhile, he confirmed that the speed of ship has a significant impact on the fatigue damage accumulation. In a similar way, the trailing suction hopper dredger not only has a large deck opening, but also has several big holes

at the bottom structure, and it always work at various speeds in different working conditions. Cross sections at the centreline of each hopper door or adjustable overflow well are worth considering, and their fatigue damage is derived from wave induced loads for dredgers at various normal speeds. Another study of Li, et al. (2013) advised that the time-domain-based procedure, which contained more factors, is more realistic than the spectral method for analysing the fatigue of the ship side-shell structure. This recommendation is useful for this dissertation, as it is conducive to exploring the fatigue damage of suction inlets over side-shell for dredgers. Fortunately, Mao, et al. (2015) proposed an accurate method to calculate fatigue damage in detailed for hatch corners and side shell structures of ship with more complex stress. Meanwhile, Li, et al. (2011) presented a novel procedure of calculating fatigue damage of ship structure details directly, and he also argued “it is believed to give more accurate predictions in fatigue assessment”. These two calculation methods for fatigue damage of ship structure are suitable for dredging ships, whose structural features are similar to that of the models in these papers; thus, they could be adopted for analysing fatigue damage details of specific parts for dredgers, for example, hatch corners, corners of side-shell around suction inlets, the detailed corners of hopper doors, and etc.

The studies on fatigue analysis highlight the importance of identifying and assessing critical regions in marine vessels, particularly those with structural discontinuities like large deck and bottom openings. For dredgers, which operate under varying speeds and complex loading conditions, these regions include amidships hatch corners, engine room areas, and bilge regions. Research suggests that traditional methods may not adequately address the unique fatigue challenges posed by such structures, emphasizing the need for more realistic time-domain-based procedures and advanced analysis tools like SESAM. By applying these advanced methodologies, this thesis aims to fill the gaps in fatigue analysis for TSHDs, providing more accurate predictions and effective strategies for enhancing structural durability and safety in the design and operational phases.

2.6. Summary of Chapter 2

In Chapter 2, the literature review comprehensively examines various aspects related to dredgers, dynamic analysis of marine structures, and the impact of hydrodynamic and time-varying mass effects. For TSHDs, structural challenges due to large deck and

bottom openings necessitate in-depth research, yet an integrated model addressing these discontinuities under operational conditions is lacking. Existing studies on excitation loads, hydrodynamic behaviours, and dynamic analysis primarily treat these factors in isolation, missing the combined effects crucial for TSHDs. While classical hydrodynamic methods and recent advancements in time-varying structure analysis provide valuable insights, they often fall short in addressing the complex geometries and operational profiles of TSHDs. Moreover, strength and fatigue analysis methods need refinement to accurately predict the behaviour of TSHDs, highlighting a gap in applying these methods to vessels with significant structural discontinuities and variable operational profiles. This thesis aims to fill these gaps by developing a comprehensive model that integrates structural dynamics, hydrodynamic responses, and fatigue analysis for TSHDs, ensuring a holistic understanding of their behaviour under various conditions.

Chapter 3. Methodology

This chapter gives the fundamental theories and methodologies of the proposed novel mathematical and numerical model and outline of self-developed programme TVM_HullGirder for dynamic analysis of mass-varying marine vessels in time-domain.

3.1. Fundamentals of proposed mathematical and numerical model

The hull girder model employed in this study perceives the ship structure as a variable cross-section Euler-Bernoulli beam with free-free boundary condition. Based on ideally finite segment idea, it typically divides hull girder into twenty beam elements. The hull girder model consists of twenty beam elements interconnected through nodes, with mass and stiffness properties of each beam element being calculated from the geometric model of the full-scale vessel. Accurate calculations necessitate prior knowledge of the geometric characteristics of twenty-one stations along the ship's structure and the mass properties of twenty beam elements, as depicted in the diagram below (Figure 18). Theoretically speaking, increasing the number of subdivided beam elements brings the hull girder model closer to the actual ship structure, enhancing the accuracy of calculation results.

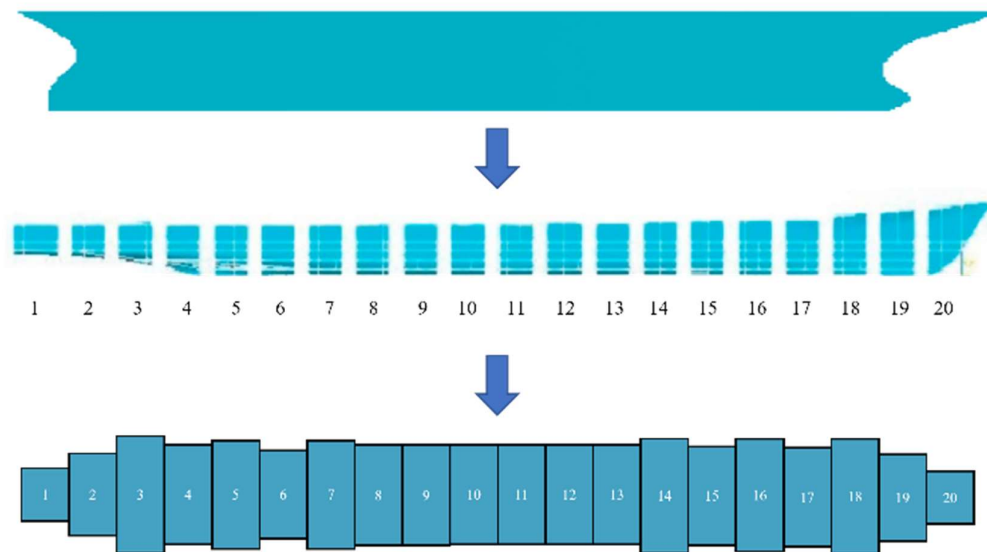


Figure 18. Classical hull girder with variable cross-sections.

The derived key theories and methodologies behind the proposed mathematical model include:

- (1) The modified Euler-Bernoulli beam theory to achieve the capability of handling variable mass function.
- (2) A semi-analytical approach based on the transfer matrix method for vibration analysis of the variable cross-section hull girder with analytical modal solutions.
- (3) The calculation method of time-varying hydrodynamic loads.
- (4) The calculation method of other excitation loads generated by key components installed on the vessel.
- (5) Improved Kane's dynamic equation to accommodate the dynamic analysis of rigid-flexible coupled offshore floating structure with time-varying mass systems.

The Figure 19 shows the outline of the proposed mathematical model in this study.

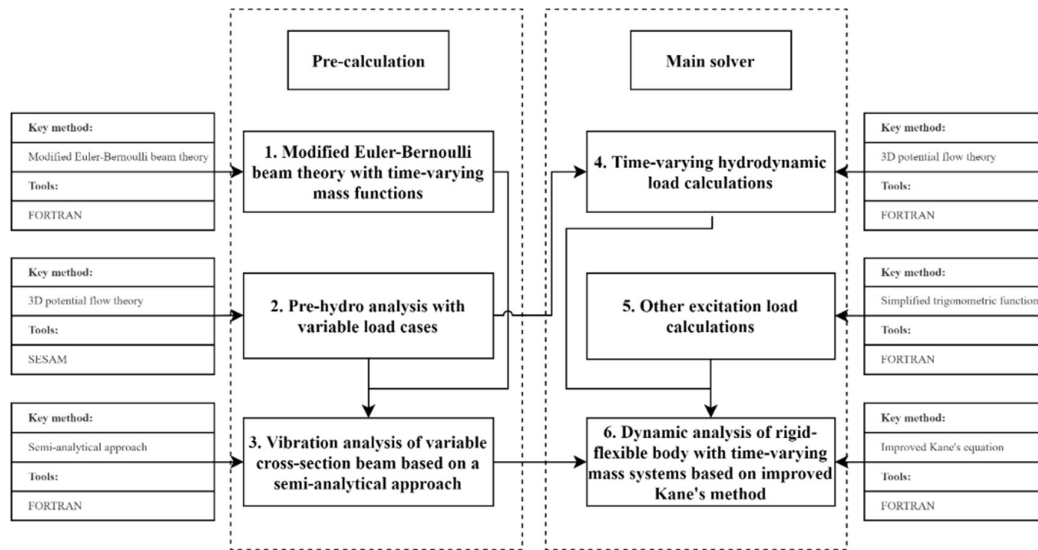


Figure 19. The outline of proposed math model.

In this outline of proposed mathematical model, it separates the model as two main sections which are pre-calculation section includes part 1, part 2, part 3 and main solver section includes part 4, part 5, part 6 respectively based on corresponding key methodologies and tool applications. The mathematical model proposed in this paper is developed to address the challenges posed by the structural dynamic analysis of offshore floating structures with variable-mass characteristics. This mathematical model is primarily based on several key theories to provide supports as below:

- (1) Beam theory of hull girder for mass-varying property

The hull girder model is based on a modified Euler-Bernoulli beam theory, allowing for the simulation of structural motion and flexible deformation, particularly in structures with variable mass characteristics.

(2) Semi-analytical vibration analysis approach

This part would introduce a semi-analytical approach based on the transfer matrix method, specifically focusing on the computation of natural frequency with numerical solutions and mode shape with analytical solutions, which tailored for the study of the vibration characteristics of variable cross-section Euler-Bernoulli beam. Moreover, this method provides a foundation for subsequent dynamic analysis.

(3) Time-varying hydrodynamic analysis

In the hydrodynamic analysis section, the three-dimensional potential flow theory will serve as the foundation. It will employ the hydrodynamics software SESAM to precompute hydrodynamic parameters for various load cases. The output files from this precomputation will be used as input files for self-developed program to calculate time-varying hydrodynamic loads for the target vessel under loading or unloading conditions.

(4) Excitation loads simulation

The program employs trigonometric functions to model and compute the excitation forces from diesel engines and propellers.

(5) Dynamic analysis of time-varying mass systems

A dynamic analysis solver for that considers time-varying mass systems based on modified Kane's dynamic equation is used in this study. The dynamical equations of the model will be reformulated into matrix form to facilitate subsequent numerical simulation computations.

The principal theories and methods of the proposed novel mathematical and numerical model consist of parts (1) – (5) and a self-developed program TVM_HullGirder in FORTRAN is implemented to perform dynamic response calculations for the hull girder subjected to complicated loads with time-varying mass systems, as shown in the Figure 20.

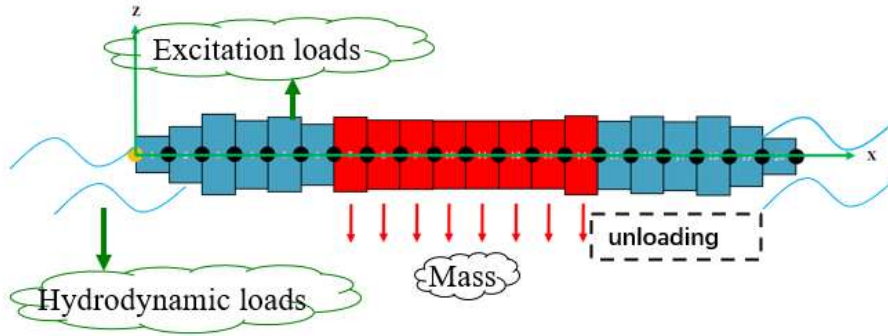


Figure 20. Hull girder model subjected to complex excitation loads with variable mass systems.

(6) Results transformation by MPC in FEM

Dynamic response results calculated by TVM_HullGirder programme can be transferred into FEM by Multiple Point Constraints (MPC) technology (Figure 21) in finite element software for further structural assessments.

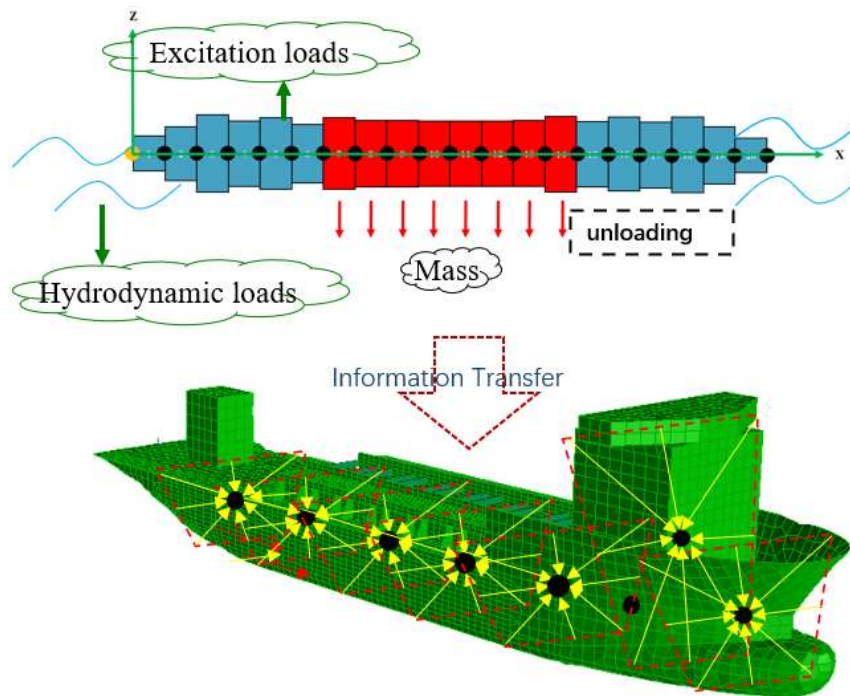


Figure 21. Results transferred from calculation programme into FEM by MPC technology.

Subsequent parts introduce and derive the relevant theories with regards to modules in program.

3.2. Modified Euler-Bernoulli beam theory with time-varying mass function

The flexural properties of a hull girder are derived from the transverse vibration of a Euler-Bernoulli beam with time-varying mass functions applied in further dynamic model without mass point at boundary conditions as shown in Figure 22, (Craig Jr & Kurdila, 2006). In this part, the basic theory of Euler-Bernoulli beam was modified for achieving time-varying mass functions to make sure that could be applied in target vessel and further dynamic analysis based on improved Kane's dynamic equation.

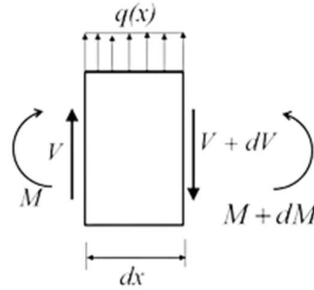


Figure 22. Force diagram of classical Euler-Bernoulli beam element.

It is assumed that no distributed load over the length of beam, the transverse vibration equation of general Euler-Bernoulli beam in the partial differential equation (PDE) form as an example (Figure 22) is shown below (Bauchau & Craig, 2009; Thekinen & Datta, 2019):

$$EI \frac{\partial^4 \phi(x,t)}{\partial x^4} + \rho A \frac{\partial^2 \phi(x,t)}{\partial t^2} = 0 \quad (1)$$

Where, the density of the beam is expressed as ρ , which is constant in general analysis. The beam stiffness, EI , is constant over the length of the beam as well as A which is the cross-section area of the beam, $\phi(x, t)$ expresses the deflect function of the beam.

Drawing inspiration from earlier research that employed the Rayleigh-Ritz method to account for added mass in beam theory (Ilanko et al., 2014; Lamb, 1920), by integrating the capabilities of the established commercial finite element software SESAM (DNV, 2017), the conventional beam theory has been adapted for marine structures to incorporate the consideration of added mass, as outlined below:

$$EI \frac{\partial^4 \phi(x,t)}{\partial x^4} + [\rho A + \rho^a A^a] \frac{\partial^2 \phi(x,t)}{\partial t^2} = 0 \quad (2)$$

Where, $\rho^a A^a$ expresses added mass of marine structures which can be pre-calculated by SESAM software.

In the analysis of a variable-mass Euler-Bernoulli beam, the density of the beam $\rho(t)$ is treated as a time function to characterize variations in mass. Due to loading or unloading working condition, the wetted surface of target vessel would be time-varying changed accordingly. As a result, added mass part is supposed to be changed in time domain as $\rho^a(t)A^a(t)$. Consequently, the transverse deflection of the Euler-Bernoulli beam with time-dependent mass properties can be mathematically expressed as:

$$EI \frac{\partial^4 \phi(x,t)}{\partial x^4} + [\rho(t)A + \rho^a(t)A^a(t)] \frac{\partial^2 \phi(x,t)}{\partial t^2} = 0 \quad (3)$$

The separation of variables is used to solve the PDE in general Euler-Bernoulli beam, the mode shape is assumed to be the product of a function of the position along the beam (mode function) and a function of time (mode coordinate) by mode superposition method. Therefore,

$$\phi(x,t) = \Phi(x)\eta(t) \quad (4)$$

Where $\Phi(x)$ is the spatial function and $\eta(t)$ is the mode coordinate function.

Based on mode superposition method, the PDE of a Euler-Bernoulli beam becomes:

$$EI \frac{d^4 \Phi(x)}{dx^4} \eta(t) = -[\rho(t)A + \rho^a(t)A^a(t)] \Phi(x) \frac{d^2 \eta(t)}{dt^2} \quad (5)$$

Collecting like terms yields:

$$\frac{EI}{\Phi(x)} \frac{d^4 \Phi(x)}{dx^4} = -\frac{[\rho(t)A + \rho^a(t)A^a(t)]}{\eta(t)} \frac{d^2 \eta(t)}{dt^2} = \omega^2 = \text{const.} \quad (6)$$

As typically done in the method of separation of variables, when it considers the spatial equation involving $\Phi(x)$ to be equal to the temporal equation involving $\eta(t)$, the middle part of above equation, they have to equate to a constant represented as the squared eigenvalue ω^2 . Consequently, the PDE is decomposed into two ordinary differential equations as shown below:

$$\begin{cases} EI \frac{d^4 \Phi(x)}{dx^4} - \omega^2 \Phi(x) = 0 \\ \frac{d^2 \eta(t)}{dt^2} + \frac{\omega^2}{[\rho(t)A + \rho^a(t)A^a(t)]} \eta(t) = 0 \end{cases} \quad (7)$$

The second equation in above has a time varying coefficient, which makes the solution difficult. That means the spatial equation $\Phi(x)$ has relationship with two time varying functions not only temporal equation $\eta(t)$ but also the presence of part of density changes $[\rho(t)A + \rho^a(t)A^a(t)]$, which violates the assumption of separation of variables in Equation (4). Thus, it has to assume that the rate at which the beam's mass changes over time is minimal compared to natural frequencies. Consequently, the Equation (6) can be rewritten as:

$$\frac{EI}{[\rho A + \rho^a A^a]} \frac{d^4 \Phi(x)}{dx^4} = -\frac{1}{\eta(t)} \frac{d^2 \eta(t)}{dt^2} = \omega^2 = const. \quad (8)$$

This leads to:

$$\begin{cases} EI \frac{d^4 \Phi(x)}{dx^4} - [\rho A + \rho^a A^a] \omega^2 \Phi(x) = 0 \\ \frac{d^2 \eta(t)}{dt^2} + \omega^2 \eta(t) = 0 \end{cases} \quad (9)$$

Hence, the analytical mode solution to the above equation base on boundary conditions of the beam can be expressed as the below form with invariant nature frequencies:

$${}_i \phi(x) = C^1 \sin {}_i \lambda x + C^2 \cos {}_i \lambda x + C^3 \sinh {}_i \lambda x + C^4 \cosh {}_i \lambda x \quad (10)$$

Where,

$${}_i \lambda_i^4 = \frac{[(\rho A + \rho^a A^a)]_i}{(EI)_i} \omega^2 \quad (11)$$

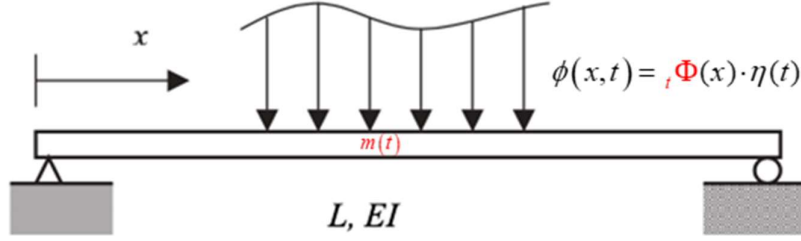


Figure 23. Time-varying mass beam with variable mode shape in time domain.

In addition, it is also possible to update nature frequency in each time step according to mass changed as well as mode shape accordingly, then the coefficient λ would be defined as below:

$${}_t\lambda_i^4 = \frac{\left[({}_t\rho A + {}_t\rho^a {}_tA^a) \right]_i}{{(EI)}_i} {}_t\omega^2 \quad (12)$$

The time-varying natural frequency has more accurate results, but time-consuming calculations as natural frequencies and mode shape need to be updated in very time step due to variable mass.

3.3. Semi-analytical of vibration analysis of variable cross-section beam

In light of the above section, an analytical solution for the vibration analysis of the Euler-Bernoulli beam with time-varying mass characteristics can be approached in time-domain analysis. However, for the investigation of the hull girder in this study, which inherently constitutes a variable cross-sectional beam, a homogeneous beam analysis is deemed insufficient. Consequently, there arises the necessity for an analytical mode shape solution tailored to variable cross-section Euler-Bernoulli beams, which not only enables the vibration analysis of the hull girder but also finds application in dynamic analysis based on improved Kane's dynamic equation method with time-varying mass systems.

Leveraging the Euler-Bernoulli beam theory, it formulates the vibration equation for the beam with variable cross-sections, where the bending stiffness and mass distribution may exhibit continuous or discontinuous variations along the beam. This method treats the variable cross-section beam as an equivalent assembly of multiple uniform beam segments. It establishes relationships for modal functions between two adjacent uniform beam segments based on the continuity conditions of displacements (including

translational and rotational) and forces (including bending moments and shear forces) at the interfaces between them. After addressing boundary conditions of the beam, it formulates non-linear eigen equation and modal functions can be computed by obtained natural frequencies from the non-linear eigen equation. The Bisection method or Newton-Raphson can be subsequently applied to solve the non-linear eigen equation for corresponding natural frequencies. The following derivation details of this approach take transverse vibration equation of variable cross-section Euler-Bernoulli beam as an example.

3.3.1. Modelling assumptions and simplification

Based on the idea of segmentation, the variable cross-section beam can be divided into a combination of several uniform beam segments connected to each other. When the number of beam segments is sufficient, each beam segment is regarded as an isometric homogeneous beam as shown in the Figure 24.

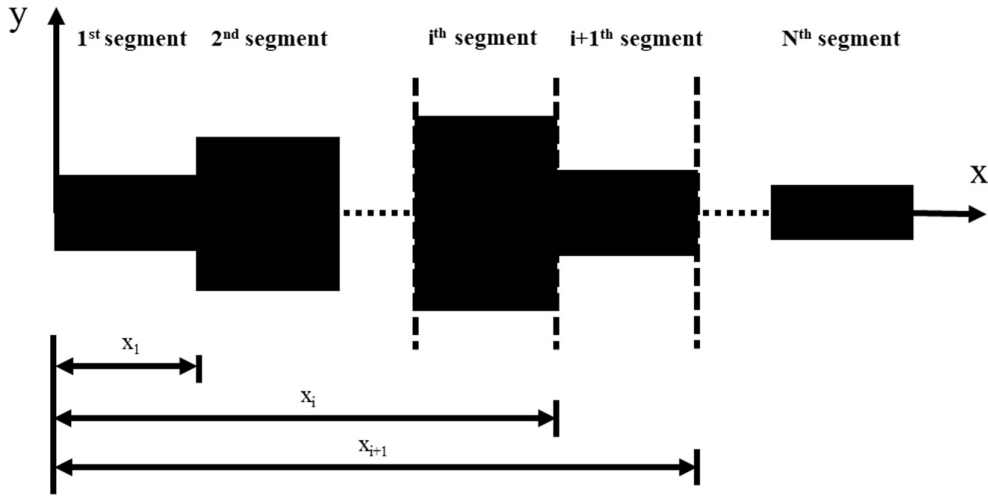


Figure 24. N segments of variable cross-section beam.

The equivalent bending stiffness and cross-sectional density of the i^{th} beam segment can be expressed as:

$$(EI)_i = \frac{1}{l_i} \int_{x_{i+1}}^{x_i} EI(x) dx \quad (13)$$

$$(\rho A)_i = \frac{1}{l_i} \int_{x_{i+1}}^{x_i} \rho A(x) dx \quad (14)$$

Where, $EI(x)$ stands for the bending stiffness at x position of the beam, $\rho A(x)$ expresses the cross-sectional density at x position of the beam, l_i expresses the length of the i^{th} beam segment ($i = 1, 2, \dots, N$).

Based on the Equation (10) in above section, the mode shape function of the i^{th} beam segment can be expressed as:

$$\begin{aligned}\phi_i(x) = & C_i^1 \sin \lambda_i(x - x_{i-1}) + C_i^2 \cos \lambda_i(x - x_{i-1}) \\ & + C_i^3 \sinh \lambda_i(x - x_{i-1}) + C_i^4 \cosh \lambda_i(x - x_{i-1})\end{aligned}\quad (15)$$

Where, $x_0 = 0$, $C_i^1, C_i^2, C_i^3, C_i^4$ are modal coefficients of the i^{th} beam segment.

Similarly, the mode shape function of the $i + 1^{th}$ beam segment can be expressed as:

$$\begin{aligned}\phi_{i+1}(x) = & C_{i+1}^1 \sin \lambda_{i+1}(x - x_i) + C_{i+1}^2 \cos \lambda_{i+1}(x - x_i) \\ & + C_{i+1}^3 \sinh \lambda_{i+1}(x - x_i) + C_{i+1}^4 \cosh \lambda_{i+1}(x - x_i)\end{aligned}\quad (16)$$

It is noted that natural frequencies here in λ stand for the whole beam rather than that of i^{th} beam segment.

According to above 3.2 section, the coefficients $C_i^1, C_i^2, C_i^3, C_i^4$ from Equation (10) are determined by boundary conditions of the beam.

3.3.2. Relationship of continuity and transfer matrix for lateral beam equation

From the continuity of displacement, rotation, bending moment and shear force between the i^{th} beam and the $i + 1^{th}$ beam at the connection point x_i , the following relationships can be obtained:

(1) Displacement:

$${}_i\phi_{i+1}(x_i) = {}_i\phi_i(x_i) \quad (17)$$

Hence, based on Equation (17), the following derivations can be derived:

$$\begin{aligned}{}_i\phi_{i+1}(x_i) = & A_{i+1} \sin {}_i\beta_{i+1}(x_i - x_i) + B_{i+1} \cos {}_i\beta_{i+1}(x_i - x_i) \\ & + C_{i+1} \sinh {}_i\beta_{i+1}(x_i - x_i) + D_{i+1} \cosh {}_i\beta_{i+1}(x_i - x_i) \\ = & 0 + B_{i+1} + 0 + D_{i+1} \\ = & B_{i+1} + D_{i+1}\end{aligned}\quad (18)$$

$$\begin{aligned}
{}_t\phi_i(x_i) &= A_i \sin {}_t\beta_i(x_i - x_{i-1}) + B_i \cos {}_t\beta_i(x_i - x_{i-1}) \\
&\quad + C_i \sinh {}_t\beta_i(x_i - x_{i-1}) + D_i \cosh {}_t\beta_i(x_i - x_{i-1}) \\
&= A_i \sin {}_t\beta_i l_i + B_i \cos {}_t\beta_i l_i + C_i \sinh {}_t\beta_i l_i + D_i \cosh {}_t\beta_i l_i
\end{aligned} \tag{19}$$

Consequently, from relationship of displacement, the following relationship of coefficients can be found:

$$B_{i+1} + D_{i+1} = A_i \sin {}_t\beta_i l_i + B_i \cos {}_t\beta_i l_i + C_i \sinh {}_t\beta_i l_i + D_i \cosh {}_t\beta_i l_i \tag{20}$$

(2) Rotation:

$${}_t\phi'_{i+1}(x_i) = {}_t\phi'_i(x_i) \tag{21}$$

Hence, based on Equation (21), the following derivations can be derived:

$$\begin{aligned}
{}_t\phi'_{i+1}(x_i) &= A_{i+1} {}_t\beta_{i+1} \cos {}_t\beta_{i+1}(x_i - x_i) - B_{i+1} {}_t\beta_{i+1} \sin {}_t\beta_{i+1}(x_i - x_i) \\
&\quad + C_{i+1} {}_t\beta_{i+1} \cosh {}_t\beta_{i+1}(x_i - x_i) + D_{i+1} {}_t\beta_{i+1} \sinh {}_t\beta_{i+1}(x_i - x_i) \\
&= A_{i+1} {}_t\beta_{i+1} - 0 + C_{i+1} {}_t\beta_{i+1} + 0 \\
&= A_{i+1} {}_t\beta_{i+1} + C_{i+1} {}_t\beta_{i+1}
\end{aligned} \tag{22}$$

$$\begin{aligned}
{}_t\phi'_i(x_i) &= A_i {}_t\beta_i \cos {}_t\beta_i(x_i - x_{i-1}) - B_i {}_t\beta_i \sin {}_t\beta_i(x_i - x_{i-1}) \\
&\quad + C_i {}_t\beta_i \cosh {}_t\beta_i(x_i - x_{i-1}) + D_i {}_t\beta_i \sinh {}_t\beta_i(x_i - x_{i-1}) \\
&= A_i {}_t\beta_i \cos {}_t\beta_i l_i - B_i {}_t\beta_i \sin {}_t\beta_i l_i + C_i {}_t\beta_i \cosh {}_t\beta_i l_i + D_i {}_t\beta_i \sinh {}_t\beta_i l_i
\end{aligned} \tag{23}$$

Consequently, from relationship of rotation, the following relationship of coefficients can be found:

$$\begin{aligned}
A_{i+1} {}_t\beta_{i+1} + C_{i+1} {}_t\beta_{i+1} &= A_i {}_t\beta_i \cos {}_t\beta_i l_i - B_i {}_t\beta_i \sin {}_t\beta_i l_i \\
&\quad + C_i {}_t\beta_i \cosh {}_t\beta_i l_i + D_i {}_t\beta_i \sinh {}_t\beta_i l_i
\end{aligned} \tag{24}$$

(3) Bending moment:

$$(EI)_{i+1} {}_t\phi''_{i+1}(x_i) = (EI)_i {}_t\phi''_i(x_i) \tag{25}$$

Hence, based on Equation (25), the following derivations can be derived:

$$\begin{aligned}
(EI)_{i+1} \phi''_{i+1}(x_i) &= (EI)_{i+1} \begin{bmatrix} -A_{i+1} \beta_{i+1}^2 \sin {}_t\beta_{i+1}(x_i - x_i) \\ -B_{i+1} \beta_{i+1}^2 \cos {}_t\beta_{i+1}(x_i - x_i) \\ +C_{i+1} \beta_{i+1}^2 \sinh {}_t\beta_{i+1}(x_i - x_i) \\ +D_{i+1} \beta_{i+1}^2 \cosh {}_t\beta_{i+1}(x_i - x_i) \end{bmatrix} \\
&= (EI)_{i+1} (0 - B_{i+1} \beta_{i+1}^2 + 0 + D_{i+1} \beta_{i+1}^2) \\
&= (EI)_{i+1} (-B_{i+1} \beta_{i+1}^2 + D_{i+1} \beta_{i+1}^2)
\end{aligned} \tag{26}$$

$$\begin{aligned}
(EI)_i \phi''_i(x_i) &= (EI)_i \begin{bmatrix} -A_i \beta_i^2 \sin {}_t\beta_i(x_i - x_{i-1}) \\ -B_i \beta_i^2 \cos {}_t\beta_i(x_i - x_{i-1}) \\ +C_i \beta_i^2 \sinh {}_t\beta_i(x_i - x_{i-1}) \\ +D_i \beta_i^2 \cosh {}_t\beta_i(x_i - x_{i-1}) \end{bmatrix} \\
&= (EI)_i \begin{pmatrix} -A_i \beta_i^2 \sin {}_t\beta_i l_i - B_i \beta_i^2 \cos {}_t\beta_i l_i \\ +C_i \beta_i^2 \sinh {}_t\beta_i l_i + D_i \beta_i^2 \cosh {}_t\beta_i l_i \end{pmatrix}
\end{aligned} \tag{27}$$

Consequently, from relationship of bending moment, the following relationship of coefficients can be found:

$$(EI)_{i+1} (-B_{i+1} \beta_{i+1}^2 + D_{i+1} \beta_{i+1}^2) = (EI)_i \begin{pmatrix} -A_i \beta_i^2 \sin {}_t\beta_i l_i - B_i \beta_i^2 \cos {}_t\beta_i l_i \\ +C_i \beta_i^2 \sinh {}_t\beta_i l_i + D_i \beta_i^2 \cosh {}_t\beta_i l_i \end{pmatrix} \tag{28}$$

(4) Shear Force:

$$(EI)_{i+1} \phi'''_{i+1}(x_i) = (EI)_i \phi'''_i(x_i) \tag{29}$$

Hence, based on Equation (29), the following derivations can be derived:

$$\begin{aligned}
(EI)_{i+1} \phi'''_{i+1}(x_i) &= (EI)_{i+1} \begin{bmatrix} -A_{i+1} \beta_{i+1}^3 \cos {}_t\beta_{i+1}(x_i - x_i) \\ +B_{i+1} \beta_{i+1}^3 \sin {}_t\beta_{i+1}(x_i - x_i) \\ +C_{i+1} \beta_{i+1}^3 \cosh {}_t\beta_{i+1}(x_i - x_i) \\ +D_{i+1} \beta_{i+1}^3 \sinh {}_t\beta_{i+1}(x_i - x_i) \end{bmatrix} \\
&= (EI)_{i+1} (-A_{i+1} \beta_{i+1}^3 + 0 + C_{i+1} \beta_{i+1}^3 + 0) \\
&= (EI)_{i+1} (-A_{i+1} \beta_{i+1}^3 + C_{i+1} \beta_{i+1}^3)
\end{aligned} \tag{30}$$

$$\begin{aligned}
(EI)_{i,t} \phi_i'''(x_i) &= (EI)_i \begin{bmatrix} -A_{i,t} \beta_i^3 \cos {}_t\beta_i (x_i - x_{i-1}) \\ +B_{i,t} \beta_i^3 \sin {}_t\beta_i (x_i - x_{i-1}) \\ +C_{i,t} \beta_i^3 \cosh {}_t\beta_i (x_i - x_{i-1}) \\ +D_{i,t} \beta_i^3 \sinh {}_t\beta_i (x_i - x_{i-1}) \end{bmatrix} \\
&= (EI)_i \begin{pmatrix} -A_{i,t} \beta_i^3 \cos {}_t\beta_i l_i + B_{i,t} \beta_i^3 \sin {}_t\beta_i l_i \\ +C_{i,t} \beta_i^3 \cosh {}_t\beta_i l_i + D_{i,t} \beta_i^3 \sinh {}_t\beta_i l_i \end{pmatrix}
\end{aligned} \tag{31}$$

Consequently, from relationship of shear force, the following relationship of coefficients can be found:

$$(EI)_{i+1} (-A_{i+1,t} \beta_{i+1}^3 + C_{i+1,t} \beta_{i+1}^3) = (EI)_i \begin{pmatrix} -A_{i,t} \beta_i^3 \cos {}_t\beta_i l_i \\ +B_{i,t} \beta_i^3 \sin {}_t\beta_i l_i \\ +C_{i,t} \beta_i^3 \cosh {}_t\beta_i l_i \\ +D_{i,t} \beta_i^3 \sinh {}_t\beta_i l_i \end{pmatrix} \tag{32}$$

Then here, it can build a relationship between i^{th} beam segment and $i + 1^{th}$ beam segment with a transfer matrix based on above continuity relationships:

$$A_{(i+1)} = Z_{(i)} A_{(i)} \tag{33}$$

Where, $A_i = [C_i^1, C_i^2, C_i^3, C_i^4]^T$ and $A_{i+1} = [C_{i+1}^1, C_{i+1}^2, C_{i+1}^3, C_{i+1}^4]^T$ are undetermined coefficients of i^{th} beam segment and $i + 1^{th}$ beam segment respectively, $Z_{(i)}$ is noted as transfer matrix between i^{th} beam segment and $i + 1^{th}$ beam segment as below:

$$[Z_i] = \begin{bmatrix} m_{3i} n_{2i} & -m_{3i} n_{1i} & -m_{4i} n_{4i} & -m_{4i} n_{3i} \\ m_{1i} n_{1i} & m_{1i} n_{2i} & -m_{2i} n_{3i} & -m_{2i} n_{4i} \\ -m_{4i} n_{2i} & m_{4i} n_{1i} & m_{3i} n_{4i} & m_{3i} n_{3i} \\ -m_{2i} n_{1i} & -m_{2i} n_{2i} & m_{1i} n_{3i} & m_{1i} n_{4i} \end{bmatrix} \tag{34}$$

Where,

$$m_{1i} = \frac{(p_i + 1)}{2}, \quad m_{2i} = \frac{(p_i - 1)}{2}, \quad m_{3i} = \frac{\beta_i (p_i + 1)}{(2\beta_{i+1})}, \quad m_{4i} = \frac{\beta_i (p_i - 1)}{(2\beta_{i+1})}$$

$$n_{1i} = \sin(\beta_i l_i), \quad n_{2i} = \cos(\beta_i l_i), \quad n_{3i} = \sinh(\beta_i l_i), \quad n_{4i} = \cosh(\beta_i l_i)$$

$$p_i = \frac{(EI)_{i,t} \beta_i^2}{[(EI)_{i+1,t} \beta_{i+1}^2]}$$

Thus, the relationship between undetermined coefficients of first beam segment and final beam segment can be expressed as below:

$$A_{(N)} = ZA_{(1)} \quad (35)$$

Where, $Z = Z_{(N-1)}Z_{(N-2)} \cdots Z_{(2)}Z_{(1)}$ expresses the transfer matrix between first beam segment and final beam segment.

3.3.3. Boundary conditions and non-linear eigen equation for lateral beam equation

In this section, it will derive the eigen equation for calculating the natural frequencies of transverse vibration of the variable cross-section beam with fixed-free boundary condition. For cantilevered beams, boundary conditions with respect to displacements (including translational and rotational) and forces (including bending moment and shear force) are as follows:

(1) Boundary condition at fixed end

i. Displacement:

$${}_t\phi_1(0) = 0 \quad (36)$$

$$\begin{aligned} {}_t\phi_1(0) &= A_1 \sin {}_t\beta_1(0-0) + B_1 \cos {}_t\beta_1(0-0) \\ &\quad + C_1 \sinh {}_t\beta_1(0-0) + D_1 \cosh {}_t\beta_1(0-0) \\ &= 0 + B_1 + 0 + D_1 = 0 \\ &= B_1 + D_1 = 0 \end{aligned} \quad (37)$$

ii. Rotation:

$${}_t\phi_1'(0) = 0 \quad (38)$$

$$\begin{aligned} {}_t\phi_1'(0) &= A_1 {}_t\beta_1 \cos {}_t\beta_1(0-0) - B_1 {}_t\beta_1 \sin {}_t\beta_1(0-0) \\ &\quad + C_1 {}_t\beta_1 \cosh {}_t\beta_1(0-0) + D_1 {}_t\beta_1 \sinh {}_t\beta_1(0-0) \\ &= A_1 {}_t\beta_1 - 0 + C_1 {}_t\beta_1 + 0 = 0 \\ &= A_1 {}_t\beta_1 + C_1 {}_t\beta_1 = 0 \end{aligned} \quad (39)$$

(2) Boundary condition at free end

i. Bending Moment:

$$(EI)_N {}_t\phi_N''(L) = 0 \quad (40)$$

$$(EI)_{N,t} \phi_N''(L) = (EI)_N \begin{pmatrix} -A_{N,t} \beta_N^2 \sin {}_t\beta_N l_N - B_{N,t} \beta_N^2 \cos {}_t\beta_N l_N \\ + C_{N,t} \beta_N^2 \sinh {}_t\beta_N l_N + D_{N,t} \beta_N^2 \cosh {}_t\beta_N l_N \end{pmatrix} = 0 \quad (41)$$

ii. Shear Force:

$$(EI)_{N,t} \phi_N'''(L) = 0 \quad (42)$$

$$(EI)_{N,t} \phi_N'''(L) = (EI)_N \begin{pmatrix} -A_{N,t} \beta_N^3 \cos {}_t\beta_N l_N + B_{N,t} \beta_N^3 \sin {}_t\beta_N l_N \\ + C_{N,t} \beta_N^3 \cosh {}_t\beta_N l_N + D_{N,t} \beta_N^3 \sinh {}_t\beta_N l_N \end{pmatrix} = 0 \quad (43)$$

In terms of Equation (37), (39), (41) and (43), the following matrix equation can be written:

$$\begin{bmatrix} 0 & 1 & 0 & 1 \\ {}_t\beta_1 & 0 & {}_t\beta_1 & 0 \end{bmatrix} \begin{bmatrix} A_1 \\ B_1 \\ C_1 \\ D_1 \end{bmatrix} = 0 \quad (44)$$

Where, the third row in left matrix is:

$$\left[-(EI)_{N,t} \beta_N^2 \sin {}_t\beta_N l_N \quad -(EI)_{N,t} \beta_N^2 \cos {}_t\beta_N l_N \quad (EI)_{N,t} \beta_N^2 \sinh {}_t\beta_N l_N \quad (EI)_{N,t} \beta_N^2 \cosh {}_t\beta_N l_N \right] [Z] \quad (45)$$

The fourth row in matrix is:

$$\left[-(EI)_{N,t} \beta_N^3 \cos {}_t\beta_N l_N \quad (EI)_{N,t} \beta_N^3 \sin {}_t\beta_N l_N \quad (EI)_{N,t} \beta_N^3 \cosh {}_t\beta_N l_N \quad (EI)_{N,t} \beta_N^3 \sinh {}_t\beta_N l_N \right] [Z] \quad (46)$$

Where, the matrix Z is the transfer matrix as below:

$$[Z]_{4 \times 4} = Z_{(N-1)} Z_{(N-2)} \cdots Z_{(2)} Z_{(1)} \quad (47)$$

If combined above equations, a matrix equation can be rewritten as below:

$$T A_{(1)} = 0 \quad (48)$$

Where $A_{(1)} = [A_1 \quad B_1 \quad C_1 \quad D_1]^T$.

For the above equation to have a non-zero solution, the determinant of its coefficient matrix has to be zero, so a non-linear eigen equation of the beam is obtained:

$$\det = \begin{bmatrix} T_{11} & T_{12} & T_{13} & T_{14} \\ T_{21} & T_{22} & T_{23} & T_{24} \\ T_{31} & T_{32} & T_{33} & T_{34} \\ T_{41} & T_{42} & T_{43} & T_{44} \end{bmatrix} = 0 \quad (49)$$

The above eigen equation is a nonlinear function of natural frequencies, which can be solved by the Bisection method or the Newton-Raphson iteration method to obtain natural frequencies of the variable cross-section beam under the corresponding boundary conditions; Substituting solved natural frequencies into Equation (15) and Equation (33), mode shape functions of the beam can be obtained with regards to each mode order.

3.3.4. Relationship of continuity and transfer matrix for axial beam equation

The analytical solution of mode shape for i^{th} beam and the $i + 1^{th}$ beam in axial are shown as below respectively:

$$\begin{cases} {}_i\phi_i(x) = A_i \sin {}_i\beta_i(x - x_{i-1}) + B_i \cos {}_i\beta_i(x - x_{i-1}) \\ {}_i\phi_{i+1}(x) = A_{i+1} \sin {}_i\beta_{i+1}(x - x_i) + B_{i+1} \cos {}_i\beta_{i+1}(x - x_i) \end{cases} \quad (50)$$

Where, the coefficient of natural frequency is expressed as $\beta_i = \omega_n \sqrt{\frac{\rho}{E}}$.

From the continuity of displacement and axial force between the i^{th} beam and the $i + 1^{th}$ beam at the connection point x_i , the following relationships are obtained:

(1) Relationship of displacement:

$${}_i\phi_{i+1}(x_i) = {}_i\phi_i(x_i) \quad (51)$$

Hence, based on Equation (51), the following derivations can be derived:

$$\begin{aligned} {}_i\phi_{i+1}(x_i) &= A_{i+1} \sin {}_i\beta_{i+1}(x_i - x_i) + B_{i+1} \cos {}_i\beta_{i+1}(x_i - x_i) \\ &= B_{i+1} \end{aligned} \quad (52)$$

$$\begin{aligned} {}_i\phi_i(x_i) &= A_i \sin {}_i\beta_i(x_i - x_{i-1}) + B_i \cos {}_i\beta_i(x_i - x_{i-1}) \\ &= A_i \sin({}_i\beta_i l_i) + B_i \cos({}_i\beta_i l_i) \end{aligned} \quad (53)$$

Consequently, from relationship of displacement, the following relationship of coefficients can be found:

$$B_{i+1} = A_i \sin({}_i\beta_i l_i) + B_i \cos({}_i\beta_i l_i) \quad (54)$$

(2) Relationship of axial force:

$$(EA)_{i+1} {}_i\phi'_{i+1}(x_i) = (EA)_i {}_i\phi'_i(x_i) \quad (55)$$

Hence, based on Equation (55), the following derivations can be derived:

$${}_t\phi'_{i+1}(x) = A_{i+1}{}_t\beta_{i+1} \cos {}_t\beta_{i+1}(x - x_i) - B_{i+1}{}_t\beta_{i+1} \sin {}_t\beta_{i+1}(x - x_i) \quad (56)$$

$${}_t\phi'_i(x) = A_i{}_t\beta_i \cos {}_t\beta_i(x - x_{i-1}) - B_i{}_t\beta_i \sin {}_t\beta_i(x - x_{i-1}) \quad (57)$$

$$\begin{aligned} (EA)_{i+1}{}_t\phi'_{i+1}(x) &= (EA)_{i+1} [A_{i+1}{}_t\beta_{i+1} \cos {}_t\beta_{i+1}(x_i - x_i) - B_{i+1}{}_t\beta_{i+1} \sin {}_t\beta_{i+1}(x_i - x_i)] \\ &= (EA)_{i+1} (A_{i+1}{}_t\beta_{i+1}) \end{aligned} \quad (58)$$

$$\begin{aligned} (EA)_i{}_t\phi'_i(x_i) &= (EA)_i [A_i{}_t\beta_i \cos {}_t\beta_i(x_i - x_{i-1}) - B_i{}_t\beta_i \sin {}_t\beta_i(x_i - x_{i-1})] \\ &= (EA)_i [A_i{}_t\beta_i \cos({}_t\beta_i l_i) - B_i{}_t\beta_i \sin({}_t\beta_i l_i)] \end{aligned} \quad (59)$$

Consequently, from relationship of axial force, the following relationship of coefficients can be found:

$$(EA)_{i+1} (A_{i+1}{}_t\beta_{i+1}) = (EA)_i [A_i{}_t\beta_i \cos({}_t\beta_i l_i) - B_i{}_t\beta_i \sin({}_t\beta_i l_i)] \quad (60)$$

Then here, it can build a relationship between i^{th} beam segment and $i + 1^{th}$ beam segment with a transfer matrix based on above continuity relationships, which is similar to Equation (33):

$$A_{(i+1)} = Z_{(i)} A_{(i)} \quad (61)$$

Where, $A_{(i)} = [A_i \ B_i]^T$ and $A_{(i+1)} = [A_{i+1} \ B_{i+1}]^T$ are undetermined coefficients of i^{th} beam segment and $i + 1^{th}$ beam segment respectively, $Z_{(i)}$ is noted as transfer matrix between i^{th} beam segment and $i + 1^{th}$ beam segment as below:

$$[Z_i] = \begin{bmatrix} p_i n_{2i} & -p_i n_{1i} \\ n_{1i} & n_{2i} \end{bmatrix} \quad (62)$$

Where,

$$p_i = \frac{(EA)_i{}_t\beta_i}{(EA)_{i+1}{}_t\beta_{i+1}}$$

$$n_{1i} = \sin(\beta_i l_i)$$

$$n_{2i} = \cos(\beta_i l_i)$$

3.3.5. Boundary conditions and non-linear eigen equation for axial beam equation

In this section, it will derive the eigen equation for calculating the natural frequencies of axial vibration of the variable cross-section beam with fixed-free boundary condition. For cantilevered beams, boundary conditions with respect to displacements and axial forces are shown as follows:

(1) Boundary condition at fixed end

Displacement:

$${}_i\phi_1(0) = 0 \quad (63)$$

$$\begin{aligned} {}_i\phi_1(0) &= A_1 \sin {}_i\beta_1(0-0) + B_1 \cos {}_i\beta_1(0-0) \\ &= B_1 = 0 \end{aligned} \quad (64)$$

(2) Boundary condition at free end

Axial force:

$$(EA)_{N \ i}\phi'_N(L) = 0 \quad (65)$$

$$(EA)_{N \ i}\phi'_N(L) = (EA)_N [A_N {}_i\beta_N \cos({}_i\beta_N l_N) - B_N {}_i\beta_N \sin({}_i\beta_N l_N)] = 0 \quad (66)$$

In terms of Equation (64) and (66), the following matrix equations can be written:

$$\begin{bmatrix} 0 & 1 \end{bmatrix} \begin{bmatrix} A_1 \\ B_1 \end{bmatrix} = 0 \quad (67)$$

$$\left[(EA)_{N \ i}\beta_N \cos({}_i\beta_N l_N) \quad - (EA)_{N \ i}\beta_N \sin({}_i\beta_N l_N) \right] [Z] = 0 \quad (68)$$

Rest of solving procedures are similar to the section 3.3.3.

3.4. Hydrodynamic load calculation for draft-varying conditions

In this section, it introduces various methods for calculating hydrodynamic loads on hull girders, including wave calculation method in time-domain, first-order wave excitation force calculation method, radiation hydrodynamic calculation method, and static water restoring force calculation method. Based on these theoretical foundations and using the existing commercial finite element software SESAM for pre-calculation, it would obtain hydrodynamic calculation results in frequency-domain for different loading conditions. These calculations consider not only the characteristics of mass

variation but also the characteristics of time-varying wet surfaces and trim changes. This approach is designed to fulfil the requirements of calculating time-varying hydrodynamic loads for the ships under study in this paper.

3.4.1. Coordinate Definition

It is necessary to define two Cartesian coordinate systems when calculating the hydrodynamic load of the floating structure on the sea as shown in Figure 25: the inertial (global) coordinate system: $O - xyz$; and the ship body (local) coordinate system: $O_0 = x_0y_0z_0$.

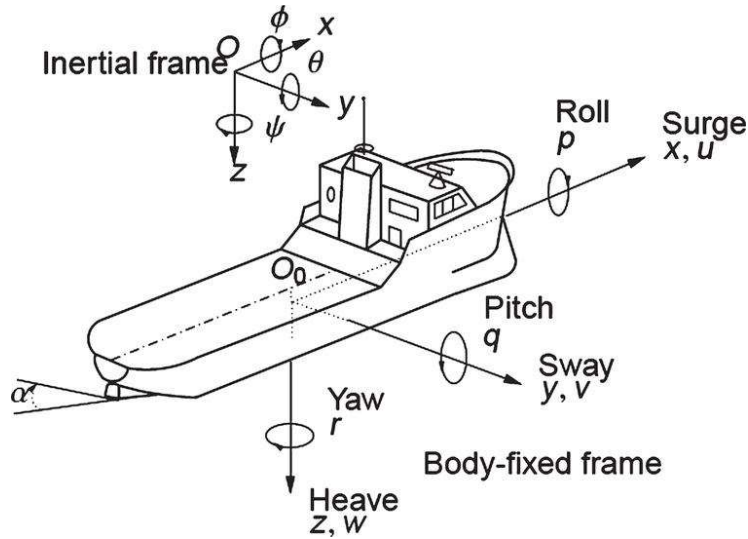


Figure 25. Coordinate systems defined in hydrodynamic calculation.

The translational displacement is described by the space coordinates through the origin of the ship's body coordinate system $O_0 = x_0y_0z_0$ in inertial coordinates $O - xyz$, which are the surge displacement along the x -axis of the inertial coordinate system, the sway displacement along the y -axis, and the heave displacement along the z -axis respectively. The three angular rotations of the ship are determined by the spatial relationship between the ship body coordinate system and the inertial coordinate system. The descriptions are the roll motion rotating around the x axis, the pitch motion rotating around the y axis and yaw motion rotating about the z axis.

3.4.2. Linear potential flow theory

The motion of large floating structures can be obtained from the linear potential flow theory. It is considered that the floating structure is in a wave field and producing six degrees of freedom under the disturbance of the waves. Moreover, it is assuming that

the flow is ideal with irrotational, incompressible and inviscid characteristics. The velocity potential exists and meets the Laplace equation and boundary conditions as below:

$$\nabla^2\Phi = 0 \quad (69)$$

$$\frac{\partial^2\Phi}{\partial t^2} + g \frac{\partial\Phi}{\partial z} = 0, z = 0 \quad (70)$$

$$\frac{\partial\Phi}{\partial z} = 0, z = -d \quad (71)$$

$$\frac{\partial\Phi}{\partial n} = V_n \quad (72)$$

Where, the Equation (69) is for the boundary conditions of the flow field, the Equation (72) is for the boundary conditions on the body surface, Φ is the total velocity potential in the flow field, which can be split into the incident wave potential Φ_I , the diffraction wave potential Φ_S and the scattering wave potential Φ_T . The following formula is the total velocity potential:

$$\Phi = \Phi_I + \Phi_S + \Phi_T \quad (73)$$

Furthermore, different boundary conditions for Φ_I , Φ_S and Φ_T is in order to solve the velocity potential as shown below:

$$\Phi_I \left\{ \begin{array}{l} \nabla^2\Phi_I = 0 \\ \frac{\partial^2\Phi_I}{\partial t^2} + g \frac{\partial\Phi_I}{\partial z} = 0, z = 0 \\ \frac{\partial\Phi_I}{\partial z} = 0, z = -d \end{array} \right. \quad (74)$$

$$\Phi_S \left\{ \begin{array}{l} \nabla^2\Phi_S = 0 \\ \frac{\partial^2\Phi_S}{\partial t^2} + g \frac{\partial\Phi_S}{\partial z} = 0, z = 0 \\ \frac{\partial\Phi_S}{\partial z} = -\frac{\partial\Phi_I}{\partial n} \end{array} \right. \quad (75)$$

$$\Phi_T \begin{cases} \Phi_T = \sum_{j=1}^6 x_j \phi_j, j = 1, 2, \dots, 6 \\ \nabla^2 \phi_j = 0 \\ -\omega^2 \phi_j + g \frac{\partial \phi_j}{\partial z} = 0, z = 0 \\ \frac{\partial \phi_j}{\partial z} = 0, z = -d \\ \frac{\partial \phi_j}{\partial z} = -i\omega n_j \end{cases} \quad (76)$$

The target researching ships are not working in a complex ocean environment. Hence, the linear wave theory (Airy wave theory) could be applied in this project as hydrodynamic loads calculation (J. Chen et al., 2019).

Wave height of regular wave:

$$\eta(x, t) = A \cdot \cos(kx - \omega t + \varepsilon) \quad (77)$$

Where, A , ω , k , ε are expressed wave amplitude, angular frequency, wave number and wave phase.

The dispersion relation in deep water:

$$\omega^2 = gk \cdot \tanh(kh) \quad (78)$$

Where, g is the gravity acceleration and h is the depth of water.

In actual sea conditions, waves are random and irregular. Assuming a stationary stochastic process with ergodicity, when simulating irregular waves using the linear wave theory mentioned above, irregular waves can be considered as the linear superposition of numerous individual waves with different wave lengths, amplitudes, and phases, as illustrated in Figure 26.

Therefore, wave height of irregular waves can be expressed as below:

$$\eta(x, t) = \sum_{i=1}^{\infty} A_i \cdot \cos(k_i x - \omega_i t + \varepsilon_i) \approx \sum_{i=1}^N A_i \cdot \cos(k_i x - \omega_i t + \varepsilon_i) \quad (79)$$

Where, N is a sufficiently large positive integer used as an approximation for an infinite series. A_i represents the wave amplitude of the i^{th} wave component, k_i is the wave number of the i^{th} wave component, ω_i is the angular frequency of the i^{th} wave

component, and ε_i is the phase angle of the i^{th} wave component. The wave amplitude A_i can be obtained through the wave spectrum $S(\omega)$ and is expressed as:

$$\frac{1}{2} A_j^2 = S(\omega_j) \Delta\omega \quad (80)$$

Here, $\Delta\omega$ represents the frequency interval between adjacent evenly spaced sampled frequency points. The instantaneous wave height of the wave follows a Gaussian distribution with a mean of 0 and a variance of $\int_0^\infty S(\omega) d\omega$.

The velocity and acceleration of the water mass point at each section of the underwater structure are also the linear superposition of the velocity and acceleration of the water mass point caused by the wave of each element component.

$$u = \sum_{i=1}^N A_i \omega_i \frac{\cosh(k_i(z+h))}{\sinh(k_i h)} \cos(k_i x - \omega_i t + \varepsilon_i) \quad (81)$$

$$w = \sum_{i=1}^N A_i \omega_i \frac{\sinh(k_i(z+h))}{\sinh(k_i h)} \sin(k_i x - \omega_i t + \varepsilon_i) \quad (82)$$

$$a_u = \sum_{i=1}^N A_i \omega_i^2 \frac{\cosh(k_i(z+h))}{\sinh(k_i h)} \sin(k_i x - \omega_i t + \varepsilon_i) \quad (83)$$

$$a_w = -\sum_{i=1}^N A_i \omega_i^2 \frac{\sinh(k_i(z+h))}{\sinh(k_i h)} \cos(k_i x - \omega_i t + \varepsilon_i) \quad (84)$$

Where, u and w are the horizontal and vertical velocity of the water mass point respectively; a_u and a_w are the horizontal and vertical acceleration of the water mass point respectively; z is the water depth of the calculation target, and h is the still water surface to the depth of the sea.

The spectrum represents the wave energy distribution of each wave frequency in stationary sea conditions. The most relevant spectra for ships are the two-parameter Pierson-Moskowitz (PM) and JONSWAP (Joint North Sea Wave Project) wave spectrum. In this section, JONSWAP wave spectrum $S(\omega)$ is applied.

$$S(\omega) = \alpha H_s^2 \frac{1}{T_p^4 \omega^5} \exp \left[-\frac{5}{4} \left(\frac{1}{T_p \omega} \right)^4 \right] \gamma \exp \left[\frac{(T_p \omega - 1)^2}{2\sigma^2} \right] \quad (85)$$

Where, ω = wave frequency in rad/s, ω_p = spectral peak frequency = $2\pi/T_p$, in rad/s,
 H_S = significant wave height, in m, $\alpha = \frac{0.0624}{[0.0230 + .366\gamma - 0.185(1.9 + \gamma)^{-1}]}$ and $\sigma =$
 $\begin{cases} 0.07, \omega \leq 1/T_p \\ 0.09, \omega > 1/T_p \end{cases}$

In above equations, γ is the spectral shape parameter, H_S and T_p represent the significant wave height and peak period of the spectrum, respectively. To avoid the additional periodic characteristics introduced by the periodicity of frequency ω values in the time history of wave elevation, a random treatment is applied to the frequency ω values. This study adopts the correction method proposed by Faltinsen (1993), as shown in Figure 26, the spectrum is evenly divided into N segments, and the frequency ω_j is randomly selected within the j^{th} segment.

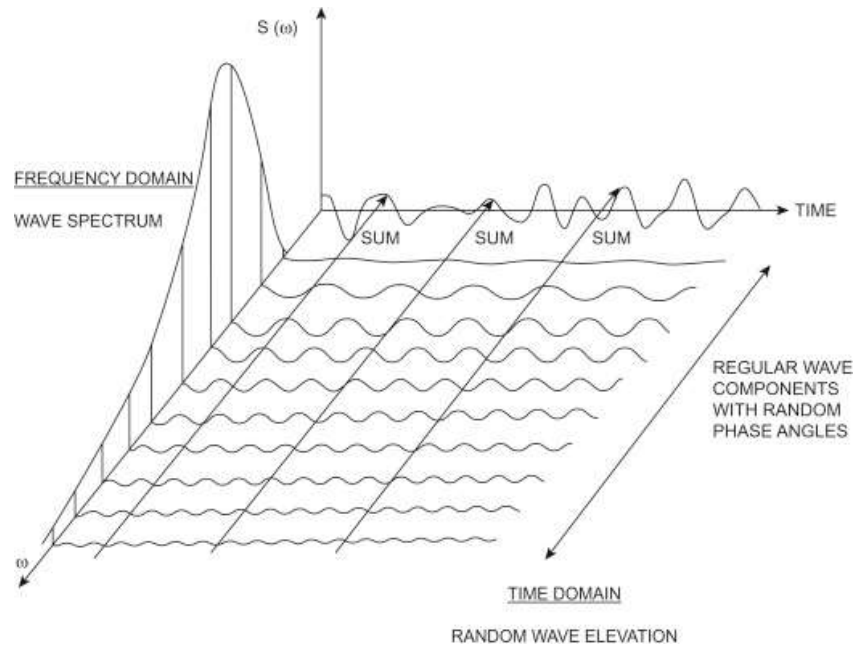


Figure 26. Transformation from wave spectrum to wave time-series (Faltinsen, 1993).



Figure 27. Sampling method in frequency-domain.

3.4.3. First order hydrodynamic loads calculation method

In this section, the main domination of dynamic part of hydrodynamic loads as first order hydrodynamic loads has been introduced.

The velocity potential of the flow field can be solved by the boundary element method, and then the pressure on the wet surface of the floating body can be calculated through the Bernoulli equation, after that, the corresponding hydrodynamic coefficient can be obtained. The hydrodynamic coefficient in this section can be calculated by the three-dimensional frequency domain potential flow calculation software program WAMIT (Wave Analysis at Massachusetts Institute of Technology) (C.-H. Lee, 1995), including wave excitation force coefficient, wave radiation force coefficient, quadratic transfer function matrix coefficient and hydrodynamic restoring force coefficient, etc (Jonkman et al., 2014; C. H. Lee & Newman, 2006). These frequency-domain hydrodynamic coefficients will be read in by the program developed in this paper, and according to the actual sea conditions, the time-domain hydrodynamic loads of the hull girder can be obtained by the time-frequency conversion method.

The wave excitation force of the floating body includes incident wave force and diffracted wave force. Among them, only the force of the incident wave flow field on the floating body is considered, which is called the incident wave force, also known as the Froude-Krylov force. The hydrodynamic force caused by the disturbance to the incident wave flow field when the floating body is fixed is called the diffracted wave force. Under the assumption of linear wave, this paper adopts the harmonic superposition method to solve the first-order wave excitation force. This method assumes that random waves can be formed by the linear superposition of many regular waves with different frequency components. Therefore, the wave excitation force can also be superimposed by the wave loads generated by these regular waves with different frequency components, as follows:

$$F^w = \Re \left\{ \sum_{j=1}^N H(\omega_j) \cdot \tilde{\zeta}_j e^{i\omega_j t} \right\} \quad (86)$$

Where, ω_j is wave frequency of j^{th} regular wave, $H(\omega_j)$ is the frequency response function with respect to the wave frequency ω_j , $\tilde{\zeta}_j$ is the amplitude of the j^{th} complex wave component, and the symbol \Re denotes taking the real value of the expression.

3.4.4. Radiation force

The offshore floating structure usually has a large range of motion. Therefore, it is necessary to consider the linear wave radiation force of the free surface memory effect according to the indirect time domain method. The calculation is as follows:

$$F_j^R(t) = -\sum_{k=1}^6 \left\{ \mu_{jk}(\infty) \ddot{x}_k(t) + \int_{-\infty}^t K_{jk}(t-\tau) \dot{x}_k(\tau) d\tau \right\}, j=1,2,\dots,6 \quad (87)$$

$$F^R(t) = -\sum_{k=1}^6 F_j^R(t) \quad (88)$$

Here, j, k represent the motion modes, including six motion modes: heave, sway, surge, roll, pitch and yaw motion mode. $\mu_{jk(\infty)}$ denotes the added mass coefficient at infinite frequency, which is only related to the shape of the object. The second term on the right side of the equation $\int_{-\infty}^t K_{jk}(t-\tau) \dot{x}_k(\tau) d\tau$ represents the potential flow damping term of the k^{th} modal motion caused by the free surface memory effect for the j^{th} motion mode, where $K_{jk}(t)$ is the corresponding time delay function. According to the relationship between the impulse response function and the frequency response function of linear systems, there exists the following relationship between the damping coefficient λ_{jk} and the added mass coefficient μ_{jk} :

$$K_{jk}(t) = \frac{2}{\pi} \int_0^\infty \lambda_{jk}(\omega) \cos(\omega t) d\omega \quad (89)$$

$$\mu_{jk}(\infty) = \mu_{jk}(\omega) + \frac{1}{\omega} \int_0^\infty K_{jk}(\tau) \sin(\omega \tau) d\tau \quad (90)$$

3.4.5. Static restoring force

In addition to considering the above-mentioned wave force, the offshore floating structure will also be affected by the hydrostatic restoring force due to the change of the wet surface caused by the movement of the floating body in the hydrostatic flow field, resulting in the change of the hydrostatic pressure. Generally speaking, the horizontal motion modes of the floating body, such as surge, sway and yaw, do not cause significant changes in the wet surface of the platform and the volume of the displaced water, so there is no hydrostatic restoring force and moment. For vertical motions, such as roll, pitch, and heave, changes in the wet surface of the marine structure and the volume of displaced water are usually caused, resulting in hydrostatic

restoring forces. According to the changes of the wet surface, the volume of the discharged water, the centre of buoyancy and the centre of gravity of the floating structure caused by the movement of each degree of freedom when the floating structure is in motion, the hydrostatic restoring force and the buoyancy of the offshore structure can be obtained.

$$F^s = [0 \quad 0 \quad \rho g V_0 \quad 0 \quad 0 \quad 0]^T - C \cdot X \quad (91)$$

Where, first term of Equation (91) represents the buoyance force, second term expresses static restoring force.

$$C = \begin{bmatrix} 0 & 0 & 0 & 0 & 0 & 0 \\ 0 & 0 & 0 & 0 & 0 & 0 \\ 0 & 0 & \rho g A_w & 0 & 0 & 0 \\ 0 & 0 & 0 & \rho g (I_x + z_B V_{\nabla}) & 0 & 0 \\ 0 & 0 & 0 & 0 & \rho g (I_y + z_B V_{\nabla}) & 0 \\ 0 & 0 & 0 & 0 & 0 & 0 \end{bmatrix} \quad (92)$$

Here, V_{∇} is displaced water volume. C is the static restoring force coefficient matrix, which depends on the changes in wet surface and metacentric height. In the case of symmetric ship design, it can be expressed in the form of Equation (92), where A_w represents the waterplane area of the offshore floating structure, ρ is the density of seawater (assumed to be 1025.0 kg/m^3), g is the acceleration due to gravity (taken as 9.806 m/s^2), I_x and I_y are the moments of inertia of the waterplane about the local coordinate x_1 and y_1 , z_B is the metacentric height, and X is the column vector representing the six degrees of freedom motion of the vessel.

According to the above hydrodynamic load components, the total hydrodynamic load of the offshore floating structure can be written as

$$F_H = F^w + F^R + F^s \quad (93)$$

3.4.6. Pre-calculation in SESAM based on boundary element method

The boundary element method discretizes only the boundary interface, reducing the dimensionality of the computation by one compared to fluid finite elements. This reduction decreases the amount of original information and degrees of freedom, leading to improved computational efficiency. The boundary element method employs

fundamental solutions for infinite domains and singularities, making it highly effective for solving problems involving infinite or semi-infinite domains. Unlike the finite element method, which discretizes elements throughout the entire fluid domain, the boundary element method only discretizes the boundary region. Therefore, its errors are limited to the boundary interface. By combining numerical and analytical approaches, the boundary element method is recognized for its reliability and accuracy, surpassing finite element methods in computing the added mass effects of external water.

In the SESAM finite element software, the Laplace equation for fluid motion is solved using the source-sink method by defining fluid density, draft height, and wet surface elements. The vibration of the draft structure and the effect of the flow field can be distributed as pulsating sources on the fluid-structure coupling interface. Nodal forces can be obtained by solving the pressure and velocity vector equations of the flow field points. Added mass is obtained by inversely solving the mass matrix, along with other hydrodynamic parameters (C.-H. Lee & Newman, 2005)

The motion of the structure and the interaction with incident waves, when solved using the source-sink method, can be viewed as pulsating sources distributed at the fluid-structure interface. These pulsating sources can be discretized into a finite number of source points, as shown in Figure 28.

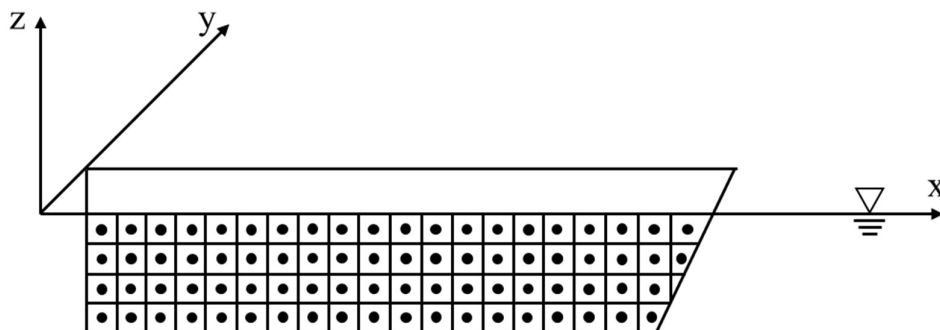


Figure 28. Source point on wetted interface of ship hull structure.

With the help of SESAM software, it is possible to calculate hydrodynamic parameters in the frequency domain.

3.5. Other excitation loads

Hull vibrations primarily stem from propeller-induced forces, with historical concerns related to substantial vibrations originating from the vessel's engines. Propellers and diesel engines are fundamentally regarded as the principal excitation sources in the ship structures. Diesel engines, integral to propulsion, generate dynamic forces and moments due to variations in torque and power output. Simultaneously, propellers, interacting with the surrounding fluid, produce hydrodynamic forces, leading to fluctuations in thrust and torque. The intricate interplay between these two systems significantly influences the dynamic response and overall structural behaviour of marine vessels.

3.5.1 Excitation loads from propeller

Vibration generated by ship propeller is a multifaceted subject of study, involving the geometric and structural attributes of the propeller, as well as the intricate interactions of numerous factors during its operation. This vibrational phenomenon can be primarily categorized into two main aspects: hydrodynamic-induced vibrations arising from the propeller's interaction with water and structural vibrations emanating from the mechanical dynamics of the propeller itself. These complex vibrations have a significant impact on the performance and structural integrity of the vessel, making their thorough analysis and control imperative in the realm of maritime engineering. Consequently, model experiments and empirical formulas are often employed to address this issue (Jensen, 2001). In addition, the majority of articles focusing on analysis of propeller excitation force indicate that the pulsating excitation force generated by the propeller on the ship's structure can be approximated as a trigonometric waveform function (Dyson, 2000; G. Zhang et al., 2014).

3.5.2 Excitation loads from diesel engine

The vibration of a diesel engine is a complex dynamic phenomenon caused by the motion and interactions of internal mechanical components. These sources of vibration can be categorized into two main types. Firstly, there are periodic mechanical vibrations resulting from the motion of pistons, connecting rods, and the rotation of the crankshaft. These include inertia vibrations and rod vibrations. The second category comprises non-periodic vibrations generated by the explosive forces and pressure fluctuations during the combustion process of the internal combustion engine. Zheng et al. (2001)

and Yuan et al. (2016) have presented some relevant findings from vibration research of the diesel engine. It is evident that the vibration loads of the diesel engine are primarily trigonometric waveforms in the time domain.

In order to investigate the impact of the excitation forces generated by the diesel engine and the propeller on the hull girder, this paper employs trigonometric waveforms as the format for simulating the vibration loads of both the diesel engine and the propeller. These waveforms are applied as external loads in the dynamic model as below:

$$F_p(t) = Am_p \cdot \sin(\omega_p t) \quad (94)$$

$$F_D(t) = Am_D \cdot \sin(\omega_D t) \quad (95)$$

Where, $F_p(t)$ is the excitation force generated by propellers, Am_p is the amplitude of force caused by propeller and ω_p is the vibrational frequency of propellers. Similarly, $F_D(t)$ is the excitation force generated by diesel engines, Am_D is the amplitude of force caused by diesel engines and ω_D is the vibrational frequency of diesel engines.

3.6. Numerical solver for dynamic analysis of proposed mathematical model by improved Kane's dynamic equation

Kane's method was chosen for this study due to its exceptional capability to handle complex dynamic systems with time-varying parameters. The structural design of offshore specialized engineering vessels like TSHDs presents unique challenges, such as inherent discontinuities, low stiffness, and high flexibility. These characteristics lead to significant rigid-flexible coupling effects that traditional dynamic analysis methods struggle to accurately capture. Kane's method offers a systematic approach to derive equations of motion for systems with complex interactions between rigid and flexible components. Its ability to incorporate time-dependent changes in mass and vibrational modes makes it particularly well-suited for analysing the dynamic behaviour of marine structures under varying operational conditions.

The seminal work of Meirovitch (1970) marked the initial establishment of dynamic equations for rocket structures accounting for time-varying mass associated with the flow of internal objects. These equations encompass six nonlinear ordinary differential equations governing the motion of rigid body and three additional ordinary differential equations accounting for elastic deformation. The coefficients in these equations vary

with time. Moreover, the article delves into the analysis of dynamic characteristics for structures featuring time-varying mass, playing a pivotal guiding role in the early phases of this project. Furthermore, the paper of Banerjee (2000) introduced a model for a flexible rocket structure with time-varying mass, taking into account the gradual decrease in mass for specific components during the flight of the rocket. Kane's dynamic equations (Kane, 1961; Kane et al., 1983) were employed in Banerjee's study to formulate the dynamic equations for the flexible structure with time-varying mass. The article also proposed a method to continuously update modal information, either by solving characteristic equations continuously or by calculating modal shapes only at specific discrete time intervals. This proposal significantly contributed to the advancement of this research.

In this section, it presents the development of a dynamic model that integrates rigid and flexible components for offshore floating structures with variable mass characteristics in the marine environment. The proposed dynamic model considers variations in mass and vibrational modes over time and is specifically designed for marine structures. It utilizes Kane's dynamic method to derive dynamical equations for this model. Subsequently, these equations will be converted into matrix form to streamline subsequent numerical simulations.

3.6.1 Basic dynamic equation of variable mass points system

It is assumed that the variable mass system is composed of "n" variable mass points $P_i (i = 1, 2, \dots, n)$, and the configuration of the variable mass system is determined by l generalized coordinates $q_j (j = 1, 2, \dots, l)$. Secondly, it is assumed that the mass of the variable mass point is a function $m_i = m_i(q_j; \dot{q}_j; t)$ with respect to generalized coordinates, generalized speed and time. It is also assumed that the position vector of the variable mass point in the inertial reference system is a function $r_i = r_i(q_j; t)$ with respect to generalized coordinates and time. Therefore, the kinetic energy function of the variable mass system can be expressed as $T = T(q_j; \dot{q}_j; t)$. In addition, it is assumed that the active force and the constraining force acting on the variable mass point are f_i and f_{ci} respectively. According to above assumptions and momentum theorem, the basic dynamic equation of variable mass point which is also named Meshchersky's equation can be expressed as (Casetta & Pesce, 2014):

$$m_i \ddot{r}_i - (f_i + f_{ci} + f_{Ri}) = 0 \quad (96)$$

Where, f_{Ri} is the reactive force which is also named Meshchersky's force caused by the change of mass of the point P_i . Its expression is

$$f_{Ri} = \dot{m}_i v_{oi} - \dot{m}_i \dot{r}_i = \dot{m}_i v_{ri} \quad (97)$$

Here, v_{oi} is the velocity vector of the point P_i released or absorbed by the mass relative to the inertial reference frame, and v_{ri} is the velocity vector of the mass released or absorbed by the mass point relative to the mass point P_i .

3.6.2. Generalized forces

It is assumed that there is a system comprised of mass point $P_k (k = 1, 2, \dots, N)$, the mass of the point P_k changes over time. Generalized velocities v are used to describe the kinematic equation of this system (Banerjee, 2000; Kane & Levinson, 1985).

It is supposed that there is a mass point P_k , the mass of the point changes over time. At t time step, the mass of the point P_k is m^k , its velocity is v^k and it is subjected to a external force F^k ; At next time step $t + \Delta t$, the mass point P_k is discharging a mass $-\dot{m}^k \Delta t$ outward at a speed v_e^k relative to the mass point P_k . Thus, the acceleration of discharging mass is $v_e^k / \Delta t$ so that the mass point gains a velocity $v^k + \Delta v^k$.

According to the Newton's second law, the force subjected to the discharging mass is:

$$F_e^k = (-\dot{m}^k \Delta t) (v_e^k / \Delta t) = -\dot{m}^k v_e^k \quad (98)$$

Hence, the reaction force of the mass point P_k is $-F_e^k = \dot{m}^k v_e^k$.

Again, according to the Newton's second law, the dynamic equation of the mass point is written as:

$$m^k a^k = m^k \frac{dv^k}{dt} = F^k - F_e^k = F^k + \dot{m}^k v_e^k \quad (99)$$

In this mass points system $P_k (k = 1, 2, \dots, N)$, the mass of each point varies with time, and the motion of the mass points system is described using v generalized velocities. For this system consisting of N mass points, Kane defines the generalized forces as (Kane, 1961; Kane et al., 1983):

(1) Generalized active force

$$F_r = \sum_{k=1}^N \vec{v}_r^k \cdot \vec{F}^k, (r=1, \dots, v) \quad (100)$$

Where, \vec{v}_r^k is the partial velocity related to the r^{th} generalized coordinate for the mass point P_k .

(2) Generalized inertia forces (due to the time rate of change of velocity)

$$F_r^* = \sum_{k=1}^N \vec{v}_r^k \cdot (-m^k \vec{a}^k), (r=1, \dots, v) \quad (101)$$

Where, m^k expresses the mass of k^{th} point, \vec{a}^k is acceleration vector of k^{th} point.

(3) Generalized inertia force (due to the time rate of change of mass)

$$F_r^{**} = \sum_{k=1}^N \vec{v}_r^k \cdot (\dot{m}^k \vec{v}_e^k), (r=1, \dots, v) \quad (102)$$

Where, \dot{m}^k is mass change rate of k^{th} point, \vec{v}_e^k is speed of mass change of k^{th} point.

Based on three types of forces described above, the dynamic equation of the mass points system P_k can be written as:

$$F_r + F_r^* + F_r^{**} = 0 \text{ or } \sum_{k=1}^N \vec{v}_r^k \cdot (\vec{F}^k - m^k \vec{a}^k + \dot{m}^k \vec{v}_e^k) = 0 \quad (103)$$

The above equation represents the Kane's dynamical equation for a system of points with variable mass.

The modal superposition method is employed to establish the dynamic response of the time-varying mass flexible structure. The vibration motion is described by the following equations of motion:

$$M\ddot{\eta} + C\dot{\eta} + K\eta = F(t) \quad (104)$$

In which, η represents the vector of generalized coordinates, local coordinates, or modal coordinates, M is the modal mass matrix, C is the modal damping matrix, and K is the modal stiffness matrix. $F(t)$ stands for the modal external force vector.

The modal mass matrix M is defined as:

$$M = \Phi^T m \Phi \quad (105)$$

Here, Φ is the modal shape matrix composed of modal shape vectors, m is the mass matrix, M is a diagonal matrix with diagonal elements being the generalized mass m_μ for each mode order.

The modal damping matrix C is defined as:

$$C = \Phi^T c \Phi \quad (106)$$

Where, c is the damping matrix. C is a diagonal matrix with diagonal elements equal to twice the product of damping ratio ζ_n , modal frequency ω_n and the generalized mass m_μ .

The modal stiffness matrix K is defined as:

$$K = \Phi^T k \Phi \quad (107)$$

Where, k is the stiffness matrix. K is a diagonal matrix with diagonal elements equal to the square of the modal frequencies ω_n .

The definition of the modal force vector $F(t)$ is given by:

$$F(t) = \Phi^T f(t) \quad (108)$$

Where, $f(t)$ is the external excitation force vector applied to each point.

The subsequent derivation relies on the properties of vector products, mainly encompassing the following three equations:

$$\vec{a} \times (\vec{b} \times \vec{c}) = \vec{b} \times (\vec{c} \times \vec{a}) = \vec{c} \times (\vec{a} \times \vec{b}) \quad (109)$$

$$\vec{a} \times (\vec{b} \times \vec{c}) + (\vec{b} \times \vec{a}) \times \vec{c} = \vec{b} \times (\vec{a} \times \vec{c}) \quad (110)$$

$$\vec{a} \times (\vec{b} \times \vec{c}) = \vec{b} \cdot (\vec{a} \cdot \vec{c}) - \vec{c} \cdot (\vec{a} \cdot \vec{b}) \quad (111)$$

3.6.3. Dynamical equations

The offshore floating structure, considering the time-varying mass system, can be effectively approximated as a system of mass points capable of deformation relative to its initial position. This system consists of mass points, each endowed with six degrees of freedom, comprising three translational motions (surge, sway, heave) and three rotational motions (roll, pitch, yaw) for each individual mass point and deflection degrees of freedom as illustrated below.

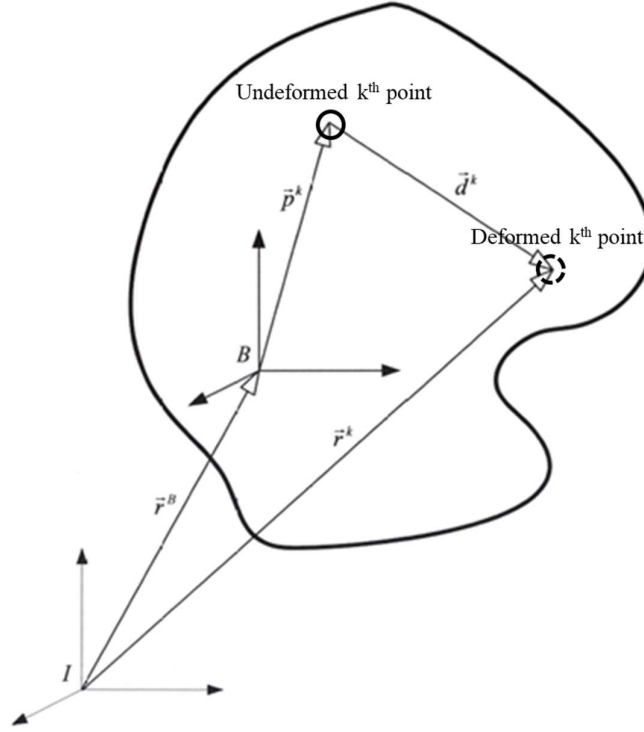


Figure 29. Schematic diagram of the motion vector relationship of the mass point.

Where, \vec{p}^k is the undeformed position of k^{th} mass point with respect to local coordinate, \vec{d}^k is the deflection of k^{th} node with respect to local coordinate. I is the original point of global coordinate stands for the hull girder. The inertial coordinate system is the reference frame in which the ship is considered with the global coordinates defined by the sea, while the local coordinate system B is the motion reference frame of the ship as the global coordinate system.

Under the assumption of small deformation, the deformation of the flexible body can be expressed using the modal superposition method. That is, the deformation of point P relative to the local coordinate system B , fixed on the flexible body as shown in Figure 29, can be expressed as the sum of the product of the μ modal shapes and their corresponding generalized modal coordinates η_i :

$$\vec{d}^k = \sum_{i=1}^{\mu} \vec{\phi}_i^k \eta_i \quad (112)$$

In the inertial reference coordinate system I , the position vector of any point P can be expressed as:

$$\vec{r}^k = \vec{r}^B + (\vec{p}^k + \vec{d}^k) \quad (113)$$

Here, \vec{r}^B is the position vector of the origin B in the local coordinate system with respect to the global coordinate system.

The expression for the velocity vector of any point P with respect to the global coordinate system I is given by the sum of the velocity of the point when the flexible body undergoes rigid body motion and the velocity when the flexible body undergoes only elastic deformation:

$$\vec{v}^k = \vec{v}^B + \vec{\omega}^B \times (\vec{p}^k + \vec{d}^k) + \vec{v}_{K/B} \quad (114)$$

where, $\vec{\omega}^B$ is the angular velocity of local coordinate system with respect to global coordinate system, $v_{K/B}$ is the relative velocity of the point p^k with respect to the local coordinate system B , where the point coincides with the position of the point p^k .

Due to the vectors p^k and d^k being defined in the local coordinate system B , their differentials in the global coordinate system I inevitably include cross-product terms with the angular velocity ω^B . According to the Equation (111), the last term on the right of Equation (114) can be written as:

$$\vec{v}_{K/B} = \dot{\vec{d}}^k = \sum_{i=1}^{\mu} (\bar{\phi}_i^k \dot{\eta}_i) \quad (115)$$

Substituting Equation (115) into Equation (114) yields the expression for the velocity of point P relative to the global coordinate system I :

$$\vec{v}^k = \vec{v}^B + \vec{\omega}^B \times (\vec{p}^k + \vec{d}^k) + \sum_{i=1}^{\mu} (\bar{\phi}_i^k \dot{\eta}_i) \quad (116)$$

Similarly, the expression for the acceleration of point P relative to the global coordinate system I is given by

$$\vec{a}^k = \vec{a}^B + \dot{\vec{\omega}}^B \times (\vec{p}^k + \vec{d}^k) + \vec{\omega}^B \times \dot{\vec{\omega}}^B \times (\vec{p}^k + \vec{d}^k) + \vec{a}_{K/B} + 2\vec{\omega}^B \times \vec{v}_{K/B} \quad (117)$$

Here, \vec{a}^k is the acceleration of point P in the global coordinate system, \vec{a}^B is the acceleration of point P in the local coordinate system, $a_{K/B}$ is the acceleration of the local reference coordinate system relative to the global reference coordinate system,

ω^B is the angular velocity of the local reference coordinate system relative to the global reference coordinate system,

Substituting Equation (115) into Equation (117), the expression for the acceleration of point P in the global coordinate system I is obtained as follows:

$$\vec{a}^k = \vec{a}^B + \vec{\alpha}^B \times (\vec{p}^k + \vec{d}^k) + \vec{\omega}^B \times \left[\vec{\omega}^B \times (\vec{p}^k + \vec{d}^k) + 2 \sum_{i=1}^{\mu} (\vec{\phi}_i^k \dot{\eta}_i) \right] + \sum_{i=1}^{\mu} (\vec{\phi}_i^k \ddot{\eta}_i) \quad (118)$$

To develop the Kane's equation, it is first necessary to obtain the partial derivative vector of the velocity vector with respect to the r^{th} generalized velocity. The expression for the partial derivative vector of the velocity vector of point P with respect to the r^{th} generalized velocity is given by:

$$\vec{v}_r^k = \vec{v}_r^B + \vec{\omega}_r^B \times (\vec{p}^k + \vec{d}^k) + \sum_{i=1}^{\mu} \left(\vec{\phi}_i^k \frac{\partial \dot{\eta}_i}{\partial \dot{\eta}_r} \right) \quad (119)$$

The above equation can be rewritten in the following form:

$$\vec{v}_r^k = \vec{v}_r^B + \vec{\omega}_r^B \times (\vec{p}^k + \vec{d}^k) + \delta_{ri} \vec{\phi}_i^k \quad (120)$$

Or

$$\vec{v}_r^k = \vec{v}_r^B + \vec{\omega}_r^B \times (\vec{p}^k + \vec{d}^k) + \vec{\phi}_r^k \quad (121)$$

Where, δ_{ri} is the Kronecker delta, when $r = i$, $\delta_{ri} = 1$, otherwise, $\delta_{ri} = 0$

The translational, rotational and vibrational equation based on Kane's method can be obtained by substituting Equation (116), (118) and (121) into Equation (100), (101), (102) and (103), which gives:

$$\begin{aligned}
& \sum_{k=1}^N \left\{ \bar{F}^k \cdot \left[\bar{v}_r^B + \bar{\omega}_r^B \times (\bar{p}^k + \bar{d}^k) + \sum_{i=1}^{\mu} \left(\bar{\phi}_i^k \frac{\partial \dot{\eta}_i}{\partial \dot{\eta}_r} \right) \right] \right\} \\
& + \left[\bar{v}_r^B + \bar{\omega}_r^B \times (\bar{p}^k + \bar{d}^k) + \sum_{i=1}^{\mu} \left(\bar{\phi}_i^k \frac{\partial \dot{\eta}_i}{\partial \dot{\eta}_r} \right) \right] \\
& \cdot \left\langle \begin{aligned} & \bar{a}^B + \sum_{i=1}^{\mu} (\bar{\phi}_i^k \ddot{\eta}_i) + \\ & -m^k \left\{ \bar{\alpha}^B \times (\bar{p}^k + \bar{d}^k) + \right. \\ & \left. \bar{\omega}^B \times \left[\bar{\omega}^B \times (\bar{p}^k + \bar{d}^k) + 2 \sum_{i=1}^{\mu} (\bar{\phi}_i^k \dot{\eta}_i) \right] \right\} \end{aligned} \right\rangle \\
& + \left[\bar{v}_r^B + \bar{\omega}_r^B \times (\bar{p}^k + \bar{d}^k) + \sum_{i=1}^{\mu} \left(\bar{\phi}_i^k \frac{\partial \dot{\eta}_i}{\partial \dot{\eta}_r} \right) \right] \cdot (-\dot{m}^k \bar{v}^k) \\
& = 0
\end{aligned} \tag{122}$$

The Equation (122) can be simplified based on Equation (121) as below:

$$\begin{aligned}
& \sum_{k=1}^N \left\{ \bar{F}^k \cdot \left[\bar{v}_r^B + \bar{\omega}_r^B \times (\bar{p}^k + \bar{d}^k) + \bar{\phi}_r^k \right] \right\} + \\
& \left[\bar{v}_r^B + \bar{\omega}_r^B \times (\bar{p}^k + \bar{d}^k) + \bar{\phi}_r^k \right] \\
& \cdot \left\langle \begin{aligned} & \bar{a}^B + \sum_{i=1}^{\mu} (\bar{\phi}_i^k \ddot{\eta}_i) + \\ & -m^k \left\{ \bar{\alpha}^B \times (\bar{p}^k + \bar{d}^k) + \right. \\ & \left. \bar{\omega}^B \times \left[\bar{\omega}^B \times (\bar{p}^k + \bar{d}^k) + 2 \sum_{i=1}^{\mu} (\bar{\phi}_i^k \dot{\eta}_i) \right] \right\} \end{aligned} \right\rangle \\
& + \left[\bar{v}_r^B + \bar{\omega}_r^B \times (\bar{p}^k + \bar{d}^k) + \bar{\phi}_r^k \right] \cdot \dot{m}^k \bar{v}_e^k \\
& = 0
\end{aligned} \tag{123}$$

Where, the mass change velocity, \bar{v}_e^k of the k^{th} mass point is shown below or user-defined value:

$$\bar{v}_e^k = - \left\{ \bar{v}^B + \bar{\omega}^B \times (\bar{p}^k + \bar{d}^k) + \sum_{i=1}^{\mu} (\bar{\phi}_i^k \dot{\eta}_i) \right\} \tag{124}$$

The following is dynamical equations for rigid-flexible body with variable mass system based on improved Kane's dynamic equation:

(1) Translational equation

The translational equation can be obtained by dot multiplying Equation (123) with the first term of Equation (121), which gives:

$$\begin{aligned} & \vec{v}_r^B \cdot \sum_{k=1}^v \left\langle m^k \left\{ \begin{aligned} & \vec{a}^B + \sum_{i=1}^{\mu} \vec{\phi}_i^k \ddot{\eta}_i + \vec{\alpha}^B \times (\vec{p}^k + \vec{d}^k) \\ & + \vec{\omega}^B \times \left[\vec{\omega}^B \times (\vec{p}^k + \vec{d}^k) + 2 \sum_{i=1}^{\mu} \vec{\phi}_i^k \dot{\eta}_i \right] \end{aligned} \right\} - \dot{m}^k \vec{v}_e^k \right\rangle \\ & = \vec{v}_r^B \cdot \sum_{k=1}^v \vec{F}^k \quad (r=1,2,3) \end{aligned} \quad (125)$$

Where, $\vec{d}^k = \sum_{i=1}^{\mu} \vec{\phi}_i^k \eta_i$ is the deflection of k^{th} mass point with respect to local coordinate system, $\vec{\omega}^B$ is the angular velocity of body with respect to global coordinate system, $\vec{\alpha}^B$ is the angular acceleration of body with respect to global coordinate system.

(2) Rotational equation

Similarly, the rotational equation can be derived from taking the scalar product of Equation (123) with second term of Equation (121). It gives as below:

$$\begin{aligned} & \vec{\omega}_r^B \cdot \left\langle \begin{aligned} & \sum_{k=1}^N (\vec{p}^k + \vec{d}^k) \times \left\{ m^k \left[\vec{a}^B + \sum_{i=1}^{\mu} (\vec{\phi}_i^k \ddot{\eta}_i) \right] + \dot{m}^k \vec{v}_e^k \right\} + \\ & \sum_{k=1}^N (\vec{p}^k + \vec{d}^k) \times m^k \left\{ \begin{aligned} & \vec{\alpha}^B \times (\vec{p}^k + \vec{d}^k) + \\ & \vec{\omega}^B \times \left[\vec{\omega}^B \times (\vec{p}^k + \vec{d}^k) + 2 \sum_{i=1}^{\mu} (\vec{\phi}_i^k \dot{\eta}_i) \right] \end{aligned} \right\} \end{aligned} \right\rangle \\ & = \vec{\omega}_r^B \cdot \sum_{k=1}^N (\vec{p}^k + \vec{d}^k) \times \vec{F}^k \quad (r=4,5,6) \end{aligned} \quad (126)$$

The expression for the angular momentum \vec{H} of the mass points system is given by:

$$\vec{H} = \hat{I} \vec{\omega}^B = \sum_{k=1}^N \left\{ m^k (\vec{p}^k + \vec{d}^k) \times \left[\vec{\omega}^B \times (\vec{p}^k + \vec{d}^k) \right] \right\} \quad (127)$$

Where, \hat{I} is the body inertial tensor. Similarly, the rate of change of the moment of inertia is given by:

$$\dot{\vec{H}} = \hat{I} \vec{\alpha}^B = \sum_{k=1}^N \left\{ m^k (\vec{p}^k + \vec{d}^k) \times \left[\vec{\alpha}^B \times (\vec{p}^k + \vec{d}^k) \right] \right\} \quad (128)$$

Hence, the rotational equation can be rewritten by:

$$\begin{aligned}
& \bar{\omega}_r^B \cdot \left\langle \begin{aligned} & \sum_{k=1}^v (\bar{p}^k + \bar{d}^k) \times \left\{ m^k \left[\bar{a}^B + \sum_{i=1}^{\mu} \bar{\phi}_i^k \ddot{\eta}_i \right] - \dot{m}^k \bar{v}_e^k \right\} \\ & + I \bar{\alpha}^B + \bar{\omega}^B \times I \bar{\omega}^B + \sum_{k=1}^v 2m^k (\bar{p}^k + \bar{d}^k) \times \left[\bar{\omega}^B \times \sum_{i=1}^{\mu} \bar{\phi}_i^k \dot{\eta}_i \right] \end{aligned} \right\rangle \quad (129) \\
& = \bar{\omega}_r^B \cdot \sum_{k=1}^v (\bar{p}^k + \bar{d}^k) \times \bar{F}^k \quad (r = 4, 5, 6)
\end{aligned}$$

(3) Vibrational equation

Similarly, if only the third term on the right-hand side of Equation (121) is nonzero, Equation (123) can be simplified to the vibration equation:

$$\begin{aligned}
& \sum_{k=1}^N \bar{\phi}_r^k \cdot \left\langle \begin{aligned} & \bar{a}^B + \sum_{i=1}^{\mu} (\bar{\phi}_i^k \ddot{\eta}_i) + \\ & -m^k \left\{ \bar{\alpha}^B \times (\bar{p}^k + \bar{d}^k) + \right. \\ & \left. \bar{\omega}^B \times \left[\bar{\omega}^B \times (\bar{p}^k + \bar{d}^k) + 2 \sum_{i=1}^{\mu} (\bar{\phi}_i^k \dot{\eta}_i) \right] \right\} - \dot{m}^k \bar{v}_e^k \end{aligned} \right\rangle \quad (130) \\
& = \sum_{k=1}^N \bar{\phi}_r^k \cdot \bar{F}^k
\end{aligned}$$

If neglecting geometric stiffness terms and incorporating the flexible terms in Equation (104), (105), (106), (107) and (108), the above vibration equation can be rewritten as:

$$\begin{aligned}
& \sum_{k=1}^v \bar{\phi}_r^k \cdot \left\langle \begin{aligned} & \bar{a}^B + \bar{\alpha}^B \times (\bar{p}^k + \bar{d}^k) \\ & m^k \left\{ + \bar{\omega}^B \times \left[\bar{\omega}^B \times (\bar{p}^k + \bar{d}^k) + 2 \sum_{i=1}^{\mu} \bar{\phi}_i^k \dot{\eta}_i \right] \right. \\ & \left. + \sum_{i=1}^{\mu} \bar{\phi}_i^k \ddot{\eta}_i \right\} - \dot{m}^k \bar{v}_e^k \end{aligned} \right\rangle \quad (131) \\
& = -m^B (\Omega_i^2 \eta_i + 2\xi \Omega_i \dot{\eta}_i) + \sum_{k=1}^v \bar{\phi}_i^k \cdot f_{ext}^k \quad (i, r = 1, 2, \dots, \mu)
\end{aligned}$$

Where, Ω_i is i^{th} natural frequency; ξ is the modal damping coefficient; f_{ex}^k is the external force on k^{th} mass point.

3.6.4. Matrix form of dynamical equations

The equations in vector form for translational, rotational, and vibrational motion of the variable mass rigid-flexible coupled body were derived in the aforementioned sections 3.6.1 - 3.6.3. To implement this algorithm in a programme, it is necessary to transform

these vector equations into scalar equations which are the matrix form of the dynamic equations.

The translational Equation (125) and rotational Equation (129) can be rewritten in matrix form as:

$$M_1 \begin{Bmatrix} \vec{a}^B \\ \vec{\alpha}^B \end{Bmatrix} + A_1^T \dot{\eta} + X_1 = \begin{Bmatrix} 0 \\ 0 \end{Bmatrix} \quad (132)$$

Where M_1 is the inertial matrix of rigid body, A_1^T is structural coupling vector of rigid and flexible motion, and X_1 is force vector of rigid body in translational and rotational motion.

Expanding Equation (125), the following translational equation can be obtained:

$$\begin{aligned} & \sum_{k=1}^N m^k \vec{a}^B + \sum_{k=1}^N m^k \vec{\alpha}^B \times (\vec{p}^k + \vec{d}^k) + \sum_{k=1}^N m^k \left(\sum_{i=1}^{\mu} \vec{\phi}_i^k \ddot{\eta}_i \right) \\ & + \sum_{k=1}^N \left\langle m^k \left\{ \vec{\omega}^B \times \left[\vec{\omega}^B \times (\vec{p}^k + \vec{d}^k) + 2 \sum_{i=1}^{\mu} (\vec{\phi}_i^k \dot{\eta}_i) \right] \right\} - \dot{m}^k \vec{v}_e^k - \vec{F}^k \right\rangle = 0 \end{aligned} \quad (133)$$

Similarly, expanding Equation (129), the following rotational equation can be obtained:

$$\begin{aligned} & \sum_{k=1}^N m^k (\vec{p}^k + \vec{d}^k) \times \vec{a}^B + \hat{I} \vec{\alpha}^B + \vec{\omega}^B \times \hat{I} \vec{\omega}^B \\ & + \sum_{k=1}^N m^k (\vec{p}^k + \vec{d}^k) \times \sum_{i=1}^{\mu} (\vec{\phi}_i^k \dot{\eta}_i) \\ & + \sum_{k=1}^N m^k (\vec{p}^k + \vec{d}^k) \times (-\dot{m}^k \vec{v}_e^k) \\ & + \sum_{k=1}^N 2m^k (\vec{p}^k + \vec{d}^k) \times \left[\vec{\omega}^B \times \sum_{i=1}^{\mu} (\vec{\phi}_i^k \dot{\eta}_i) \right] - \sum_{k=1}^N (\vec{p}^k + \vec{d}^k) \times \vec{F}^k = 0 \end{aligned} \quad (134)$$

The inertia matrix is a six times six symmetric partitioned matrix. The upper left three times three matrix is associated with the translational components of the rigid body. The lower right three by three matrix is associated with the rotational components of the rigid body. The upper right and lower left matrix are associated with coupling between the translational and rotational components of the rigid body.

The \vec{a}^B term in Equation (125) is three by three diagonal matrix in the upper left of M_1 , which is:

$$m^B U = m^B \begin{bmatrix} 1 & 0 & 0 \\ 0 & 1 & 0 \\ 0 & 0 & 1 \end{bmatrix} \quad (135)$$

Where U is the three-by-three identify matrix and m^B is the total mass of the body.

In terms of Equation (125), some modal integral items, which are \vec{S} and \vec{b} respectively, can be defined as below:

$$S = \sum_{k=1}^N \vec{p}^k m^k + b\eta \quad (136)$$

And

$$b = \sum_{k=1}^N m^k \vec{\phi}^k \quad (137)$$

The term $\vec{\alpha}^B$ in Equation (125) can be expressed as below:

$$\begin{aligned} m^k \vec{\alpha}^B \times (\vec{p}^k + \vec{d}^k) &= -m^k (\vec{p}^k + \vec{d}^k) \times \vec{\alpha}^B \\ &= -(m^k \vec{p}^k + m^k \vec{d}^k) \times \vec{\alpha}^B \\ &= -\vec{S} \times \vec{\alpha}^B \end{aligned} \quad (138)$$

Similarly, the term \vec{a}^B in Equation (129) can be written as below:

$$\sum_{k=1}^N (\vec{p}^k + \vec{d}^k) \times m^k \vec{a}^B = \vec{S} \vec{a}^B \quad (139)$$

Where it is noted that the term \vec{S} on above is expressed as below in assumption of rigid body dynamic analysis:

$$\vec{S} = \begin{bmatrix} 0 & -s_3 & s_2 \\ s_3 & 0 & -s_1 \\ -s_2 & s_1 & 0 \end{bmatrix} \quad (140)$$

The inertia tensor \hat{I} is expressed as:

$$\hat{I} = \hat{I}_0 + \sum_{i=1}^{\mu} (N_i + N_i^T) \eta_i \quad (141)$$

Here, the term \hat{I}_0 is inertial tensor of the rigid body:

$$\hat{I}_0 = \begin{bmatrix} y^2 + z^2 & -xy & -xz \\ -yx & x^2 + z^2 & -yz \\ -zx & -zy & x^2 + y^2 \end{bmatrix} \quad (142)$$

The term of production of N_i and η_i is the inertia tensor of the flexible body which will be introduced in the following derivations.

Therefore, the inertial matrix M_1 can be written as:

$$M_1 = \begin{bmatrix} m^B U_{3 \times 3} & -\tilde{S}_{3 \times 3} \\ \tilde{S}_{3 \times 3} & \hat{I}_{3 \times 3} \end{bmatrix}_{6 \times 6} \quad (143)$$

The term $\ddot{\eta}$ in translational dynamical Equation (125) can be written as below based on the modal integral, \vec{b} , mentioned in Equation (137) above:

$$\sum_{k=1}^N m^k \sum_{i=1}^{\mu} \vec{\phi}_i^k \ddot{\eta}_i = \sum_{k=1}^N m^k \vec{\phi}^k \ddot{\eta} = b \ddot{\eta} \quad (144)$$

If defined another modal integral term, \vec{g} , as:

$$g = \sum_{k=1}^N \tilde{p}^k \vec{\phi}^k m^k \quad (145)$$

The expression with respect to term $\ddot{\eta}$ in rotational Equation (129) can be written as below:

$$\begin{aligned} \sum_{k=1}^N (\vec{p}^k + \vec{d}^k) \times m^k \sum_{i=1}^{\mu} \vec{\phi}_i^k \ddot{\eta}_i &= \sum_{k=1}^N [(\vec{p}^k + \vec{d}^k) \times m^k \vec{\phi}^k] \ddot{\eta} \\ &= \sum_{k=1}^N [(\vec{p}^k \times m^k \vec{\phi}^k) + (\vec{\phi}^k \eta \times m^k \vec{\phi}^k)] \ddot{\eta} \\ &= g \ddot{\eta} \end{aligned} \quad (146)$$

Consequently, the structural coupling vector for flexible and rigid body motion in Equation (132) can be written as:

$$A_1^T = \begin{Bmatrix} \vec{b} \\ \vec{g} \end{Bmatrix} \quad (147)$$

Comparing Equation (132) with Equation (133), the expression for the force component in the translational equation is obtained as:

$$X_1^{trans} = \sum_{k=1}^N \left\langle m^k \left\{ \bar{\omega}^B \times \left[\bar{\omega}^B \times (\bar{p}^k + \bar{d}^k) + 2 \sum_{i=1}^{\mu} (\bar{\phi}_i^k \dot{\eta}_i) \right] \right\} - \dot{m}^k \bar{v}_e^k \right\rangle - \sum_{k=1}^N \bar{F}^k \quad (148)$$

Which can be rewritten as:

$$X_1^{trans} = \tilde{\omega}_B [\tilde{\omega}_B S + 2b\dot{\eta}] - \sum_{k=1}^N \dot{m}^k \bar{v}_e^k - \sum_{k=1}^N \bar{F}^k \quad (149)$$

Where $\tilde{\omega}^B$ can be expressed as below which similar to \tilde{S} :

$$\tilde{\omega}_B = \begin{bmatrix} 0 & -\omega_3 & \omega_2 \\ \omega_3 & 0 & -\omega_1 \\ -\omega_2 & \omega_1 & 0 \end{bmatrix}$$

Comparing Equation (132) with Equation (134), the expression for the force component in the translational equation is obtained as:

$$\begin{aligned} X_1^{rot} &= \sum_{k=1}^N (\bar{p}^k + \bar{d}^k) \times (-\dot{m}^k \bar{v}_e^k) + \bar{\omega}^B \times \hat{I} \bar{\omega}^B \\ &+ 2 \sum_{k=1}^N m^k (\bar{p}^k + \bar{d}^k) \times \left(\bar{\omega}^B \times \sum_{i=1}^{\mu} \bar{\phi}_i^k \dot{\eta}_i \right) - \bar{t}_{ext}^B \end{aligned} \quad (150)$$

If the higher-order terms in the above equation are neglected, the Equation (150) can be simplified to:

$$X_1^{rot} = -\dot{m} \tilde{r}_c V_e + \tilde{\omega}^B \hat{I} \bar{\omega}^B + 2 \sum_{k=1}^N N_r^T \dot{\eta}_r \bar{\omega}^B - \bar{t}_{ext}^B \quad (151)$$

Where \tilde{r}_c expresses the average position of the particles, \bar{t}_{ext}^B is the total resultant external torque on the body as below respectively.

$$N_i = \sum_{k=1}^{\nu} \left[(\bar{p}^{kT} \bar{\phi}_i^k) U - \bar{p}^k (\bar{\phi}_i^k)^T \right] m^k \quad (152)$$

$$\tilde{r}_c = \frac{1}{\nu} \sum_{k=1}^{\nu} (\bar{p}^k + \bar{d}^k) \quad (153)$$

$$\bar{t}_{ext}^B = \sum_{k=1}^{\nu} (\bar{p}^k + \bar{d}^k) \times \bar{F}^k = \sum_{k=1}^{\nu} (\bar{p}^k + \bar{d}^k) \bar{F}^k \quad (154)$$

The vibration Equation (131) can be rewritten in matrix form as:

$$A_2 \begin{Bmatrix} \vec{a}^B \\ \vec{\alpha}^B \end{Bmatrix} + E_1 \ddot{\eta} + Z_1 = \begin{Bmatrix} 0 \\ 0 \end{Bmatrix} \quad (155)$$

Where A_2 is the coupling vector of deflection motion and rigid motion of the body, E_1 is the generalized mass matrix, Z_1 is the flexural motion forcing vector.

Expanding the Equation (130), the following equation can be obtained:

$$\sum_{k=1}^{\nu} \vec{\phi}_r^k \cdot \left\langle \begin{array}{l} \vec{a}^B + \vec{\alpha}^B \times (\vec{p}^k + \vec{d}^k) + \\ m^k \left\{ \vec{\omega}^B \times \left[\vec{\omega}^B \times (\vec{p}^k + \vec{d}^k) + 2 \sum_{i=1}^{\mu} (\vec{\phi}_i^k \dot{\eta}_i) \right] + \right. \\ \left. \sum_{i=1}^{\mu} (\vec{\phi}_i^k \ddot{\eta}_i) \right\} + \\ \left. -\dot{m}^k \vec{v}_e^k - F^k \right\rangle = 0 \quad (i, r = 1, 2, \dots, \mu) \quad (156)$$

The terms including \vec{a}^B in Equation (156) can be simplified as below:

$$\sum_{k=1}^N \vec{\phi}_r^k \cdot m^k \vec{a}^B = \sum_{k=1}^N \vec{\phi}_r^{kT} m^k \vec{a}^B = \vec{b}_r^T \vec{a}^B \quad (r = 1, 2, \dots, \mu) \quad (157)$$

The terms including $\vec{\alpha}^B$ in Equation (156) can be simplified as below:

$$\begin{aligned} \sum_{k=1}^N \vec{\phi}_r^k \cdot m^k \vec{\alpha}^B \times (\vec{p}^k + \vec{d}^k) &= \sum_{k=1}^N \vec{\alpha}^B \cdot [(\vec{p}^k + \vec{d}^k) \times m^k \vec{\phi}_r^k] \\ &= \vec{g}_r^T \vec{\alpha}^B \end{aligned} \quad (158)$$

In terms of Equation (155), (157) and (158), the term A_2 can be expressed as below:

$$A_2 = \left\{ \vec{b}^T \quad \vec{g}^T \right\} = A_1 \quad (159)$$

In Equation (156), the terms including $\ddot{\eta}$ can be simplified as below:

$$\sum_{k=1}^N \vec{\phi}_r^k \cdot m^k \sum_{i=1}^{\mu} \vec{\phi}_i^k \ddot{\eta}_i = \sum_{k=1}^N \vec{\phi}_r^k \cdot m^k \vec{\phi}^k \ddot{\eta}_i \quad (160)$$

Hence, the generalized mass matrix E_1 can be expressed as below:

$$E_1 = \sum_{k=1}^N \vec{\phi}_i^{kT} \dot{m}^k \vec{\phi}_j^k \quad (161)$$

The remaining terms in Equation (156) are the flexural motion forcing vector Z_1 , which can be expanded as below:

$$\begin{aligned}
Z_1 &= \sum_{k=1}^{\nu} \vec{\phi}_r^k \cdot \left[m^k \left\{ \vec{\omega}^B \times \left[\vec{\omega}^B \times (\vec{p}^k + \vec{d}^k) + 2 \sum_{i=1}^{\mu} (\vec{\phi}_i^k \dot{\eta}_i) \right] \right\} - \dot{m}^k \vec{v}_e^k - \vec{F}^k \right] \\
&= \sum_{r=1}^n \sum_{k=1}^{\nu} \vec{\phi}_r^{kT} m^k \left\{ \vec{\omega}^B \times \left[\vec{\omega}^B \times \left(\vec{p}^k + \sum_{i=1}^{\mu} \vec{\phi}_i^k \eta_i \right) \right] \right\} \\
&\quad + \sum_{r=1}^n \sum_{k=1}^{\nu} \vec{\phi}_r^{kT} m^k \left\{ \vec{\omega}^B \times 2 \sum_{i=1}^{\mu} \vec{\phi}_i^k \dot{\eta}_i \right\} \\
&\quad - \sum_{r=1}^n \sum_{k=1}^{\nu} \vec{\phi}_r^{kT} \dot{m}^k \vec{v}_e^k - \sum_{r=1}^n \sum_{k=1}^{\nu} \vec{\phi}_r^{kT} \vec{F}^k
\end{aligned} \tag{162}$$

The terms including $\vec{\phi}_i^k \dot{\eta}_i$ in the Equation (162) can be simplified to the following expression:

$$\begin{aligned}
&\sum_{k=1}^N \vec{\phi}_r^k \cdot m^k \left[\omega^B \times \left(2 \sum_{i=1}^{\mu} \vec{\phi}_i^k \dot{\eta}_i \right) \right] = \sum_{k=1}^N m^k \omega^B \cdot \left[\left(2 \sum_{i=1}^{\mu} \vec{\phi}_i^k \dot{\eta}_i \right) \times \vec{\phi}_r^k \right] \\
&= \sum_{k=1}^N m^k \omega^{BT} \cdot \left(2 \sum_{i=1}^{\mu} \vec{\phi}_i^k \times \vec{\phi}_r^k \dot{\eta}_i \right) = 2 \omega^{BT} \sum_{k=1}^N m^k \left(\sum_{i=1}^{\mu} \vec{\phi}_i^k \times \vec{\phi}_r^k \dot{\eta}_i \right) \\
&= 2 \omega^{BT} \sum_{i=1}^{\mu} \left(\sum_{k=1}^N m^k \vec{\phi}_i^k \times \vec{\phi}_r^k \right) \dot{\eta}_i
\end{aligned} \tag{163}$$

If let

$$d_{ir} = \sum_{k=1}^{\nu} \vec{\phi}_i^k \times \vec{\phi}_r^k m^k \quad (i, r = 1, 2, \dots, \mu) \tag{164}$$

Then the Equation (163) can be simplified to:

$$\sum_{k=1}^N \vec{\phi}_r^k \cdot m^k \left[\omega^B \times \left(2 \sum_{i=1}^{\mu} \vec{\phi}_i^k \dot{\eta}_i \right) \right] = 2 \omega^{BT} \sum_{i=1}^{\mu} d_{ir} \dot{\eta}_i \tag{165}$$

The terms including $\vec{\phi}_i^k \eta_i$ in the Equation (162) can be simplified to the following expression:

$$\begin{aligned}
&\sum_{k=1}^N \vec{\phi}_r^{kT} m^k \left\{ \vec{\omega}^B \left[\vec{\omega}^B \left(\vec{p}^k + \sum_{i=1}^{\mu} \vec{\phi}_i^k \eta_i \right) \right] \right\} = \sum_{k=1}^N \omega^B \cdot m^k \left\{ \left[\vec{\omega}^B \left(\vec{p}^k + \sum_{i=1}^{\mu} \vec{\phi}_i^k \eta_i \right) \right] \times \vec{\phi}_r^k \right\} \\
&= \omega^{BT} \sum_{k=1}^N \left[\vec{\omega}^B \left(\vec{p}^k + \sum_{i=1}^{\mu} \vec{\phi}_i^k \eta_i \right) \right] \times m^k \vec{\phi}_r^k = -\omega^{BT} \sum_{k=1}^N m^k \vec{\phi}_r^k \times \left[\vec{\omega}^B \left(\vec{p}^k + \sum_{i=1}^{\mu} \vec{\phi}_i^k \eta_i \right) \right] \\
&= -\omega^{BT} \omega^B \left[N_r + \sum_{k=1}^N \sum_{i=1}^{\mu} \eta_i \left(\vec{\phi}_i^{kT} \vec{\phi}_r^k U - \vec{\phi}_r^k \vec{\phi}_i^{kT} \right) m^k \right]
\end{aligned} \tag{166}$$

If let

$$D_r = N_r + \sum_{k=1}^N \sum_{i=1}^{\mu} \eta_i \left(\bar{\phi}_i^{k^T} \bar{\phi}_r^k U - \bar{\phi}_r^k \bar{\phi}_i^{k^T} \right) m^k \quad (r=1, 2, \dots, \mu) \quad (167)$$

Then the Equation (166) can be simplified to:

$$\sum_{k=1}^N \bar{\phi}_r^{k^T} m^k \left\{ \bar{\omega}^B \left[\bar{\omega}^B \left(\bar{p}^k + \sum_{i=1}^{\mu} \bar{\phi}_i^k \eta_i \right) \right] \right\} = -\omega^{B^T} \omega^B D_r \quad (168)$$

Substituting Equations (165) and (168) into Equation (162), the expression for the vibration force vector of the flexible structure is as follows:

$$Z_1 = Y_1 + \left(m_{gen} \Omega^2 + k^g f \right) \eta + 2m_{gen} \xi \Omega \dot{\eta} - \phi^T f_{ext} \quad (169)$$

Where m_{gen} is the generalized mass, k^g is the geometrix stiffness, Ω is the modal frequency, and the ξ is the modal damping coefficient, the Y_{1r} can be expressed as below:

$$Y_{1r} = -\bar{\omega}^{B^T} \left(D_r \bar{\omega}^B - 2 \sum_{i=1}^{\mu} d_{1r} \dot{\eta}_i \right) - \sum_{k=1}^N \bar{\phi}_1^{k^T} \dot{m}^k \bar{V}_e \quad (r=1, 2, \dots, \mu) \quad (170)$$

Then,

$$Y_1 = \left\{ \begin{array}{c} -\bar{\omega}^{B^T} \left(D_1 \bar{\omega}^B - 2 \sum_{i=1}^{\mu} d_{1r} \dot{\eta}_i \right) - \sum_{k=1}^N \bar{\phi}_1^{k^T} \dot{m}^k \bar{v}_e^k \\ \vdots \\ -\bar{\omega}^{B^T} \left(D_{\mu} \bar{\omega}^B - 2 \sum_{i=1}^{\mu} d_{\mu i} \dot{\eta}_i \right) - \sum_{k=1}^N \bar{\phi}_{\mu}^{k^T} \dot{m}^k \bar{v}_e^k \end{array} \right\} \quad (171)$$

Assembling the translational, rotational, and vibrational equations in matrix form together, the dynamic equations in matrix for the rigid-flexible structure system can be obtained as below:

$$\left[\begin{array}{cc} M_{1(6 \times 6)} & A_{1(6 \times \mu)}^T \\ A_{1(\mu \times 6)} & E_{1(\mu \times \mu)} \end{array} \right] \left\{ \begin{array}{c} \bar{a}_{(3 \times 1)}^B \\ \bar{\alpha}_{(3 \times 1)}^B \\ \ddot{\eta}_{(\mu \times 1)} \end{array} \right\} = \left\{ \begin{array}{c} -X_{1(6 \times 1)} \\ -Z_{1(\mu \times 1)} \end{array} \right\} \quad (172)$$

High-order state variables can be obtained by left-multiplying the inverse of the system matrix with the right-hand vector of Equation (172). Given the initial conditions for

low-order state variables, the values of high-order state variables at each time step can be obtained through numerical integration.

3.7. Determinations in improved Kane's dynamic equation for marine structures

To formulate the mathematical model for ship motion accurately, it is imperative to determine the added mass components (D. T. Sen & Vinh, 2016). With the improved Kane's dynamic equation, in this study, the influence due to added mass is also included.

The objective of this part is to develop a comprehensive methodology for calculating all components of added mass and inertia moment in all six degrees of freedom, thereby facilitating the simulation of ship's movement.

The inertia matrix of the system, denoted as M_1 from above section which is with respect to time history due to variable mass, encompasses the inertia contributions from both the rigid body and added mass as shown below:

$${}_tM_1 = {}_tM_I + {}_tM^a \quad (173)$$

Where, M_I is inertia matrix of rigid body in global coordinate, M^a stands for added inertia moment matrix of hull girder in the ocean.

$${}_tM_I = \begin{bmatrix} {}_t m^B & 0 & 0 & 0 & {}_t m z_g & -{}_t m y_g \\ 0 & {}_t m^B & 0 & -{}_t m z_g & 0 & {}_t m x_g \\ 0 & 0 & {}_t m^B & {}_t m y_g & -{}_t m x_g & 0 \\ 0 & -{}_t m z_g & {}_t m y_g & {}_t I_x & -{}_t I_{xy} & -{}_t I_{xz} \\ {}_t m z_g & 0 & -{}_t m x_g & -{}_t I_{yx} & {}_t I_y & -{}_t I_{yz} \\ -{}_t m y_g & {}_t m x_g & 0 & -{}_t I_{zx} & -{}_t I_{zy} & {}_t I_z \end{bmatrix} \quad (174)$$

$${}_tM^a = \begin{bmatrix} {}_t m_{11}^a & {}_t m_{12}^a & {}_t m_{13}^a & {}_t m_{14}^a & {}_t m_{15}^a & {}_t m_{16}^a \\ {}_t m_{21}^a & {}_t m_{22}^a & {}_t m_{23}^a & {}_t m_{24}^a & {}_t m_{25}^a & {}_t m_{26}^a \\ {}_t m_{31}^a & {}_t m_{32}^a & {}_t m_{33}^a & {}_t m_{34}^a & {}_t m_{35}^a & {}_t m_{36}^a \\ {}_t m_{41}^a & {}_t m_{42}^a & {}_t m_{43}^a & {}_t m_{44}^a & {}_t m_{45}^a & {}_t m_{46}^a \\ {}_t m_{51}^a & {}_t m_{52}^a & {}_t m_{53}^a & {}_t m_{54}^a & {}_t m_{55}^a & {}_t m_{56}^a \\ {}_t m_{61}^a & {}_t m_{62}^a & {}_t m_{63}^a & {}_t m_{64}^a & {}_t m_{65}^a & {}_t m_{66}^a \end{bmatrix} \quad (175)$$

In the case of ships, where the hull exhibits symmetry along the port-starboard (x-y) plane, it can be deduced that vertical motions caused by heave and pitch do not generate transverse forces, hence:

$${}_i m_{32}^a = {}_i m_{34}^a = {}_i m_{36}^a = {}_i m_{52}^a = {}_i m_{54}^a = {}_i m_{56}^a = 0 \quad (176)$$

Thanks to the symmetry of the added mass matrix, it can be inferred that $m_{ij}^a = m_{ji}^a$, then the following components in added matrix can be generated as below:

$${}_i m_{23}^a = {}_i m_{43}^a = {}_i m_{63}^a = {}_i m_{25}^a = {}_i m_{45}^a = {}_i m_{65}^a = 0 \quad (177)$$

Similarly, the same rationale applies to longitudinal motions induced by acceleration in a particular direction $i = (2,4,6)$:

$${}_i m_{12}^a = {}_i m_{14}^a = {}_i m_{16}^a = 0 \quad (178)$$

$${}_i m_{21}^a = {}_i m_{41}^a = {}_i m_{61}^a = 0 \quad (179)$$

Consequently, for a ship experiencing motion in six degrees of freedom, the thirty-six components of added mass have been reduced to eighteen components as below:

$${}_i M^a = \begin{bmatrix} {}_i m_{11}^a & 0 & {}_i m_{13}^a & 0 & {}_i m_{15}^a & 0 \\ 0 & {}_i m_{22}^a & 0 & {}_i m_{24}^a & 0 & {}_i m_{26}^a \\ {}_i m_{31}^a & 0 & {}_i m_{33}^a & 0 & {}_i m_{35}^a & 0 \\ 0 & {}_i m_{42}^a & 0 & {}_i m_{44}^a & 0 & {}_i m_{46}^a \\ {}_i m_{51}^a & 0 & {}_i m_{53}^a & 0 & {}_i m_{55}^a & 0 \\ 0 & {}_i m_{62}^a & 0 & {}_i m_{64}^a & 0 & {}_i m_{66}^a \end{bmatrix} \quad (180)$$

The challenge lies in predicting and determining the remaining components in the added mass matrix could be solved by commercial software such as SESAM.

Ultimately, under the assumption of symmetry in marine structures, the final time-varying inertia tensor can be expressed as follows:

$${}_i M_1 = \begin{bmatrix} {}_i m^B + {}_i m_{11}^a & 0 & {}_i m_{13}^a & 0 & {}_i m z_g + {}_i m_{15}^a & -{}_i m y_g \\ 0 & {}_i m^B + {}_i m_{22}^a & 0 & -{}_i m z_g + {}_i m_{24}^a & 0 & {}_i m x_g + {}_i m_{26}^a \\ {}_i m_{31}^a & 0 & {}_i m^B + {}_i m_{33}^a & {}_i m y_g & -{}_i m x_g + {}_i m_{35}^a & 0 \\ 0 & -{}_i m z_g + {}_i m_{42}^a & {}_i m y_g & {}_i I_x + {}_i m_{44}^a & -{}_i I_{xy} & -{}_i I_{xz} + {}_i m_{46}^a \\ {}_i m z_g + {}_i m_{51}^a & 0 & -{}_i m x_g + {}_i m_{53}^a & -{}_i I_{yx} & {}_i I_y + {}_i m_{55}^a & -{}_i I_{yz} \\ -{}_i m y_g & {}_i m x_g + {}_i m_{62}^a & 0 & -{}_i I_{zx} + {}_i m_{64}^a & -{}_i I_{zy} & {}_i I_z + {}_i m_{66}^a \end{bmatrix} \quad (181)$$

3.8. The Runge-Kutta time integration method

Once the aforementioned modules have independently computed the loads and the second derivative of the degrees of freedom (acceleration) of the variable-mass hull girder, it is necessary to link these modules through a time integral module to iteratively

update the displacement and first derivatives (velocity) of the degrees of freedom for the next time step.

In this study, the Fourth Order Runge-Kutta (RK4) method is primarily employed for the time integral module. The RK4 method is selected for time integration due to its high accuracy, stability, and computational efficiency. It significantly improves accuracy over lower-order methods by evaluating derivatives at multiple points within each time step, which is crucial for capturing dynamic behaviour accurately. RK4 also maintains stability, essential for stiff equations and long-term integrations, while balancing complexity and performance better than higher-order methods. Its widespread use and proven reliability, combined with ease of implementation, make RK4 a trusted and practical choice for dynamic analysis of complex systems like marine vessels.

Assuming that at time t_0 , the displacements and velocities of the system degrees of freedom are known to be X_n and \dot{X}_n respectively, the second derivative of the degrees of freedom with respect to time (acceleration) at next time step can be obtained through the dynamic control equation:

$$\ddot{X}_n = f(X_n, \dot{X}_n, t_n) \quad (182)$$

Where t_n stands for the current time, X_n and \dot{X}_n express the vector of system states (positions and velocities respectively) at time t_n , $f(X_n, \dot{X}_n, t_n)$ is the acceleration (second derivative \ddot{X}_n) calculated at time based on the current states.

To construct the first intermediate term based on the fourth-order Runge Kutta method, it calculates the values at the midpoint of the time step, which can denote

$$t_n^{(1)} = t_n + \frac{\Delta t}{2} \quad (183)$$

$$X_n^{(1)} = X_n + \frac{\Delta t}{2} \cdot \dot{X}_n \quad (184)$$

$$\dot{X}_n^{(1)} = \dot{X}_n + \frac{\Delta t}{2} \cdot \ddot{X}_n \quad (185)$$

$$\ddot{X}_n^{(1)} = f(X_n^{(1)}, \dot{X}_n^{(1)}, t_n^{(1)}) \quad (186)$$

Where Δt as the time step.

To construct the second intermediate term for the Runge-Kutta method:

$$t_n^{(2)} = t_n + \frac{\Delta t}{2} \quad (187)$$

$$X_n^{(2)} = X_n + \frac{\Delta t}{2} \cdot \dot{X}_n^{(1)} \quad (188)$$

$$\dot{X}_n^{(2)} = \dot{X}_n + \frac{\Delta t}{2} \cdot \ddot{X}_n^{(1)} \quad (189)$$

$$\ddot{X}_n^{(2)} = f\left(X_n^{(2)}, \dot{X}_n^{(2)}, t_n^{(2)}\right) \quad (190)$$

To construct the third intermediate term for the Runge-Kutta method:

$$t_n^{(3)} = t_n + \Delta t \quad (191)$$

$$X_n^{(3)} = X_n + \Delta t \cdot \dot{X}_n^{(2)} \quad (192)$$

$$\dot{X}_n^{(3)} = \dot{X}_n + \Delta t \cdot \ddot{X}_n^{(2)} \quad (193)$$

$$\ddot{X}_n^{(3)} = f\left(X_n^{(3)}, \dot{X}_n^{(3)}, t_n^{(3)}\right) \quad (194)$$

The final values of the system's degrees of freedom (displacements and velocities) at time $t_n + \Delta t$ can be obtained by using the Runge-Kutta method as below

$$X_{n+1} = X_n + \frac{\Delta t}{6} \left(\dot{X}_n + 2\dot{X}_n^{(1)} + 2\dot{X}_n^{(2)} + \dot{X}_n^{(3)} \right) \quad (195)$$

$$\dot{X}_{n+1} = \dot{X}_n + \frac{\Delta t}{6} \left(\ddot{X}_n + 2\ddot{X}_n^{(1)} + 2\ddot{X}_n^{(2)} + \ddot{X}_n^{(3)} \right) \quad (196)$$

Where $t_n^{(1)}, t_n^{(2)}, t_n^{(3)}$ represent the successive time intervals computed by the Runge-Kutta method, X_{n+1} indicates the degrees of freedom information for the next time step, $X_n^{(1)}, X_n^{(2)}, X_n^{(3)}$ represent the intermediate values of the degrees of freedom during the Runge-Kutta method calculations.

3.9. Multiple point constraints technology in FEA

Multiple Point Constraints (MPC) technology in Finite Element Analysis (FEA) is a numerical technique used to model and analyse complex structural systems where traditional constraints are complex. In FEA, constraints are used to define the

relationships between degrees of freedom (DOFs) at different nodes in a finite element model. MPC technology extends this concept to allow the imposition of constraints on multiple points or nodes simultaneously, providing a more flexible and powerful approach to modelling certain physical behaviours.

The theoretical underpinnings of ANSYS Workbench MPC technology are deeply rooted in structural mechanics and numerical analysis. The key formulations include:

(1) Equation of motion

The dynamic behaviour of structures is governed by the equations of motion. For a dynamic system with mass M , damping C , and stiffness K matrices, the equation of motion is given by:

$$M\ddot{U} + C\dot{U} + KU = F \quad (197)$$

Where \ddot{U} is the acceleration vector, \dot{U} is the velocity vector, U is the displacement vector, F is the force vector.

(2) Compatibility and equilibrium

MPCs ensure compatibility and equilibrium among multiple points in a surface structure. The compatibility equation is given by:

$$CU = 0 \quad (198)$$

Where C is the compatibility matrix, U is the displacement vector.

(3) Matrix algebra

Matrix algebra is employed to efficiently handle interconnected DOFs. The overall system matrix equation is:

$$KU = F \quad (199)$$

Where K is the global stiffness matrix, U is the displacement vector and F is the force vector.

(4) Constraint enforcement

MPC technology enforces constraints by introducing relationships between selected DOFs. The MPC equation is formulated as:

$$C_{MPC}U_{MPC} = 0 \quad (200)$$

Where C_{MPC} is the MPC constraint matrix and U_{MPC} is the MPC displacement vector.

(5) Lagrange multipliers:

The introduction of Lagrange multipliers facilitates the incorporation of constraints into the equations of motion. The augmented equations become:

$$M\ddot{U} + C\dot{U} + KU = F + C_{MPC}^T \lambda \quad (201)$$

Where the λ is the vector of Lagrange multipliers.

(6) Virtual work principle:

The virtual work principle is employed to derive the equations of motion with constraints. The virtual work done by applied forces and constraint forces must be zero:

$$\delta W = \delta \left(\frac{1}{2} U^T K U \right) - \delta \left(\frac{1}{2} U^T F \right) = 0 \quad (202)$$

In traditional FEA, constraints are typically applied between pairs of nodes, specifying how the displacements or rotations at one node are related to those at another node. However, there are situations where a constraint needs to involve more than two nodes or where a complex relationship between multiple nodes must be defined. This is where MPC technology comes into play.

MPCs enable the user to define more sophisticated constraints involving multiple nodes, allowing for the modelling of various physical scenarios. This can include simulating interactions between different parts of a structure, enforcing symmetry conditions, or representing complex connections such as hinges or sliding interfaces.

In this study, the dynamic response information of each node on the hull girder, computed by using in-house program, is applied to the corresponding cross-sections of a three-dimensional ship finite element model using MPC technology to facilitate finite element analysis.

3.10. Outline of proposed mathematical and numerical model

Utilizing the foundational methodologies elucidated in the preceding sections, this section provides a detailed exposition of the outline and application of the proposed mathematical and numerical model. The complexity of the model is visually distilled in the illustrative depiction presented in the following Figure 30, offering a

comprehensive representation of the model's conceptual framework and its practical implementation.

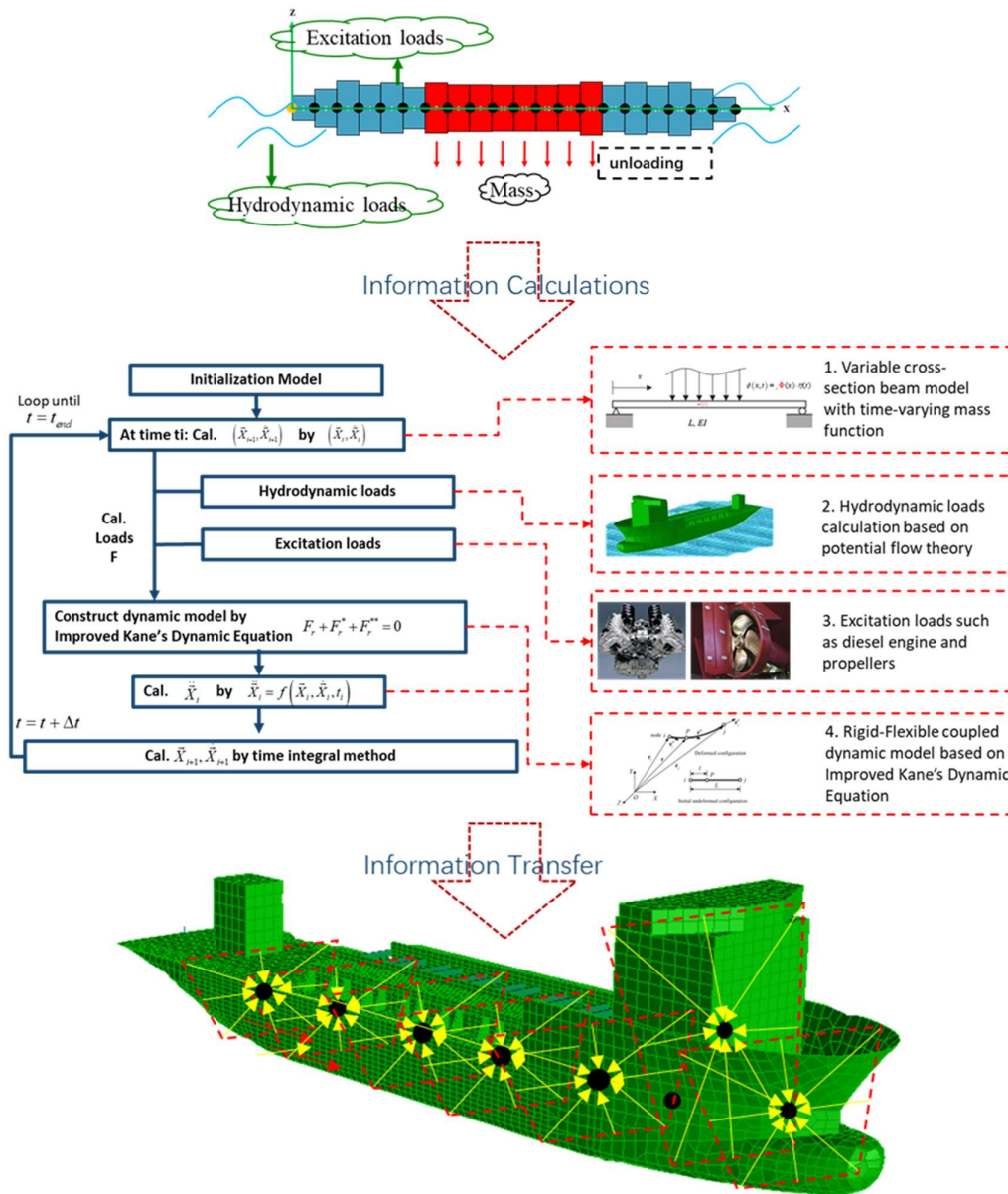


Figure 30. Outline and application of proposed model.

3.10.1. Outline of TVM_HullGirder program

The outline of the TVM_HullGirder program based on proposed model in this paper is shown in Figure 31. The proposed model is a dynamic response calculation program in time-domain compiled by FORTRAN language for analysing variable cross-section hull girder with time-varying mass characteristics subjected to various complex loads.

Firstly, the program is initialized by pre-defined input parameters including structure data, environment data and simulation data by users as well as pre-calculated files from SESAM for hydrodynamic analysis. Based on input data, the vibration analysis of the hull girder and pre-computed hydrodynamic files are calculated and generated as an initial task.

Secondly, all user-defined excitation loads are computed and updated at every time step to construct dynamic equation with results generated by initial module based on improved Kane's dynamic equation. Then the acceleration vector at current time step would be solved.

Finally, the displacement and velocity information of the next time step would be calculated by the time integral method such as fourth order Runge-Kutta method based on current results program stored to realize the closed-loop calculation of the user-defined simulation time.

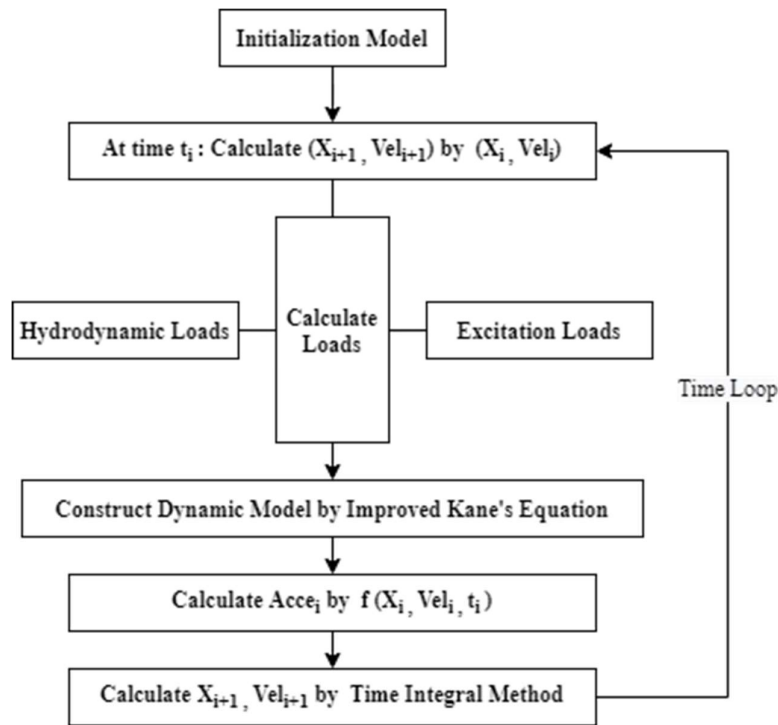


Figure 31. The outline of TVM_HullGirder program.

3.10.2. Application of TVM_HullGirder program in FEA

The dynamic response calculation results of the TVM_HullGirder program, including the motion response results of the hull girder in the global coordinate system and the

structural dynamic response results in the local coordinate system, can be seamlessly transferred to the three-dimensional finite element model of the vessel by using MPC technology. Further analysis, such as stress, strain, strength, and fatigue analysis and assessments etc, can be conducted using commercial finite element software, as illustrated in the Figure 32.

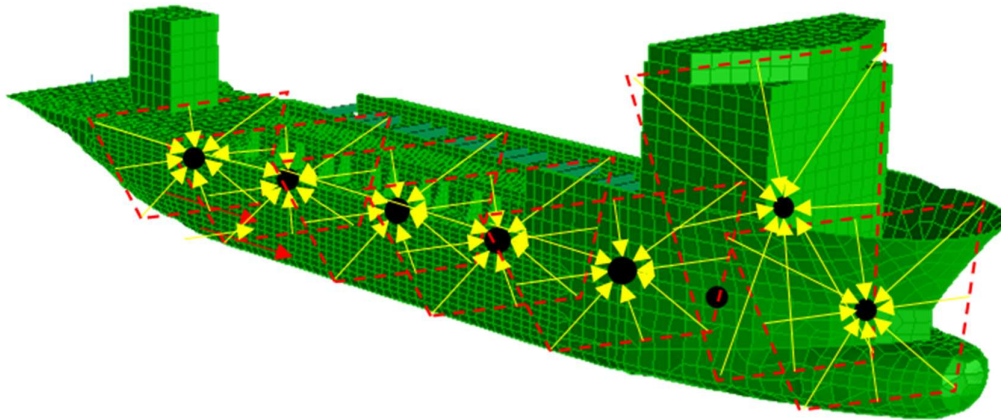


Figure 32. Dynamic response information transferred into FEM by MPC in selected cross-section.

3.11. Summary of Chapter 3

In Chapter 3, it concludes by presenting the foundational theories and methodologies underlying the innovative mathematical and numerical model developed for this research. This includes an in-depth exploration of the time-varying mass Euler-Bernoulli beam theory, semi-analytical methods for analysing vibration characteristics of beams with variable cross-sections, and advanced techniques for calculating time-varying hydrodynamic and excitation loads. Additionally, the chapter details the improved Kane's dynamic equations adapted for systems with time-varying mass, which serve as the primary approach for dynamic analysis. The chapter also introduces the self-developed program, TVM_HullGirder, which is designed for the comprehensive dynamic analysis of marine vessels with varying mass in the time domain.

Chapter 4. Case studies and discussions

This chapter firstly verified the feasibility and efficiency of the semi-analytical approach for the vibration analysis of the variable cross-section beam compared with FEA results. Secondly, SESAM software is utilized to pre-calculate hydro parameters for ten load cases during unloading working conditions. Thirdly, a self-developed program TVM_HullGirder is employed for vibration analysis of the three-dimensional hull girder model, and its effects on time-varying hydrodynamic results are assessed and compared. Fourthly, the program is utilized to calculate the dynamic response of the three-dimensional hull girder model, producing results that encompass the rigid-flexible coupling motion response of the hull girder and structural dynamic response outcomes for selected cross-section of the hull girder. Finally, results outputted by TVM_HullGirder program are transferred into the corresponding sections of the ship's finite element model using MPC technology for structural response assessment by FEA.

4.1. Verifications of the semi-analytical approach

In this part, it employs the finite element software ABAQUS to conduct a comparative analysis and validation of the proposed semi-analytical approach in pre-calculation module of the TVM_HullGirder program for vibration analysis of a designed variable cross-section Euler-Bernoulli beam.

The purpose of this calculation and comparison are to verify the semi-analytical approach proposed in this research. To verify the semi-analytical solutions of variable cross-section Euler-Bernoulli beam, the compared results between this approach and ABAQUS software have been shown in part 4.1.1 and 4.1.2 for axial and transverse vibration analysis of two-dimensional cantilever Euler-Bernoulli beam respectively (Y. Zhang & Hu, 2023).

4.1.1. Vibration analysis results of the cantilever Euler-Bernoulli beam in axial direction

A designed example and calculation results to prove the accuracy of proposed semi-analytical approach in axial direction of a three-dimensional cantilever Euler-Bernoulli beam is shown as below.

Table 1 shows the designed model of a three-dimensional cantilever Euler-Bernoulli beam with detailed parameters and the Figure 33 shows the geometric model of this Euler-Bernoulli beam in ABAQUS.

Table 1. The Euler-Bernoulli beam parameters for vibration analysis in axial direction.

Section num.	Cross-section shape	Area of cross-section (m ²)	Length of beam element (m)	Young's Modulus (Pa)	Density of material (kg/m ³)
Section 1	Circle	4.00E-04	0.25	2.10E+11	7800
Section 2	Circle	3.00E-04	0.25	2.10E+11	7800
Section 3	Circle	2.00E-04	0.25	2.10E+11	7800
Section 4	Circle	1.00E-04	0.25	2.10E+11	7800

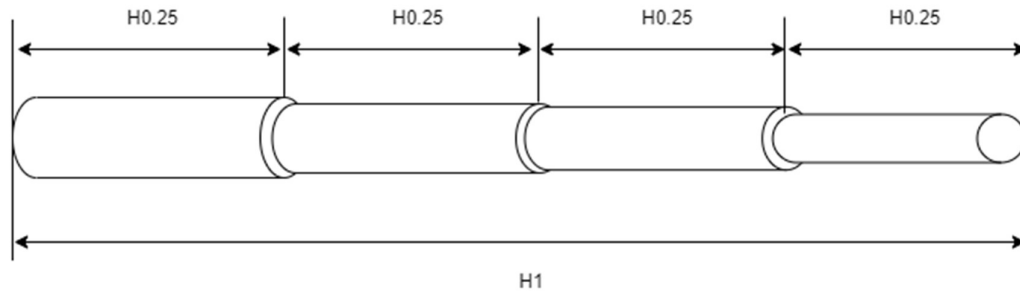


Figure 33. The geometric model of the cantilever Euler-Bernoulli beam in ABAQUS.

To verify the suitability of the semi-analytical method for vibration analysis of a variable cross-section beam, results were compared with FEA. The selection of a variable cross-section beam with circular sections and the provided parameters for this analysis is justified for several reasons:

- (1) Simplicity and clarity: Circular sections with varying areas simplify the geometry, making it easier to isolate and evaluate the numerical method's performance against FEA without additional geometric complexities.

(2) Analytical benchmark: The simplicity of circular sections allows for more accessible analytical solutions, providing a reliable benchmark for verifying the accuracy of the numerical method.

(3) Material consistency: Using the same material properties (Young's Modulus and density) across sections ensures that any variations in the results are due to changes in the cross-sectional area rather than material inconsistencies.

(4) Gradient complexity: The gradual change in the cross-sectional area provides a clear gradient, testing the numerical method's ability to handle varying stiffness and mass distribution along the beam length.

(5) Comprehensive testing: The given sections with specific lengths and material properties provide a comprehensive test scenario to evaluate the numerical method's robustness in handling both stiffness and mass variations.

Natural frequency results of first eight mode orders of the designed cantilever Euler-Bernoulli beam in axial direction are shown in the Table 2 computed by two calculation methods, which are FEA from ABAQUS and the proposed semi-analytical approach respectively. It also shows the difference percentage between these two methods.

Table 2. Natural frequency analysis results of the cantilever Euler-Bernoulli beam in axial direction outputted from ABAQUS software and the semi-analytical approach.

Mode order num.	Natural frequency from ABAQUS (rad/s)	Natural frequency from semi-analytical approach (rad/s)	Difference percentage (%)
1 st	11067.20	11068.54	0.01
2 nd	25385.95	25402.01	0.06
3 rd	39740.52	39801.68	0.15
4 th	53981.99	54135.15	0.28
5 th	75844.33	76272.24	0.56
6 th	89887.25	90605.71	0.80
7 th	103886.20	105005.40	1.08

8 th	117702.90	119338.80	1.39
-----------------	-----------	-----------	------

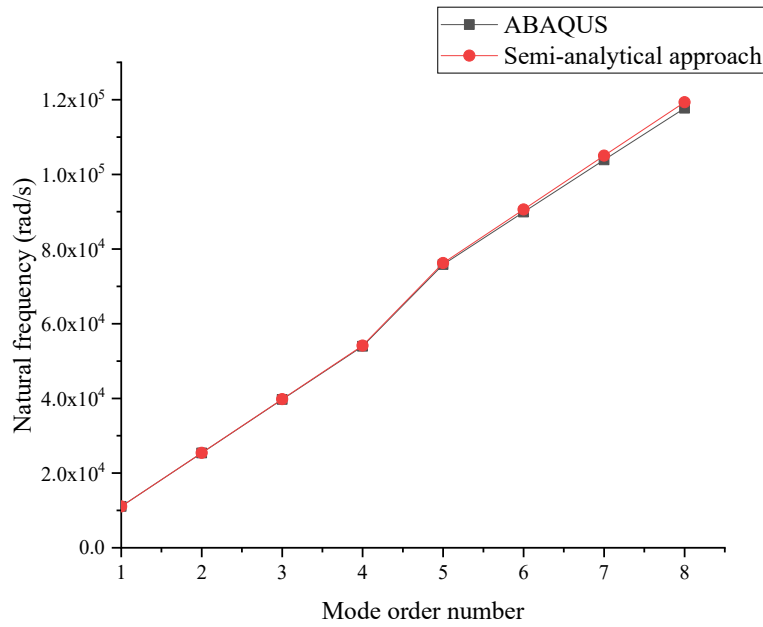


Figure 34. Natural frequency results in axial calculated by ABAQUS and the semi-analytical approach.

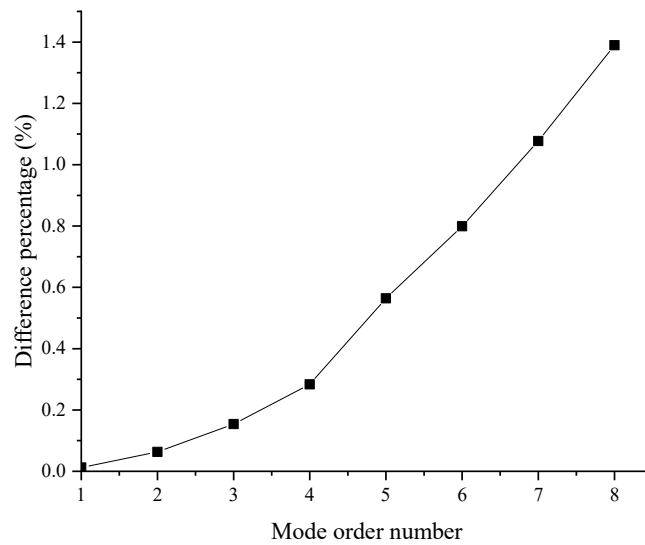


Figure 35. Difference percentage in axial of ABAQUS and the semi-analytical approach.

From the detailed results of Table 2 and the comparison curves of Figure 34 and Figure 35, it can be readily observed that the results of the two methods in calculating the natural frequencies of axial beam vibration are almost identical. In this computational case, the natural frequencies of eight mode orders were selected for comparisons. For large structures like ships, the chosen mode order is sufficient to assess the accuracy and applicability of the methods.

Moreover, from the comparison results, it can be observed that the natural frequency calculation results of the two methods are nearly identical in low-order modes, with only minor deviations appearing in higher-order modes. The results of the semi-analytical approach are consistently slightly higher than the FEA calculation results in all selected mode orders. The higher the mode order, the greater the discrepancy between the natural frequency calculation results of the two methods. However, overall, the percentage deviation is entirely acceptable.

4.1.2. Vibration analysis results of the cantilever Euler-Bernoulli beam in transverse

A designed example and calculation results to prove the accuracy of proposed semi-analytical approach in transverse direction of a three-dimensional cantilever Euler-Bernoulli beam is shown below.

Table 3 shows the designed model of a three-dimensional cantilever Euler-Bernoulli beam with detailed parameters and the Figure 36 shows the geometric model of this Euler-Bernoulli beam in ABAQUS.

Table 3. The Euler-Bernoulli beam parameters for vibration analysis in transverse direction.

Section num.	Cross-section shape	Radius of cross-section (m)	Length of beam element (m)	Young's Modulus (Pa)	Density of material (kg/m ³)
Section 1	Circle	9.40E-03	0.25	2.10E+11	7900
Section 2	Circle	8.15E-03	0.25	2.10E+11	7900
Section 3	Circle	6.90E-03	0.25	2.10E+11	7900
Section 4	Circle	5.65E-03	0.25	2.10E+11	7900

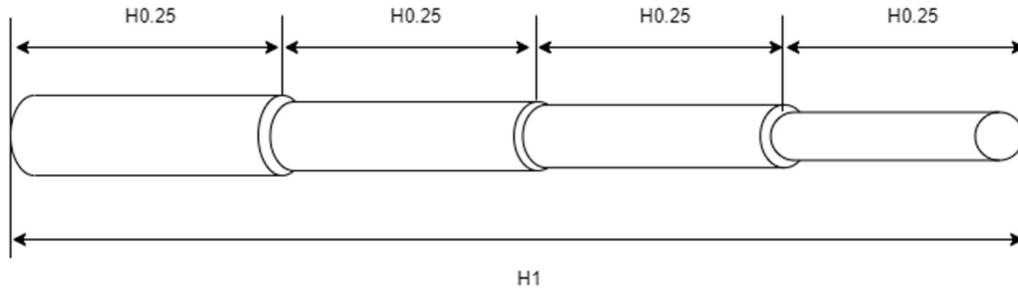


Figure 36. Geometric model of the cantilever Euler-Bernoulli beam in ABAQUS.

The natural frequency results of first eight mode orders of the designed cantilever Euler-Bernoulli beam in transverse direction are shown in the Table 4 computed by two calculation methods, which are FEA from ABAQUS and the proposed semi-analytical approach respectively. It also shows the difference percentage between these two methods.

Table 4. Natural frequency analysis results of the cantilever Euler-Bernoulli beam in transverse direction outputted from ABAQUS software and the semi-analytical approach.

Mode order num.	Natural frequency from ABAQUS (rad/s)	Natural frequency from semi-analytical approach (rad/s)	Difference percentage (%)
1 st	114.44	114.46	0.02
2 nd	479.13	479.56	0.09
3 rd	1187.21	1189.71	0.21
4 th	2230.09	2238.45	0.37
5 th	3804.66	3829.34	0.65
6 th	5569.73	5620.61	0.91
7 th	7707.58	7801.40	1.22
8 th	10224.63	10388.75	1.61

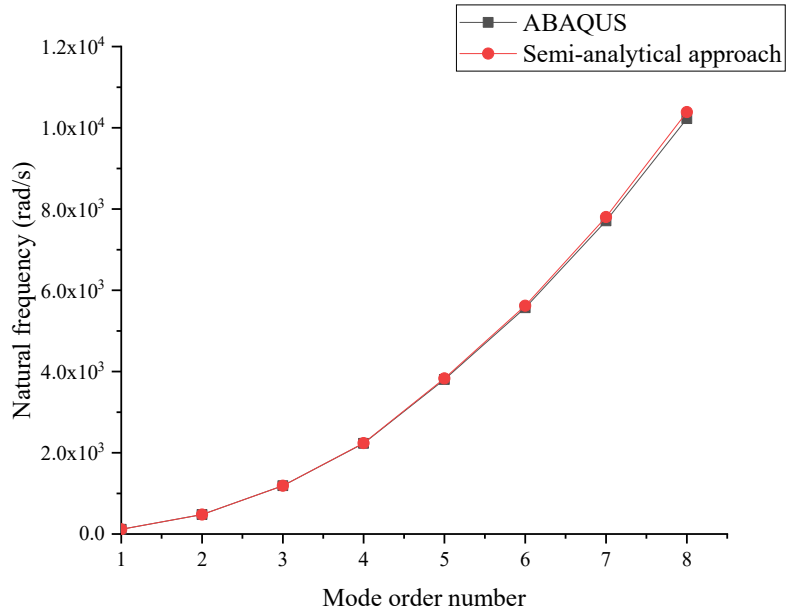


Figure 37. Natural frequency results in transverse calculated by ABAQUS and the semi-analytical approach.

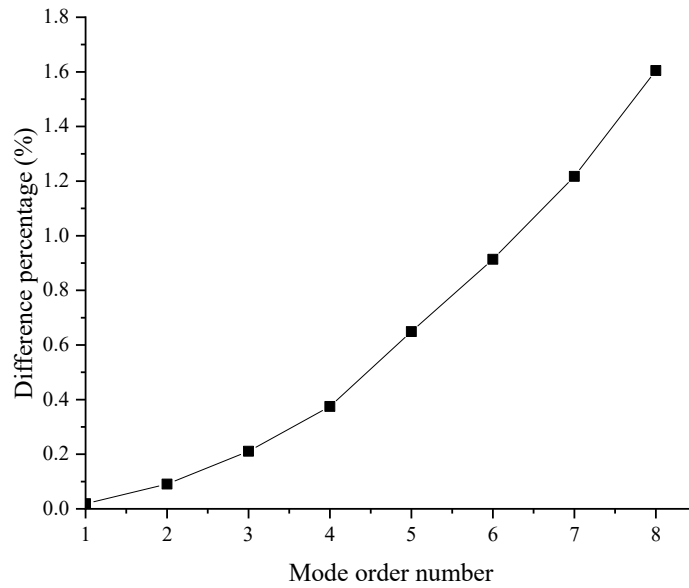


Figure 38. Difference percentage in transverse of ABAQUS and the semi-analytical approach.

Similar to the results in section 4.1.1, from the comparison results, it can be observed that the natural frequency calculation results of the two methods are nearly identical in low-order modes, with only minor deviations appearing in higher-order modes. The results of the semi-analytical approach are consistently slightly higher than the FEA calculation results in all selected mode orders. The higher the mode order, the greater the discrepancy between the natural frequency calculation results of the two methods. However, overall, the percentage deviation is entirely acceptable.

Furthermore, for transverse vibration analysis by using the semi-analytical approach in the TVM_HullGirder program, it is necessary to generate the mode shapes of the beam in selected mode orders to effectively prove that the mode shape results are also reasonable. The **Error! Reference source not found.** shows transverse mode shapes in eight selected mode orders computed by the semi-analytical method.

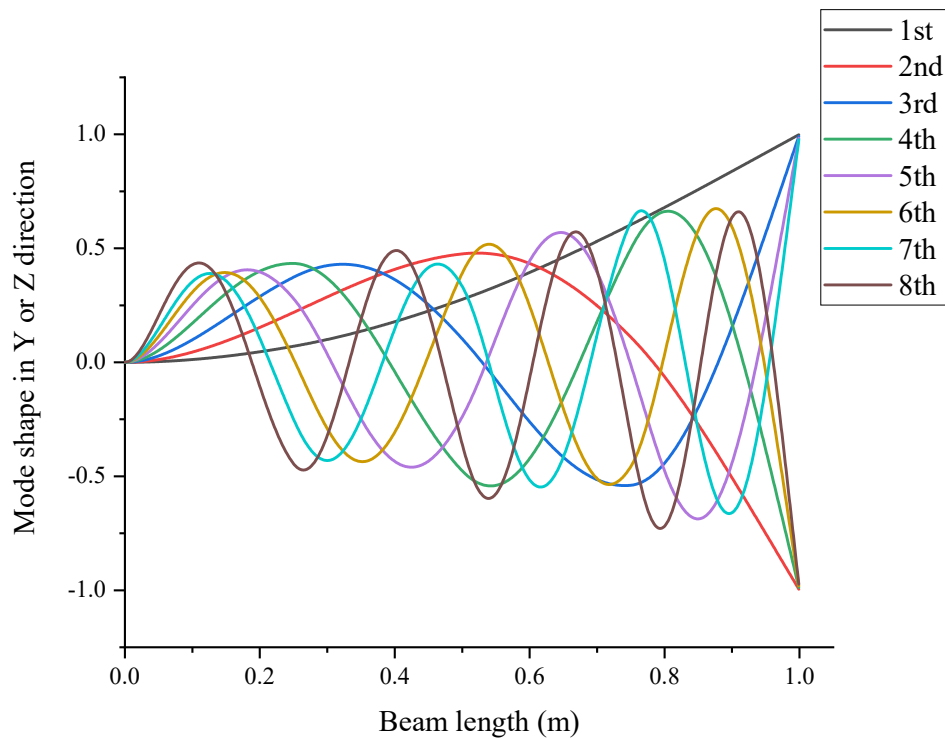


Figure 39. Mode shape generated by the semi-analytical approach.

In terms of the above results, the proposed semi-analytical approach has performed a good result as well as FEA. That proves this approach not only has the same accuracy as results of the FE analysis, but also has higher computational efficiency than FEA and

can obtain the mode analytical solution of the variable cross-section beam to support further dynamic analysis based on improved Kane’s dynamic equation with time-varying mass system. That means this method could be applied to the further dynamic model constructed by Kane’s dynamic method.

4.2. Model descriptions and case settings

In pursuit of examining the structural dynamic responses of TSHDs with variable-mass features operating under rapid unloading conditions, this chapter presents a case of study with a numerical model, which is built for a TSHD vessel. The self-developed programme, TVM_HullGirder, was employed to generate essential data, encompassing the vessel’s motions during unloading scenarios and the dynamic responses of specific cross-sections on the hull structure. The main scantlings of the TSHD vessel are shown in Table 5.

Table 5. The main scantlings of the dredging ship.

The main scantlings	
Overall length (m)	138.0
Length between perpendiculars (m)	128.60
Breadth (m)	27.15
Depth (m)	10.40
International freeboard draft (m)	7.35
Dredging freeboard draft (m)	8.90
Displacement (t)	22000.0
Light weight (t)	9060.0
Dead weight (t)	13000.0

The following figures show basic structural diagram of a TSHD from the side and top views, and the hull lines plan of the target research TSHD (Figure 40, Figure 41 and Figure 42).

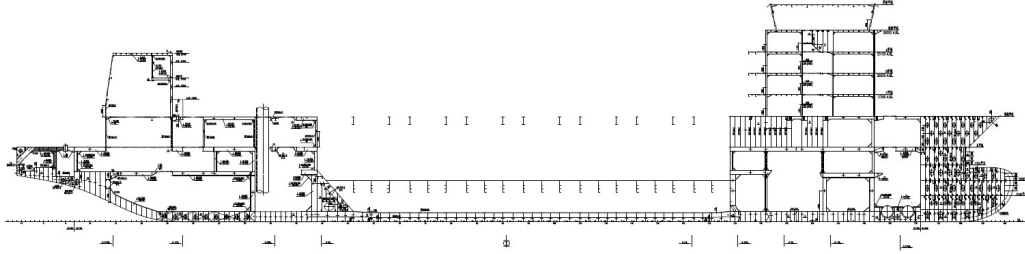


Figure 40. Basic structural diagram of a TSHD from the side view.

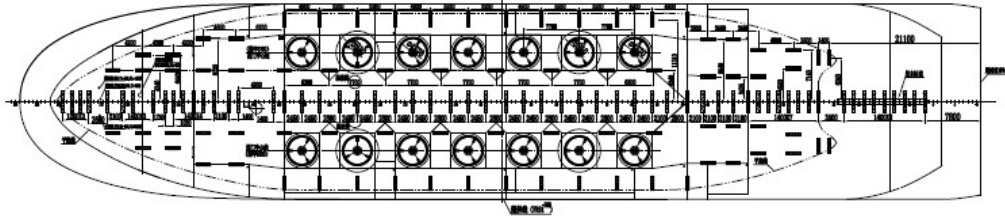


Figure 41. Basic structural diagram of a TSHD from the top view.

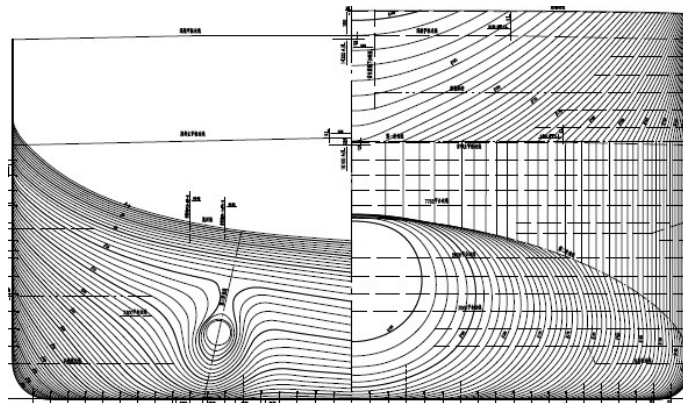


Figure 42. Hull lines plan of a TSHD.

In the initial stage of numerical simulation, this model is strategically segmented and approximated to determine structural profile parameters for equivalent beam elements along different segments of the hull girder. These parameters calculated by ANSYS/Spaceclaim are then utilized as input data for TVM_HullGirder programme to complete the model's establishment.

Within the pre-calculation module, a hydrodynamic model was generated by SESAM software. Additionally, different mass models are defined for various loading conditions and corresponding drafts. These results serve as input files for TVM_HullGirder program, thus finalizing the preparation of input data for the pre-calculation module. Finally, using the TVM_HullGirder programme, the dynamic

response results of the hull girder are generated under specific unloading condition. In post-progress, dynamic response results outputted by the TVM_HullGirder programme are transferred to FEM in ANSYS by MPC technology for stress, strain and other further assessments.

The program initialization process involves a series of file inputs, model establishment and parameters configuration.

(1) Numerical modelling

As in shown in the Figure 43, the middle section of the hull girder, consisting of beam elements numbered 07 to 14, is defined as the variable-mass beam elements, representing the hopper of the TSHD. This section experiences a significant mass variation during unloading conditions. Beam elements numbered 01 - 06 represent the stern part of the vessel, while beam elements numbered 15 - 20 represent the bow part of the ship's structure, meanwhile, they are all considered as invariant-mass beam elements.

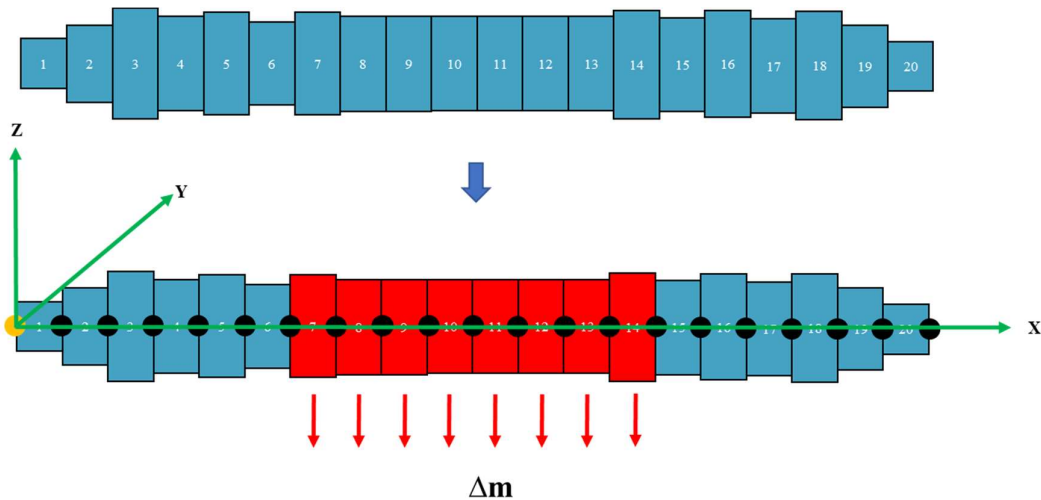


Figure 43. Hull girder model with defined variable-mass beam elements in the middle.

Using the rigid-flexible coupled hull girder dynamics model based on Kane's equation, the aftmost point of the stern on the hull girder is chosen as the reference point to represent the rigid body motion of the vessel. This is because it is the easiest way to simulate the flexible deformation of the hull girder by employing mode shapes of a cantilever beam when the reference point represented for the rigid body is located on the end of the hull girder. By combining the rigid body motion and flexible deformation

modelling, this way provides a comprehensive understanding of the hull girder's dynamics, ensuring precise and reliable analysis.

Therefore, the left node in the beam element 01 serves as the reference point for the hull girder (highlighted in yellow in Figure 43) and is considered the reference point for rigid body motion in the dynamic model. The other nodes (highlighted in black in Figure 43) represent the dynamic response data of the hull girder's cross-section at their respective positions.

(2) Structural properties

The structural section attributes are those matching the structural property of the real-scale TSHD vessel (Table 6 and Table 7).

Table 6. Structural property data as input.

Structure data	
Young's modulus (Pa)	2.10E+11
Num. of beam elements	20
Num. of modal orders selected	2
Coefficient of density change (kg/m ³)	8150
Damping ratio of structure	0.05
Length of each beam element (m)	6.75

The following figure (Figure 44) show example of the cross-section parameter calculation in ANSYS/Spaceclaim for inputs of structural parameters in the programme. The key cross-section parameters are calculated for relevant ship frames in three-dimensional geometric model of full-scale vessel by ANSYS/Spaceclaim module, which are cross-section areas, second moment of areas about Y and Z axis respectively.

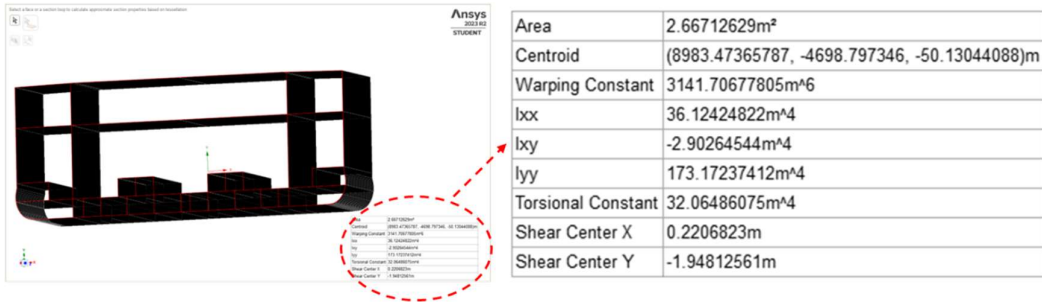


Figure 44. Example of cross-sectional parameters calculation in ANSYS/Spaceclaim.

Based on above calculations of key cross-sectional parameters by ANSYS/Spaceclaim, main structural parameters for each equivalent beam element as a representative in the variable cross-section hull girder can be obtained as shown in the following table (Table 7) in this case study.

Table 7. Main parameters in each beam element.

Main parameters of each beam element					
Element ID	Variable mass (1-No / 2-Yes)	Equivalent Cross-section area (m ²)	Equivalent material density (kg/m ³)	Equivalent second moment of area about Y axis I _{yy} (m ⁴)	Equivalent second moment of area about Z axis I _{zz} (m ⁴)
1	1	1.5968	337500.00	4.5564	78.4726
2	1	2.1114	506250.00	17.1229	113.8862
3	1	2.2839	573750.00	30.6364	138.2759
4	1	2.2944	607500.00	33.9115	156.3682
5	1	2.9126	742500.00	42.6458	186.9058
6	1	2.0597	877500.00	35.2697	165.6185
7	2	2.1303	2497500.00	21.5129	179.9092

8	2	2.1303	2666250.00	21.5129	179.9092
9	2	2.1303	2801250.00	21.5129	179.9092
10	2	2.1303	2666250.00	21.5129	179.9092
11	2	2.1303	2565000.00	21.5129	179.9092
12	2	2.1303	2598750.00	21.5129	179.9092
13	2	2.1303	2598750.00	21.5129	179.9092
14	2	2.1303	2531250.00	21.5129	179.9092
15	1	2.6671	540000.00	36.1242	173.1724
16	1	2.253	573750.00	34.5681	168.3403
17	1	1.8127	405000.00	25.7684	87.8449
18	1	1.5439	371250.00	21.1778	55.7969
19	1	1.3147	303750.00	14.0321	25.5842
20	1	0.7729	121500.00	3.624	6.1909

(3) Hydrodynamic analysis parameters settings.

The pre-calculation of hydrodynamic analysis for TSHD vessel is described here. The hydrodynamic model built in SESAM as panel model is shown in Figure 45.

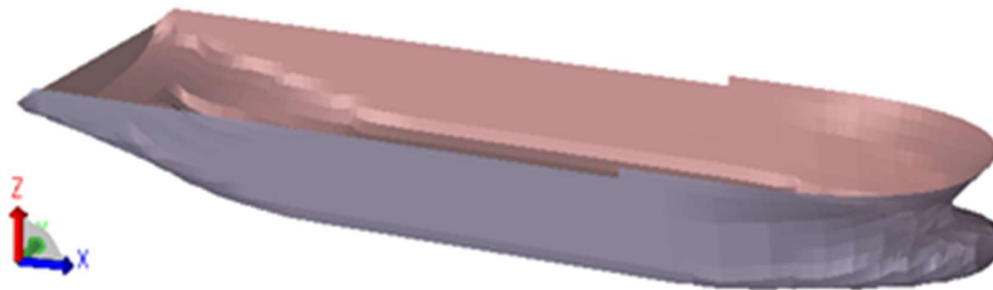


Figure 45. Panel model in SESAM.

Ten different drafts are defined in Table 8. The pre-processing results of hydrodynamic analysis in SESAM software, which mainly establishing panel model of the dredging vessel with variable mass models for defining different loading condition to compare key hydrodynamic parameters. Based on the loading manual of target vessel, it is

assumed that ten loading conditions are adopted during the unloading operation from fully weighted load to lighted load and vary approximately linearly (Figure 46) with drafts and trim characteristics (Table 8).

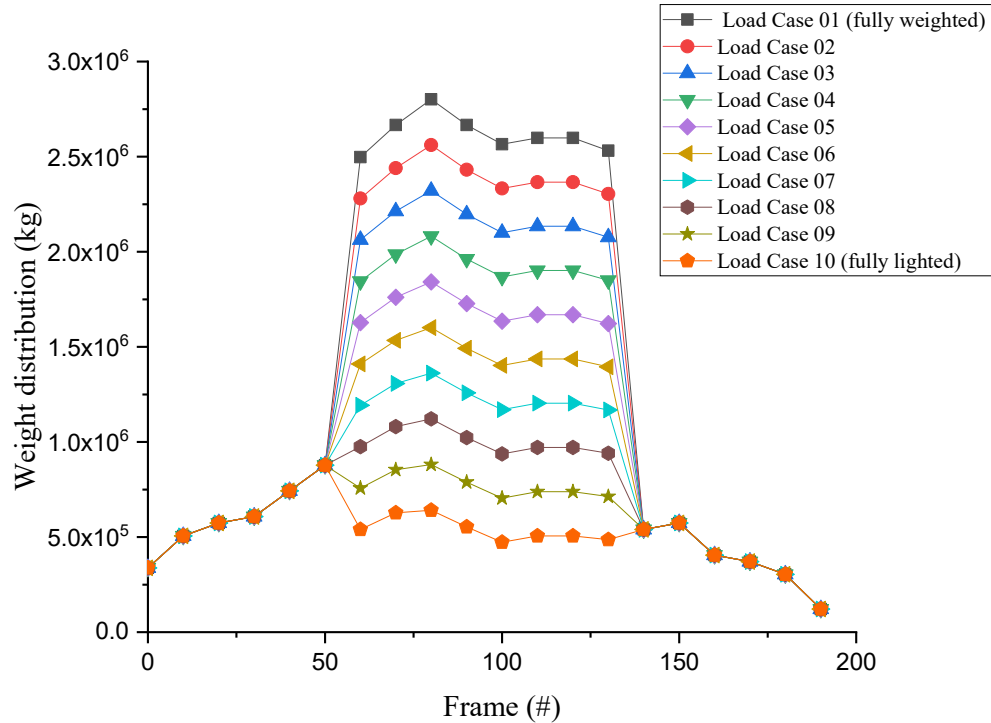


Figure 46. Weight distribution along with ship frame in ten load cases.

Table 8. Hydro parameters in ten load cases.

Load case	LC01	LC02	LC03	LC04	LC05	LC06	LC07	LC08	LC09	LC10
Z-waterline (m)	1.56	1.22	0.87	0.52	0.18	-0.17	-0.52	-0.87	-1.21	-1.56
Trim (deg)	-0.19	-0.36	-0.54	-0.72	-0.90	-1.07	-1.25	-1.43	-1.60	-1.78
Draft AP (m)	1.56	1.22	0.87	0.52	0.18	-0.17	-0.52	-0.87	-1.21	-1.56
Draft FP (m)	1.24	0.58	-0.08	-0.73	-1.39	-2.04	-2.70	-3.36	-4.01	-4.67

(4) Simulation parameters settings

In this case study, the duration of the unloading operation is defined as 4 minutes (240 seconds). This duration represents the typical operation time required for a TSHD to

transition from a fully loaded condition to a completely lighted condition. The total simulation time is set to 360 seconds. The time when mass variation begins is set at 60 seconds, and the time when mass variation ends is defined at 300 seconds. The time step size for dynamic analysis calculations is set as 0.0125 seconds. Table 9 shows key simulation parameters settings as inputs in the TVM_HullGirder programme.

Table 9. Simulation parameters as input.

Simulation data	
Total simulation time (s)	360.0
Time step (s)	0.0125
Mass changed start time (s)	60.0
Mass changed end time (s)	300.0

(5) Sea environmental parameters settings

Moreover, the hydrodynamic parameters settings are shown in Table 10. The irregular wave is chosen for wave type in this case study. The JONSWAP is selected for wave spectrum as most common case and gamma value is set with 3.3 being a commonly used value for moderately peaked spectra. Significant wave height is set as 0.8 meters. Wave direction is set with 0-degree as heading wave and 45-degree as oblique wave for different simulation cases to compare and discuss further respectively. Furthermore, in terms of recent study on TSHD, it presents that the structures of TSHDs play a crucial role in the dredging construction process, especially when encountering medium to long-period waves (Qi et al., 2023). Therefore, in this case study, the wave period is set as 20.0 meters.

Table 10. Sea environmental data as input.

Sea environmental data	
Wave type	Irregular wave
Wave spectrum	JONSWAP
Wave direction (°)	0° heading wave / 45° oblique wave

Significant wave height (m)	0.8
Peak period (s)	20.0
Gamma	3.3

(6) Definition of simulation cases

For the purpose of facilitating comparisons between the simulation results of different variable settings, Table 11 defines the simulation case descriptions used in this paper. These descriptions encompass the types of dynamic models, the types of hydrodynamic analysis, and whether added mass is considered in the dynamic model and vibration analysis module.

Table 11. Definitions for users as input.

Simulation cases (*/*/*/*)		Definitions
Dynamic analysis type (*/*/*/*)	5	3D rigid body (No mass changes)
	6	3D rigid body (mass changes)
	7	3D rigid-flexible body (No mass changes & No 'X' deflection)
	8	3D rigid-flexible body (mass changes & No 'X' deflection)
Hydrodynamic analysis type (-/*/*/*)	0	No time-varying wet surface - input pre-hydro analysis results of LC01 as constants
	1	Time-varying hydro cal. – input pre-hydro analysis results of LC01-10 as constants for relevant time period
	2	Time-varying hydro cal. – input pre-hydro analysis results of LC01-10 by linear interpolate method for each time step
Added mass function switch	0	Turn off - not take account to added mass in dynamic analysis

(-/-/*/-)	1	Turn on - take account to added mass in dynamic analysis
Wet mode function switch	0	Turn off – (Dry) not take account to added mass in vibration analysis
(-/-/*/*)	1	Turn on – (Wet) take account to added mass in vibration analysis

4.3. Pre-calculation results by SESAM

The status of deadweight of the TSHD with time-varying mass system can be expressed as below (Figure 47 and Figure 48):

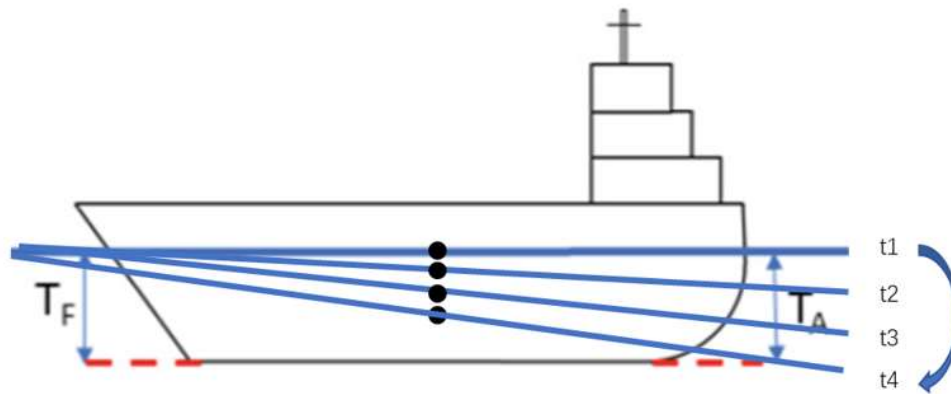


Figure 47. Variation in TSHD draft line.

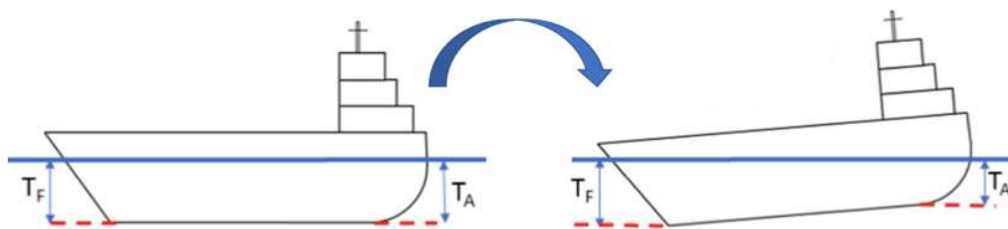


Figure 48. Variable draft line at the bow and stern of the TSHD.

The pre-calculation of hydrodynamic analysis for TSHD vessel is described here. The hydrodynamic model built in SESAM is shown in Figure 49. Ten different drafts and trims are based on Table 8 in section 4.2. The pre-processing results of hydrodynamic analysis in SESAM software, which mainly establishing panel model of the dredging

vessel with variable mass models for defining different loading condition to compare key hydrodynamic parameters.

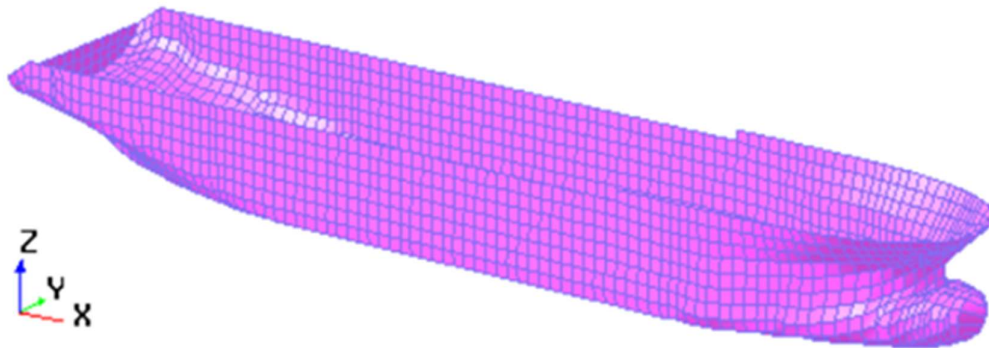


Figure 49. Approximation of the objective ship hull by 2408 quadrilateral elements.

In terms of data of real ship from loading manual, the following figure shows panel model with related mass model in fully weighted and lighted load case respectively in SESAM/HydroD program (Figure 50 and Figure 51).

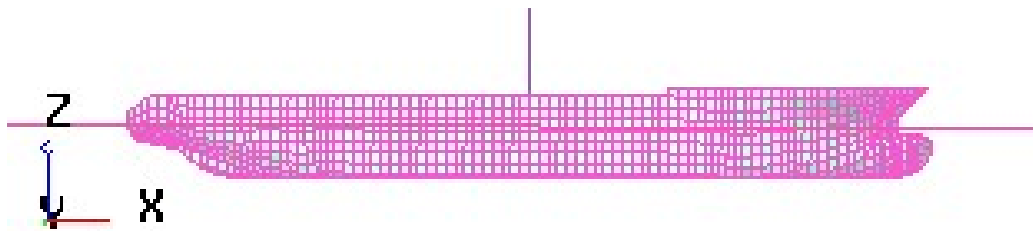


Figure 50. The panel model in fully weighted load case 01.

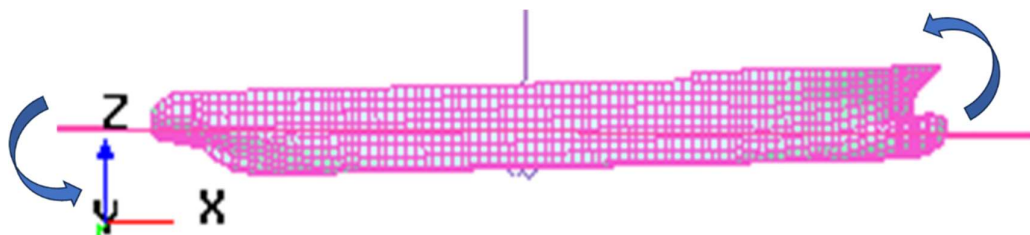


Figure 51. The panel model for fully lighted load case 10.

The following parts show added mass, damping coefficients and RAOs of the ten different load cases calculated by SESAM/WADAM during the unloading operation conditions of the TSHD.

4.3.1. Added mass

The following figures show added mass of ten different load cases calculated by SESAM/WADAM.

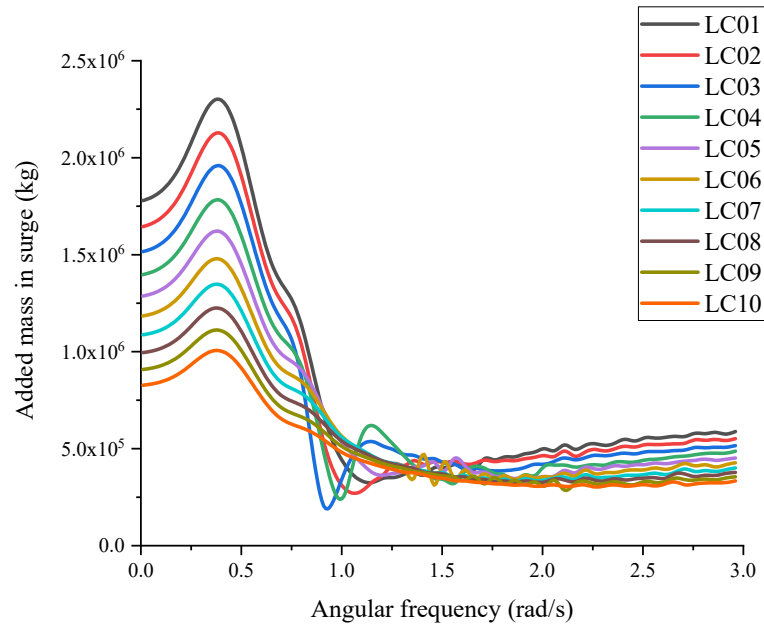


Figure 52. Added mass in surge with 10 load cases.

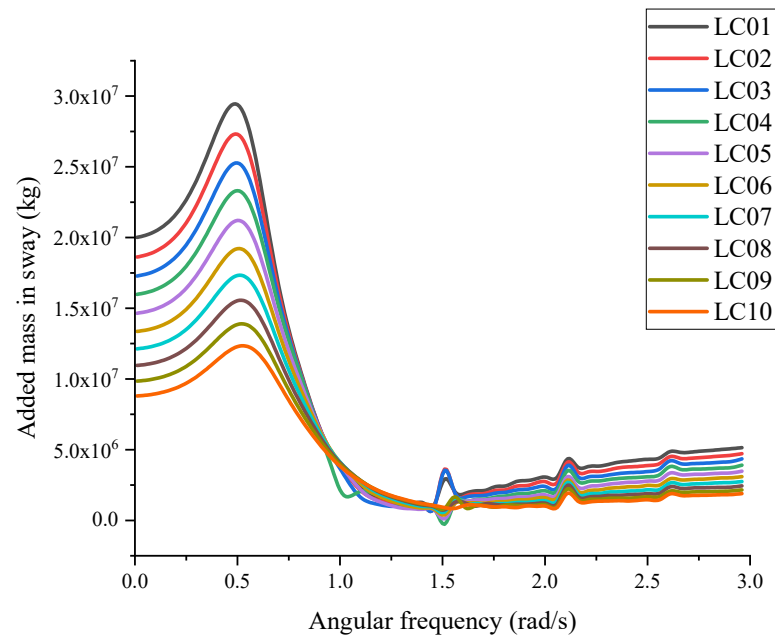


Figure 53. Added mass in sway with 10 load cases.

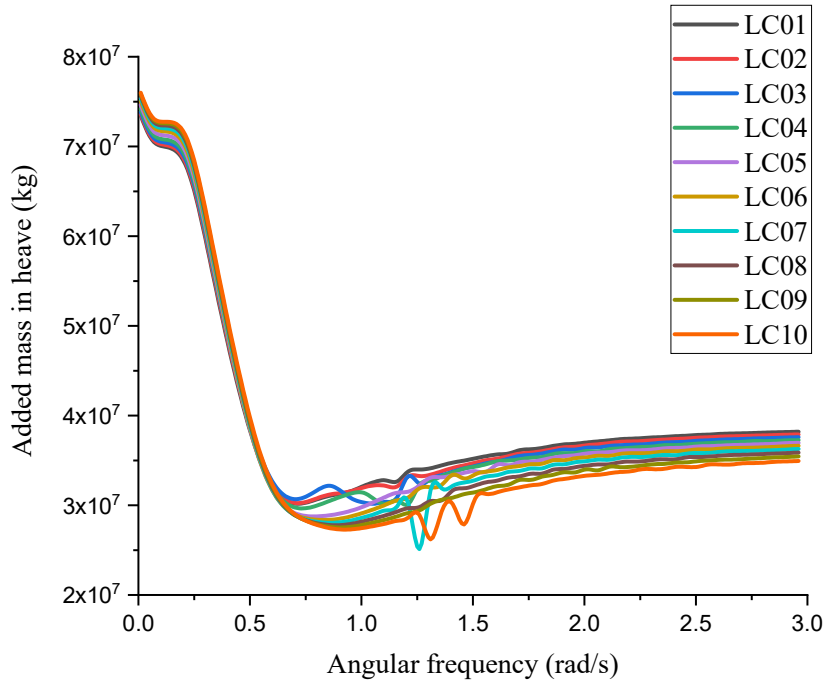


Figure 54. Added mass in heave with 10 load cases.

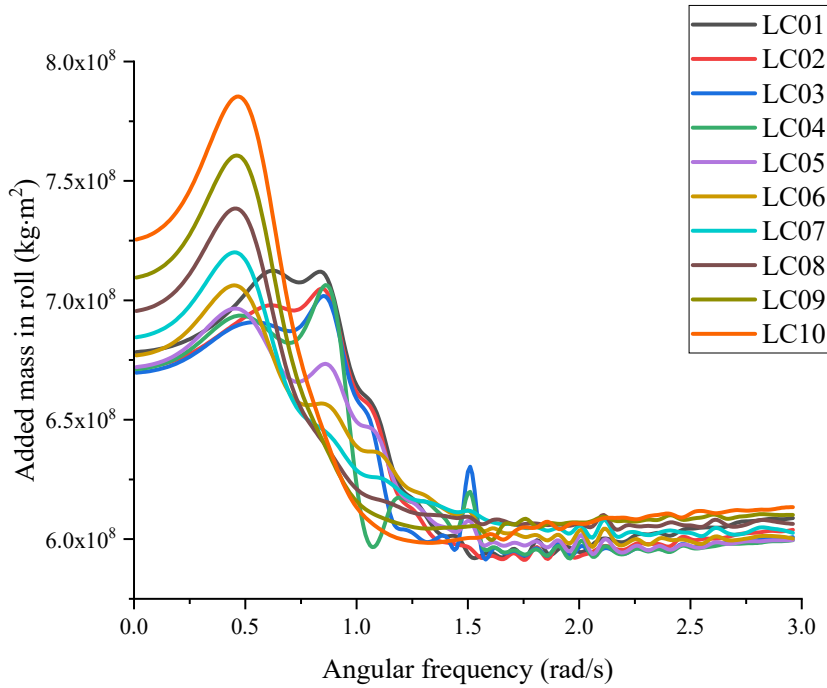


Figure 55. Added mass in roll with 10 load cases.

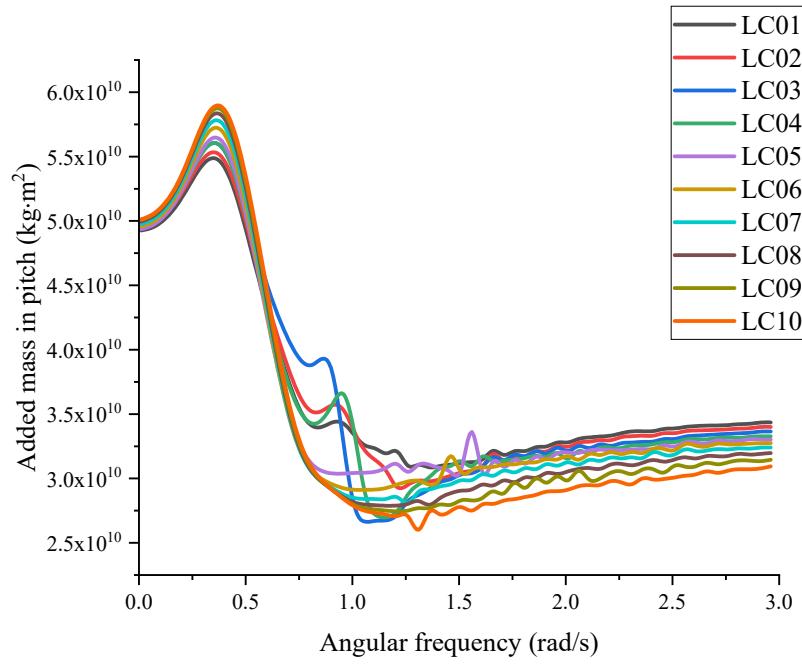


Figure 56. Added mass in pitch with 10 load cases.

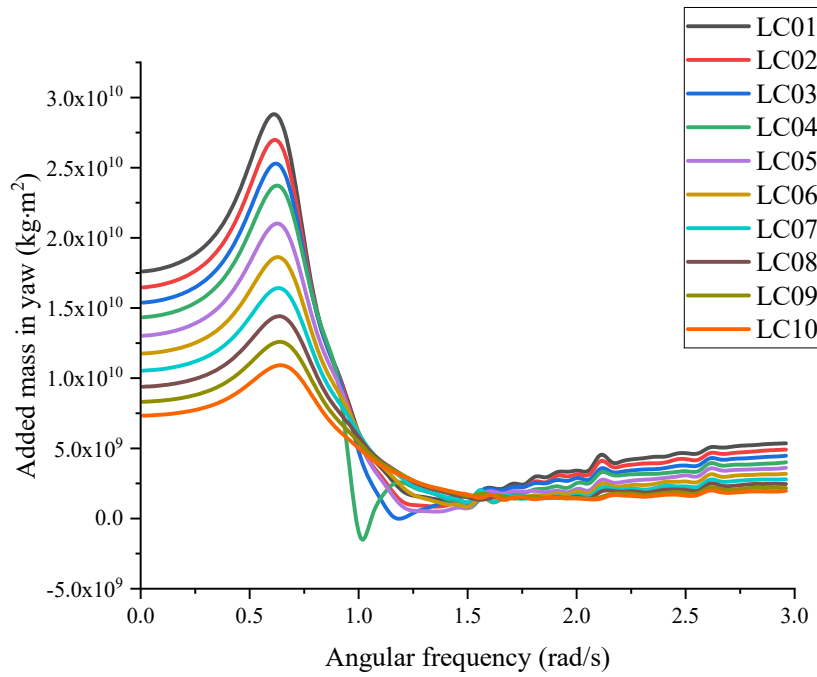


Figure 57. Added mass in yaw with 10 load cases.

4.3.2. Damping coefficients

The following figures show damping coefficients of ten different load cases calculated by SESAM/WADAM.

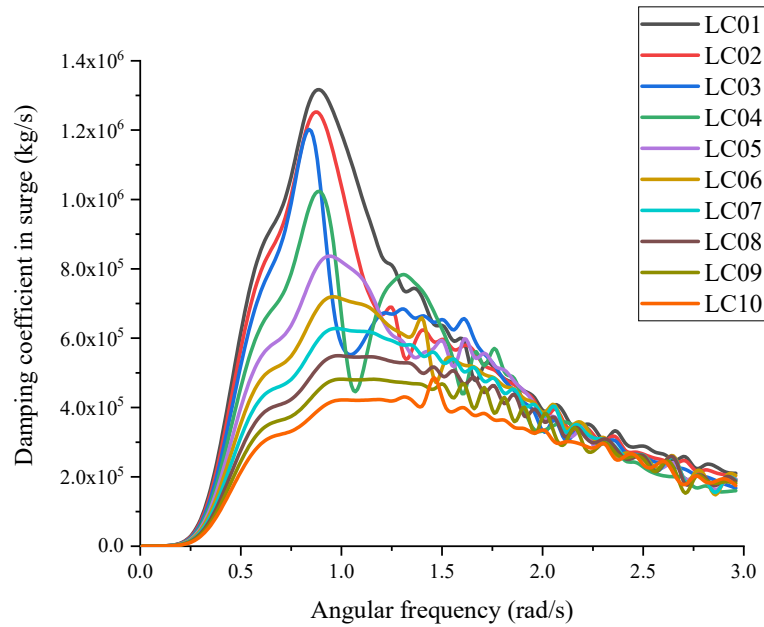


Figure 58. Damping coefficients in surge with 10 load cases.

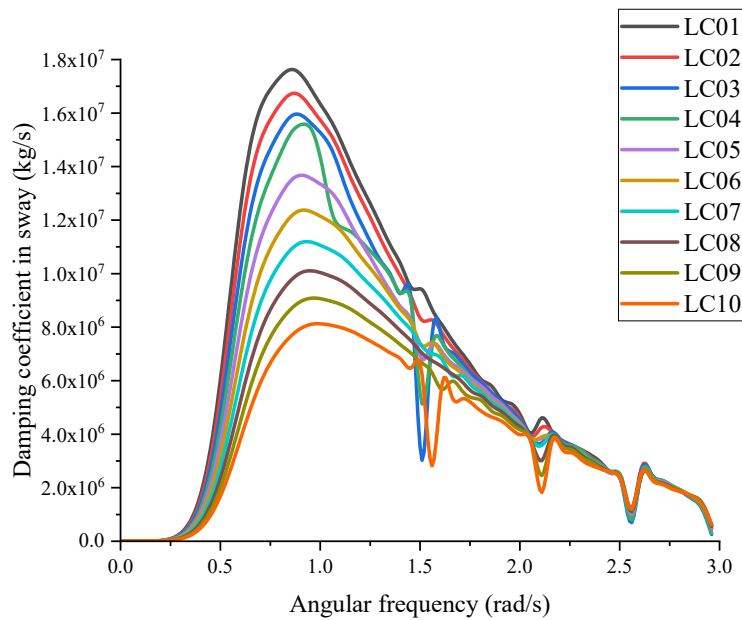


Figure 59. Damping coefficients in sway with 10 load cases.

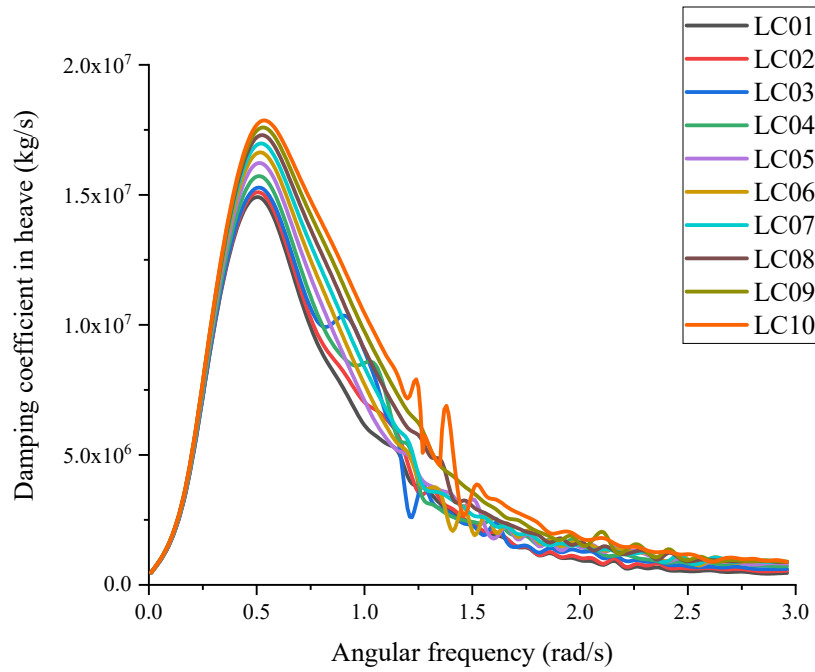


Figure 60. Damping coefficients in heave with 10 load cases.

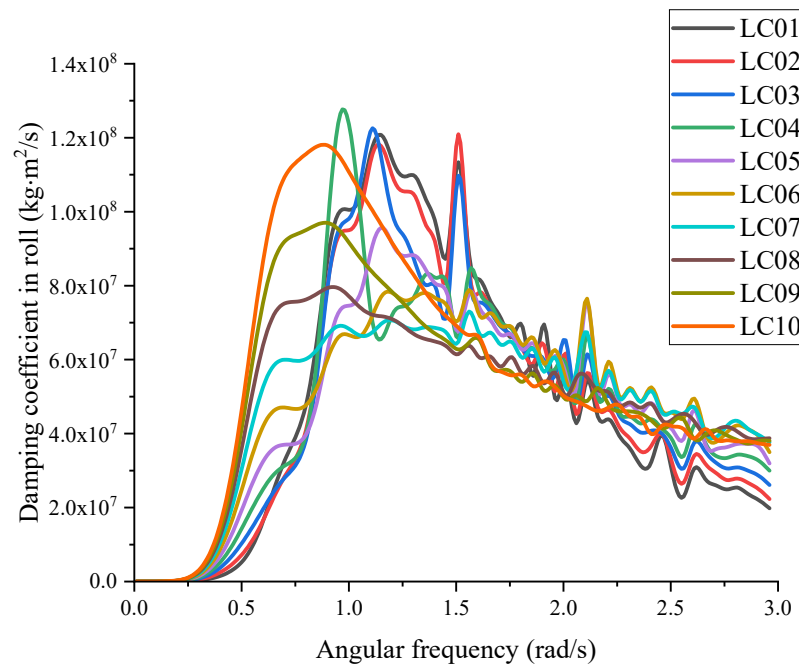


Figure 61. Damping coefficients in roll with 10 load cases.

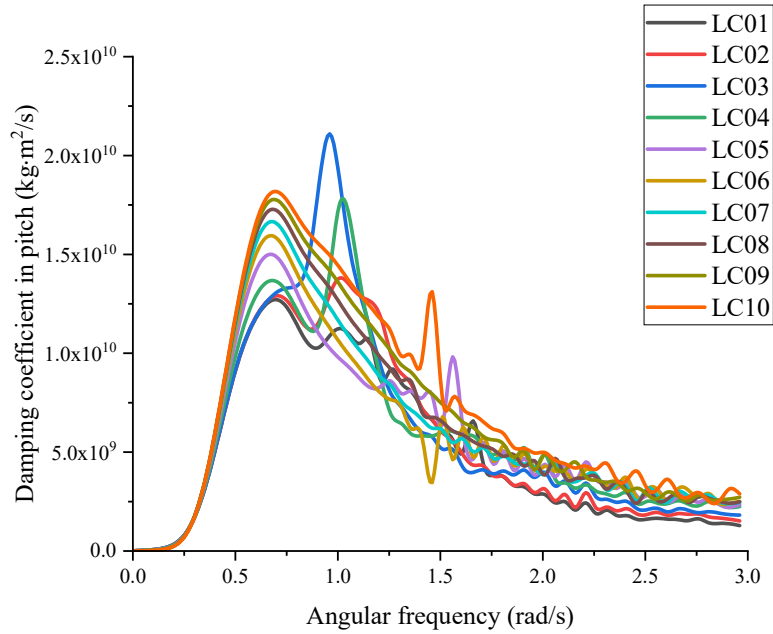


Figure 62. Damping coefficients in pitch with 10 load cases.

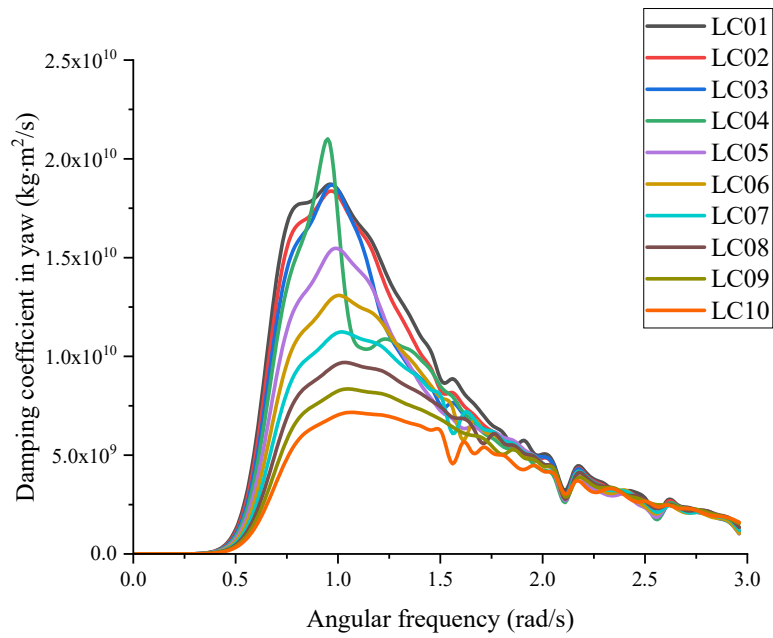


Figure 63. Damping coefficients in yaw with 10 load cases.

4.3.3. RAOs

The following figures show RAOs of ten different load cases calculated by SESAM/WADAM for 0-degree and 45-degree wave direction respectively.

(1) RAOs in 0-degree wave direction

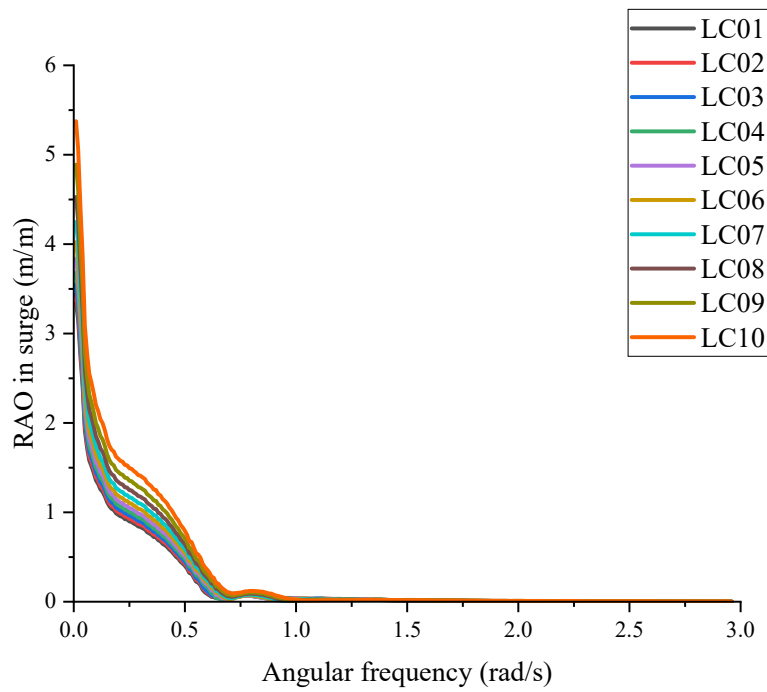


Figure 64. RAOs in surge with 10 load cases in 0-degree wave.

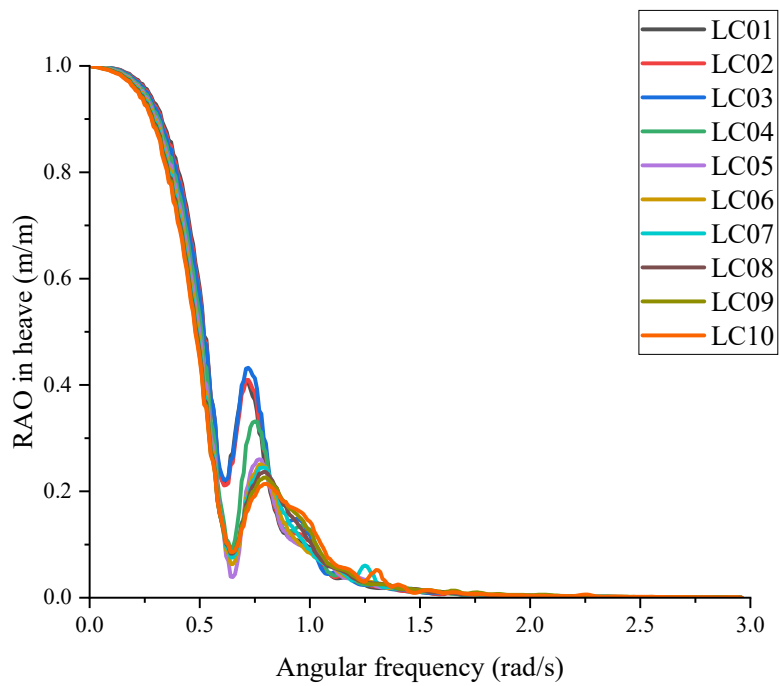


Figure 65. RAOs in heave with 10 load cases in 0-degree wave.

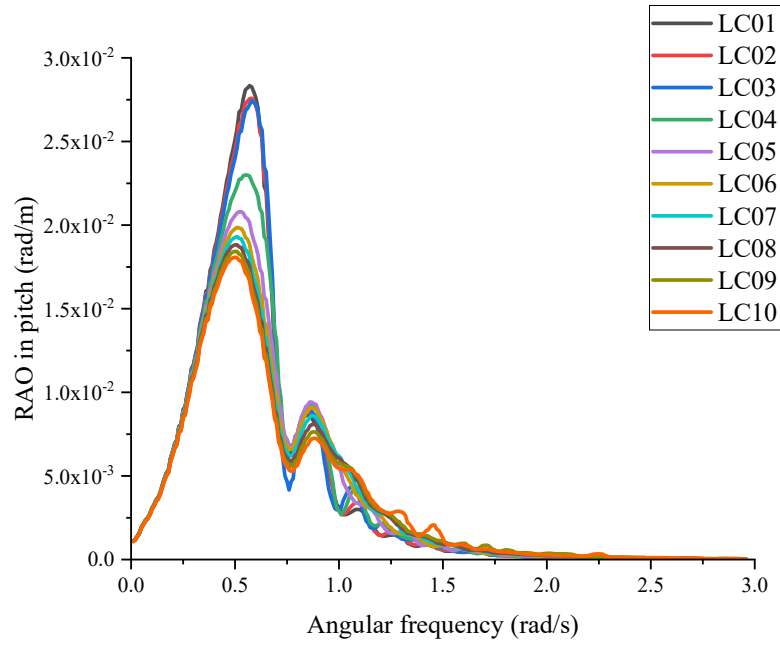


Figure 66. RAOs in pitch with 10 load cases in 0-degree wave.

(2) RAOs in 45-degree wave direction

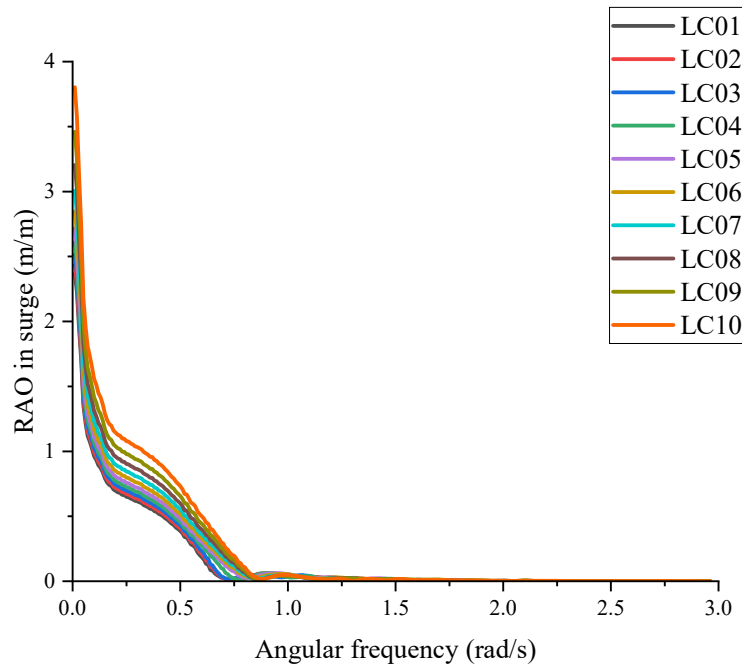


Figure 67. RAOs in surge with 10 load cases in 45-degree wave.

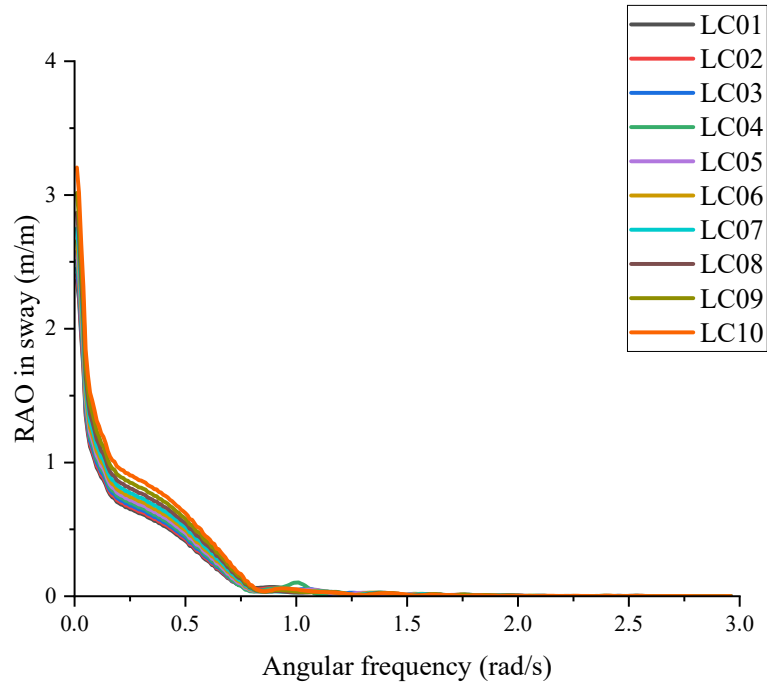


Figure 68. RAOs in sway with 10 load cases in 45-degree wave.

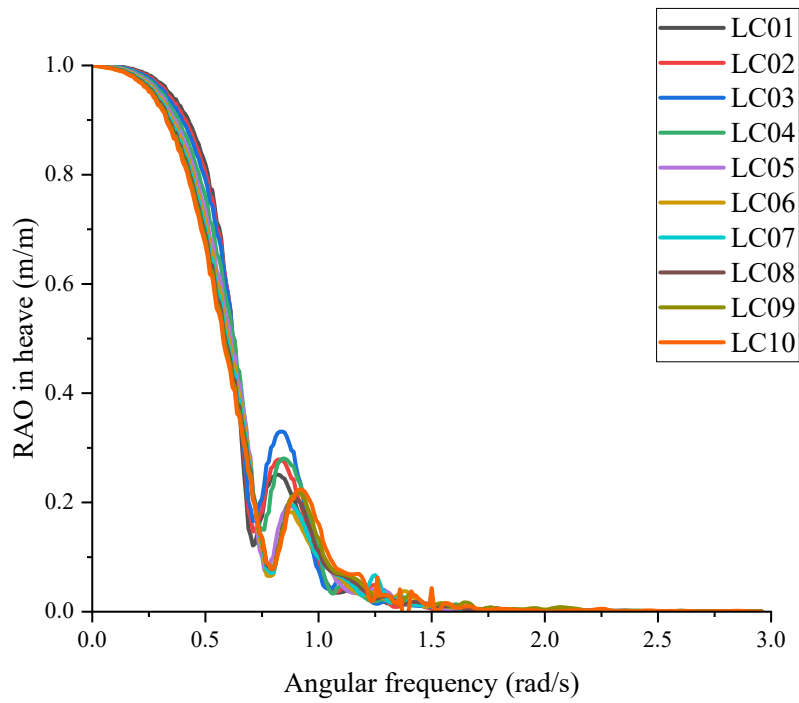


Figure 69. RAOs in heave with 10 load cases in 45-degree wave.

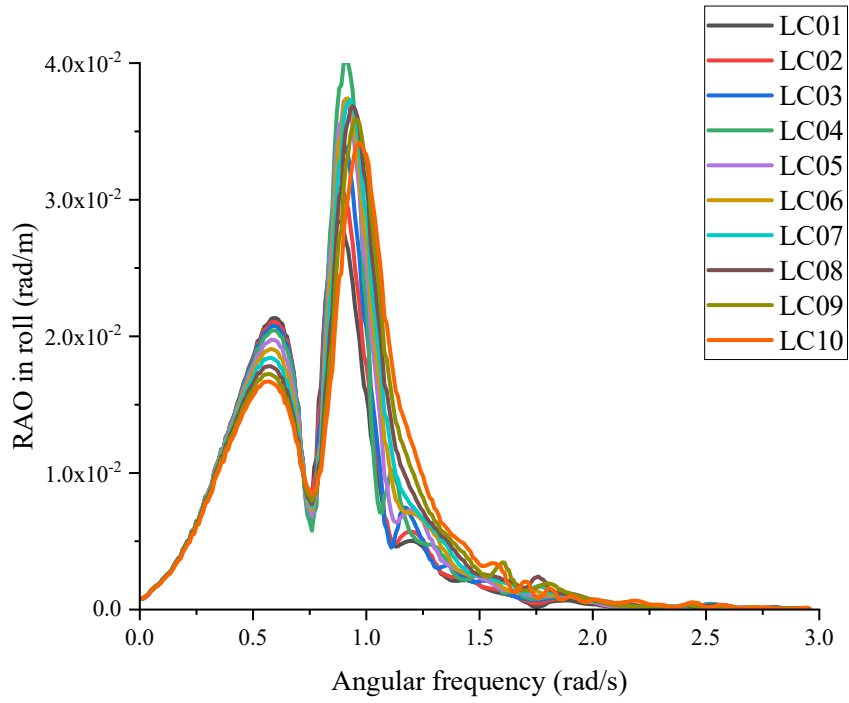


Figure 70. RAOs in roll with 10 load cases in 45-degree wave.

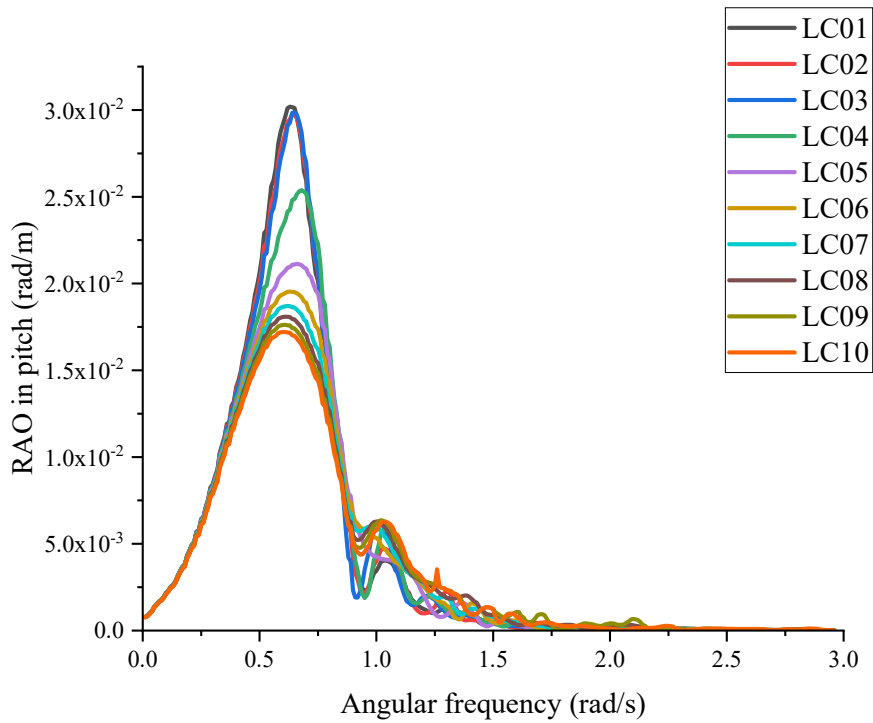


Figure 71. RAOs in pitch with 10 load cases in 45-degree wave.

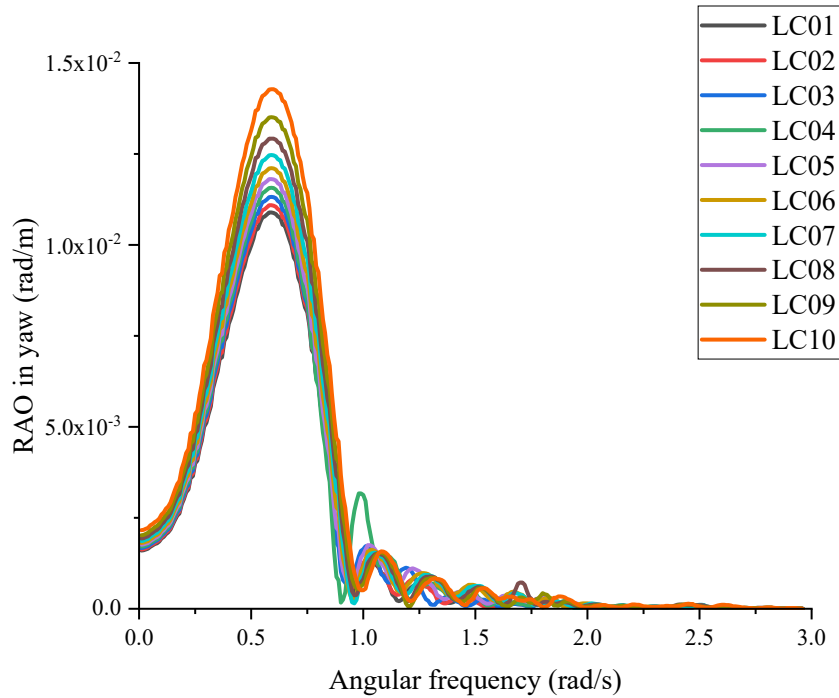


Figure 72. RAOs in yaw with 10 load cases in 45-degree wave.

It is evident from above figures that a significant nonlinear behaviour is exhibited between LC03 and LC04, primarily within the frequency range of 0.5-1.5 rad/s. This frequency range experiences notable nonlinearity due to the initial exposure of the bulbous bow of the vessel's hull to the water surface, which triggers this nonlinear hydrodynamic response (Figure 73). Conversely, in other load cases and their respective frequency domain ranges, a predominantly linear response is also observed.

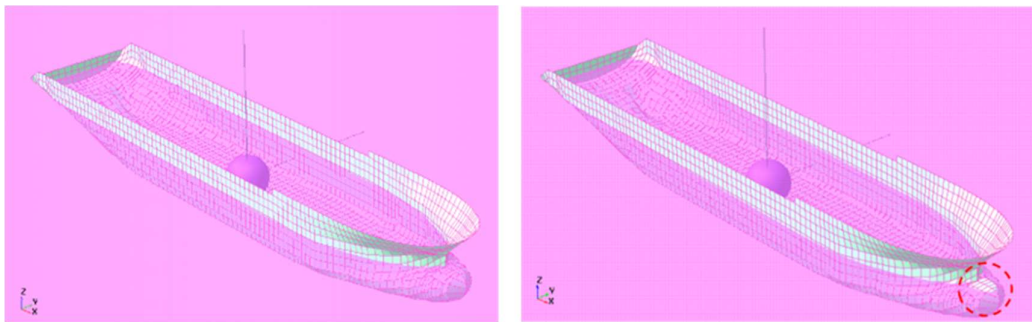


Figure 73. Dredger in load case 03 (left) and load case 04 (right).

The design features of a dredger's bulbous hull expose it to complex hydrodynamic due to the sudden change of water surface area at this draft. This variation demonstrates

pronounced nonlinearity in a specific frequency range, highlighting its critical importance for the hydrodynamic performance of TSHDs. It is primarily attributed to two factors:

(i) Influence due to draft variation and bow exposure

During the unloading operation, the TSHD's draft undergoes changes during the transition from fully weight load to light load conditions. In this process, the increased exposure of the submerged bulbous hull affects the variation in hydrodynamic parameters. This nonlinearity may manifest different trends within various frequency ranges and can significantly impact the TSHD's vibration response and stability. For instance, in RAO in heave (Figure 65 and Figure 69), within the frequency range of 0.5-1.5, the reduction in hydrodynamic parameters may be more pronounced compared to those in other frequency ranges.

The exposure of the bulbous bow of the TSHD to the water surface is another crucial factor which relates to the changing of draft. When the bow becomes exposed, it triggers a rapid change in hydrodynamic parameters, resulting in a noticeable nonlinear effect. This effect may exhibit different characteristics within specific frequency ranges, such as Figure 62 damping coefficient in pitch within the 0.5-1.5 frequency range. It may create peaks or troughs in the response amplitude function. Understanding this effect is vital for the safety and stability of TSHDs.

(ii) Frequency dependency

The nonlinear variation in hydrodynamic parameters can exhibit distinct trends within different frequency ranges. This implies that TSHDs may be subject to varying types of hydrodynamic effects across different frequency ranges. This frequency dependency is crucial for the design and operational strategies of TSHDs. For example, during the dredging process, different operational measures may be required in various frequency ranges to ensure the vessel's stability and performance.

In summary, the above results provide a deeper understanding of the hydrodynamic performance of TSHDs under unloading conditions, emphasizing the significance of nonlinear effects. These findings have important implications for the design, operation, and performance enhancement of TSHDs. Therefore, special attention must be paid to the impact of this nonlinearity in the design and operation of TSHDs to ensure stable hydrodynamic performance under different conditions.

4.4. Vibration natural frequency due to mass-variation

Based on the hydrodynamic data computed in previous section 4.3, the programme initiates its calculations by utilizing this data as the input with time-varying added mass, in conjunction with user-defined parameters and other data for vibration characteristics analysis of the hull girder model.

The pre-calculation module of the program is configured with various drafts and trim features as well as switches for different functionalities related to the proposed mathematical and numerical model. To emphasize the importance of parameters in vibration analysis, the format of results for different cases are defined in this section. In the figures from Figure 74 to Figure 81, ‘Dry’ calculation results indicate natural frequencies without consideration of the added mass, representing dry modal natural frequencies. ‘Wet’ calculation results consider the added mass in vibration analysis, categorized into ‘Wet – 8011’ for time-invariant added mass from load case 01, ‘Wet – 8111’ for added mass from 10 load cases at each time interval, and ‘Wet – 8211’ for time-varying added mass through linear interpolation of the 10 load cases for natural frequency analysis.

As shown in the figures from Figure 74 to Figure 77, they present the first-order natural frequency calculation results of the reference hull girder during an unloading scenario over a simulation period of 360 seconds.

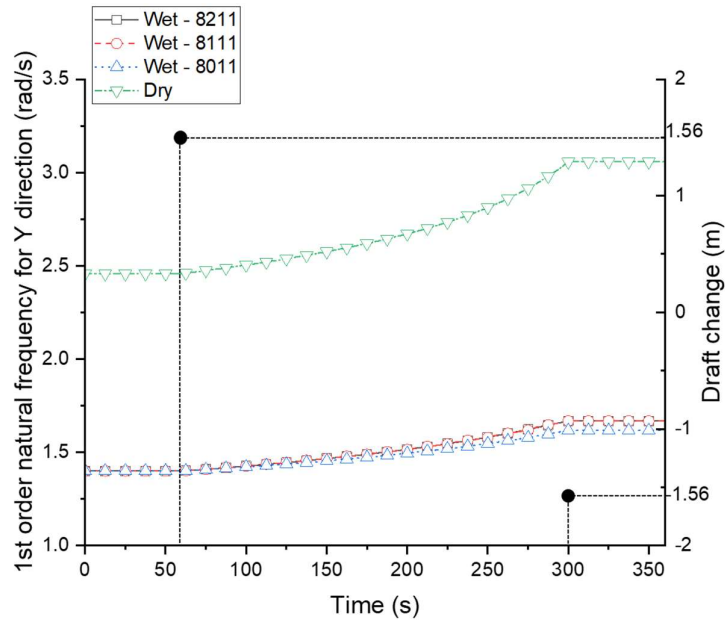


Figure 74. The first-order natural frequency results with four different simulation cases involving three various added mass calculation methods (Wet) and the case without consideration of added mass (Dry) in Y direction.

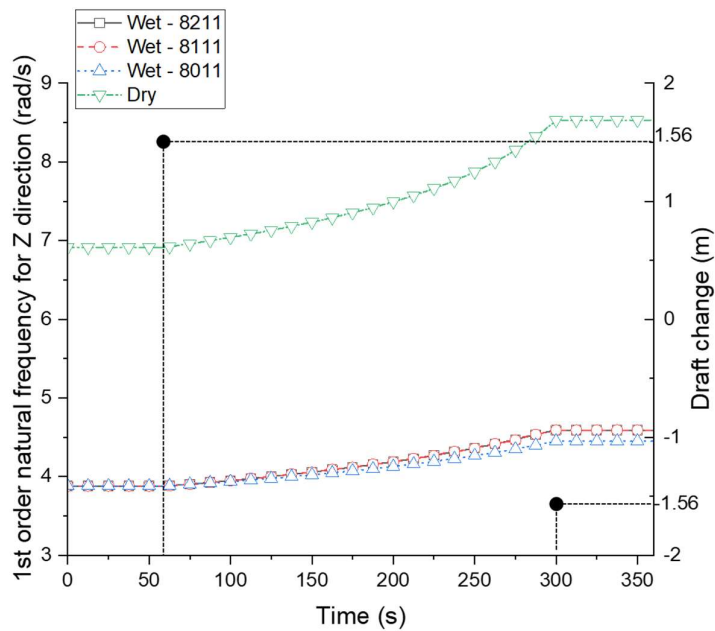


Figure 75. The first-order natural frequency results with four different simulation cases involving three various added mass calculation methods (Wet) and the case without consideration of added mass (Dry) in Z direction.

In the Figure 74 and Figure 75, the labels serve as indicators for the different scenarios that were examined during the vibration analysis of hull girder concerning the inclusion of the added mass effect for both of Y and Z direction respectively. The graph provides a clear and compelling depiction of how the added mass has a profound impact on the natural frequencies of the hull girder. In this case of study, when conducting the natural frequency calculations for the first-order vibration mode, the influence of added mass is notably pronounced, exceeding a range of 3 - 4 rad/s especially for Z direction. This substantial effect serves to underscore the critical importance of accounting for the added mass when delving into the dynamic response analysis of the hull girder. As the mass of the hull girder decreases, the differences in considering added mass in vibration analysis gradually become more pronounced. This significance is particularly highlighted in scenarios where variations in mass conditions come into play. The findings emphasize the need for a comprehensive approach that incorporates added mass considerations, as it significantly affects the structural behaviour and performance of the hull girder in practical applications.

The Figure 76 and Figure 77 provide a zoomed view of the first-order natural frequency calculation results for the hull girder vibration for both of Y and Z direction respectively, considering different added mass calculation methods during the mass-variation process to compare importance of time-varying hydrodynamic analysis.

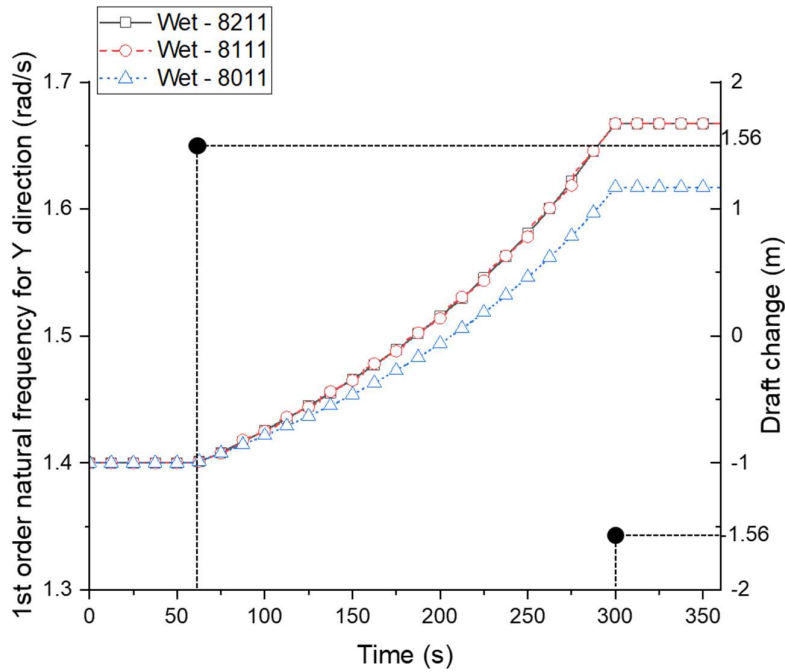


Figure 76. The first-order natural frequency results with three various added mass calculation methods (Wet) in Y direction.

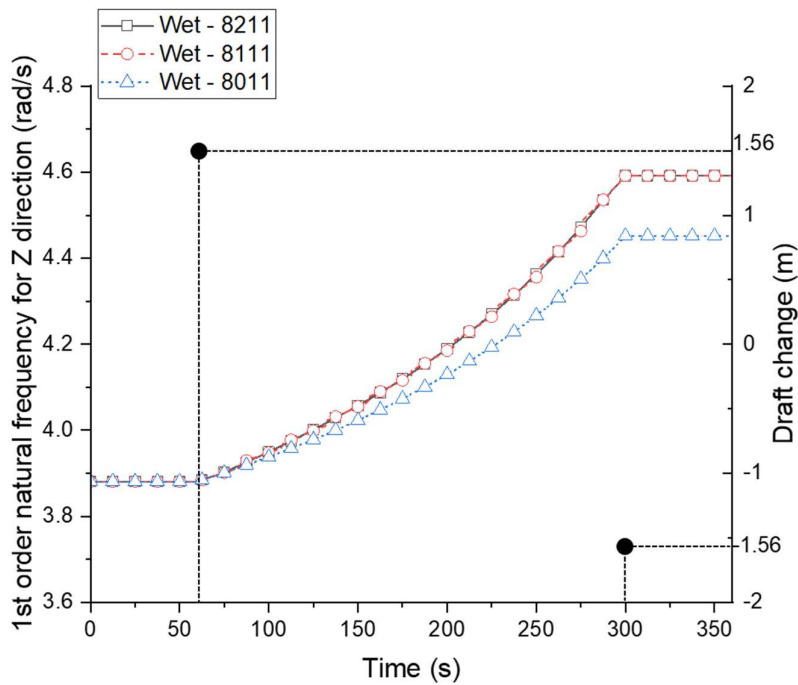


Figure 77. The first-order natural frequency results with three various added mass calculation methods (Wet) in Z direction.

It is evident from the figures above that different time-varying added mass calculation methods yield different results. Specifically, in the vibration analysis, when considering only structural mass changes without accounting for time-varying added mass, the differences in first-order natural frequencies compared to simulations that consider time-varying added mass become increasingly significant. In this case, the maximum difference can reach up to 0.2 rad/s (8011 vs. 8211&8111) in analysis results of Z direction. This implies that the method of calculating time-varying added mass is highly significant for the vibration analysis of hull girders with variable mass. In other words, while changes in structural mass have a dominant impact on structural inherent characteristics in the short term, the variations in added mass due to changing wet surfaces in water also influence the structural inherent characteristics to a certain extent and should not be neglected. On the other hand, the two methods for calculating time-varying hydrodynamics show similar results in vibration analysis (8211&8111). This means that if time-varying added mass is considered in vibration analysis, the results will only slightly differ within certain time periods without introducing significant errors. Theoretically speaking, employing linear interpolation for time-varying added mass can yield more precise results, although this method requires a longer computational time compared to other approaches.

Similarly, Figure 78 to Figure 81 display the natural frequency calculation results for the second-order mode in Y and Z direction respectively.

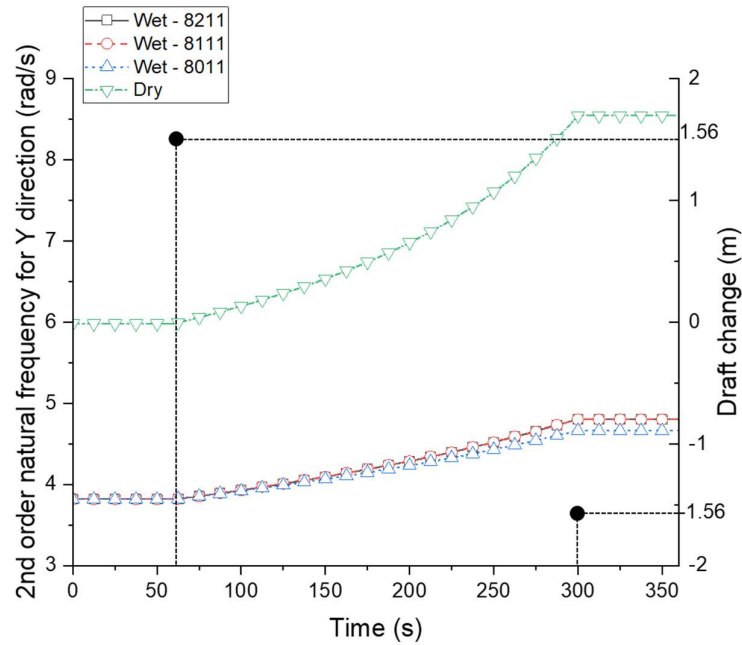


Figure 78. The second-order natural frequency results with four different simulation cases involving three various added mass calculation methods (Wet) and the case without consideration of added mass (Dry) in Y direction.

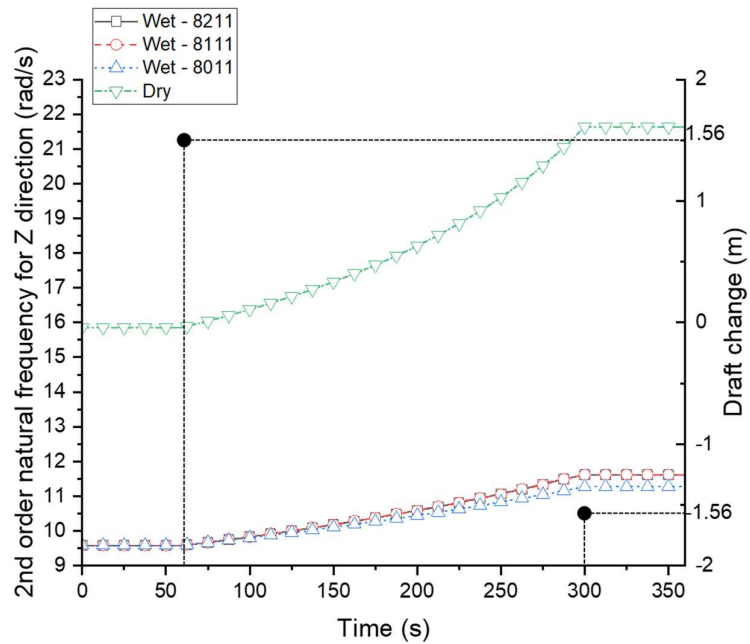


Figure 79. The second-order natural frequency results with four different simulation cases involving three various added mass calculation methods (Wet) and the case without consideration of added mass (Dry) in Z direction.

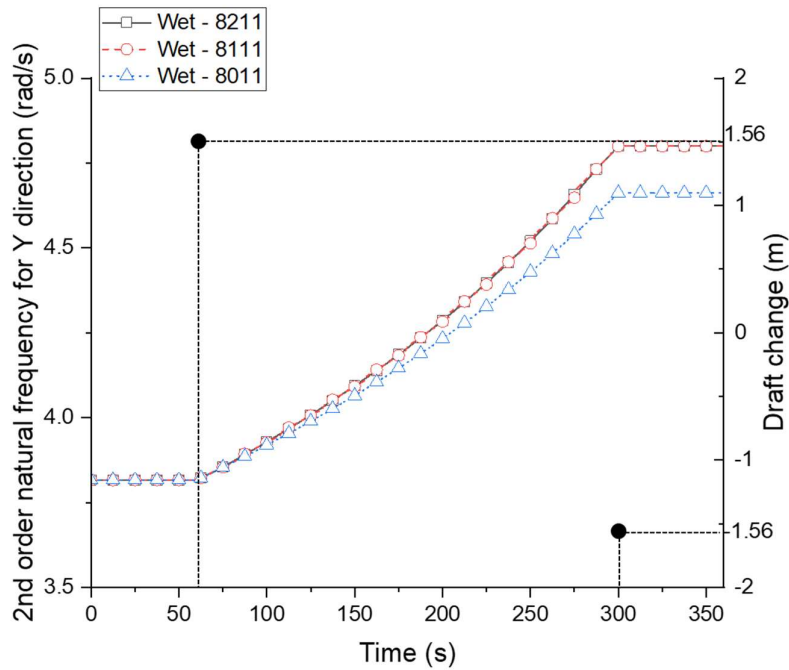


Figure 80. The second-order natural frequency results with three various added mass calculation methods (Wet) in Y direction.

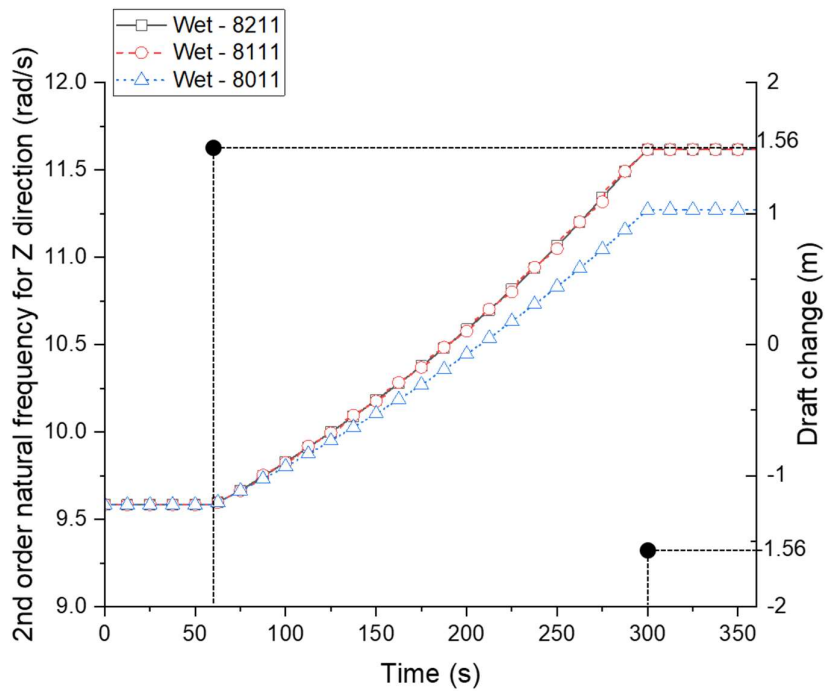


Figure 81. The second-order natural frequency results with three various added mass calculation methods (Wet) in Z direction.

Figures from Figure 74 to Figure 81 illustrate the vibration characteristics analysis of the hull girder, particularly the changes in its natural frequency during the unloading process. The low order natural frequencies are a critical parameter in understanding the structural response and vibration behaviour of the hull girder under mass-variation conditions. The ability to predict these characteristics is essential for ensuring the structural integrity and safety of specialized vessels like TSHDs.

Based on these results, it is evident that, in vibration analysis, the consideration of added mass has a substantial impact on the analysis outcome. Additionally, the time-varying hydrodynamic parameters also influence the accuracy of the vibration analysis results to a significant extent. These different approaches allow for a comprehensive exploration of the added mass effect under various conditions during the variable mass process. The results help in understanding how the vibration characteristics of the hull girder change with respect to the inclusion of added mass in different ways over time.

4.5. TVM_HullGirder simulation results during unloading conditions

The objective of developing a dynamic response calculation program in time-domain is to investigate the motion and structural dynamic responses of a hull girder with time-varying mass systems subjected to various coupled complex loads. In this section, building upon the outcomes of the pre-calculation module described in section 4.3 and section 4.4, the TVM_HullGirder programme is employed to conduct dynamic analysis based on the improved Kane’s dynamic equation. Subsequently, the post-processing work was conducted to output the dynamic responses from the hull girder model. It conducts discussions on the structural analysis of the time-varying mass hull girder by comparing different parameter settings and variations in the proposed mathematical model. Figure 82 describes key outputs from positions on the hull girder model by the TVM_HullGirder program.

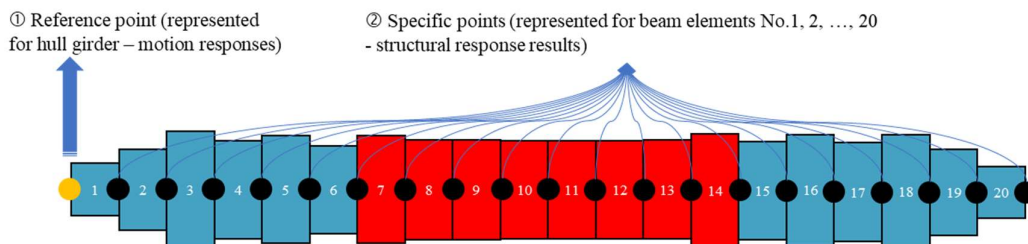


Figure 82. Descriptions for outputted results from the hull girder model.

The subsequent parts are primarily divided into two sections. Section 4.5.1 presents the motion responses of the hull girder as a single rigid-flexible coupled body under complex operational and sea environmental loads, particularly during mass unloading working conditions. Section 4.5.2 focuses on the structural dynamic responses of the hull girder, with an emphasis on some specific cross-section on the hull girder model, also subjected to complex loads under unloading working conditions.

4.5.1. Motion responses of the hull girder

In this section, the motion response results for the reference point of the hull girder are given, corresponding to the yellow point on the left of beam element 01 in Figure 82. These results include the displacement of the reference point, representing changes in the draft of hull girder, as well as velocity and acceleration responses. Furthermore, it analyses and discuss the impact of these results on the structure by comparing them under various operating conditions and model parameter settings.

(1) Unloading operation analysis with 0-degree wave sea condition

Figure 83 illustrates the dynamic calculation results of the draft at the reference point of the hull girder under various mathematical model configurations.

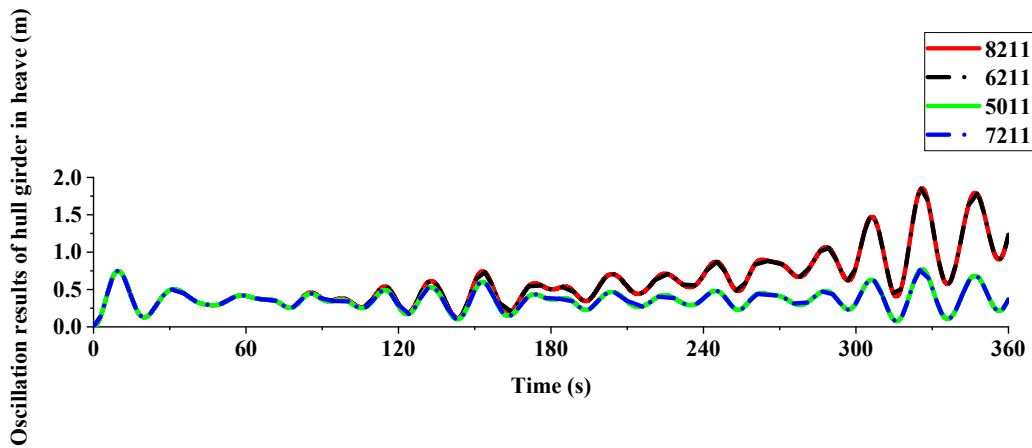


Figure 83. Oscillation results of hull girder in heave with various dynamic model and mass change settings.

The curves in Figure 83 clearly demonstrate that starting from 60 seconds (mass change start settings), the changing mass condition significantly affects the vibration of the hull girder (representing the mass-changing conditions of the TSHD during unloading operations, indicated by 8211 and 6211). In the variable-mass working condition, after

300 seconds when mass changing ceases, it is evident from the graph that the oscillation responses in heave in unloading conditions (8211 and 6211) significantly exceeds that in invariant mass working conditions (7211 and 5011). In this case, the change in amplitude is nearly twice as much as that in the constant mass condition. However, whether in the mass-changing conditions (8211 and 6211) or in the invariant-mass conditions (7211 and 5011), the influence of considering flexible deformation terms in the dynamic model on the oscillatory response of the hull girder is almost negligible.

Specifically, as time progresses, the mass variation gradually exerts an impact on the draft variation. In the 8211 and 6211 conditions, as the mass gradually decreases, the oscillation of the hull girder in heave increases significantly, especially after 300 seconds when the mass stops losing. In the same sea conditions, the oscillation of the hull girder is noticeably large under the mass-variation condition due to the effective mass the hull bears decrease relative to its inertial and dynamic characteristics, affecting the vessel's dynamic responses. Mass change significantly influences the hull's free vibration responses and frequency characteristics, making it more susceptible to external excitation forces, typically resulting in a pronounced increase in oscillation in heave. This phenomenon is crucial for understanding the vessel's oscillatory responses and oscillation amplitude variations under different conditions, particularly when mass variation is significant.

In contrast, under invariant-mass working conditions (5011 and 7211), the oscillation of the hull girder in heave remains relatively stable. These results emphasize the significant impact of mass change on the oscillatory responses of the hull girder. Simultaneously, the effect of the flexible deformation terms on the oscillatory responses is minimal, whether under conditions of mass change or invariant mass. This finding holds significant implications for gaining a deeper understanding of the dynamic behaviour of the hull girder and for design considerations.

The following figures respectively illustrate the acceleration responses of the reference point on the hull girder as a rigid-flexible coupled body and as a rigid body in heave (Figure 84 and Figure 85) and pitch (Figure 86 and Figure 87).

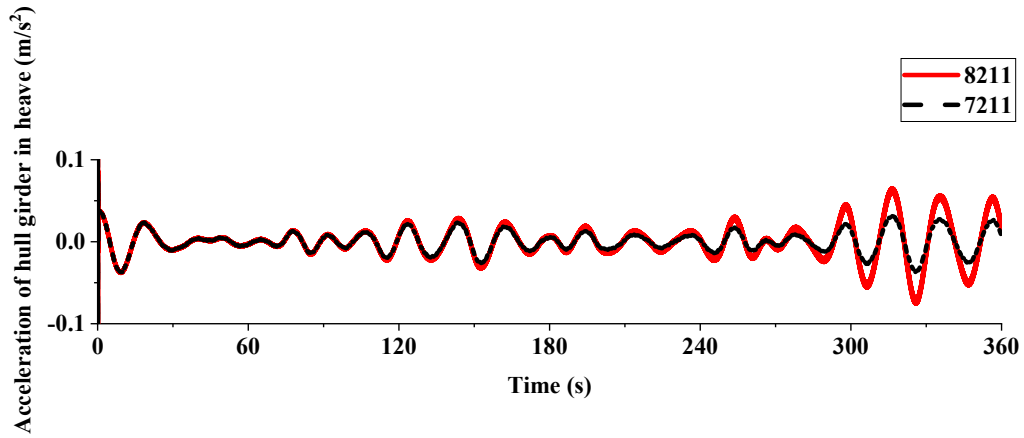


Figure 84. Acceleration of hull girder in heave as a rigid-flexible coupled body with variable mass (8211) and invariant-mass (7211) working conditions.

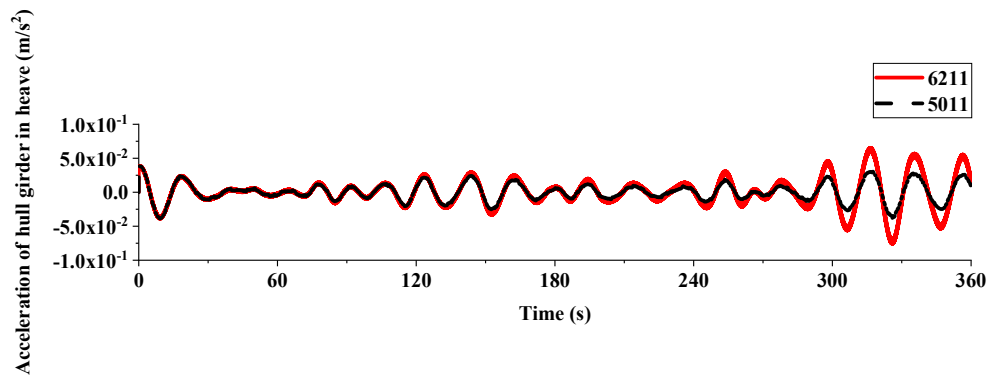


Figure 85. Acceleration of hull girder in heave as a rigid body with variable mass (6211) and invariant-mass (5011) working conditions.

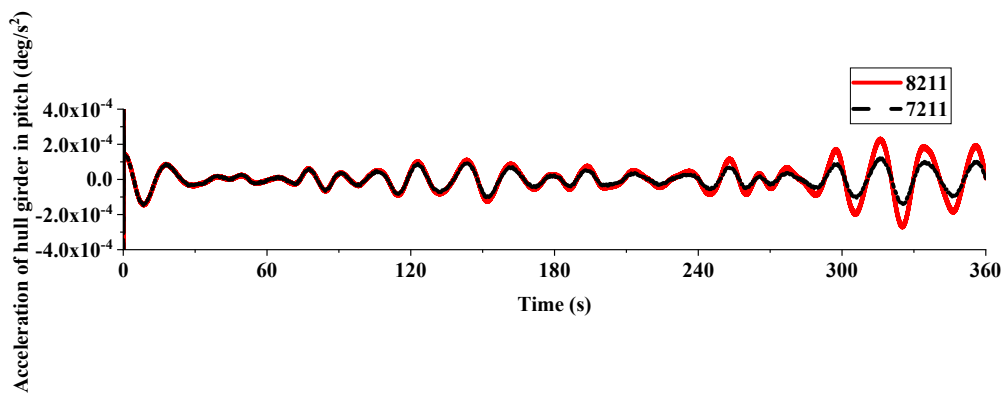


Figure 86. Acceleration of hull girder in pitch as a rigid-flexible coupled body with variable mass (8211) and invariant-mass (7211) working conditions.

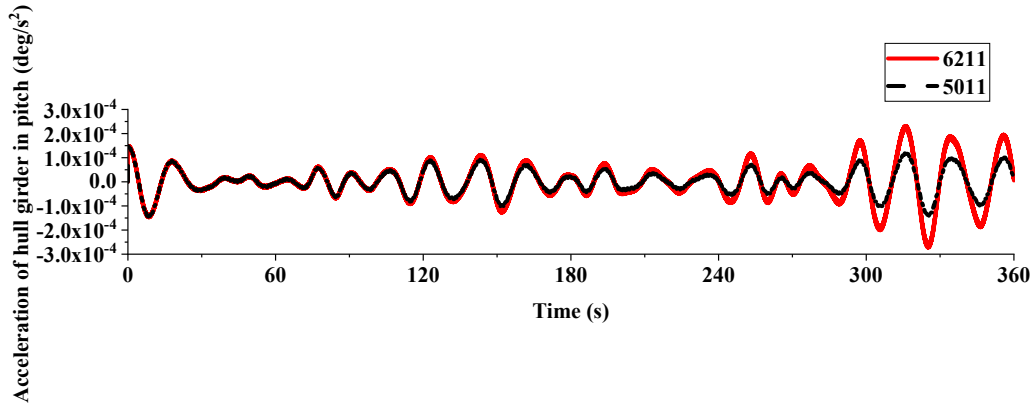


Figure 87. Acceleration of hull girder in pitch as a rigid body with variable mass (6211) and invariant-mass (5011) working conditions.

Upon a more in-depth examination of these results, it becomes essential to conduct a comprehensive analysis of the hull girder's structural dynamics and the impact of variable mass conditions on its performance. Firstly, the critical distinctions between treating the hull girder as a rigid body and employing a rigid-flexible coupled structure model should be further explored. When the hull girder is regarded as a rigid body, the inherent flexible characteristics, encompassing natural vibration modes and bending deformations, are essentially overlooked. In this context, the analysis predominantly revolves around rigid body vibration modes, often limiting the accuracy of acceleration responses. This limitation becomes apparent as acceleration responses substantially diminish due to the inadequate consideration of flexible characteristics.

Conversely, when employing the rigid-flexible coupled structure model, the internal flexible features are incorporated, including bending vibrations and deformations. This model more accurately captures the dynamic behaviour of the hull girder, leading to more pronounced acceleration responses in the analysis. This underscores the vital significance of considering flexible characteristics in structural dynamic analysis, particularly when addressing high-frequency responses or complex vibration modes.

Furthermore, it is evident that the variation in mass significantly influences the vibration response of the hull girder. As mass decreases, effective mass diminishes as well, resulting in an increased vibration amplitude. This phenomenon arises due to the close relationship between effective mass and the hull's inertia and dynamic characteristics. Consequently, mass variations exert a substantial impact on the hull

girder's free vibration response and frequency characteristics. This understanding is crucial for gaining insight into the vessel's vibration response under various operational conditions, especially in scenarios featuring substantial mass variations as explored in this study.

(2) Unloading operation analysis with 45-degree wave sea condition

To investigate the impact of different wave conditions on the motion response of the vessel during unloading operations, this part presents the displacement responses in heave and angular responses in pitch of the vessel under 0-degree heading waves and 45-degree oblique waves sea conditions respectively.

The Figure 88 and Figure 89 respectively illustrate the oscillation responses in heave and angular responses in pitch of the vessel under 0-degree and 45-degree wave conditions during the unloading operations.

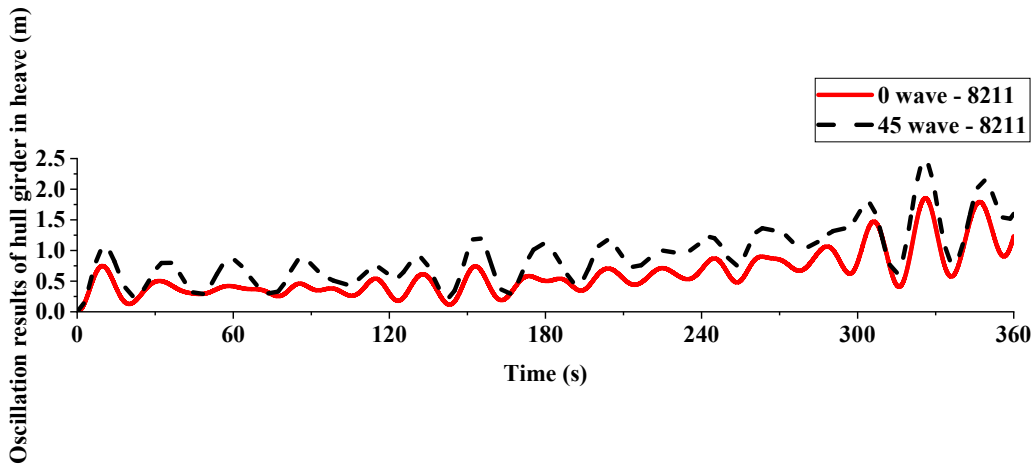


Figure 88. Oscillation results of the hull girder in heave in 0-degree and 45-degree wave direction during unloading operations.

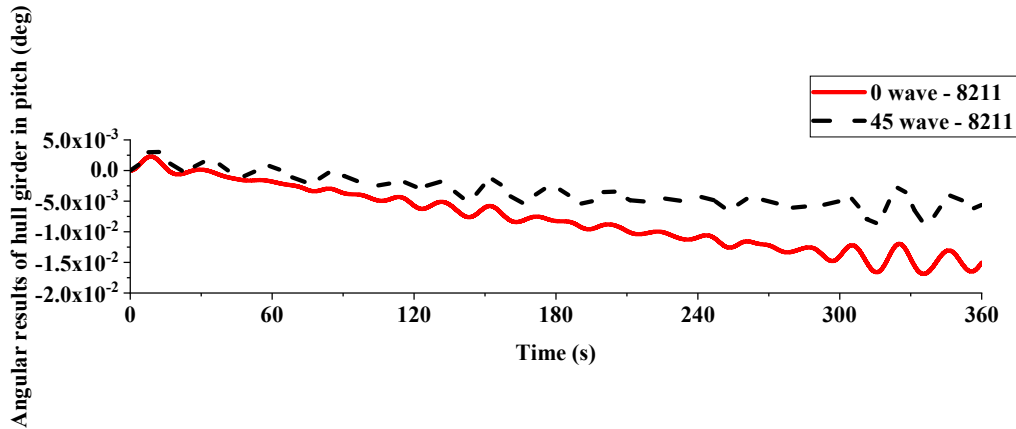


Figure 89. Angular results of the hull girder in pitch in 0-degree and 45-degree wave direction during unloading operations.

The motion responses of the hull girder are significantly influenced by the wave conditions, as evident from the above results. Specifically, for motion responses of the vessel in heave, the oblique wave condition has a more pronounced impact. In contrast, for the motion response of the vessel in pitch, the head wave condition exerts a greater influence.

To further investigate the motion responses under varying wave conditions accurately, the following presents the motion response analysis results for the invariant-mass condition as output by the TVM_HullGirder programme. The preceding analysis focused on the motion responses of the hull girder in unloading working conditions under different wave scenarios.

The Figure 90 and Figure 91 respectively illustrate the oscillation responses in heave and angular responses in pitch of the vessel under 0-degree and 45-degree wave conditions during the invariant-mass working conditions.

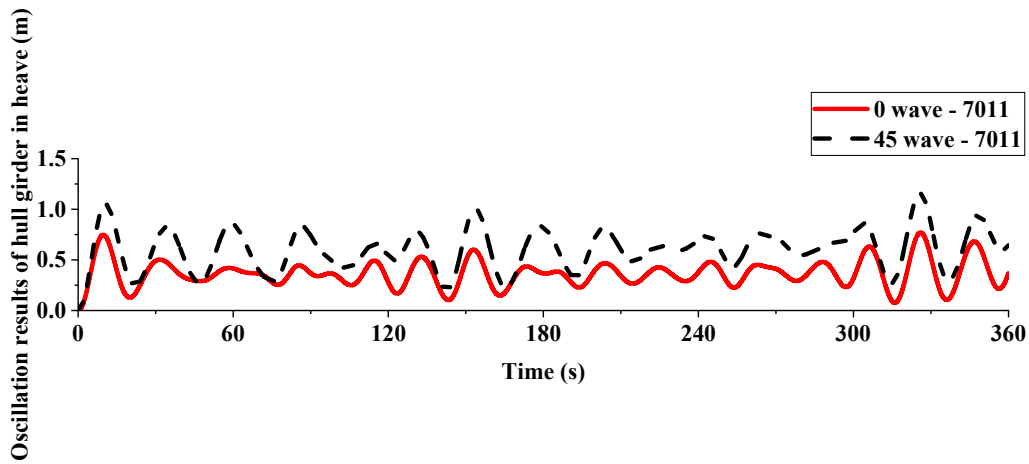


Figure 90. Oscillation results of the hull girder in heave in 0-degree and 45-degree wave direction during invariant-mass working conditions.

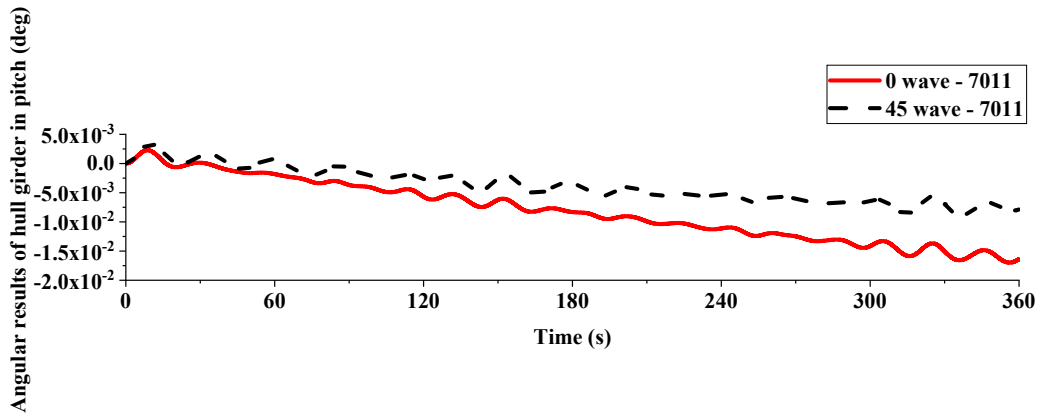


Figure 91. Angular results of the hull girder in pitch in 0-degree and 45-degree wave direction during invariant-mass working conditions.

The above hull girder motion response results further demonstrate that, whether in unloading working conditions or under constant mass conditions, different wave conditions exert a significant influence on various motion components of the vessel.

The Figure 92 and Figure 93 respectively illustrate the acceleration responses in heave and in pitch of the vessel under 0-degree and 45-degree wave conditions during the unloading operations.

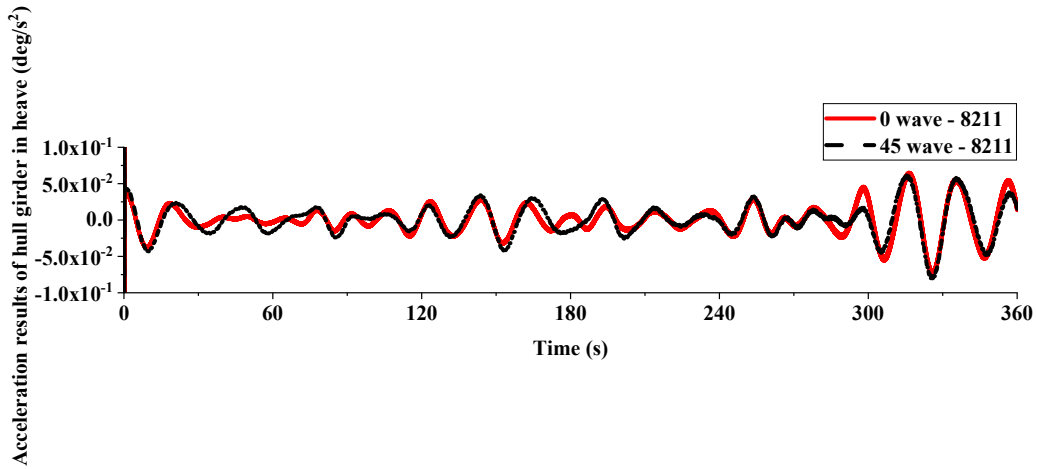


Figure 92. Acceleration results of the hull girder in heave under 0-degree and 45-degree wave sea condition respectively.

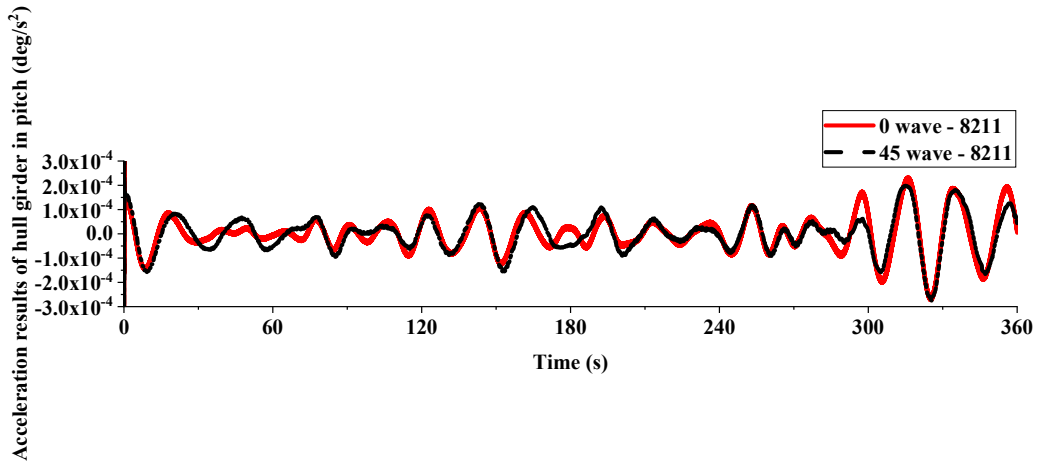


Figure 93. Angular acceleration results of the hull girder in pitch under 0-degree and 45-degree wave sea condition respectively.

4.5.2. Structural vibration responses

To investigate dynamic responses of the hull girder presented as displacements and rotational angles on each node at the ends of beam elements in local coordinate system, this section will provide comparative analysis and discussions of calculated results for user-defined cross-sections on the hull girder under various working conditions and sea environments. Furthermore, it is noteworthy that these results regarding displacements and rotational angles in six degrees of freedoms will be employed in further FEA in next section to determine stress distribution across the dredger's structure and other structural assessments.

(1) Unloading operation analysis with 0-degree wave sea condition

In this part, it mainly takes calculation results of several cross-section of beam elements on the hull girder model in Z axis with dynamic displacements and about Y axis with rotational dynamic responses.

The following figures present dynamic displacement results of invariant-mass beam elements numbered 01 – 06 at the stern part (Figure 94) and 15 – 20 at the bow part (Figure 96) of the hull girder model as well as variable mass beam elements numbered 07 – 14 represented the middle part of the hull girder model (Figure 95).

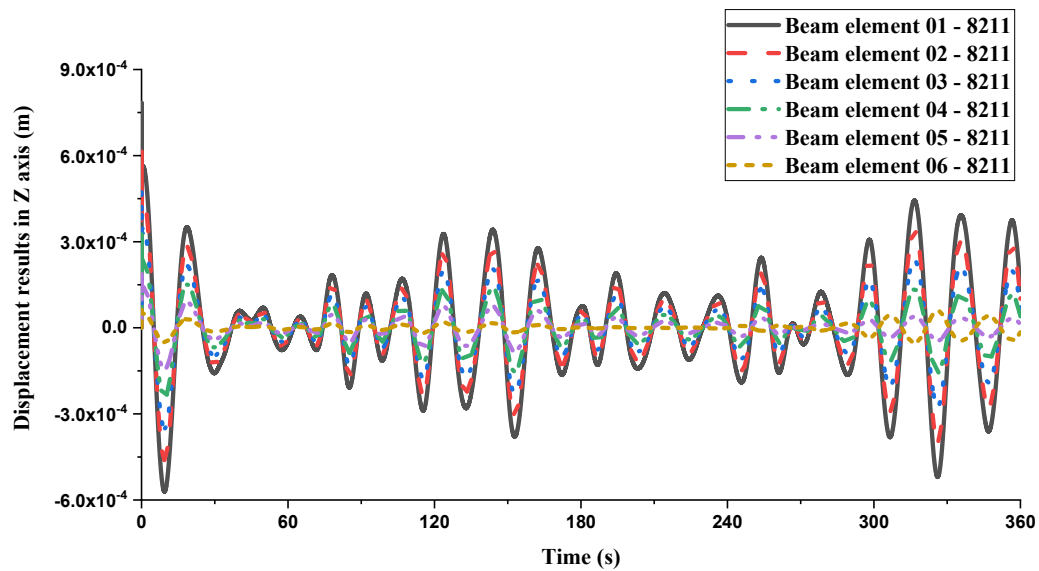


Figure 94. Displacement results of invariant-mass beam element 01 - 06 in Z direction under unloading working conditions.

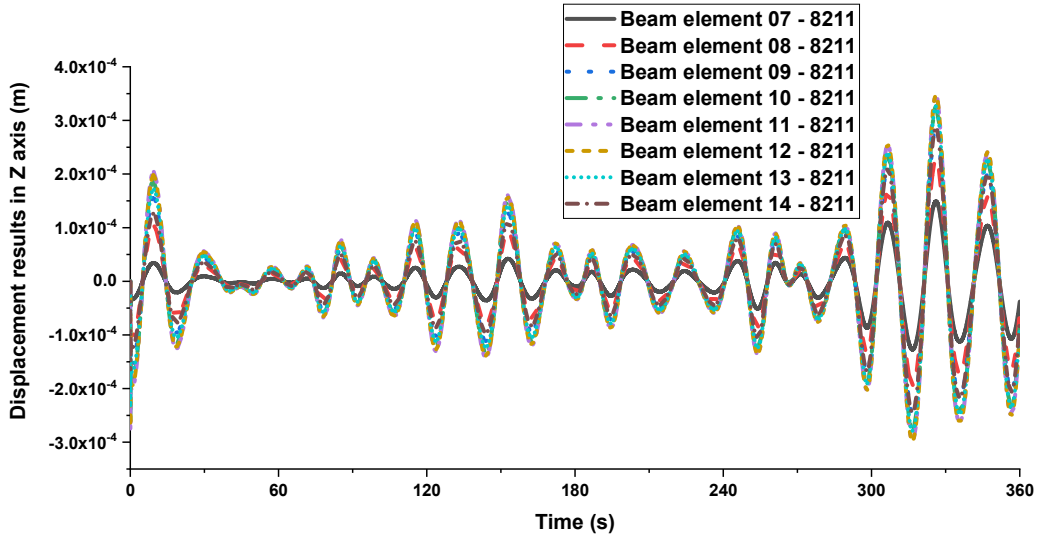


Figure 95. Displacement results of time-varying mass beam element 07 - 14 in Z direction under unloading working conditions.

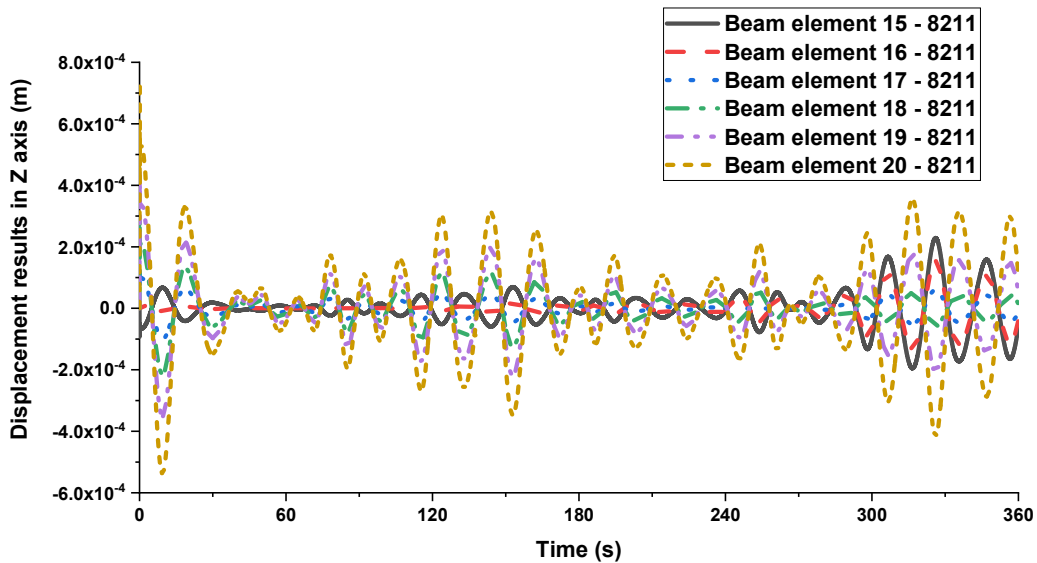


Figure 96. Displacement results of invariant-mass beam element 15 - 20 in Z direction under unloading working conditions.

From above figures, it proves that the dynamic response amplitudes of the bow (beam element 20), middle (beam element 10 and 11), and stern (beam element 01) structures of the hull girder are relatively large, whereas the dynamic responses at approximately 1/4 (beam element 06 and 07) and 3/4 (beam element 15 and 16) of the vessel is minimal. This pattern aligns with the common dynamic response behaviour of a hull girder.

The following figures take displacement results of illustrate the displacement responses of beam elements 01, 06, 10, 16, and 20 with comparison results under unloading working conditions and invariant mass working conditions. These beam elements respectively represent key cross-sectional locations of interest: the stern, 1/4 length from the vessel, midship, 3/4 length from the vessel, and the bow. These positions are crucial for analysing the dynamic behaviour of the ship's structure.

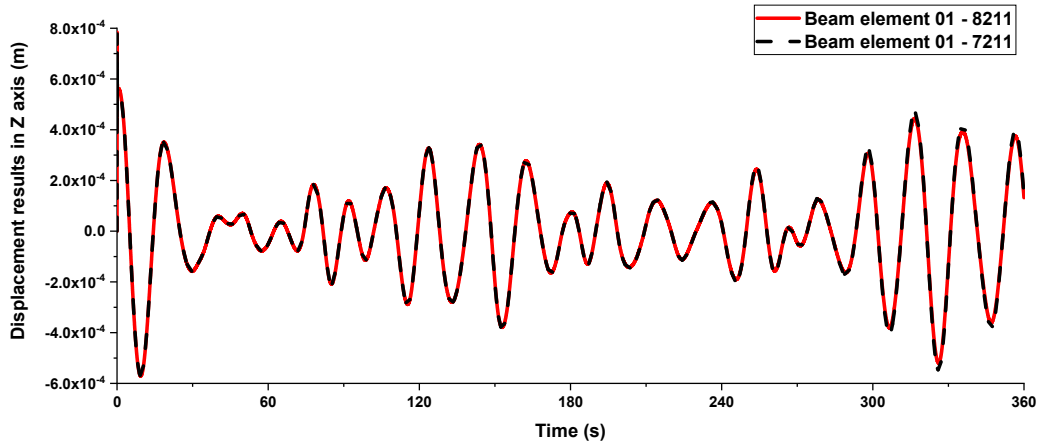


Figure 97. Displacement results of beam element 01 in Z direction with variable mass (8211) and invariant mass (7211) working conditions respectively.

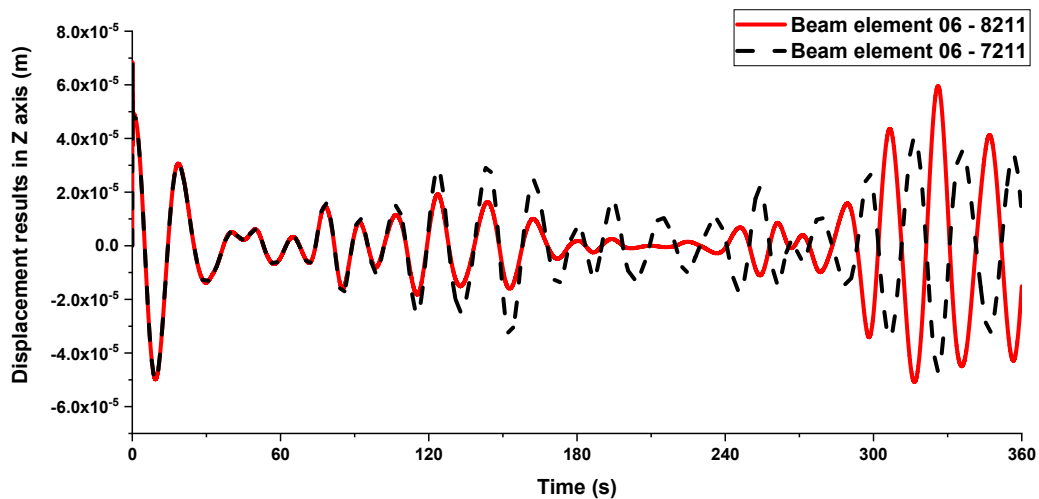


Figure 98. Displacement results of beam element 06 in Z direction with variable mass (8211) and invariant mass (7211) working conditions respectively.

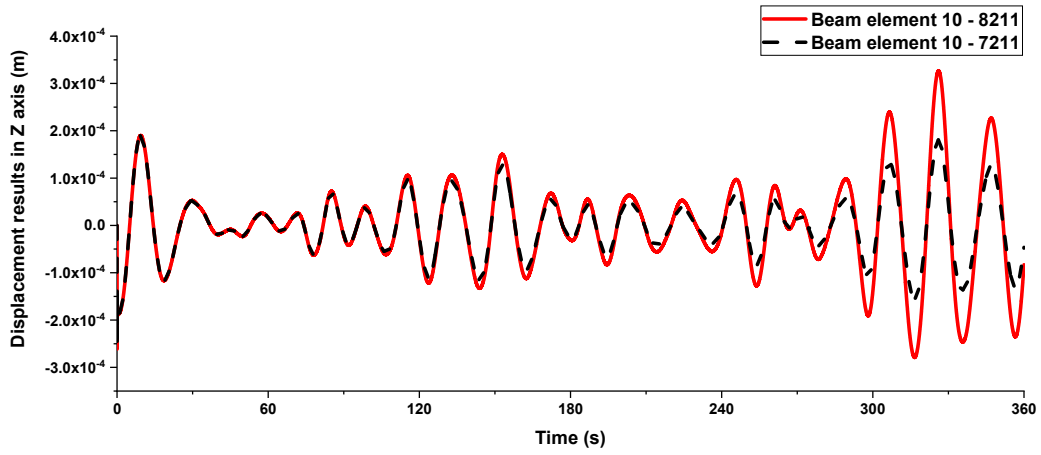


Figure 99. Displacement results of beam element 10 in Z direction with variable mass (8211) and invariant mass (7211) working conditions respectively.

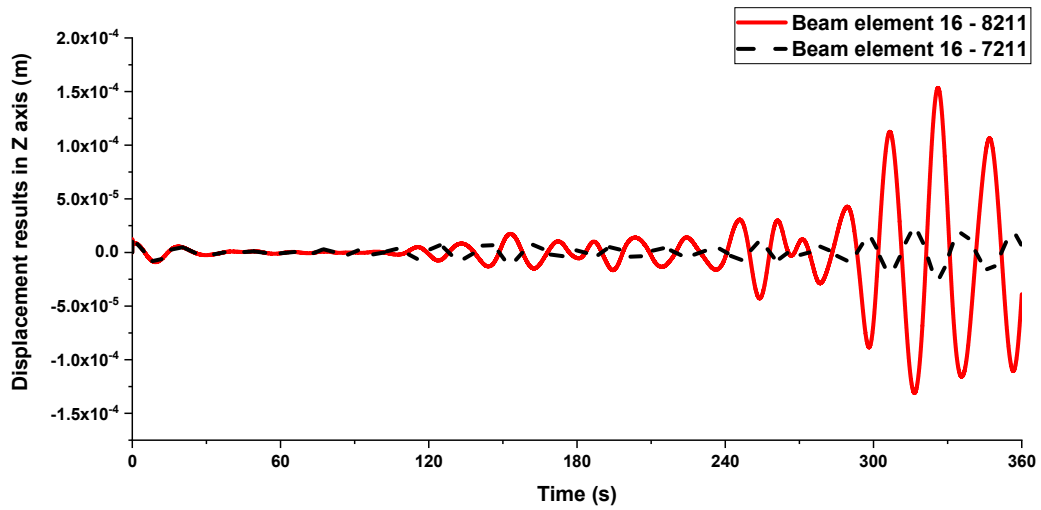


Figure 100. Displacement results of beam element 16 in Z direction with variable mass (8211) and invariant mass (7211) working conditions respectively.

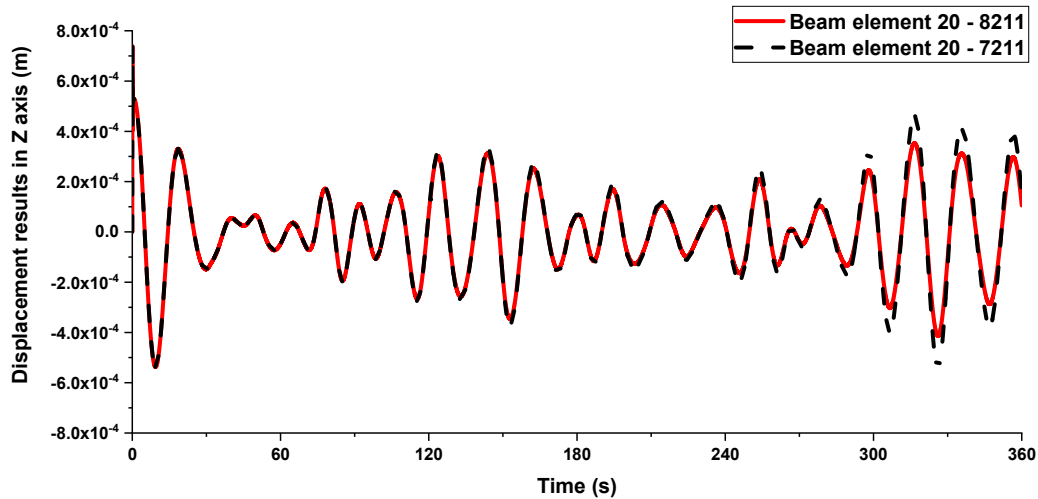


Figure 101. Displacement results of beam element 20 in Z direction with variable mass (8211) and invariant mass (7211) working conditions respectively.

From the above results, it is evident that the dynamic responses at the stern (beam element 01) and the bow (beam element 20) show minimal differences between the working conditions of variable mass and invariant mass. However, at the 1/4 length of the hull girder (beam element 06), midship (beam element 10), and 3/4 length of the hull girder (beam element 16), the dynamic responses exhibit significant differences. Notably, under variable mass conditions, the amplitude of dynamic response is considerably larger compared to the invariant-mass working condition. This highlights the substantial impact of mass variation on the ship's dynamic behaviour at these critical sections.

On the other hand, from a ship structural design perspective, the angular response of the vessel's structure is of paramount importance. Design engineers typically pay close attention to the angular response of the ship's cross-section and the subsequent implications for structural strength and fatigue analysis. Therefore, it is essential to provide the computed results of the cross-sectional angular response for both variable-mass and constant-mass beam elements. The following figures present angular dynamic results of invariant-mass beam elements numbered 01 – 06 at the stern part (Figure 102) and 15 – 20 at the bow part (Figure 104) of the hull girder model as well as variable mass beam elements numbered 07 – 14 represented the middle part of the hull girder model (Figure 103).

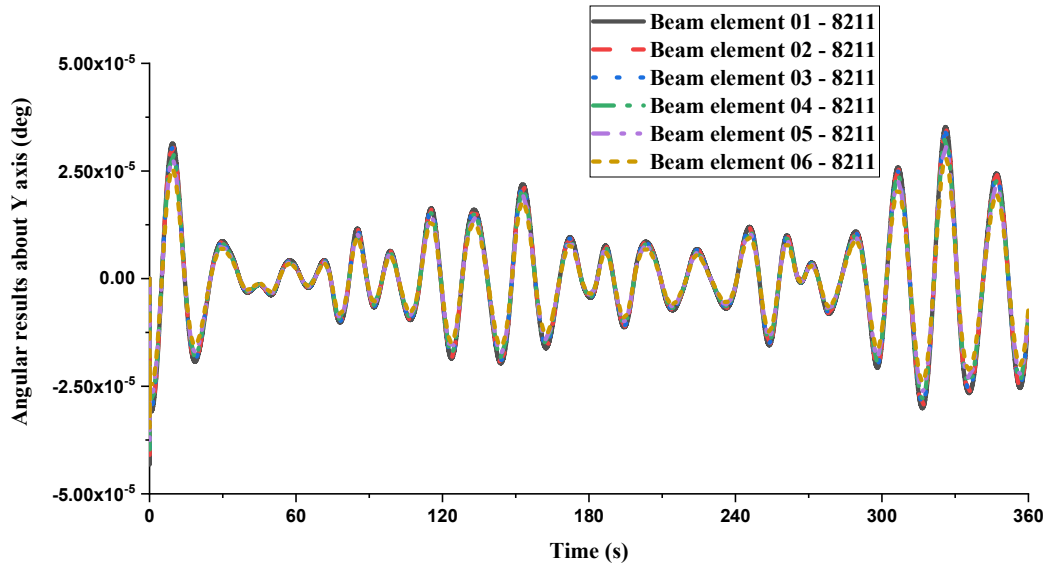


Figure 102. Angular results of invariant-mass beam element 01 - 06 about Y axis under unloading working conditions.

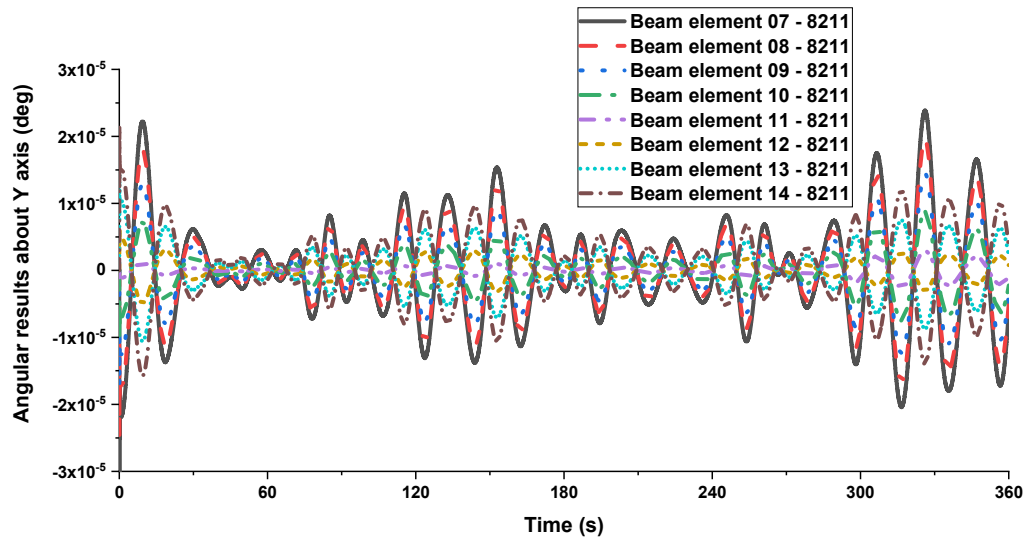


Figure 103. Angular results of time-varying mass beam element 07 - 14 about Y axis under unloading working conditions.

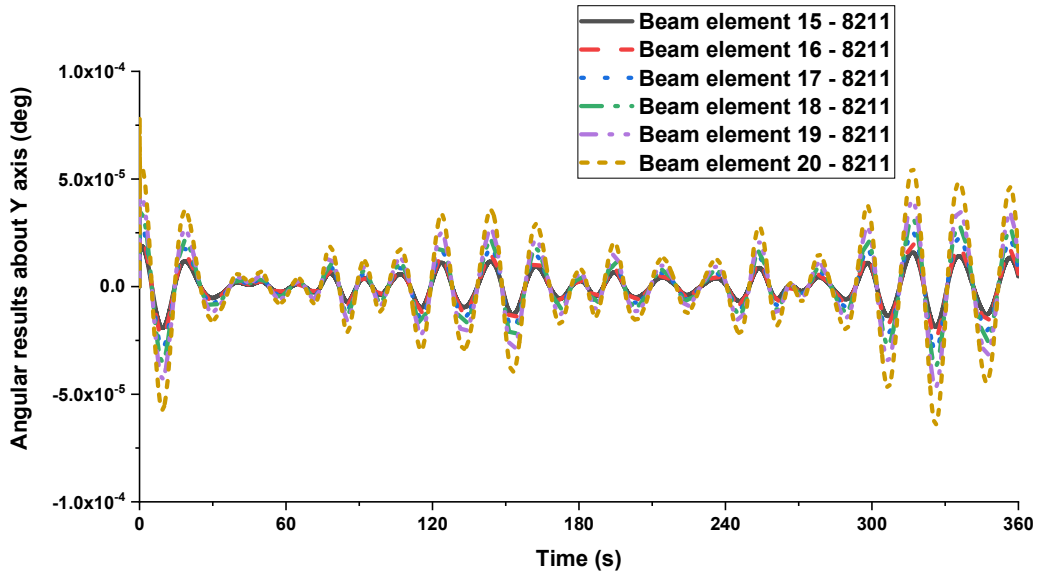


Figure 104. Angular results of invariant-mass beam element 15 - 20 about Y axis under unloading working conditions.

Similarly, the following figures take angular dynamic results of beam elements 01, 06, 10, 16, and 20 with comparison results under unloading working conditions and invariant mass working conditions.

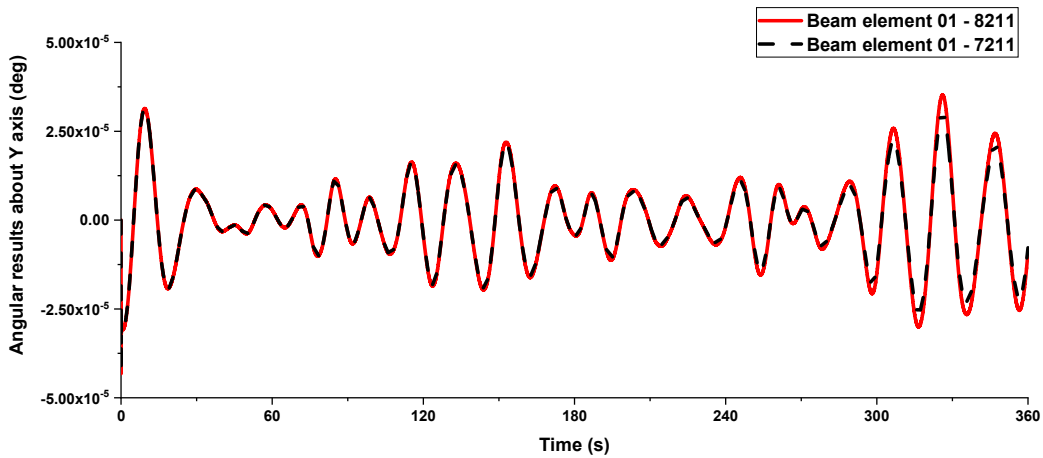


Figure 105. Angular results of beam element 01 about Y axis with variable mass (8211) and invariant mass (7211) working conditions respectively.

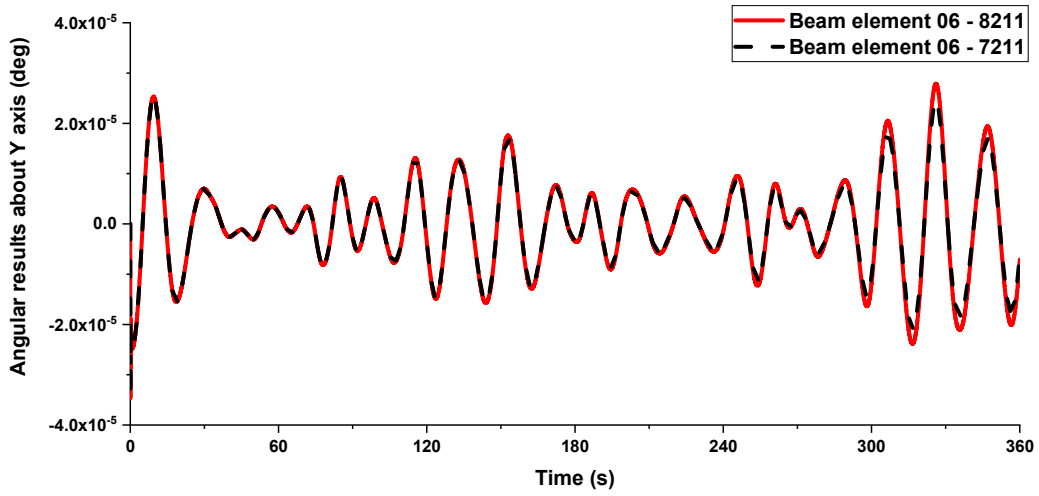


Figure 106. Angular results of beam element 06 about Y axis with variable mass (8211) and invariant mass (7211) working conditions respectively.

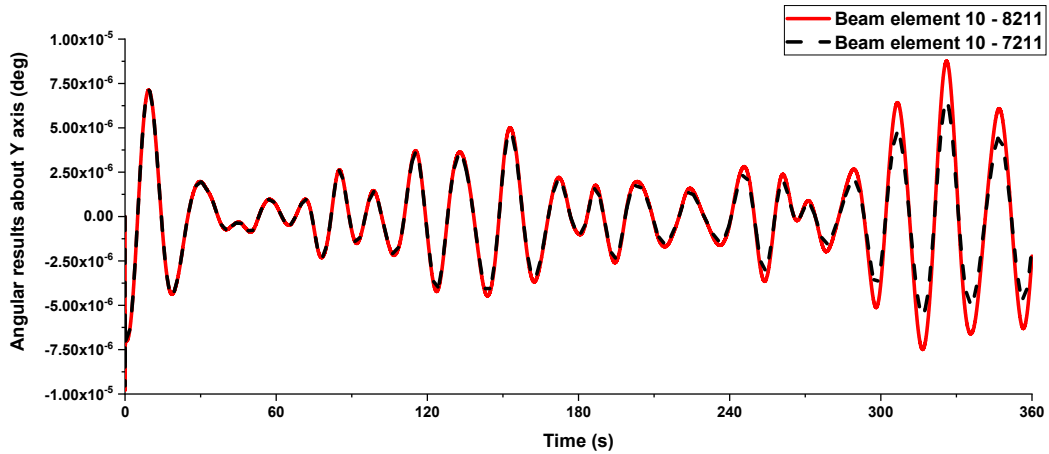


Figure 107. Angular results of beam element 10 about Y axis with variable mass (8211) and invariant mass (7211) working conditions respectively.

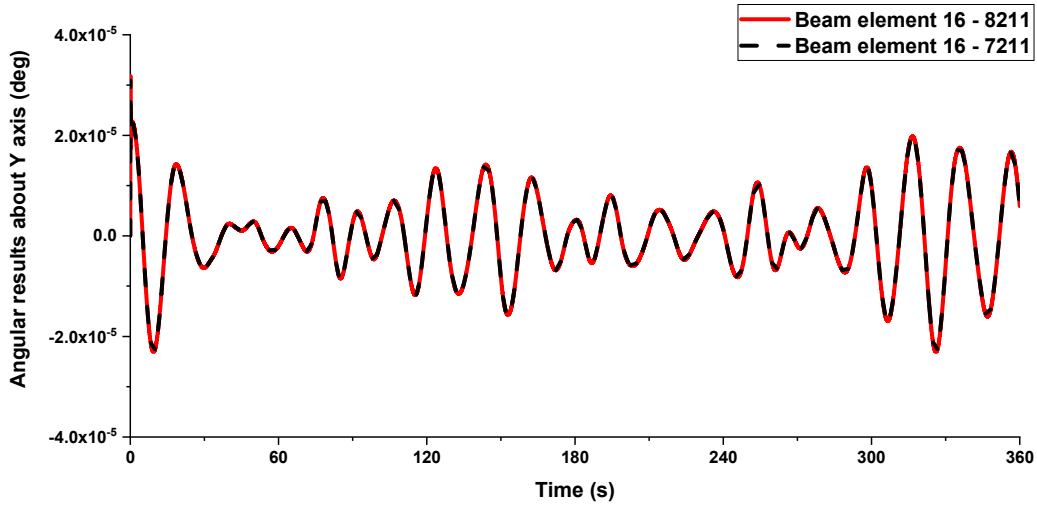


Figure 108. Angular results of beam element 16 about Y axis with variable mass (8211) and invariant mass (7211) working conditions respectively.

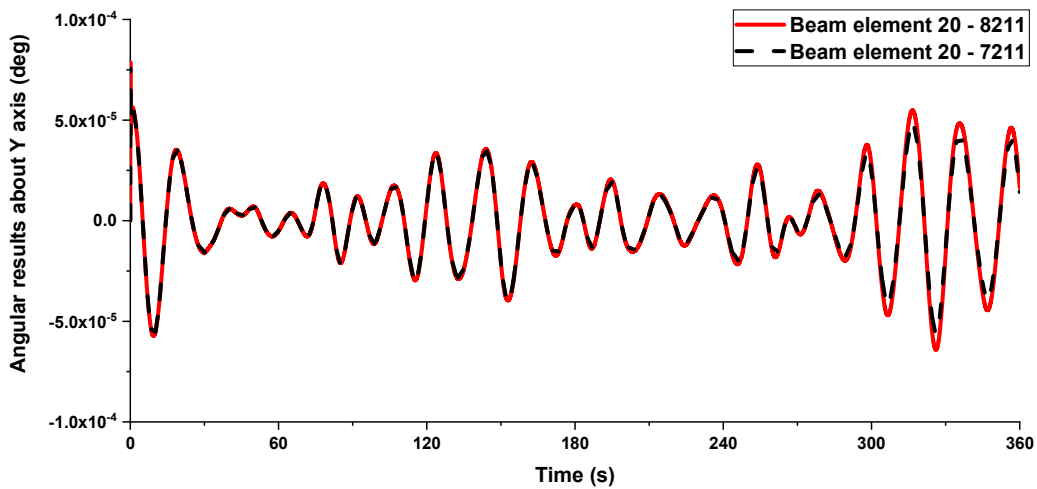


Figure 109. Angular results of beam element 20 about Y axis with variable mass (8211) and invariant mass (7211) working conditions respectively.

Overall, the results clearly indicate that the dynamic response in terms of angular results is greater under varying mass working conditions compared to invariant mass conditions. This underscores the pronounced impact that changes in mass have on the torsional dynamics of the vessel.

The comparison between variable-mass and constant-mass operational conditions, as depicted in the figures above, reveals that the additional loads induced by mass variation result in substantial extra torsional loads on the vessel's cross-sections. This effect is particularly evident in the structural elements located at the stern, midship, and bow sections of the hull girder correspondence to beam elements 01, 10, and 20, which bear a greater share of these additional torsional loads. As a result, these areas experience a more significant impact from the dynamic response under variable mass operational conditions.

The findings highlight the critical importance of accounting for mass changes in the design and analysis of such vessels. Ignoring these changes could lead to an underestimation of the torsional loads and, consequently, the structural demands on key sections of the hull. Therefore, it is essential to incorporate considerations of mass variation to ensure the integrity and performance of the vessel under operational conditions.

(2) Unloading operation analysis with 45-degree wave sea condition

To comprehensively analyse the dynamic response of the ship's hull girder under different wave conditions, in this part, it examined the displacement and angular responses at various key sections of the hull.

The following figures illustrate the dynamic responses of five critical beam elements located at the stern (beam element 01), one-quarter length from the stern (beam element 06), midship (beam element 10), three-quarter length from the stern (beam element 16), and the bow (beam element 20). These sections were chosen to represent the overall behaviour of the hull girder. Each figure compares the displacement responses under 0-degree (head-on) wave conditions and 45-degree (oblique) wave conditions, providing insights into the impact of wave direction on the structural dynamics of the vessel.

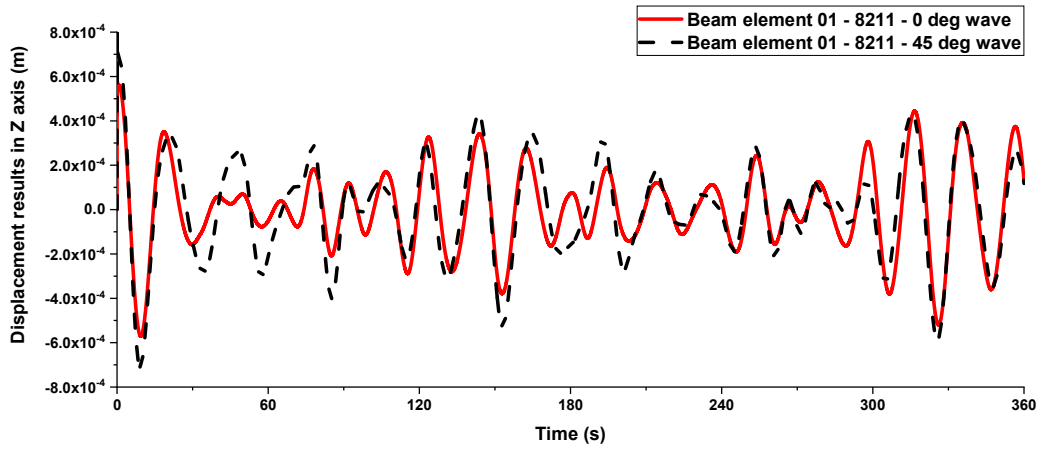


Figure 110. Displacement results of the beam element 01 in Z direction with 0-degree and 45-degree sea wave conditions respectively.

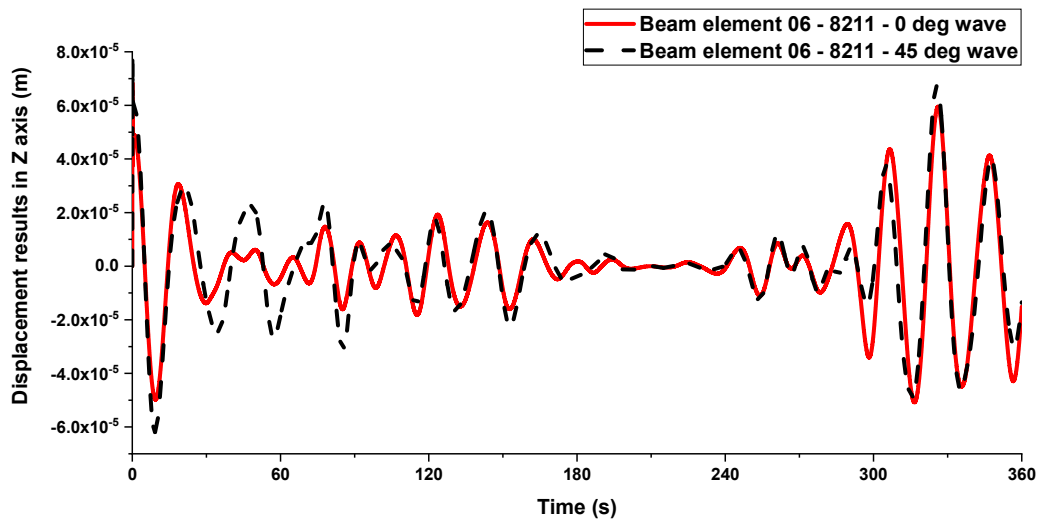


Figure 111. Displacement results of the beam element 06 in Z direction with 0-degree and 45-degree sea wave conditions respectively.

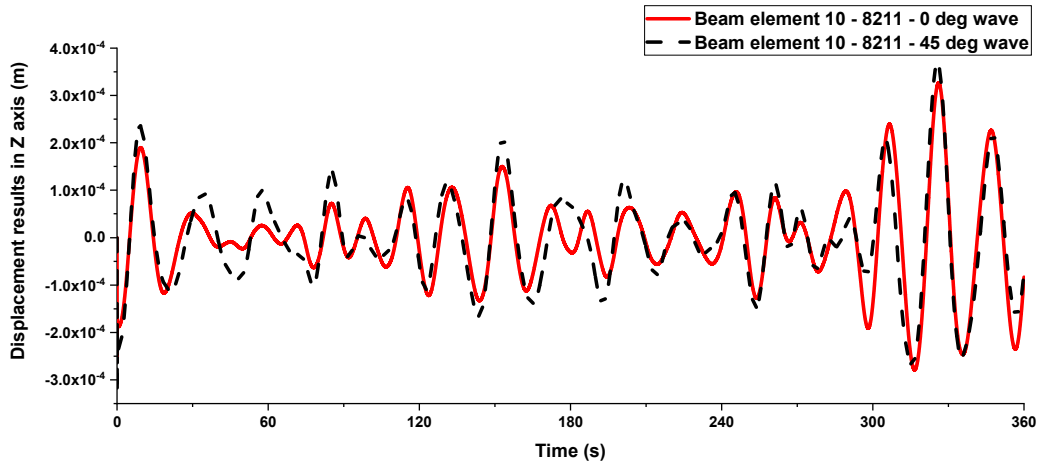


Figure 112. Displacement results of the beam element 10 in Z direction with 0-degree and 45-degree sea wave conditions respectively.

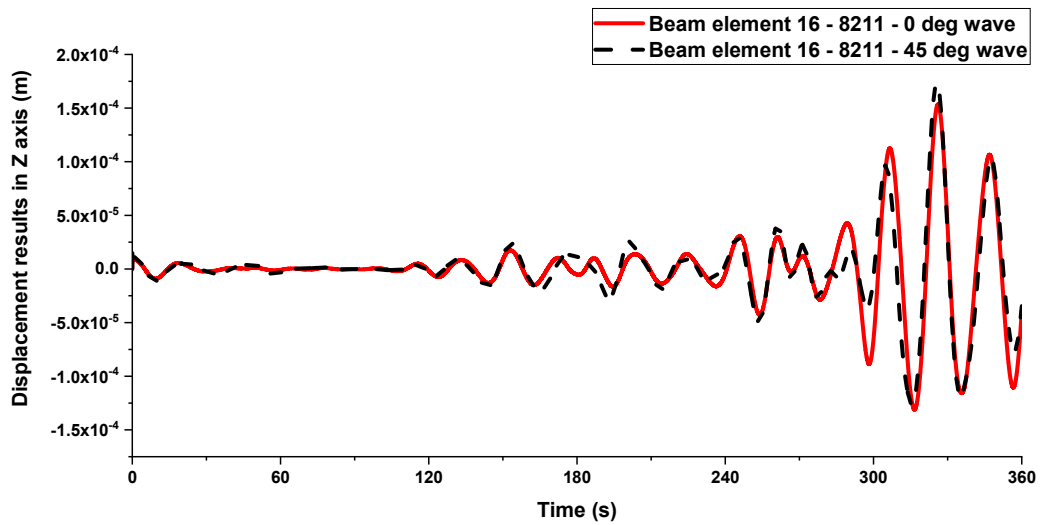


Figure 113. Displacement results of the beam element 16 in Z direction with 0-degree and 45-degree sea wave conditions respectively.

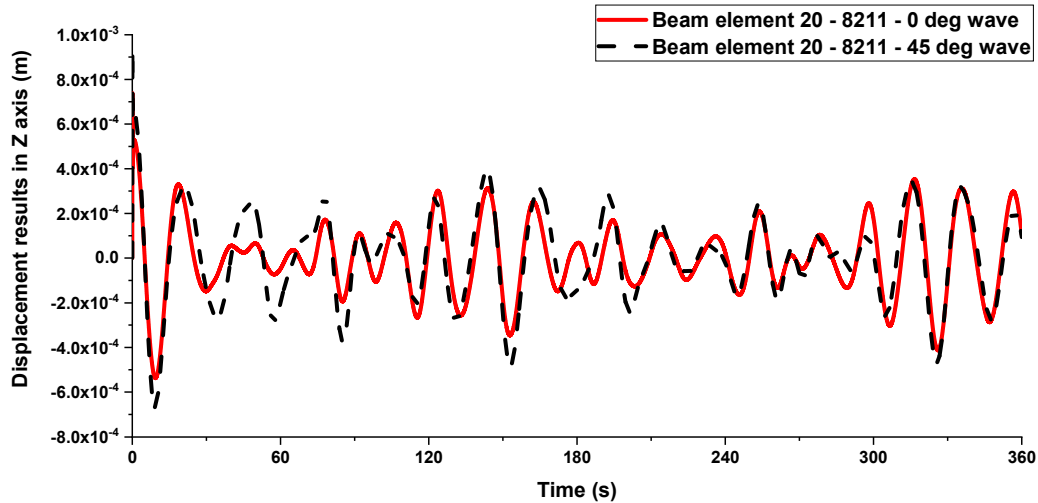


Figure 114. Displacement results of the beam element 20 in Z direction with 0-degree and 45-degree sea wave conditions respectively.

Based on the above figures, it can analyse and discuss the dynamic response of the ship's hull girder under different wave conditions (0-degrees and 45-degrees) for various beam elements representing different sections of the ship. The displacement response for beam element 01 (stern) shows similar patterns for both 0-degree and 45-degree wave conditions, indicating minimal variation in dynamic response due to the change in wave direction. For beam element 06 (quarter length from stern), the displacement response demonstrates a noticeable difference between 0-degree and 45-degree wave conditions, with more pronounced amplitude and frequency of oscillations in the 45-degree wave condition. Beam element 10 (midship) shows a distinct increase in amplitude for the 45-degree wave condition compared to the 0-degree wave condition, suggesting greater sensitivity to oblique wave impacts. Beam element 16 (three-quarter length from stern) exhibits significant differences between the two wave conditions, with higher amplitude oscillations in the 45-degree wave condition. Similarly, the displacement response for beam element 20 (bow) shows minimal differences between 0-degree and 45-degree wave conditions, with slight variations in amplitude.

The dynamic response of the ship's hull girder is significantly influenced by the direction of the waves, as observed in the above figures. The midship and sections near the midship (beam elements 06, 10, and 16) exhibit greater sensitivity to changes in

wave direction compared to the bow and stern (beam elements 01 and 20). The amplitude of the dynamic response is generally higher in the 45-degree wave condition compared to the 0-degree wave condition, suggesting that oblique waves impose greater dynamic loads on the hull girder, leading to increased structural response. The midship region (beam element 10) and sections close to it are more susceptible to dynamic loads induced by varying wave directions, indicating the need for special consideration in the design and analysis phase to ensure structural integrity under different sea conditions. Conversely, the stern and bow sections show consistent dynamic responses irrespective of the wave direction, indicating these areas are less affected by changes in wave approach angles, likely due to their inherent structural stiffness and design characteristics. Understanding the dynamic response under different wave conditions is crucial for optimizing the design and ensuring the safety and longevity of the ship's structure. These observations highlight the importance of considering wave direction and dynamic loading conditions in the structural analysis of marine vessels to ensure robust and resilient design.

On the other hand, similarly, the following figures illustrate the angular responses for these sections, providing insights into how different wave directions impact the ship's structural dynamics.

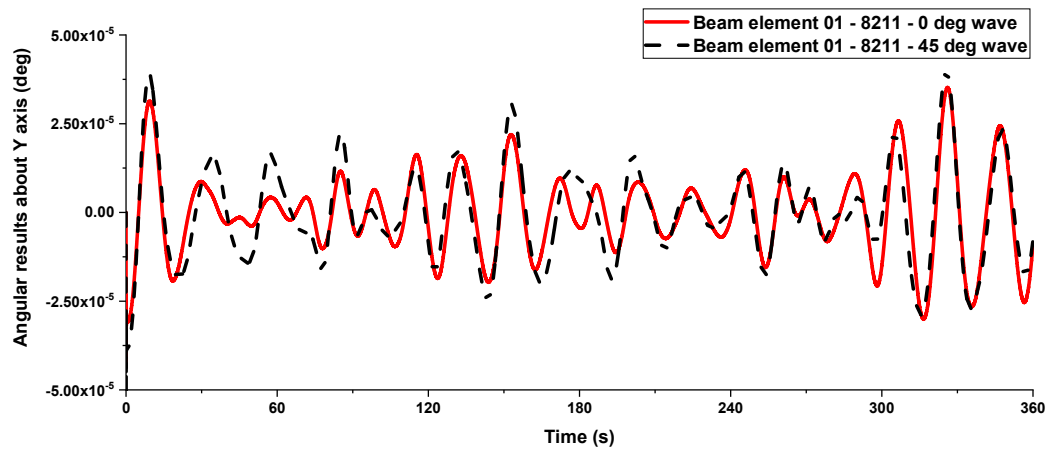


Figure 115. Angular results of the beam element 01 in Z direction with 0-degree and 45-degree sea wave conditions respectively.

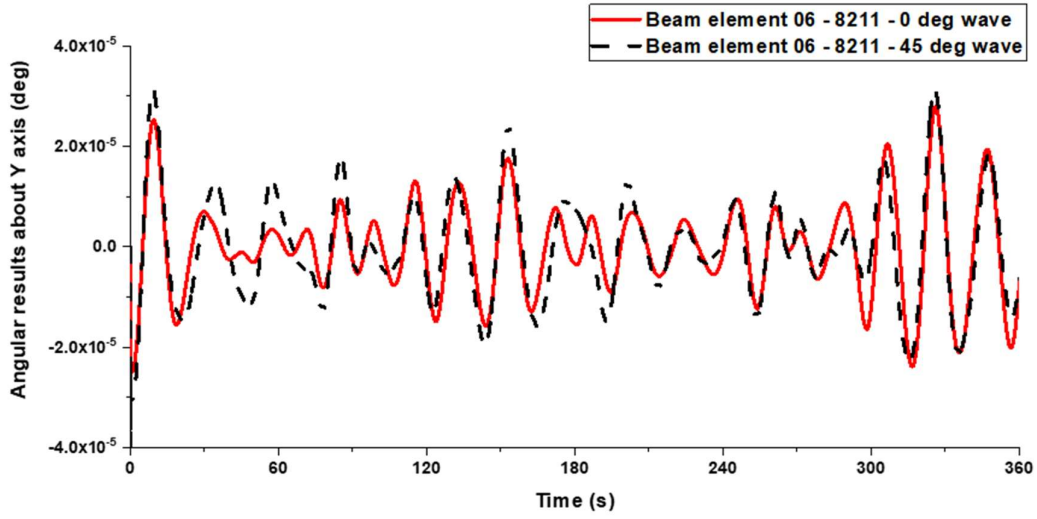


Figure 116. Angular results of the beam element 06 in Z direction with 0-degree and 45-degree sea wave conditions respectively.

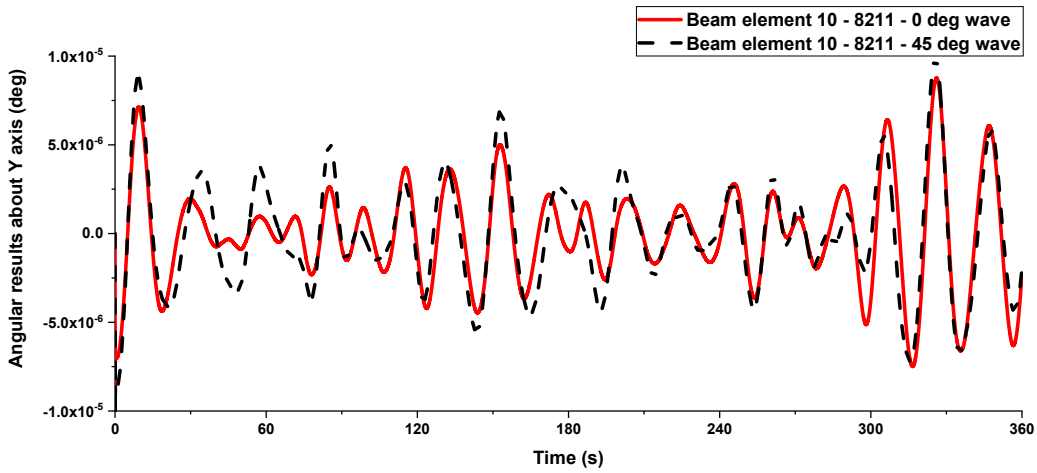


Figure 117. Angular results of the beam element 10 in Z direction with 0-degree and 45-degree sea wave conditions respectively.

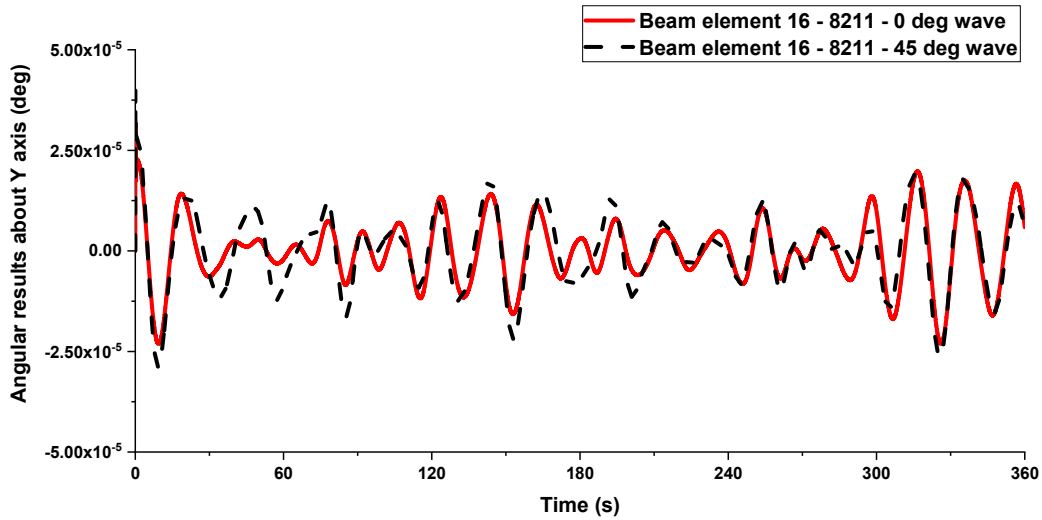


Figure 118. Angular results of the beam element 16 in Z direction with 0-degree and 45-degree sea wave conditions respectively.

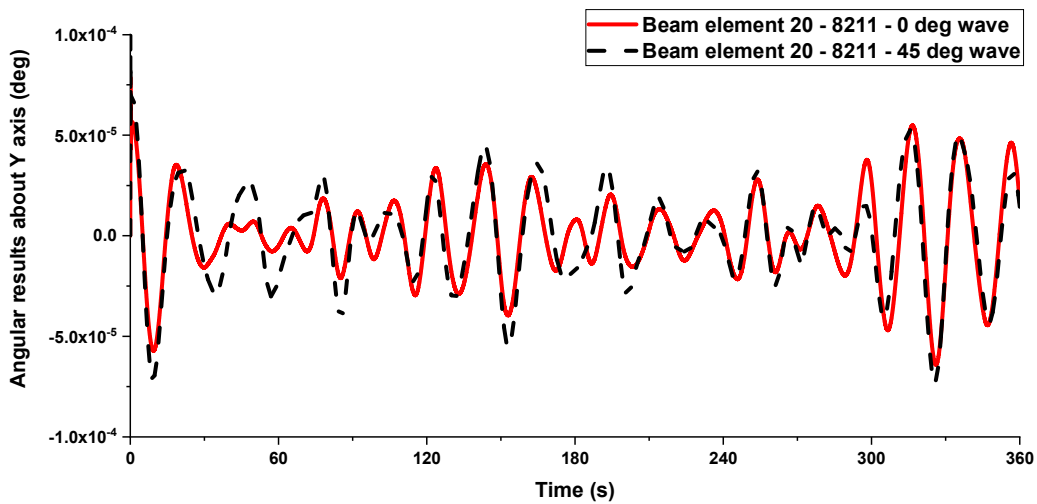


Figure 119. Angular results of the beam element 20 in Z direction with 0-degree and 45-degree sea wave conditions respectively.

Based on the above figures, the angular response for beam element 01 (stern) shows similar patterns for both wave conditions, indicating minimal variation. For beam element 06 (quarter length from stern), there is a noticeable difference, with higher amplitude and frequency in the 45-degree wave condition. Beam element 10 (midship) also shows increased amplitude under the 45-degree wave condition, suggesting greater sensitivity to oblique wave impacts. Beam element 16 (three-quarter length from stern)

exhibits significant differences between the wave conditions, with higher amplitude oscillations in the 45-degree wave condition. Lastly, beam element 20 (bow) shows minimal differences between the two conditions, similar to the stern, with slight variations in amplitude.

The angular response results highlight that the dynamic response of the ship's hull girder is significantly influenced by the direction of the waves. The midship and sections near the midship (beam elements 06, 10, and 16) exhibit greater sensitivity to changes in wave direction compared to the bow and stern (beam elements 01 and 20). The amplitude of the dynamic response is generally higher in the 45-degree wave condition, indicating that oblique waves impose greater dynamic loads on the hull girder. This suggests that the midship region and its adjacent sections should be given special consideration in the design and analysis phase to ensure structural integrity under different sea conditions. The stern and bow sections show consistent dynamic responses irrespective of the wave direction, likely due to their inherent structural stiffness and design characteristics. Overall, these observations underscore the importance of considering wave direction and dynamic loading conditions in the structural analysis of marine vessels to ensure robust and resilient design.

In this section, all the results presented are expressed in the local coordinate system of the hull girder. Whether they are angular or translational displacement responses, these results can be transferred to the corresponding sections of the ship's finite element model using MPC technology in ANSYS software. This will enable the sectional motion in the finite element model to be based on the computed time-history response results, ultimately allowing for stress computations in the finite element model. This step is crucial for in-depth stress distribution analysis and a more comprehensive structural response assessment.

4.6. Results by FE analysis

This section gives FEM analysis results of target research vessel in ANSYS and its further structural analysis results throughout the MPC technology based on dynamic responses results calculated by the TVM_HullGirder programme from section 4.5.

4.6.1. FE Model settings in ANSYS

A significant number of discontinuous ship structural components are primarily distributed in the midship section of the TSHD vessel. Therefore, in this section, a real-size model is established in ANSYS for the midship section of the TSHD, which is also a variable mass structure, as shown in Figure 120 and Figure 121.



Figure 120. Geometric model of middle sections in ANSYS from main view.

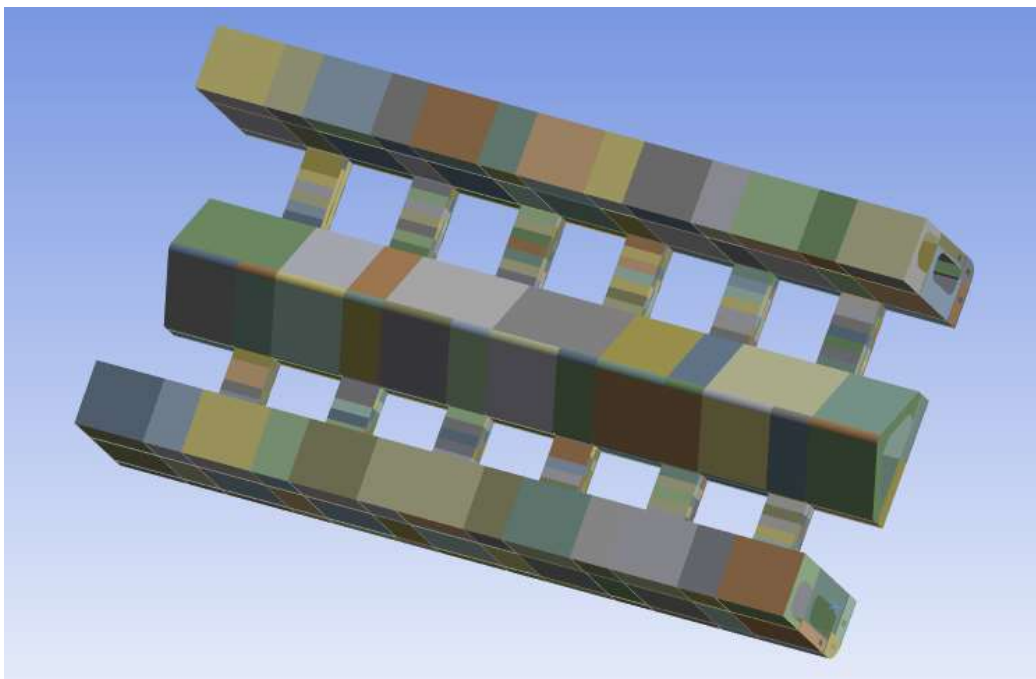


Figure 121. Geometric model of middle sections in ANSYS from top view.

The geometric model above is based on the actual ship dimensions and plate thickness, with appropriate structural simplifications and modifications to achieve more accurate computational results with maximum computational efficiency.

Figure 122 illustrates the meshing of the finite element model using predominantly quadrilateral shell elements in ANSYS.

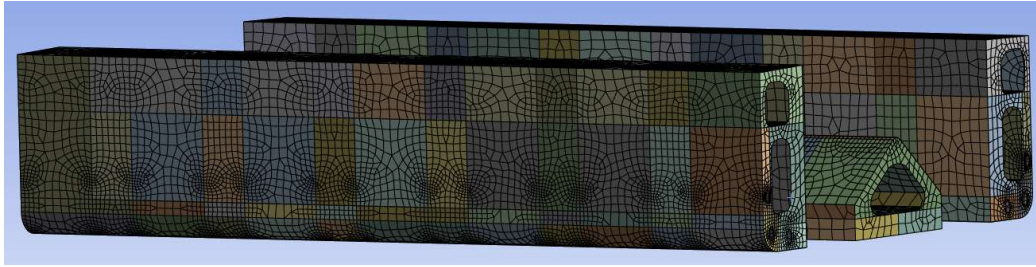


Figure 122. Finite element model of middle sections in ANSYS.

Figure 123 displays the configuration of MPC surfaces in the finite element model. In this context, the definition of the MPC surfaces from A, B, C, D, E, F (shown in Figure 123) corresponds to the right nodes of beam elements 7, 8, 9, 10, 11, 12, 13 in the hull girder model (Figure 82).

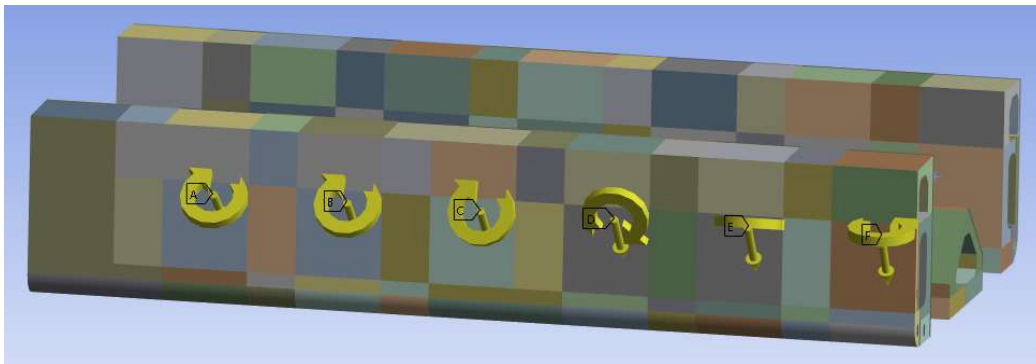


Figure 123. MPC settings in six cross sections of middle parts.

Figure 124 and Figure 125 illustrate examples of MPC technology settings in ANSYS at points A (beam element 07) and C (beam element 09). In this case study, the dynamic response results for translational and rotational degrees of freedom are applied to the corresponding FEM ship cross-sections using MPC technology.

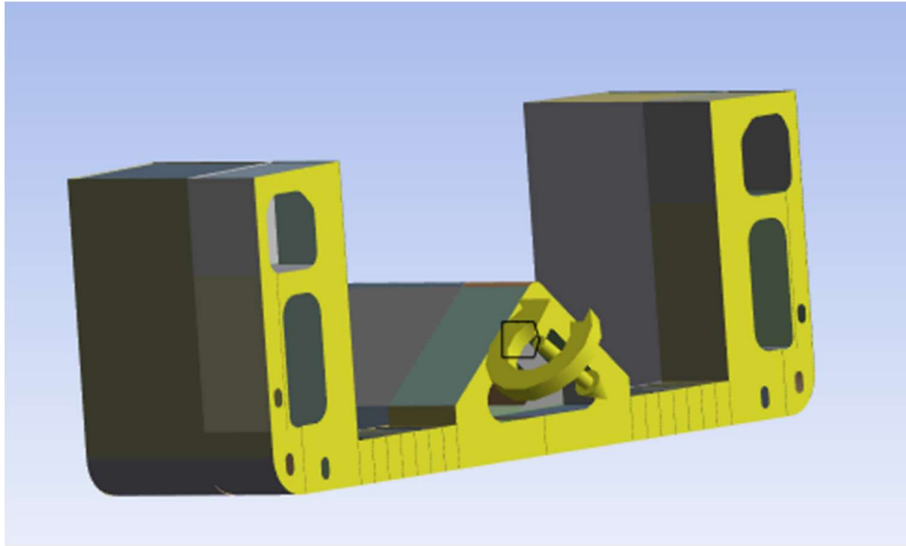


Figure 124. MPC setting at A surface corresponds to beam element 07.

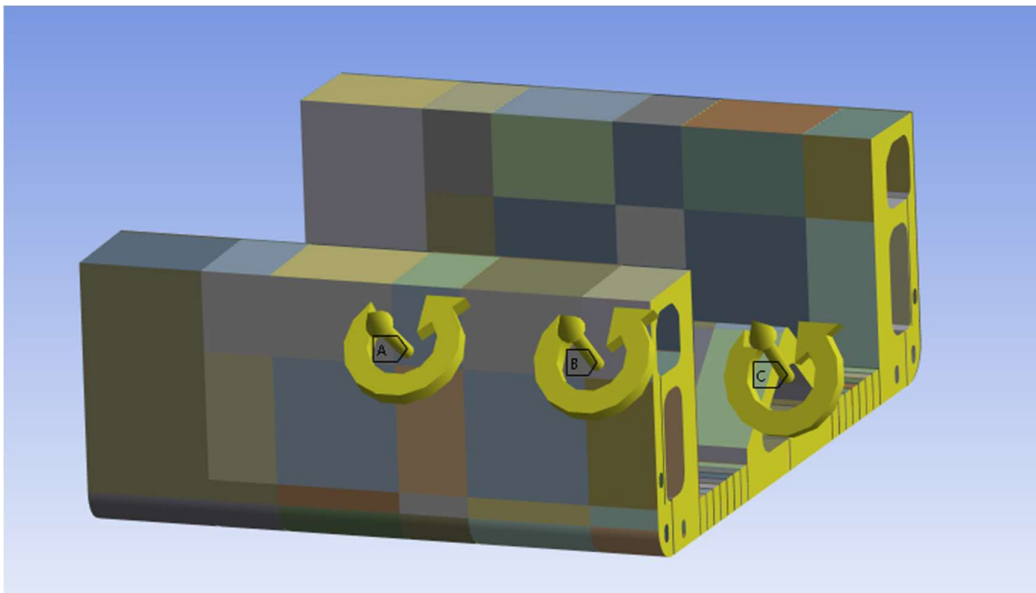


Figure 125. MPC setting at C surface corresponds to beam element 09.

4.6.2. FEA results in ANSYS by MPC

Based on the calculation results outputted by the TVM_HullGirder program from 4.5 section, this section selects the structural vibration dynamic response results expressed in local coordinate system with the 0-degree heading wave and 45-degree oblique wave sea states during the unloading working conditions. These results account for the coupled effects of rigid motion and flexible deformation of the TSHD. They are inputted into the FEM in ANSYS using MPC technology. The post-processing analysis

results for the following structure are all outputted by the ANSYS finite element software.

The following figures illustrate the stress analysis results for the hull girder under various wave conditions and mass scenarios, specifically focusing on the maximum equivalent von-Mises stress (Figure 126), maximum principal stress (Figure 127), and maximum stress intensity (Figure 128).

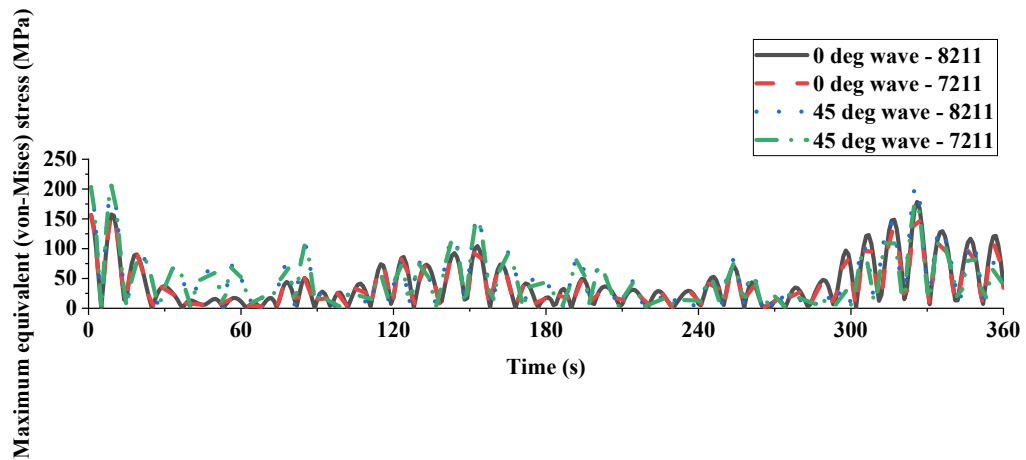


Figure 126. Maximum von-Mises stress during the simulation time with different case settings.

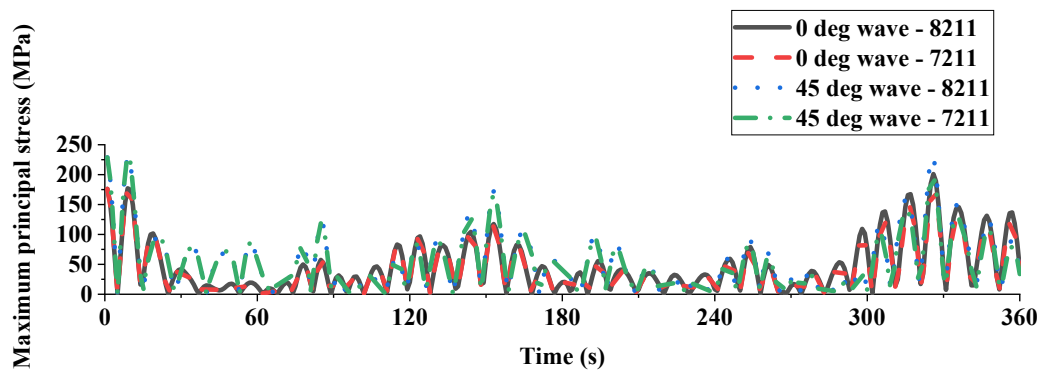


Figure 127. Maximum principal stress during the simulation time with different case settings.

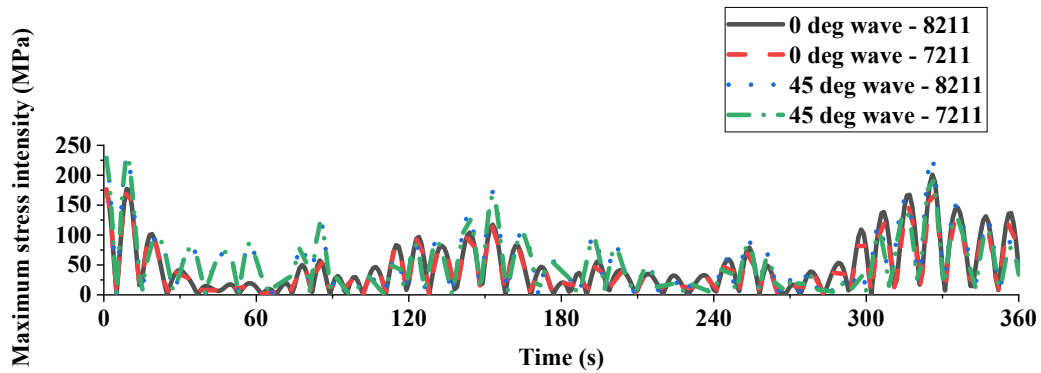


Figure 128. Maximum stress intensity during the simulation time with different case settings.

The above figures illustrate the stress analysis results for the hull girder under various wave conditions and mass scenarios. Figure 126 displays the maximum equivalent von-Mises stress over the simulation time, comparing stress levels between 0-degree wave (heading wave) and 45-degree wave (oblique wave) under both unloading (variable mass, labelled as 8211) and invariant mass (labelled as 7211) conditions. Figure 127 presents the maximum principal stress during the simulation time for the same conditions, and Figure 128 shows the maximum stress intensity throughout the simulation period, comparing different wave directions and mass scenarios.

The analysis of the stress response of the hull girder under different wave directions and mass conditions reveals significant insights into the vessel's structural behaviour. The stress responses exhibit considerable variation between 0-degree and 45-degree wave conditions, with the 45-degree wave direction resulting in higher stress levels across all measures, indicating that oblique waves exert more substantial dynamic loads on the hull girder. In 8211 scenarios, representing unloading (variable mass) conditions, generally show higher stress values compared to the 7211 scenarios (invariant mass conditions), demonstrating that mass variation during unloading significantly influences stress distribution and magnitude, necessitating careful consideration during the design and operational phases. Stress peaks are more pronounced in the 45-degree wave conditions, suggesting greater stress concentrations and potential fatigue issues under oblique wave impacts. These findings underscore the importance of accounting for both wave direction and mass variability in the structural analysis of marine vessels, ensuring that the structural design can withstand these dynamic loads to maintain

structural integrity and prevent fatigue damage over time. In summary, the results highlight the critical role of dynamic loading conditions, particularly wave direction and mass variation, in the stress response of marine vessels, essential for optimizing design and ensuring long-term durability and safety.

Similarly, the following figures illustrate the strain analysis results for the hull girder under various wave conditions and mass scenarios, specifically focusing on the maximum equivalent strain (Figure 129), maximum principal elastic strain (Figure 130), and maximum elastic strain intensity (Figure 131).

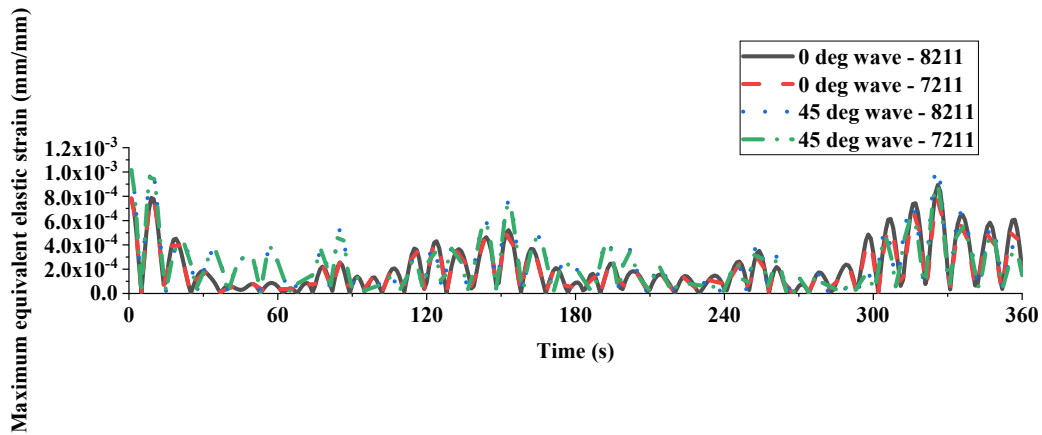


Figure 129. Maximum equivalent strain during the simulation time with different case settings.

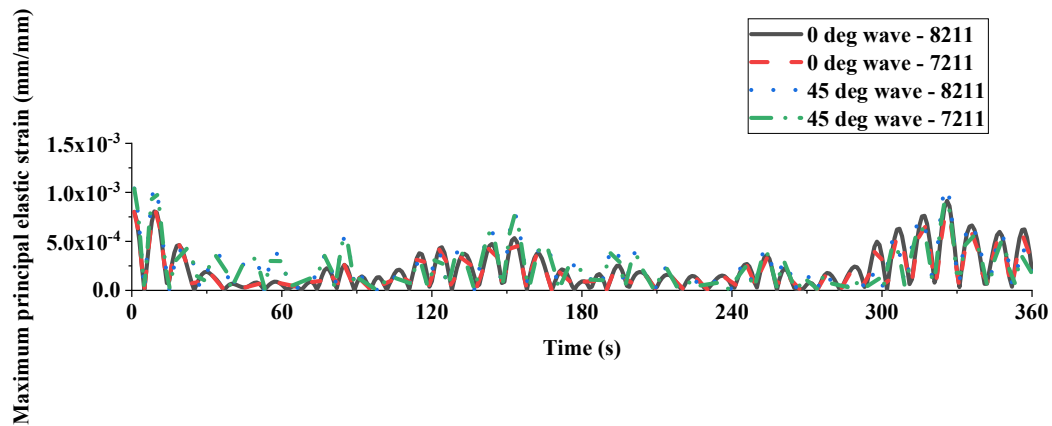


Figure 130. Maximum principal elastic strain during the simulation time with different case settings.

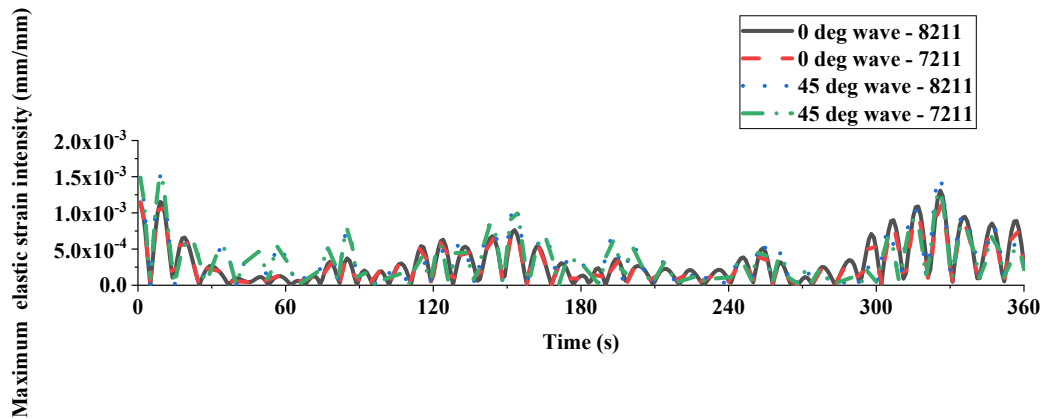


Figure 131. Maximum elastic strain intensity during the simulation time with different case settings.

Based on the above figures, the analysis of the strain responses of the hull girder under different wave directions and mass conditions reveals significant insights into the vessel's structural behaviour. The strain responses exhibit considerable variation between 0-degree and 45-degree wave conditions, with the 45-degree wave direction resulting in higher strain levels across all measures, indicating that oblique waves exert more substantial dynamic loads on the hull girder. In the 8211 scenarios, representing unloading (variable mass) conditions, strain values are generally higher compared to the 7211 scenarios (invariant mass conditions), indicating that mass variation during unloading significantly influences strain distribution and magnitude, necessitating careful consideration during design and operational phases. The peaks in strain are more pronounced in the 45-degree wave conditions, suggesting greater strain concentrations and potential fatigue issues under oblique wave impacts.

Additionally, the following Figure 132 illustrate maximum total deformation analysis results for the hull girder under various wave conditions and mass scenarios.

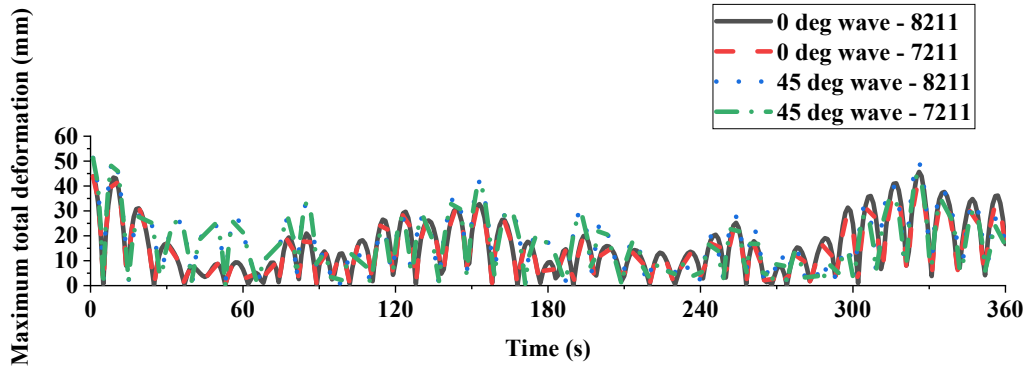


Figure 132. Maximum total deformation during the simulation time with different case settings.

The deformation responses show significant variation between 0-degree (heading wave) and 45-degree (oblique wave) conditions. The 45-degree wave direction results in higher deformation levels, indicating that oblique waves exert greater dynamic loads on the hull girder. The variable mass scenarios (8211) exhibit generally higher deformation values compared to the invariant mass scenarios (7211). This suggests that mass variation during unloading significantly impacts the deformation distribution and magnitude. Deformation peaks are more pronounced under 45-degree wave conditions, highlighting greater deformation concentrations. This indicates that the hull girder faces more significant structural loads and potential fatigue issues under oblique wave impacts. The analysis underscores the importance of considering both wave direction and mass variability in the structural design and analysis of marine vessels. The findings highlight that oblique waves and variable mass conditions lead to higher deformation.

In summary, the structural analysis of stress, strain, and total deformation conducted in ANSYS clearly indicates that both the oblique wave condition and variable mass condition significantly impact the ship's structure. The analysis reveals that oblique waves exert greater dynamic loads, leading to higher stress, strain, and deformation levels. Similarly, the variable mass conditions during unloading also result in increased structural responses compared to constant mass conditions. Consequently, for the TSHD vessel structure, it is crucial to account for the combined effects of oblique waves and variable mass during the design and operational phases. Among the various conditions analysed, the head wave dumping condition exerts the least influence on the

vessel's structural integrity, making it the most favourable scenario in terms of minimizing structural impact.

The following figures provide a visual representation of the maximum equivalent von-Mises stress distribution in the middle parts of real-scale ship's FEM under different wave directions and mass conditions at 326s. These images help to analyse the structural integrity of the hull under various operational scenarios.

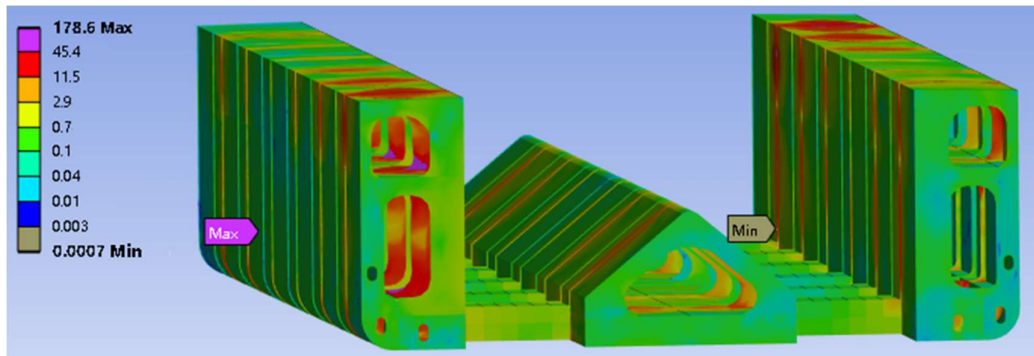


Figure 133. Maximum equivalent von-Mises stress in 0-degree wave - 8211.

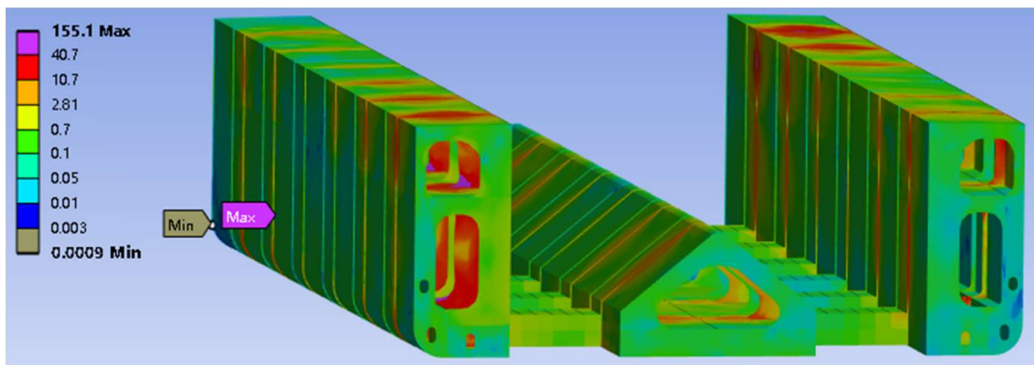


Figure 134. Maximum equivalent von-Mises stress in 0-degree wave - 7211.

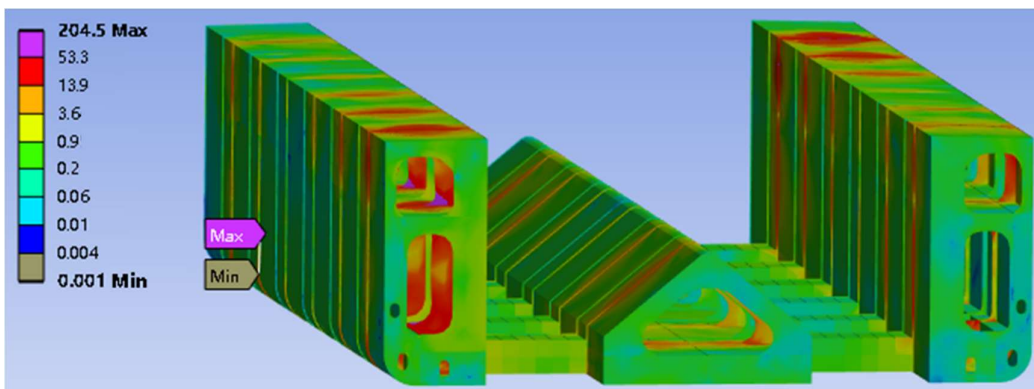


Figure 135. Maximum equivalent von-Mises stress in 45-degree wave - 8211.

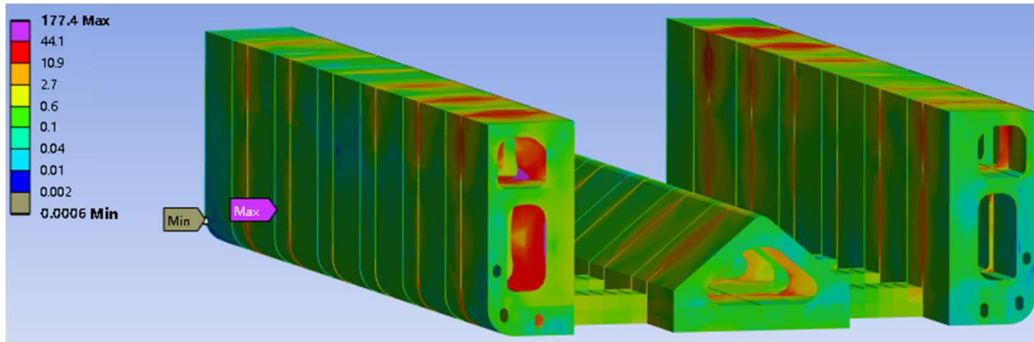


Figure 136. Maximum equivalent von-Mises stress in 45-degree wave - 7211.

The analysis of the von-Mises stress distribution under different wave directions and mass conditions reveals significant insights into the structural behaviour of the vessel. When comparing the stress responses between the 0-degree and 45-degree wave conditions, it becomes evident that the oblique waves exert greater dynamic loads on the vessel. Specifically, the maximum stress under the 45-degree wave condition with invariant mass (7211) reaches 177.4 MPa (Figure 136), which is higher than the 155.1 MPa (Figure 134) observed under the 0-degree wave condition.

Further examining the impact of mass variation, the variable mass scenarios (8211) generally show higher stress values compared to the invariant mass scenarios. Under the 0-degree wave condition with variable mass, the maximum stress is 178.6 MPa (Figure 133), significantly higher than the invariant mass scenario. This effect is even more pronounced under the 45-degree wave condition, where the maximum stress increases to 204.5 MPa with variable mass (Figure 135). These findings suggest that mass variation during unloading significantly influences the stress distribution and magnitude, necessitating careful consideration during the design and operational phases.

The stress concentrations are more pronounced under the 45-degree wave conditions and variable mass scenarios, with the highest stress levels observed in Figure 135. This indicates that the hull girder faces more significant structural loads and potential fatigue issues under oblique wave impacts and varying mass conditions. The higher stress peaks in these scenarios highlight the need for robust design strategies to ensure the vessel's structural integrity and longevity.

In summary, the structural analysis of von-Mises stress in ANSYS demonstrates that both oblique wave conditions and variable mass scenarios significantly impact the ship's structure. The highest stress levels, reaching up to 204.5 MPa, are observed under

45-degree wave conditions with variable mass in this case study. These results underscore the necessity for meticulous design considerations to maintain the structural integrity and prevent fatigue damage over time. For TSHD vessels, accounting for dynamic loading conditions, such as wave direction and mass variation, is crucial in optimizing design and ensuring the long-term durability and safety of the ship's structure.

The design of the ship's cross-section plays a significant role in determining its ability to withstand dynamic loads. The cross-sections analysed in the following figures display varying stress distributions by selecting some key points of beam element 07 at 326s as examples under different wave and mass conditions.

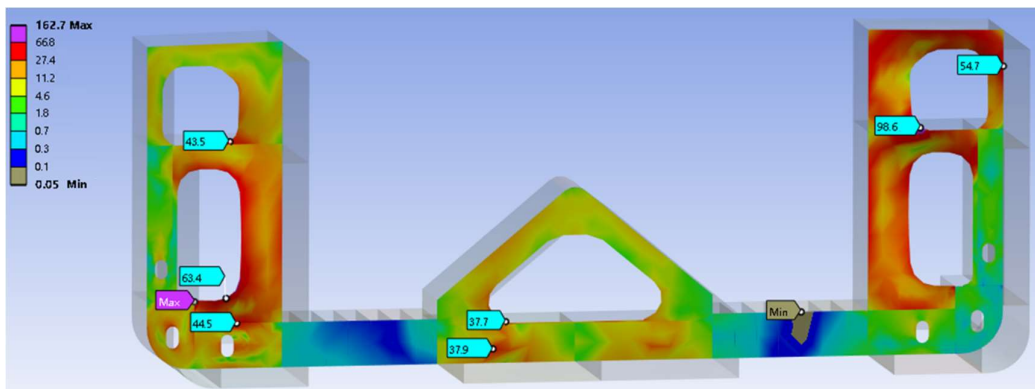


Figure 137. Selected von-Mises stress points on the cross-section of beam element 07 in 0-degree wave -8211.

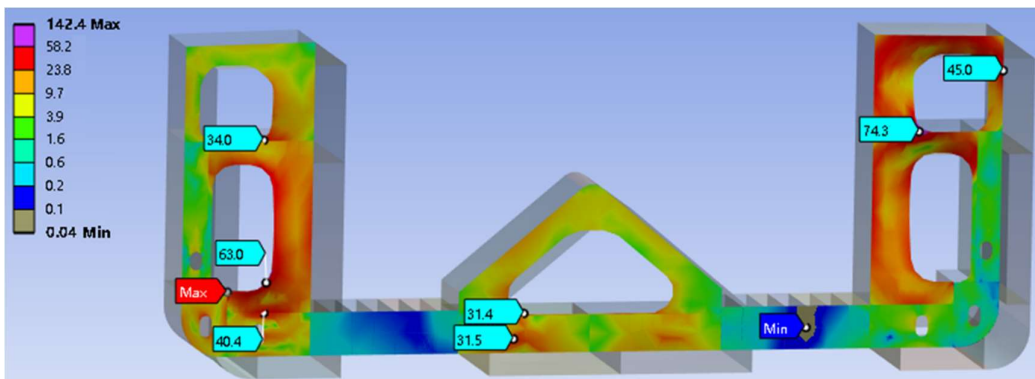


Figure 138. Selected von-Mises stress points on the cross-section of beam element 07 in 0-degree wave -7211.

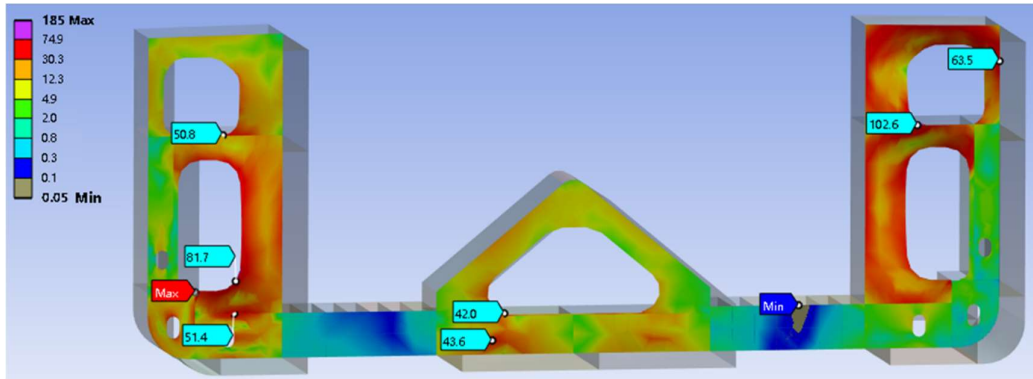


Figure 139. Selected von-Mises stress points on the cross-section of beam element 07 in 45-degree wave -8211.

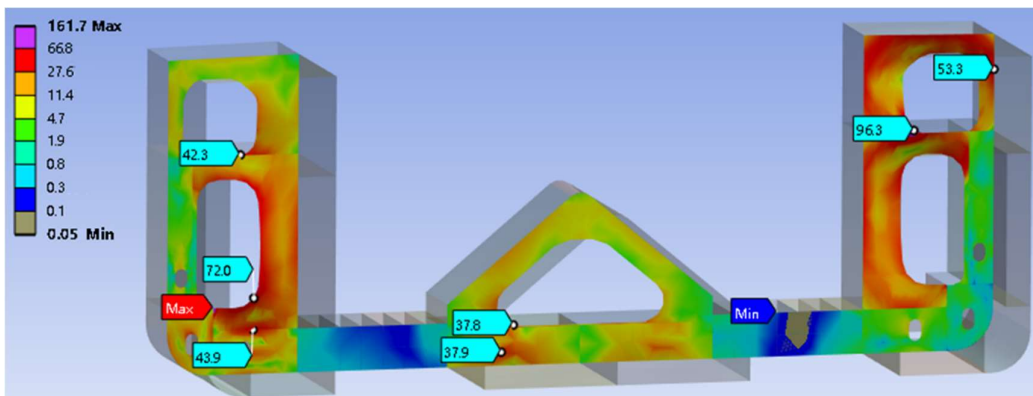


Figure 140. Selected von-Mises stress points on the cross-section of beam element 07 in 45-degree wave -7211.

The stress analysis values from the selected points on beam element 07 under various wave and mass conditions provide detailed insights into the structural performance and stress distribution in critical areas of the ship’s hull girder. Under the 0-degree wave and invariant mass scenario (7211), the stress distribution is relatively uniform, with notable stress concentrations around the structural cutouts. The stress values range from 31.4 MPa to 142.4 MPa, indicating that while the structure handles the head-on wave direction relatively well, certain areas experience higher stress due to geometric discontinuities.

In contrast, when the mass changes during unloading (8211) under the same wave conditions, the maximum stress increases significantly, ranging from 42.0 MPa to 162.2 MPa. This highlights the impact of mass variation on stress distribution. The increase in stress values compared to the invariant mass scenario indicates that dynamic loading

conditions during unloading significantly affect the structural integrity. Design improvements should focus on accommodating these variable loads, possibly through material enhancements or additional support structures.

Under oblique wave conditions (45-degree wave), the stress values show a higher range, from 37.8 MPa to 161.7 MPa, even with invariant mass (7211). This scenario demonstrates that oblique waves impose greater dynamic loads on the structure. The stress concentration near the cutouts and supports in the upper structure necessitates focused reinforcement to mitigate the effects of oblique wave impacts. When mass variation is introduced in the 45-degree wave scenario (8211), the stress levels are the highest observed, ranging from 42.0 MPa to 185.0 MPa. The combination of oblique wave direction and mass variation presents the most challenging scenario for structural integrity, indicating that these areas are highly susceptible to dynamic loads and potential fatigue issues.

The analysis of selected points on beam element 07 under different conditions reveals critical areas of high stress concentration, particularly around structural cutouts and support structures. Both wave direction and mass variation significantly influence the stress distribution, with oblique waves and variable mass conditions leading to the highest stress levels. To ensure the structural integrity and longevity of the ship's hull girder, it is essential to reinforce areas around cutouts and support structures, use higher strength materials or additional supports in high-stress regions, and consider the effects of dynamic loading conditions, particularly during unloading operations. By addressing these factors in the design phase, the ship can better withstand dynamic loads, maintain structural integrity, and reduce the risk of fatigue damage over time.

In this section, the dynamic response results calculated by the TVM_HullGirder program in Section 4.5 are applied to the FEM of the study object using the MPC technology in the finite element software ANSYS. Utilizing finite element techniques enables a more detailed post-processing analysis of ship structures, including stress analysis, strain analysis, and deformation analysis. Moreover, users can customize the selection of specific nodes or structural regions to output the time history results of structural calculations. This is not limited to stress, strain, and deformation but can also include subsequent assessments such as fatigue evaluations and strength analysis results.

4.6.3. Verifications by qualitative analysis

In this section, it performs a qualitative analysis to verify the validity of computational results of proposed model, specifically focusing on the engine room column distribution and the associated vibrations and stresses in the TSHD vessel. The analysis conducted by a dredging company in 2019 using the PRUFTECHNIK Vibxpert II vibration analyser provides critical data points for key equipment and structural regions, including the columns in the engine room. The following figure shows the columns distribution in the engine room by the measurement analysis report of a TSHD vessel provided by a dredging company.

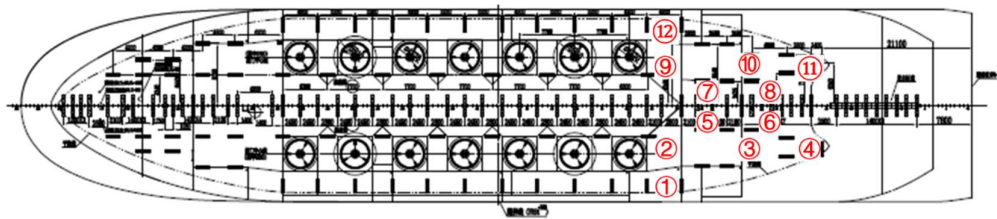


Figure 141. Column distribution diagram in engine room of the TSHD.

The measurement task primarily focused on low-frequency vibration analysis to determine whether conditions such as imbalance and misalignment fell within the DNV standards. The primary standard utilized for report analysis was the DNV Vibration Class, Ch6 Pt 15 (DNV GL, 2005), which is used for ships and offshore drilling platforms, providing guidelines for the installation of marine gearboxes, diesel engines, motors, and bearing boxes etc.

In the report, it was found that the bearing box of the high-pressure water pump exhibited rotational looseness, and resonance occurred in some of the engine room columns. The vibration measurements indicated that the vibrations in the engine room columns predominantly originated from the propeller rotation frequency and the operating frequency peaks of the main diesel engine.

During the measurement period, it was observed that the resonance phenomenon of column 1 (Figure 142) had disappeared, with the total vibration value falling below the DNV alarm standard. However, columns 2 (Figure 143) and 7 (Figure 144) exhibited resonance at 35Hz (3.5 times the main diesel engine's rotational frequency), with total vibration values exceeding the DNV warning standard. Other columns maintained total vibration values below the DNV standards, indicating minimal impact on surrounding

equipment. It was recommended that the surrounding equipment of columns 1 and 2 in the engine room be inspected before restarting after prolonged shutdowns to prevent secondary failures caused by vibrations.

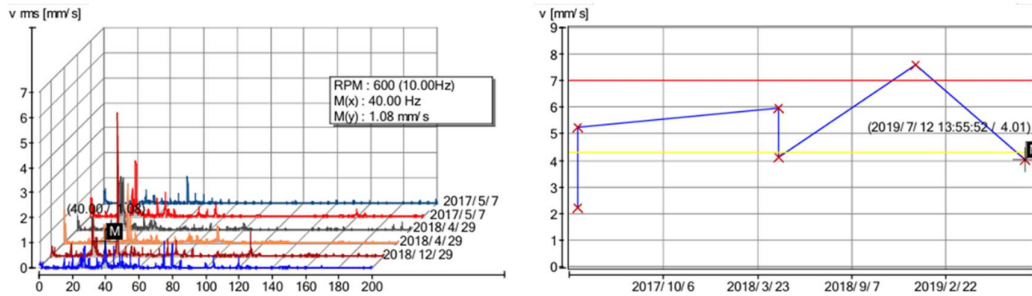


Figure 142. Velocity spectrum (left) and virtual value (right) of engine room column 1.

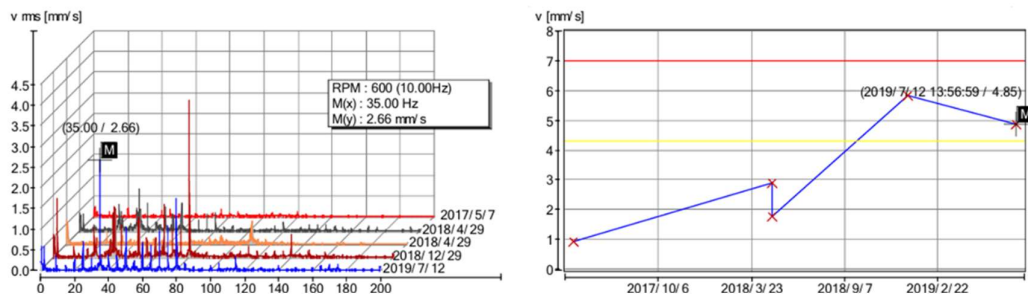


Figure 143. Velocity spectrum (left) and virtual value (right) of engine room column 2.

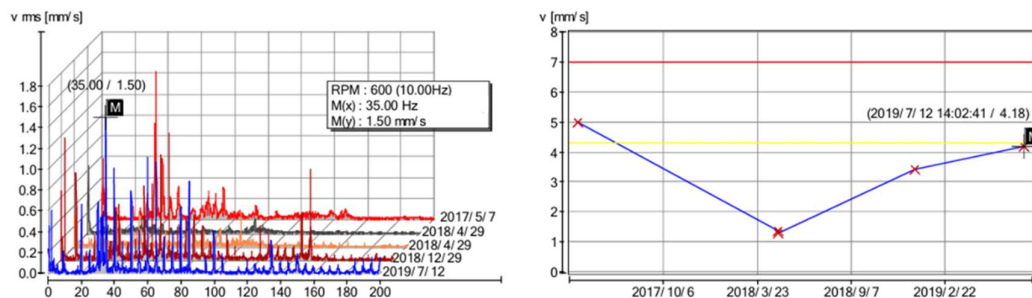


Figure 144. Velocity spectrum (left) and virtual value (right) of engine room column 7.

Based on the qualitative analysis of the engine room columns, it is evident that the vibrational responses and stress concentrations at the 1/4 positions of the ship's hull, specifically around columns 1, 2, 9, and 12, align with the computational results presented in section 4.5.2 and 4.6 in this thesis. The resonance and vibration data

corroborate the modelled dynamic responses, particularly in regions prone to higher stress and vibrational impact due to the unique structural characteristics of the TSHD vessel.

The qualitative data from the vibration measurements serve as a verification for the computational models used in this study. The alignment of observed resonance phenomena and stress concentrations with the simulated outcomes demonstrates the reliability and accuracy of the proposed models. This congruence between empirical data and simulation results strengthens the validity of proposed approach in analysing the dynamic structural responses of marine vessels with large openings and complex load distributions, such as TSHDs.

4.7. Summary of Chapter 4

In Chapter 4, it concludes with a comprehensive validation of the semi-analytical approach for analysing the vibration characteristics of variable cross-section beams by comparing it with FEA results, confirming its feasibility and efficiency. The chapter also details the use of SESAM software to pre-calculate hydrodynamic parameters for ten unloading load cases. Subsequently, the self-developed program TVM_HullGirder is employed to analyse the vibration response of a three-dimensional hull girder model, assessing the effects of time-varying hydrodynamic results. This includes the calculation of the rigid-flexible coupling motion response and the structural dynamic response of selected cross-sections of the hull girder. Finally, the dynamic response results generated by the TVM_HullGirder program are integrated into the ship's finite element model using MPC technology in ANSYS for further structural strength assessments, and the FEA results for the full-scale three-dimensional vessel model are presented. Additionally, qualitative analysis based on the engine room column data further validates the model results, showing concentrated vibration responses and stress distributions at the 1/4 sections of the hull, aligning well with the computed outcomes.

Chapter 5. Conclusions and future works

As some special vessels in the field of marine engineering, such as TSHD is designed with unique purposes and distinctive structural features to meet the requirements of marine engineering applications. These vessels, along with other types of offshore vessels exhibiting similar characteristics, such as variable mass properties and large structural discontinuities, present significant challenges in both design and assessment. The inherent complexities of their dynamic behaviours, influenced by time-varying mass and structural discontinuities, create gaps in the current understanding and capabilities of structural analysis and design methods.

To address these challenges, this thesis has developed a set of innovative time-domain programs specifically tailored for the dynamic response calculation of such specialized vessels. This programme, when combined with existing commercial software, enables efficient and versatile analysis that fills critical gaps in the field. These gaps include the accurate prediction of dynamic responses under variable mass conditions, the impact of structural discontinuities on overall vessel integrity, and the need for robust tools that integrate seamlessly with advanced finite element analysis (FEA) for detailed stress, strain, and deformation analysis. The implementation of these programs not only enhances the precision of dynamic response predictions but also provides engineers with the tools necessary for thorough and effective design assessments, ensuring the safety, reliability, and performance of specialized marine vessels.

5.1. Proposed math and numerical model

In this thesis, a novel mathematical and numerical model for dynamic analysis of marine vessel during loading or unloading working conditions based on the following key theories and approaches has been proposed (TVM_HullGirder programme):

- Modified Euler-Bernoulli beam with time-varying mass functions.
- Improved Kane's dynamic method with time-varying mass system applied in variable cross-section hull girder with support from the semi-analytical approach for the vibration characteristic analysis of variable cross-section Euler-Bernoulli beam.

- Time-varying wet surface and trim characteristics of the hull girder considered in time-varying hydrodynamic calculations.
- Complex excitation loads coupled with dynamic model.

The proposed math model has been developed and compiled as a time-history dynamic analysis programme by FORTRAN language, and it is suitable for the following purposes:

- Vibrational characteristics analysis of marine vessels with time-varying mass systems, combined with pre-analysis results from SESAM as input files.
- Motion response calculations for marine vessels with time-varying mass systems, treated as either rigid body or rigid-flexible coupled body.
- Dynamic response calculations for individual cross-sections of marine vessels with time-varying mass systems, considered as rigid-flexible coupled body.

Most types of dynamic responses that engineering applications concerned about can be outputted from TVM_HullGirder programme based on the proposed model in this thesis. These dynamic results could be transferred into individual cross-sections on the FEM of the target vessel by MPC technology in commercial FE software for the further stress, strain, and strength and fatigue assessments.

5.2. Novelty and impact of the work

From pioneering new methodologies that challenge conventional paradigms to revealing innovative insights that expand the boundaries of current knowledge, and the cases of studies based on results calculated by proposed model and its programme combined with application of current finite element software, the novelties of this research are highlighted as follows:

- A novel mathematical and numerical model for dynamic analysis of marine vessels under time-varying mass conditions has been developed.
- This model has been implemented into a time-history dynamic analysis program, TVM_HullGirder, written in FORTRAN.

- The TVM_HullGirder program is capable of calculating and outputting both motion responses of the marine vessel and local structural dynamic responses in the time domain.
- The results produced by the program can be seamlessly transferred to a detailed FEM using MPC technology for further structural analysis and assessment.
- By conducting post-processing structural FEA, engineers can quickly identify design flaws or other deficiencies, facilitating rapid evaluation and optimization of the structure during the design phase.

The research conducted by this PhD study has made significant contributions to the field of marine engineering, specifically in the dynamic analysis of marine vessels with time-varying mass properties. The development and implementation of a novel mathematical and numerical model for TSHDs represent a substantial advancement in the understanding and assessment of these complex structures. Some impacts of this research are summarized as follows:

(1) Methodological advancements

One of the primary impacts of this research is the introduction of a robust time-domain program that effectively calculates the dynamic response of specialized marine vessels. This program, tailored for marine vessels, addresses the unique challenges posed by variable mass properties and large structural discontinuities. By integrating this program with existing commercial software, the research has bridged significant gaps in current analytical capabilities, providing a more comprehensive and accurate tool for structural analysis.

(2) Contribution to structural design and assessment

This PhD work has improved the design and assessment processes for marine vessels, ensuring better safety and performance. The ability to accurately predict the dynamic behaviour of TSHDs under various operational conditions allows for more informed design decisions and enhances the reliability of these vessels. This research also sets a precedent for the analysis of other offshore vessels with similar characteristics, broadening the applicability of the developed methodologies.

(3) Academic and industry impact

Academically, this research has added valuable knowledge to the field of marine engineering. The findings and methodologies have the potential to be widely cited and used as a foundation for further studies. For the industry, the practical implications of this research are profound. Ship designers and engineers now have access to advanced tools that can significantly improve the structural integrity and operational efficiency of TSHDs and similar vessels.

(4) Future research and development

The impact of this research extends to future studies and developments. The methodologies and tools developed can be adapted and expanded to explore new areas within marine engineering. This includes the integration of additional variables affecting ship dynamics, such as hydrostatic loads and axial vibrations, in subsequent versions of the program. The groundwork laid by this study paves the way for continuous improvements and innovations in the dynamic analysis of marine structures.

(5) Personal contributions and development

I have demonstrated a high level of expertise and innovation throughout the research process. The successful development and implementation of the proposed model underscore my capability to tackle complex engineering problems and contribute valuable solutions. This experience has not only enriched my academic and professional skills but also positioned them as a significant contributor to the field of marine engineering.

5.3. Future works

The mathematical and numerical model developed in this thesis still faces many challenges. For example, the dynamic model does not consider the hydrostatic load of the ship, etc. This part of the module calculation needs to be added and verified in future work.

From the perspective of each module in the model proposed in this thesis, the following shortcomings can be identified:

(1) The excitation force calculation module of the hybrid-drive system of TSHDs should be continuously updated and developed to obtain more accurate excitation force calculation results in the programme.

The future challenge of the excitation force calculation module for the hybrid-drive system of TSHDs can be addressed by simplifying the hybrid-drive system through a mass model and coupling it with an appropriate stiffness and damping structure model. This approach can then be programmed and embedded into the current program to accurately calculate the vibration load output and its impact on the hull girder.

(2) The hydrodynamic calculation module in the current version of the programme needs to be added calculation function of hydrostatic loads of the marine vessel.

The challenge of enhancing the hydrodynamic calculation module in the current version of the program to include the calculation function of hydrostatic loads can be addressed by integrating a dedicated hydrostatic load calculation algorithm. This integration will involve developing and embedding the necessary computational routines within the existing program to accurately assess the hydrostatic loads on the marine vessel.

(3) The current program turns off the variables affecting the ship's axial vibration, and subsequent updated versions should consider this part for more precise calculation and analysis.

The challenge of incorporating variables affecting the ship's axial vibration in subsequent versions of the program can be addressed by integrating axial vibration analysis algorithms in Kane's dynamic equation. This will involve updating the program to include the necessary computational models and routines that account for axial vibration factors, ensuring more precise calculation and analysis of the ship's dynamic response.

(4) The dynamics module in the current mathematical model does not consider the impact of vibration modes on the first-order derivative and second-order derivative variables with regard to the time. Subsequent updated versions should consider this to explore whether it has a greater impact on the dynamic response of the structure.

The challenge of incorporating the impact of vibration modes on the first-order and second-order derivative variables with respect to time in the current mathematical model can be addressed by integrating the relevant derivative terms into the dynamics module based on Kane's dynamic equation. This can be achieved by updating the program to include these derivative effects in the equations of motion, thereby providing a more comprehensive analysis of the dynamic response. This update will

allow for the exploration of whether these factors have a significant impact on the structural dynamic response.

List of references

- Andrun, M., Ban, D., Bašić, J., & Ljubenkov, B. (2020). TSHD ship opening simulation by discrete element method. *Applied Ocean Research*, 94, 102001. <https://doi.org/10.1016/j.apor.2019.102001>
- Attar, M. (2012). A transfer matrix method for free vibration analysis and crack identification of stepped beams with multiple edge cracks and different boundary conditions. *International Journal of Mechanical Sciences*, 57(1), 19–33.
- Avi, E., Laakso, A., Romanoff, J., Remes, H., & Lillemäe-Avi, I. (2021). Coarse mesh finite element model for cruise ship global and local vibration analysis. *Marine Structures*, 79, 103053.
- Bajer, C. I., & Dyniewicz, B. (2008). Space–time approach to numerical analysis of a string with a moving mass. *International Journal for Numerical Methods in Engineering*, 76(10), 1528–1543.
- Bajer, C. I., & Dyniewicz, B. (2009). Virtual functions of the space–time finite element method in moving mass problems. *Computers & Structures*, 87(7–8), 444–455.
- Bajer, C. I., & Dyniewicz, B. (2012). *Numerical analysis of vibrations of structures under moving inertial load* (Vol. 65). Springer Science & Business Media.
- Banerjee, A. K. (2000). Dynamics of a variable-mass, flexible-body system. *Journal of Guidance, Control, and Dynamics*, 23(3), 501–508.
- Bartels, R. E. (2003). A time integration algorithm based on the state transition matrix for structures with time varying and nonlinear properties. *Computers & Structures*, 81(6), 349–357.
- Basic, J., Ban, D., Degiuli, N., & Govender, N. (2017). Discrete element method simulation of a split hopper dredger discharging process. *MARINE VII: Proceedings of the VII International Conference on Computational Methods in Marine Engineering*, 848–860.
- Bauchau, O. A., & Craig, J. I. (2009). Euler-Bernoulli beam theory. In *Structural analysis* (pp. 173–221). Springer.
- Beck, R. F., & Troesch, A. W. (1980). Wave diffraction effects in head seas. *International Shipbuilding Progress*, 27(316), 306–315.

- Belgova, M. (1962). Determination of overall bending moments caused by elastic vibrations of ships. *Transactions of the Leningrad Institute of Water Transport, Issue XXVIII, BSRA Translation, 1599.*
- Bestaoui, Y. (2010). A lagrangian approach to modeling of an airship with wind and varying mass effects. *48th AIAA Aerospace Sciences Meeting Including the New Horizons Forum and Aerospace Exposition, 40.*
- Bilello, C., Bergman, L. A., & Kuchma, D. (2004). Experimental investigation of a small-scale bridge model under a moving mass. *Journal of Structural Engineering, 130(5), 799–804.*
- Bishop, R. E. D., Price, W. G., & Tam, P. K. Y. (1977). Unified dynamic analysis of ship response to waves. *Naval Architect, 6.*
- Bisschop, F., Visser, P., van Rhee, C., & Verhagen, H. J. (2010). Erosion due to high flow velocities: a description of relevant processes. *Coastal Engineering Proceedings, 32, 24.*
- Boiangiu, M., Ceausu, V., & Untaroiu, C. D. (2016). A transfer matrix method for free vibration analysis of Euler-Bernoulli beams with variable cross section. *Journal of Vibration and Control, 22(11), 2591–2602.*
- Bray, N., & Cohen, M. (2004). *Dredging for development.* International Association of Dredging Companies.
- Bray, R. N., Bates, A. D., & Land, J. M. (1997). *Dredging: a handbook for engineers.*
- Casetta, L., & Pesce, C. P. (2014). The inverse problem of Lagrangian mechanics for Meshchersky's equation. *Acta Mechanica, 225(6), 1607–1623.*
- Chen, J., Hu, Z., Liu, G., & Wan, D. (2019). Coupled aero-hydro-servo-elastic methods for floating wind turbines. *Renewable Energy, 130, 139–153.*
- Chen, N.-Z. (2016). Hull girder reliability assessment for FPSOs. *Engineering Structures, 114, 135–147.*
- Chen, Y. N., & Chiou, J. W. (1981). Evaluation of Analytical Methods for Predicting Hull Girder Dynamic Response in Waves. *American Bureau of Shipping, Ocean Engineering Division, Technical Report No. OE-81001.*

- Cowper, G. (1966). The shear coefficient in Timoshenko's beam theory. *Journal of Applied Mechanics*, 33(2), 335–340.
- Craig Jr, R. R., & Kurdila, A. J. (2006). *Fundamentals of structural dynamics*. John Wiley & Sons.
- Crisfield, M. A., & TRRL. (1975). FULL-RANGE ANALYSIS OF STEEL PLATES AND STIFFENED PLATING UNDER UNIAXIAL COMPRESSION. *Proceedings of the Institution of Civil Engineers*, 59(4), 595–624.
- Cui, C., Jiang, H., & Li, Y.-H. (2012). Semi-analytical method for calculating vibration characteristics of variable cross-section beam. *Zhendong Yu Chongji(Journal of Vibration and Shock)*, 31(14), 85–88.
- DE JONG, G. (2010). Classification of Dredgers–Technical & Regulatory Developments. *Bulletin Technique, Bureau Veritas*.
- de Wit, L., Talmon, A. M., & Van Rhee, C. (2014). 3D CFD simulations of trailing suction hopper dredger plume mixing: Comparison with field measurements. *Marine Pollution Bulletin*, 88(1–2), 34–46.
- DNV, G. L. (2017). Sesam user manual-Wadam. *DNV GL Software*.
- DNV GL. (2005). *DNV Vibration Class*. DNV Standards.
- Dragados. (2017). *Aberdeen Harbour Expansion Project*.
- Dyniewicz, B. (2012). Space–time finite element approach to general description of a moving inertial load. *Finite Elements in Analysis and Design*, 62, 8–17.
- Dyson, P. K. (2000). *Modelling, testing and design, of a surface piercing propeller drive*.
- Eisma, D. (2005). *Dredging in coastal waters*. CRC Press.
- Faltinsen, O. (1993). *Sea loads on ships and offshore structures* (Vol. 1). Cambridge university press.
- Feyzollahzadeh, M., & Bamdad, M. (2020). A modified transfer matrix method to reduce the calculation time: A case study on beam vibration. *Applied Mathematics and Computation*, 378, 125238.

- Fonseca, N., & Guedes Soares, C. (2002). Comparison of numerical and experimental results of nonlinear wave-induced vertical ship motions and loads. *Journal of Marine Science and Technology*, 6, 193–204.
- Fu, M. (2012). The high order multiplication perturbation method for time-varying dynamic system. *Scientia Sinica Physica, Mechanica & Astronomica*, 42(2), 185.
- Gaspar, B., Teixeira, A. P., & Soares, C. G. (2016). Effect of the nonlinear vertical wave-induced bending moments on the ship hull girder reliability. *Ocean Engineering*, 119, 193–207.
- Goodman, R. A. (1971). Wave-excited main hull vibration in large tankers and bulk carriers. *Naval Architect*.
- Grant, D., Chakravarthy, A., & Lind, R. (2009). Modal interpretation of time-varying eigenvectors of morphing aircraft. *AIAA Atmospheric Flight Mechanics Conference*, 5848.
- Gupta, A. K. (1985). Vibration of tapered beams. *Journal of Structural Engineering*, 111(1), 19–36.
- Hai-jun, P., & Zhi-gang, W. U. (2009). PRECISE INTEGRATION BASED ON ALGORITHMS FOR SOLVING TIME VARYING PERIODIC COEFFICIENT LYAPUNOV DIFFERENTIAL EQUATIONS. *工程力学*, 26(4), 61–67.
- Hakala, M. (1986). *Application of the finite element method to fluid-structure interaction in ship vibration*. VTT Technical Research Centre of Finland.
- Han, L., Zhang, Y., Ni, Z.-Q., Zhang, Z.-M., & Jiang, L.-H. (2012). A modified transfer matrix method for the study of the bending vibration band structure in phononic crystal Euler beams. *Physica B: Condensed Matter*, 407(23), 4579–4583.
- Henson, G. M. (2008). Response of an oscillating system to harmonic forces of time-varying frequency. *AIAA Journal*, 46(8), 2033–2041.
- Hoffman, D., & Van Hooff, R. W. (1976). Experimental and theoretical evaluation of springing on a great lakes bulk carrier. *International Shipbuilding Progress*, 23(262), 173–193.

- Holl, H., & Irschik, H. (1996). Integration of nonlinear dynamic systems with time-varying mass using a boundary element formulation in time. *Dynamics Specialists Conference*, 1240.
- Holl, H. J., Belyaev, A. K., & Irschik, H. (1998). A time integration algorithm for nonlinear rotordynamic systems with time-varying parameters. *Proceedings of the Seventh International Symposium on Transport Phenomena and Dynamics of Rotating Machinery (7th ISROMAC)*, 22–26.
- Holl, H. J., Belyaev, A. K., & Irschik, H. (1999). Simulation of the Duffing-oscillator with time-varying mass by a BEM in time. *Computers & Structures*, 73(1–5), 177–186.
- Huang, X., & Zeiler, T. (2006). Dynamics of flexible launch vehicles with variable mass. *44th AIAA Aerospace Sciences Meeting and Exhibit*, 826.
- Ilanco, S., Monterrubio, L., & Mochida, Y. (2014). *The Rayleigh-Ritz method for structural analysis*. John Wiley & Sons.
- Jensen, J. J. (1983). *Beam models for ship hull vibration analysis*.
- Jensen, J. J. (2001). *Load and global response of ships*. Elsevier.
- Jensen, J. J., & Dogliani, M. (1996). Wave-induced ship hull vibrations in stochastic seaways. *Marine Structures*, 9(3–4), 353–387.
- Jensen, J. J., & Pedersen, P. T. (1981). Bending moments and shear forces in ships sailing in irregular waves. *Journal of Ship Research*, 25(04), 243–251.
- Jiang, C. S., & Liu, Y. D. (2011). Seakeeping prediction of the large self-propelling cutter-suction dredger. *Ship and Ocean Engineering*, 33(3), 13–16.
- Jonkman, J. M., Robertson, A. N., & Hayman, G. J. (2014). HydroDyn user's guide and theory manual. *National Renewable Energy Laboratory*.
- Joshi, A. (1995). Free vibration characteristics of variable mass rockets having large axial thrust/acceleration. *Journal of Sound and Vibration*, 4(187), 727–736.
- Jung, J.-J., Park, Y.-K., Shin, H.-S., Park, I.-K., & Korobkin, A. (2003). An estimation of hull girder response due to wave excitation. *ISOPE International Ocean and Polar Engineering Conference, ISOPE-I*.

- Kane, T. R. (1961). Variable Mass Dynamics? *Bulletin of Mechanical Engineering Education*, 2(20), 62–65.
- Kane, T. R., & Levinson, D. A. (1985). *Dynamics, theory and applications*. McGraw Hill.
- Kane, T. R., Likins, P. W., & Levinson, D. A. (1983). *Spacecraft dynamics*. New York.
- Kim, M.-S., Park, J.-J., Kim, B.-W., & Eom, J.-K. (2011). Nonlinear effect on wave loads of large ships in time domain. *International Journal of Naval Architecture and Ocean Engineering*, 3(1), 95–104.
- Kim, Y., Kim, K.-H., & Kim, Y. (2009). Springing analysis of a seagoing vessel using fully coupled BEM–FEM in the time domain. *Ocean Engineering*, 36(11), 785–796.
- Kucharski, T. (2000). A method for dynamic response analysis of time-variant discrete systems. *Computers & Structures*, 76(4), 545–550.
- Kumai, T. (1967). On the estimation of natural frequencies of vertical vibration of ships. *Journal of Zosen Kiokai*, 1967(121), 175–182.
- Kumar, M. S., Alagusundaramoorthy, P., & Sundaravadivelu, R. (2007). Ultimate strength of square plate with rectangular opening under axial compression. *Journal of Naval Architecture and Marine Engineering*, 4(1), 15–26.
- Kumar, M. S., Alagusundaramoorthy, P., & Sundaravadivelu, R. (2009a). Interaction curves for stiffened panel with circular opening under axial and lateral loads. *Ships and Offshore Structures*, 4(2), 133–143.
- Kumar, M. S., Alagusundaramoorthy, P., & Sundaravadivelu, R. (2009b). Ultimate strength of stiffened plates with a square opening under axial and out-of-plane loads. *Engineering Structures*, 31(11), 2568–2579.
- Lamb, H. (1920). On the vibrations of an elastic plate in contact with water. *Proceedings of the Royal Society of London. Series A, Containing Papers of a Mathematical and Physical Character*, 98(690), 205–216.
- Laura, P. A. A., Gutierrez, R. H., & Rossi, R. E. (1996). Free vibrations of beams of bilinearly varying thickness. *Ocean Engineering*, 23(1), 1–6.

- Lee, C. C., Liu, Y. H., & Kim, C. R. (1995). Simulation of nonlinear waves and forces due to transient and steady motion of submerged sphere. *ISOPE International Ocean and Polar Engineering Conference*, ISOPE-I.
- Lee, C. H., & Newman, J. N. (2006). Wamit user manual. *WAMIT, Inc*, 42.
- Lee, C.-H. (1995). *WAMIT theory manual*. Massachusetts Institute of Technology, Department of Ocean Engineering.
- Lee, C.-H., & Newman, J. N. (2005). Computation of wave effects using the panel method. *WIT Transactions on State-of-the-Art in Science and Engineering*, 18.
- Lee, C.-K. (2012). Numerical study of hydrodynamic interaction on a vessel in restricted waterways. *International Journal of Naval Architecture and Ocean Engineering*, 4(1), 1–9.
- Lee, J. W., & Lee, J. Y. (2016). Free vibration analysis using the transfer-matrix method on a tapered beam. *Computers & Structures*, 164, 75–82.
- Lewis, E. V. (1988). Principles of naval architecture second revision. Society of Naval Architects and Marine Engineers. *Ann Arbor, MI*.
- Li, M., Lu, Q., Bai, S., Zhang, M., Tian, H., & Qin, L. (2021). Digital twin-driven virtual sensor approach for safe construction operations of trailing suction hopper dredger. *Automation in Construction*, 132, 103961.
- Li, Q. S. (2000). A new exact approach for analyzing free vibration of SDOF systems with nonperiodically time varying parameters. *J. Vib. Acoust.*, 122(2), 175–179.
- Li, X., Yang, J., & Xiao, L. (2003). Motion analysis on a large FPSO in shallow water. *ISOPE International Ocean and Polar Engineering Conference*, ISOPE-I.
- Li, Z., & Ringsberg, J. W. (2011). Direct calculation of fatigue damage of ship structure details. *International Conference on Offshore Mechanics and Arctic Engineering*, 44342, 551–558.
- Li, Z., & Ringsberg, J. W. (2012). Fatigue routing of container ships—assessment of contributions to fatigue damage from wave-induced torsion and horizontal and vertical bending. *Ships and Offshore Structures*, 7(2), 119–131.
- Li, Z., Ringsberg, J. W., & Storhaug, G. (2013). Time-domain fatigue assessment of ship side-shell structures. *International Journal of Fatigue*, 55, 276–290.

- Lin, W.-M., & Yue, D. (1991). *Numerical solutions for large-amplitude ship motions in the time domain*.
- Liu, X., Zhou, G., Zhu, S., Wang, Y., Sun, W., & Weng, S. (2014). A modified highly precise direct integration method for a class of linear time-varying systems. *Science China Physics, Mechanics & Astronomy*, 57, 1382–1389.
- Maeda, H. (1980). *On the theory of coupled ship motions and vibrations*.
- Majji, M., Juang, J.-N., & Junkins, J. L. (2010). Observer/Kalman-filter time-varying system identification. *Journal of Guidance, Control, and Dynamics*, 33(3), 887–900.
- Mao, Q. (2011). Free vibration analysis of multiple-stepped beams by using Adomian decomposition method. *Mathematical and Computer Modelling*, 54(1–2), 756–764.
- Mao, Q., & Pietrzko, S. (2010). Free vibration analysis of stepped beams by using Adomian decomposition method. *Applied Mathematics and Computation*, 217(7), 3429–3441.
- Mao, W., Li, Z., Ogeman, V., & Ringsberg, J. W. (2015). A regression and beam theory based approach for fatigue assessment of containership structures including bending and torsion contributions. *Marine Structures*, 41, 244–266.
- McGhee, D. S. (2004). *A method for incorporating changing structural characteristics due to propellant mass usage in a launch vehicle ascent simulation*.
- Meirovitch, L. (1970). General motion of a variable-mass flexible rocket with internal flow. *Journal of Spacecraft and Rockets*, 7(2), 186–195.
- Mohtaram, Y. F., Kahnamouei, J. T., Shariati, M., & Behjat, B. (2012). Experimental and numerical investigation of buckling in rectangular steel plates with groove-shaped cutouts. *Journal of Zhejiang University SCIENCE A*, 13, 469–480.
- Mourik, R., & Osnabrugge, J. (2014). Applications of artificial intelligence on the dredge controls of a hopper dredger. *WE- DA XXXIV Technical Conference & TAMU*, 45, 192–196.
- Muis Alie, M. Z., Sitepu, G., Sade, J., Mustafa, W., Nugraha, A. M., & Bin Muh. Saleh, A. (2016). Finite Element analysis on the hull girder ultimate strength of

- asymmetrically damaged ships. *International Conference on Offshore Mechanics and Arctic Engineering*, 49941, V003T02A083.
- Musriyadi, T. B., & Naifah, S. F. R. (2020). Booster Pump Performance Analysis Towards Rotation Of Impeller For CSD Dredger Type. *International Journal of Marine Engineering Innovation and Research*, 2(1).
- Naguleswaran, S. (1994). Vibration in the two principal planes of a non-uniform beam of rectangular cross-section, one side of which varies as the square root of the axial co-ordinate. *Journal of Sound and Vibration*, 172(3), 305–319.
- Newman, J. N. (1993). Deformable floating bodies. *8th International Workshop on Water Waves and Floating Bodies*, 109–112.
- Newman, J. N. (1994). Wave effects on deformable bodies. *Applied Ocean Research*, 16(1), 47–59.
- Nhleko, S. (2009). *Free vibration states of an oscillator with a linear time-varying mass*.
- Nikkhoo, A., Rofooei, F. R., & Shadnam, M. R. (2007). Dynamic behavior and modal control of beams under moving mass. *Journal of Sound and Vibration*, 306(3–5), 712–724.
- Ning, D. Z., & Teng, B. (2007). Numerical simulation of fully nonlinear irregular wave tank in three dimension. *International Journal for Numerical Methods in Fluids*, 53(12), 1847–1862.
- Ohtaka, K., Hibino, F., & Oji, M. (1964). A Study of Vertical Vibration of Ships (1st report). *Journal of Zosen Kiokai*, 1964(116), 90–99.
- Ozsoysal, R. (2004). A review of recent ship vibration papers. *Shock Vib Dig*, 36, 207–214.
- Paik, J. K., Thayamballi, A. K., Pedersen, P. T., & Park, Y. Il. (2001). Ultimate strength of ship hulls under torsion. *Ocean Engineering*, 28(8), 1097–1133.
- Paik, J. K., Thayamballi, A. K., Wang, G., Kim, B. J., STEEN, E., & ØSTVOLD, T. K. (2000). On advanced buckling and ultimate strength design of ship plating. Discussion. Authors' closure. *Transactions-Society of Naval Architects and Marine Engineers*, 108, 249–290.

- Payer, H. G., Fricke, W., SCHILLING, S. A., STEINBERGER, J. P., LEHMANN, E., & LIU, D. (1994). Rational dimensioning and analysis of complex ship structures. Discussion. Authors' closure. *Transactions-Society of Naval Architects and Marine Engineers*, 102, 395–417.
- Peng, H. J., & Wu, Z. G. (2009). Solving time-varying periodic coefficient differential equation via Fourier series and precise integration method. *Chinese Journal of Computational Mechanics*, 26, 772–777.
- Penny, J. E. T., & Howard, G. F. (1980). Time-domain finite-element solutions for single-degree-of-freedom systems with time-dependent parameters. *Journal of Mechanical Engineering Science*, 22(1), 29–33.
- Petit, F., & Loccufer, M. (2009). Torsional vibrations on a hopper dredger due to transient conditions. *International Design Engineering Technical Conferences and Computers and Information in Engineering Conference*, 48982, 1215–1224.
- Pourtakdoust, S. H., & Assadian, N. (2004). Investigation of thrust effect on the vibrational characteristics of flexible guided missiles. *Journal of Sound and Vibration*, 272(1–2), 287–299.
- Qi, J., Hao, Y., & Chai, W. (2023). Failure analysis on wave compensator and hull structure of trailing suction hopper dredger (TSHD) under Medium-Long period wave. *Engineering Failure Analysis*, 152, 107434.
- Qiu, W., Peng, H., & Hsiung, C. C. (2001). Validation of time-domain prediction of motion, sea load, and hull pressure of a frigate in regular waves. *Twenty-Third Symposium on Naval Hydrodynamics Office of Naval Research Bassin d'Essais Des Carenes National Research Council*.
- Ringsberg, J. W., Li, Z., Tesanovic, A., & Knifund, C. (2015). Linear and nonlinear FE analyses of a container vessel in harsh sea state. *Ships and Offshore Structures*, 10(1), 20–30.
- Rörup, J., Darie, I., & Maciolowski, B. (2017). Strength analysis of ship structures with open decks. *Ships and Offshore Structures*, 12(sup1), S189–S199.
- Saad-Eldeen, S., Garbatov, Y., & Guedes Soares, C. (2014). Ultimate strength assessment of steel plates with a large opening. *Developments in Maritime*

- Transportation and Exploitation of Sea Resources*. London: Taylor & Francis Group, 373–380.
- Saad-Eldeen, S., Garbatov, Y., & Soares, C. G. (2016). Ultimate strength analysis of highly damaged plates. *Marine Structures*, *45*, 63–85.
- Schlick, O. (1884). On the vibration of steam vessels. *Institution of Naval Architects*.
- Sen, D. (2002). Time-domain computation of large amplitude 3D ship motions with forward speed. *Ocean Engineering*, *29*(8), 973–1002.
- Sen, D. T., & Vinh, T. C. (2016). Determination of added mass and inertia moment of marine ships moving in 6 degrees of freedom. *International Journal of Transportation Engineering and Technology*, *2*(1), 8–14.
- Sheehan, C., Harrington, J., & Murphy, J. D. (2010). An environmental and economic assessment of topsoil production from dredge material. *Resources, Conservation and Recycling*, *55*(2), 209–220.
- Shi, W. (2013). *Dynamics of energy system behaviour and emissions of trailing suction hopper dredgers*.
- Singh, S. P., & Sen, D. (2007a). A comparative linear and nonlinear ship motion study using 3-D time domain methods. *Ocean Engineering*, *34*(13), 1863–1881.
- Singh, S. P., & Sen, D. (2007b). A comparative study on 3D wave load and pressure computations for different level of modelling of nonlinearities. *Marine Structures*, *20*(1–2), 1–24.
- Skjørdal, S. O., & Faltinsen, O. M. (1980). A linear theory of springing. *Journal of Ship Research*, *24*(02), 74–84.
- Song Chang. (2017, December 4). *How to use cutter suction dredgers to “reclam the land.”*
- Stiansen, S. G., Mansour, A., & Chen, Y. N. (1977). *Dynamic response of large great lakes bulk carriers to wave-excited loads*.
- Strzałko, J., & Grabski, J. (1995). Dynamic analysis of a machine model with time-varying mass. *Acta Mechanica*, *112*, 173–186.

- Sun, H.-H., & Bai, Y. (2003). Time-variant reliability assessment of FPSO hull girders. *Marine Structures*, 16(3), 219–253.
- Taggart, R. (1980). Ship design and construction. (*No Title*).
- Tan, S. J., & Zhong, W. X. (2006). Numerical solution of differential Riccati equation with variable coefficients via symplectic conservative perturbation method. *Journal of Dalian University of Technology*, 46(S1), S7–S13.
- Thekinen, J. D., & Datta, N. (2019). Wave-induced flexural response of idealized non-uniform hull girder in random seas. *Marine Systems & Ocean Technology*, 14, 12–22.
- Tobbe, P. A. (1995). *An application of component modes to the flexible multibody simulation problem*. The University of Alabama in Huntsville.
- Tobbe, P., Matras, A., & Wilson, H. (2009). Modeling and simulation of variable mass, flexible structures. *AIAA Modeling and Simulation Technologies Conference*, 6023.
- Troesch, A. W. (1984). Wave-induced hull vibrations: an experimental and theoretical study. *Journal of Ship Research*, 28(02), 141–150.
- Underwood, J. M., Sobey, A. J., Blake, J. I. R., & Sheno, R. A. (2015). Ultimate collapse strength assessment of damaged steel plated grillages. *Engineering Structures*, 99, 517–535.
- Valsgard, S., Svensen, T. E., & Thorkildsen, H. (1995). *A computational method for analysis of container vessels*.
- Van Gunsteren, F. F. (1974). Some Further Calculations of Wave-Induced Hull Vibrations. *Proc Int. Symposium on Dynamics of Marine Vehicles and Structures in Waves*, University College London.
- Van Horssen, W. T., & Pischansky, O. V. (2011). On the stability properties of a damped oscillator with a periodically time-varying mass. *Journal of Sound and Vibration*, 330(13), 3257–3269.
- Van Horssen, W. T., Pischansky, O. V., & Dubbeldam, J. L. A. (2010). On the forced vibrations of an oscillator with a periodically time-varying mass. *Journal of Sound and Vibration*, 329(6), 721–732.

- Vidal, R. (2001). Irruption of the trailer jumbo in the dredging industry. *Terra et Aqua*, 3–12.
- Vlasblom W. (2007). https://dredging.org/documents/ceda/downloads/vlasblom2-trailing_suction_hopper_dredger.pdf.
- Vlasblom, W. J. (2003). Designing dredging equipment. *Lecture Notes, TUDelft*, 5, 24.
- Vuijk, W. (2020). *Shape and Topology Optimized TSHD Midsection*.
- Vujasinović, J., Parunov, J., Čorak, M., Buić, V., & Radolović, V. (2012). Strukturna analiza usisnog jaružala sa skladištem. *Sorta 2012: Zbornik Radova XX. Simpozija Teorija i Praksa Brodogradnje, in Memoriam Prof. Leopold Sorta= Conference Proceedings of the 20th Symposium Theory and Practice Shipbuilding, in Memoriam Prof. Leopold Sorta*.
- Waishek, J., Dogan, A., & Bestaoui, Y. (2009). Investigation into the time varying mass effect on airship dynamics response. *47th AIAA Aerospace Sciences Meeting Including the New Horizons Forum and Aerospace Exposition*, 735.
- Waishek, J., Dogan, A., & Bestaoui, Y. (2010). Comprehensive characterization of airship response to wind and time varying mass. *AIAA Atmospheric Flight Mechanics Conference*, 7626.
- Walton, T. (1902). *Steel ships: Their construction and maintenance*. Charles Griffin & Company.
- Weaver Jr, W., Timoshenko, S. P., & Young, D. H. (1991). *Vibration problems in engineering*. John Wiley & Sons.
- Weng, C. J. (1978). Estimation of natural frequency of free vibration for riverboat. *J Wuhan Univ Technol*, 2, 45–52.
- Wu, M., & Moan, T. (2005). Efficient calculation of wave-induced ship responses considering structural dynamic effects. *Applied Ocean Research*, 27(2), 81–96.
- Xu, M. C., Song, Z. J., Pan, J., & Soares, C. G. (2017). Ultimate strength assessment of continuous stiffened panels under combined longitudinal compressive load and lateral pressure. *Ocean Engineering*, 139, 39–53.
- Yang, C., & Ertekin, R. C. (1992). *Numerical simulation of nonlinear wave diffraction by a vertical cylinder*.

- Yell, D., & Riddell, J. (1995). *Dredging*. Thomas Telford.
- Yin, Y., Zhao, D., Cui, H., & Hong, M. (2014). Predicting method of natural frequency for ship's overall vertical vibration. *Brodogradnja: Teorija i Praksa Brodogradnje i Pomorske Tehnike*, 65(3), 49–58.
- Yu, C.-L., Feng, J.-C., & Chen, K. (2015). Ultimate uniaxial compressive strength of stiffened panel with opening under lateral pressure. *International Journal of Naval Architecture and Ocean Engineering*, 7(2), 399–408.
- Yu, C.-L., & Lee, J.-S. (2012). Ultimate strength of simply supported plate with opening under uniaxial compression. *International Journal of Naval Architecture and Ocean Engineering*, 4(4), 423–436.
- Yu, K., Zou, J., Zhang, Y., & Shi, G. (1997). An algorithm for structural dynamic response based on Hamilton law. *Journal of Harbin Institute of Technology*, 29(05), 46–49.
- Yuan, C., Feng, H., He, Y., & Xu, J. (2016). Motion characteristics and mechanisms of a resonance starting process in a free-piston diesel engine generator. *Proceedings of the Institution of Mechanical Engineers, Part A: Journal of Power and Energy*, 230(2), 206–218.
- Yucel, A., & Arpaci, A. (2010). Analysis of free and forced ship vibrations using finite element method. *Engineering Systems Design and Analysis*, 49187, 147–156.
- Yue, C., Ren, X., Yang, Y., & Deng, W. (2016). A modified precise integration method based on Magnus expansion for transient response analysis of time varying dynamical structure. *Chaos, Solitons & Fractals*, 89, 40–46.
- Zhan, K., Gao, H., Chen, H., & Lin, Z. (2015). Optimal retrofitting of a hybrid propulsion system using NSGA-II algorithm for trailing suction hopper dredger. *2015 IEEE Electric Ship Technologies Symposium (ESTS)*, 201–206.
- Zhang, G., Zhao, Y., Li, T., & Zhu, X. (2014). Propeller excitation of longitudinal vibration characteristics of marine propulsion shafting system. *Shock and Vibration*, 2014.

- Zhang, Y., & Hu, Z. (2023). A mathematical model for variable cross-section hull girder with time-varying mass characteristics. In *Advances in the Analysis and Design of Marine Structures* (pp. 309–317). CRC Press.
- Zhanglan, C., Jiawei, Y., Dongjiao, W., & Hongli, Y. (2014). The numerical prediction of draghead motion of trailing suction Hopper dredger in time domain. *Ocean Engineering*, *91*, 146–151.
- Zhao, D., Hu, Z., Zhou, K., Chen, G., Chen, X., & Feng, X. (2018). Coupled analysis of integrated dynamic responses of side-by-side offloading FLNG system. *Ocean Engineering*, *168*, 60–82.
- Zhao, D. Y. (1979). On the approximate calculation of the natural frequency of vertical modes of main hull vibrating. *J Dalian Univ Technol*, *18*, 113–126.
- Zhao, W., Milne, I. A., Efthymiou, M., Wolgamot, H. A., Draper, S., Taylor, P. H., & Taylor, R. E. (2018). Current practice and research directions in hydrodynamics for FLNG-side-by-side offloading. *Ocean Engineering*, *158*, 99–110.
- Zhao, W., Yang, J., & Hu, Z. (2012). Hydrodynamic interaction between FLNG vessel and LNG carrier in side by side configuration. *Journal of Hydrodynamics*, *24*(5), 648–657.
- Zhao, W., Yang, J., Hu, Z., & Tao, L. (2014). Prediction of hydrodynamic performance of an FLNG system in side-by-side offloading operation. *Journal of Fluids and Structures*, *46*, 89–110.
- Zhao, W., Yang, J., Hu, Z., & Xie, B. (2013). Hydrodynamics of an FLNG system in tandem offloading operation. *Ocean Engineering*, *57*, 150–162.
- Zheng, H., Liu, G. R., Tao, J. S., & Lam, K. Y. (2001). FEM/BEM analysis of diesel piston-slap induced ship hull vibration and underwater noise. *Applied Acoustics*, *62*(4), 341–358.
- Zhou, B., Yu, M., & Guo, J. (n.d.). Hybrid optimization algorithm for estimating soil parameters of spoil hopper deposition model for trailing suction hopper dredgers. *Journal of Intelligent & Fuzzy Systems, Preprint*, 1–19.

- Zhou, G., & Jiang, L. (2005). DA High Precision Direct Integration Method for Periodically Time-Varying Linear System. *JOURNAL-SHANGHAI JIAOTONG UNIVERSITY-CHINESE EDITION-*, 39(6), 1016.
- Zhu, P., Wang, S., Lyu, H., & Hao, Y. (2023a). The Motion Response of Trailing Suction Hopper Dredger under the Influence of Swell. *Journal of Physics: Conference Series*, 2565(1), 012032.
- Zhu, P., Wang, S., Lyu, H., & Hao, Y. (2023b). The Motion Response of Trailing Suction Hopper Dredger under the Influence of Swell. *Journal of Physics: Conference Series*, 2565(1), 012032.
- Zhu, S., Wu, M., & Moan, T. (2011). Experimental investigation of hull girder vibrations of a flexible backbone model in bending and torsion. *Applied Ocean Research*, 33(4), 252–274.

Appendices

Appendix A. Bisection method codes for solving non-linear equation

```
SUBROUTINE BisectionMethod(T, FuncName, A, B, H, EPS, X, N, M)
INTEGER, INTENT(IN) :: FuncName
REAL(8), INTENT(IN) :: A, B, H, EPS
INTEGER, INTENT(IN) :: N
REAL(8), INTENT(IN) :: T
INTEGER, INTENT(OUT) :: M
REAL(8), DIMENSION(N), INTENT(OUT) :: X
REAL(8) :: Z, Y1, Z1, Y0, Z0, F
M = 0
Z = A
CALL BISECTION_FUNCTION_SELECT(T, FuncName, Z, F)      !%%
Y = F                                                  !%%
10 IF ((Z.GT.B + H / 2.0).OR.(M.EQ.N)) RETURN
IF (ABS(Y).LT.EPS) THEN
    M = M + 1
    X(M) = Z
    Z = Z + H / 2.0
    CALL BISECTION_FUNCTION_SELECT(T, FuncName, Z, F)  !%%
    Y = F                                              !%%
    GOTO 10
END IF
Z1 = Z + H
CALL BISECTION_FUNCTION_SELECT(T, FuncName, Z1, F)    !%%
Y1 = F                                                !%%
IF (ABS(Y1).LT.EPS) THEN
    M = M + 1
    X(M) = Z1
    Z = Z1 + H / 2.0
    CALL BISECTION_FUNCTION_SELECT(T, FuncName, Z, F)  !%%
    Y = F                                              !%%
    GOTO 10
END IF
IF (Y * Y1.GT.0.0) THEN
```

```

    Y = Y1
    Z = Z1
    GOTO 10
END IF
20 IF (ABS(Z1 - Z).LT.EPS) THEN
    M = M + 1
    X(M) = (Z1 + Z) / 2.0
    Z = Z1 + H / 2.0
    CALL BISECTION_FUNCTION_SELECT(T, FuncName, Z, F)    !%%
    Y = F                                                !%%
    GOTO 10
END IF
Z0 = (Z1 + Z) / 2.0
CALL BISECTION_FUNCTION_SELECT(T, FuncName, Z0, F)    !%%
Y0 = F                                                !%%
IF (ABS(Y0).LT.EPS) THEN
    M = M + 1
    X(M) = Z0
    Z = Z0 + H / 2.0
    CALL BISECTION_FUNCTION_SELECT(T, FuncName, Z, F)    !%%
    Y = F                                                !%%
    GOTO 10
END IF
IF (Y * Y0.LT.0.0) THEN
    Z1 = Z0
    Y1 = Y0
ELSE
    Z = Z0
    Y = Y0
END IF
GOTO 20
END SUBROUTINE BisectionMethod

```

Appendix B. Transfer matrix method codes for solving natural frequency

```

SUBROUTINE NaturalFrequencyY(T, X, NonLinearFuncY)
  USE ComData
  USE SimulData
  USE StrctData
  USE EnvirData
  IMPLICIT NONE
  REAL(8), INTENT(IN) :: X
  REAL(8), INTENT(IN) :: T
  REAL(8), INTENT(OUT) :: NonLinearFuncY
  REAL(8), DIMENSION(HullGirder%SumElement) :: PreBetaY
  REAL(8), DIMENSION(4, 4, HullGirder%SumElement - 1) :: Z
  REAL(8), DIMENSION(HullGirder%SumElement - 1) :: P, M1, M2, M3, M4, N1, N2, N3,
  N4
  REAL(8), DIMENSION(4, 4) :: TAO, TransferMatrix
  REAL(8), DIMENSION(1, 4) :: temp_row3, temp_row4
  INTEGER :: I
  REAL(8) :: y11, y12, y13, y14, y21, y22, y23, y24, y31, y32, y33, y34, y41, y42, y43, y44,
  y51, y52, y53, y54, &
  y61, y62, y63, y64, y1, y2, y3, y4, y5, y6
  REAL(8) :: Rho
  DO I = 1, HullGirder%SumElement
    IF (WetModeSwitch == 1) THEN
      IF (HullGirder%BElement(I)%BeamMass == 2) THEN
        CALL TimeVaryingRho(T, HullGirder%BElement(I)%Equiv_Rho, Rho)
        PreBetaY(I) = (((HullGirder%BElement(I)%Equiv_A * Rho
&
+ HullGirder%InfiniteAddedMass(2,2) / HullGirder%SumElement ) /
&
(HullGirder%YoungModulus * HullGirder%BElement(I)%Equiv_Iyy)) * (X **
2)) ** (1.0 / 4.0)
      ELSE
        PreBetaY(I) = (((HullGirder%BElement(I)%Equiv_A *
&
+ HullGirder%InfiniteAddedMass(2,2) / HullGirder%SumElement ) /
&
(HullGirder%YoungModulus * HullGirder%BElement(I)%Equiv_Iyy)) * (X **
2)) ** (1.0 / 4.0)
      END IF
    END IF
  END DO

```

```

ELSE
  IF (HullGirder%BElement(I)%BeamMass == 2) THEN
    CALL TimeVaryingRho(T, HullGirder%BElement(I)%Equiv_Rho, Rho)
    PreBetaY(I) = (((HullGirder%BElement(I)%Equiv_A * Rho) / &
      (HullGirder%YoungModulus * HullGirder%BElement(I)%Equiv_Iyy)) * (X **
2)) ** (1.0 / 4.0)
    ELSE
      PreBetaY(I) = (((HullGirder%BElement(I)%Equiv_A *
HullGirder%BElement(I)%Equiv_Rho) / &
      (HullGirder%YoungModulus * HullGirder%BElement(I)%Equiv_Iyy)) * (X **
2)) ** (1.0 / 4.0)
    END IF
  END IF
END DO

DO I = 1, HullGirder%SumElement - 1
  P(I) = ((HullGirder%YoungModulus * HullGirder%BElement(i)%Equiv_Iyy) *
PreBetaY(I) ** 2) / &
  ((HullGirder%YoungModulus * HullGirder%BElement(I + 1)%Equiv_Iyy) *
PreBetaY(I + 1) ** 2)

  M1(I) = (P(I) + 1) / 2.0
  M2(I) = (P(I) - 1) / 2.0
  M3(I) = PreBetaY(I) * (P(I) + 1) / (2.0 * PreBetaY(I + 1))
  M4(I) = PreBetaY(I) * (P(I) - 1) / (2.0 * PreBetaY(I + 1))
  N1(I) = SIN(PreBetaY(I) * HullGirder%BElement(I)%Length)
  N2(I) = COS(PreBetaY(I) * HullGirder%BElement(I)%Length)
  N3(I) = SINH(PreBetaY(I) * HullGirder%BElement(I)%Length)
  N4(I) = COSH(PreBetaY(I) * HullGirder%BElement(I)%Length)
  Z(1, 1, I) = M3(I) * N2(I)
  Z(1, 2, I) = - M3(I) * N1(I)
  Z(1, 3, I) = - M4(I) * N4(I)
  Z(1, 4, I) = - M4(I) * N3(I)

  Z(2, 1, I) = M1(I) * N1(I)
  Z(2, 2, I) = M1(I) * N2(I)
  Z(2, 3, I) = - M2(I) * N3(I)
  Z(2, 4, I) = - M2(I) * N4(I)

  Z(3, 1, I) = - M4(I) * N2(I)
  Z(3, 2, I) = M4(I) * N1(I)

```

```

Z(3, 3, I) = M3(I) * N4(I)
Z(3, 4, I) = M3(I) * N3(I)

Z(4, 1, I) = - M2(I) * N1(I)
Z(4, 2, I) = - M2(I) * N2(I)
Z(4, 3, I) = M1(I) * N3(I)
Z(4, 4, I) = M1(I) * N4(I)
END DO
TransferMatrix(:, :) = Z(:, :, 1)
DO I = 2, HullGirder%SumElement - 1
  TransferMatrix(:, :) = MATMUL(Z(:, :, I), TransferMatrix(:, :))
END DO

temp_row3(1, 1) = - HullGirder%YoungModulus *
HullGirder%BElement(HullGirder%SumElement)%Equiv_Iyy * &
  PreBetaY(HullGirder%SumElement) ** 2 &
  *
  SIN(PreBetaY(HullGirder%SumElement)) *
HullGirder%BElement(HullGirder%SumElement)%Length)
temp_row3(1, 2) = - HullGirder%YoungModulus *
HullGirder%BElement(HullGirder%SumElement)%Equiv_Iyy * &
  PreBetaY(HullGirder%SumElement) ** 2 &
  *
  COS(PreBetaY(HullGirder%SumElement)) *
HullGirder%BElement(HullGirder%SumElement)%Length)
temp_row3(1, 3) = HullGirder%YoungModulus *
HullGirder%BElement(HullGirder%SumElement)%Equiv_Iyy * &
  PreBetaY(HullGirder%SumElement) ** 2 &
  *
  SINH(PreBetaY(HullGirder%SumElement)) *
HullGirder%BElement(HullGirder%SumElement)%Length)
temp_row3(1, 4) = HullGirder%YoungModulus *
HullGirder%BElement(HullGirder%SumElement)%Equiv_Iyy * &
  PreBetaY(HullGirder%SumElement) ** 2 &
  *
  COSH(PreBetaY(HullGirder%SumElement)) *
HullGirder%BElement(HullGirder%SumElement)%Length)

temp_row4(1, 1) = - HullGirder%YoungModulus *
HullGirder%BElement(HullGirder%SumElement)%Equiv_Iyy * &
  PreBetaY(HullGirder%SumElement) ** 3 &
  *
  COS(PreBetaY(HullGirder%SumElement)) *
HullGirder%BElement(HullGirder%SumElement)%Length)

```

```

temp_row4(1, 2) = HullGirder%YoungModulus *
HullGirder%BElement(HullGirder%SumElement)%Equiv_Iyy * &
    PreBetaY(HullGirder%SumElement) ** 3 &
*
    SIN(PreBetaY(HullGirder%SumElement)) *
HullGirder%BElement(HullGirder%SumElement)%Length)
temp_row4(1, 3) = HullGirder%YoungModulus *
HullGirder%BElement(HullGirder%SumElement)%Equiv_Iyy * &
    PreBetaY(HullGirder%SumElement) ** 3 &
*
    COSH(PreBetaY(HullGirder%SumElement)) *
HullGirder%BElement(HullGirder%SumElement)%Length)
temp_row4(1, 4) = HullGirder%YoungModulus *
HullGirder%BElement(HullGirder%SumElement)%Equiv_Iyy * &
    PreBetaY(HullGirder%SumElement) ** 3 &
*
    SINH(PreBetaY(HullGirder%SumElement)) *
HullGirder%BElement(HullGirder%SumElement)%Length)

```

```
temp_row3 = MATMUL(temp_row3, TransferMatrix)
```

```
temp_row4 = MATMUL(temp_row4, TransferMatrix)
```

```
TAO(1, 1) = 0.0
```

```
TAO(1, 2) = 1.0
```

```
TAO(1, 3) = 0.0
```

```
TAO(1, 4) = 1.0
```

```
TAO(2, 1) = PreBetaY(1)
```

```
TAO(2, 2) = 0.0
```

```
TAO(2, 3) = PreBetaY(1)
```

```
TAO(2, 4) = 0.0
```

```
TAO(3, 1) = temp_row3(1, 1)
```

```
TAO(3, 2) = temp_row3(1, 2)
```

```
TAO(3, 3) = temp_row3(1, 3)
```

```
TAO(3, 4) = temp_row3(1, 4)
```

```
TAO(4, 1) = temp_row4(1, 1)
```

```
TAO(4, 2) = temp_row4(1, 2)
```

```
TAO(4, 3) = temp_row4(1, 3)
```

```
TAO(4, 4) = temp_row4(1, 4)
```

$$\begin{aligned}
y11 &= \text{tao}(1, 1) * \text{tao}(2, 2) * \text{tao}(3, 3) * \text{tao}(4, 4) \\
y12 &= -\text{tao}(1, 1) * \text{tao}(2, 2) * \text{tao}(3, 4) * \text{tao}(4, 3) \\
y13 &= -\text{tao}(1, 1) * \text{tao}(2, 3) * \text{tao}(3, 2) * \text{tao}(4, 4) \\
y14 &= \text{tao}(1, 1) * \text{tao}(2, 3) * \text{tao}(3, 4) * \text{tao}(4, 2) \\
y1 &= y11 + y12 + y13 + y14;
\end{aligned}$$

$$\begin{aligned}
y21 &= \text{tao}(1, 1) * \text{tao}(2, 4) * \text{tao}(3, 2) * \text{tao}(4, 3) \\
y22 &= -\text{tao}(1, 1) * \text{tao}(2, 4) * \text{tao}(3, 3) * \text{tao}(4, 2) \\
y23 &= -\text{tao}(1, 2) * \text{tao}(2, 1) * \text{tao}(3, 3) * \text{tao}(4, 4) \\
y24 &= \text{tao}(1, 2) * \text{tao}(2, 1) * \text{tao}(3, 4) * \text{tao}(4, 3) \\
y2 &= y21 + y22 + y23 + y24;
\end{aligned}$$

$$\begin{aligned}
y31 &= \text{tao}(1, 2) * \text{tao}(2, 3) * \text{tao}(3, 1) * \text{tao}(4, 4) \\
y32 &= -\text{tao}(1, 2) * \text{tao}(2, 3) * \text{tao}(3, 4) * \text{tao}(4, 1) \\
y33 &= -\text{tao}(1, 2) * \text{tao}(2, 4) * \text{tao}(3, 1) * \text{tao}(4, 3) \\
y34 &= \text{tao}(1, 2) * \text{tao}(2, 4) * \text{tao}(3, 3) * \text{tao}(4, 1) \\
y3 &= y31 + y32 + y33 + y34
\end{aligned}$$

$$\begin{aligned}
y41 &= \text{tao}(1, 3) * \text{tao}(2, 1) * \text{tao}(3, 2) * \text{tao}(4, 4) \\
y42 &= -\text{tao}(1, 3) * \text{tao}(2, 1) * \text{tao}(3, 4) * \text{tao}(4, 2) \\
y43 &= -\text{tao}(1, 3) * \text{tao}(2, 2) * \text{tao}(3, 1) * \text{tao}(4, 4) \\
y44 &= \text{tao}(1, 3) * \text{tao}(2, 2) * \text{tao}(3, 4) * \text{tao}(4, 1) \\
y4 &= y41 + y42 + y43 + y44
\end{aligned}$$

$$\begin{aligned}
y51 &= \text{tao}(1, 3) * \text{tao}(2, 4) * \text{tao}(3, 1) * \text{tao}(4, 2) \\
y52 &= -\text{tao}(1, 3) * \text{tao}(2, 4) * \text{tao}(3, 2) * \text{tao}(4, 1) \\
y53 &= -\text{tao}(1, 4) * \text{tao}(2, 1) * \text{tao}(3, 2) * \text{tao}(4, 3) \\
y54 &= \text{tao}(1, 4) * \text{tao}(2, 1) * \text{tao}(3, 3) * \text{tao}(4, 2) \\
y5 &= y51 + y52 + y53 + y54
\end{aligned}$$

$$\begin{aligned}
y61 &= \text{tao}(1, 4) * \text{tao}(2, 2) * \text{tao}(3, 1) * \text{tao}(4, 3) \\
y62 &= -\text{tao}(1, 4) * \text{tao}(2, 2) * \text{tao}(3, 3) * \text{tao}(4, 1) \\
y63 &= -\text{tao}(1, 4) * \text{tao}(2, 3) * \text{tao}(3, 1) * \text{tao}(4, 2) \\
y64 &= \text{tao}(1, 4) * \text{tao}(2, 3) * \text{tao}(3, 2) * \text{tao}(4, 1) \\
y6 &= y61 + y62 + y63 + y64
\end{aligned}$$

$$\text{NonLinearFuncY} = y1 + y2 + y3 + y4 + y5 + y6$$

END SUBROUTINE NaturalFrequencyY

Appendix C. Orthonormal basis solution codes

```
SUBROUTINE Orthonormal_Basis_Solver(Matrix, OthonormalBasis)
  IMPLICIT NONE
  REAL(8), DIMENSION(2, 2), INTENT(INOUT) :: Matrix
  REAL(8), DIMENSION(2), INTENT(OUT) :: OthonormalBasis
  INTEGER :: LDX, N, P, LDU, LDV, JOB, INFO
  INTEGER :: I, J
  REAL(8), DIMENSION(2, 2) :: S, U, V
  REAL(8) :: E(max(2 + 1, 2))
  REAL(8), ALLOCATABLE, DIMENSION(:) :: WORK
  N = 2 !row
  P = 2 !column
  JOB = 11 !或 10
  LDX = N
  LDU = N
  LDV = P
  ALLOCATE (WORK(1:N))
  Matrix = TRANSPOSE(Matrix)
  CALL DSVDC(Matrix, LDX, N, P, S, E, U, LDU, V, LDV, WORK, JOB, INFO)
  DO I = 1, 2
    DO J = 1, 2
      IF (S(I, J) /= 0.0 .AND. S(I, J) < 0.1) THEN
        OthonormalBasis(:) = U(:, I)
      END IF
    END DO
  END DO
END SUBROUTINE Orthonormal_Basis_Solver
subroutine DSVDC (X, LDX, N, P, S, E, U, LDU, V, LDV, WORK, JOB, &
  INFO)
  !
  !! DSVDC performs the singular value decomposition of a rectangular matrix.
  !
  !***LIBRARY SLATEC (LINPACK)
  !***CATEGORY D6
  !***TYPE DOUBLE PRECISION (SSVDC-S, DSVDC-D, CSVDC-C)
  !***KEYWORDS LINEAR ALGEBRA, LINPACK, MATRIX,
```

```

!          SINGULAR VALUE DECOMPOSITION
!***AUTHOR Stewart, G. W., (U. of Maryland)
!***DESCRIPTION
!
!  DSVDC is a subroutine to reduce a double precision NxP matrix X
!  by orthogonal transformations U and V to diagonal form. The
!  diagonal elements S(I) are the singular values of X. The
!  columns of U are the corresponding left singular vectors,
!  and the columns of V the right singular vectors.
!
!  On Entry
!
!    X    DOUBLE PRECISION(LDX,P), where LDX >= N.
!
!        X contains the matrix whose singular value
!        decomposition is to be computed. X is
!        destroyed by DSVDC.
!
!    LDX  INTEGER.
!        LDX is the leading dimension of the array X.
!
!    N    INTEGER.
!        N is the number of rows of the matrix X.
!
!    P    INTEGER.
!        P is the number of columns of the matrix X.
!
!    LDU  INTEGER.
!        LDU is the leading dimension of the array U.
!        (See below).
!
!    LDV  INTEGER.
!        LDV is the leading dimension of the array V.
!        (See below).
!
!    WORK DOUBLE PRECISION(N).
!        WORK is a scratch array.

```

!

! JOB INTEGER.

! JOB controls the computation of the singular

! vectors. It has the decimal expansion AB

! with the following meaning

!

! A == 0 do not compute the left singular

! vectors.

! A == 1 return the N left singular vectors

! in U.

! A >= 2 return the first MIN(N,P) singular

! vectors in U.

! B == 0 do not compute the right singular

! vectors.

! B == 1 return the right singular vectors

! in V.

!

! On Return

!

! S DOUBLE PRECISION(MM), where MM=MIN(N+1,P).

! The first MIN(N,P) entries of S contain the

! singular values of X arranged in descending

! order of magnitude.

!

! E DOUBLE PRECISION(P).

! E ordinarily contains zeros. However see the

! discussion of INFO for exceptions.

!

! U DOUBLE PRECISION(LDU,K), where LDU >= N.

! If JOBA == 1, then K == N.

! If JOBA >= 2, then K == MIN(N,P).

! U contains the matrix of right singular vectors.

! U is not referenced if JOBA == 0. If N <= P

! or if JOBA == 2, then U may be identified with X

! in the subroutine call.

!

! V DOUBLE PRECISION(LDV,P), where LDV >= P.

```

!          V contains the matrix of right singular vectors.
!          V is not referenced if JOB == 0. If P <= N,
!          then V may be identified with X in the
!          subroutine call.
!
!          INFO    INTEGER.
!          The singular values (and their corresponding
!          singular vectors) S(INFO+1),S(INFO+2),...,S(M)
!          are correct (here M=MIN(N,P)). Thus if
!          INFO == 0, all the singular values and their
!          vectors are correct. In any event, the matrix
!          B = TRANS(U)*X*V is the bidiagonal matrix
!          with the elements of S on its diagonal and the
!          elements of E on its super-diagonal (TRANS(U)
!          is the transpose of U). Thus the singular
!          values of X and B are the same.
!
!***REFERENCES J. J. Dongarra, J. R. Bunch, C. B. Moler, and G. W.
!          Stewart, LINPACK Users' Guide, SIAM, 1979.
!***ROUTINES CALLED DAXPY, DDOT, DNRM2, DROT, DROTG, DSCAL, DSWAP
!***REVISION HISTORY (YYMMDD)
!  790319 DATE WRITTEN
!  890531 Changed all specific intrinsics to generic. (WRB)
!  890531 REVISION DATE from Version 3.2
!  891214 Prologue converted to Version 4.0 format. (BAB)
!  900326 Removed duplicate information from DESCRIPTION section.
!          (WRB)
!  920501 Reformatted the REFERENCES section. (WRB)
!***END PROLOGUE DSVDC
INTEGER LDX, N, P, LDU, LDV, JOB, INFO
DOUBLE PRECISION X(LDX, *), S(*), E(*), U(LDU, *), V(LDV, *), WORK(*)
!
!
INTEGER I, ITER, J, JOBU, K, KASE, KK, L, LL, LLS, LM1, LP1, LS, LU, M, MAXIT,
&
MM, MM1, MP1, NCT, NCTP1, NCU, NRT, NRTP1
DOUBLE PRECISION DDOT, T

```

```

DOUBLE PRECISION B, C, CS, EL, EMM1, F, G, DNRM2, SCALE, SHIFT, SL, SM, SN,
&
    SMM1, T1, TEST, ZTEST
LOGICAL WANTU, WANTV
!***FIRST EXECUTABLE STATEMENT DSVDC
!
!   SET THE MAXIMUM NUMBER OF ITERATIONS.
!
MAXIT = 30
!
!   DETERMINE WHAT IS TO BE COMPUTED.
!
WANTU = .FALSE.
WANTV = .FALSE.
JOBU = MOD(JOB, 100) / 10
NCU = N
if (JOBU > 1) NCU = MIN(N, P)
if (JOBU /= 0) WANTU = .TRUE.
if (MOD(JOB, 10) /= 0) WANTV = .TRUE.
!
!   REDUCE X TO BIDIAGONAL FORM, STORING THE DIAGONAL ELEMENTS
!   IN S AND THE SUPER-DIAGONAL ELEMENTS IN E.
!
INFO = 0
NCT = MIN(N - 1, P)
NRT = MAX(0, MIN(P - 2, N))
LU = MAX(NCT, NRT)
if (LU < 1) go to 170
DO 160 L = 1, LU
    LP1 = L + 1
    if (L > NCT) go to 20
    !
    !       COMPUTE THE TRANSFORMATION FOR THE L-TH COLUMN AND
    !       PLACE THE L-TH DIAGONAL IN S(L).
    !
    S(L) = DNRM2(N - L + 1, X(L, L), 1)
    if (S(L) == 0.0D0) go to 10

```

```

if (X(L, L) /= 0.0D0) S(L) = SIGN(S(L), X(L, L))
call DSCAL(N - L + 1, 1.0D0 / S(L), X(L, L), 1)
X(L, L) = 1.0D0 + X(L, L)
10  CONTINUE
S(L) = -S(L)
20  CONTINUE
if (P < LP1) go to 50
DO 40 J = LP1, P
  if (L > NCT) go to 30
  if (S(L) == 0.0D0) go to 30
  !
  !       APPLY THE TRANSFORMATION.
  !
  T = -DDOT(N - L + 1, X(L, L), 1, X(L, J), 1) / X(L, L)
  call DAXPY(N - L + 1, T, X(L, L), 1, X(L, J), 1)
30  CONTINUE
  !
  !       PLACE THE L-TH ROW OF X INTO E FOR THE
  !       SUBSEQUENT CALCULATION OF THE ROW TRANSFORMATION.
  !
  E(J) = X(L, J)
40  CONTINUE
50  CONTINUE
if (.NOT.WANTU .OR. L > NCT) go to 70
!
!       PLACE THE TRANSFORMATION IN U FOR SUBSEQUENT BACK
!       MULTIPLICATION.
!
DO 60 I = L, N
  U(I, L) = X(I, L)
60  CONTINUE
70  CONTINUE
if (L > NRT) go to 150
!
!       COMPUTE THE L-TH ROW TRANSFORMATION AND PLACE THE
!       L-TH SUPER-DIAGONAL IN E(L).
!

```

```

E(L) = DNRM2(P - L, E(LP1), 1)
if (E(L) == 0.0D0) go to 80
if (E(LP1) /= 0.0D0) E(L) = SIGN(E(L), E(LP1))
call DSCAL(P - L, 1.0D0 / E(L), E(LP1), 1)
E(LP1) = 1.0D0 + E(LP1)
80  CONTINUE
E(L) = -E(L)
if (LP1 > N .OR. E(L) == 0.0D0) go to 120
!
!     APPLY THE TRANSFORMATION.
!
DO 90 I = LP1, N
    WORK(I) = 0.0D0
90  CONTINUE
DO 100 J = LP1, P
    call DAXPY(N - L, E(J), X(LP1, J), 1, WORK(LP1), 1)
100 CONTINUE
DO 110 J = LP1, P
    call DAXPY(N - L, -E(J) / E(LP1), WORK(LP1), 1, X(LP1, J), 1)
110 CONTINUE
120 CONTINUE
if (.NOT.WANTV) go to 140
!
!     PLACE THE TRANSFORMATION IN V FOR SUBSEQUENT
!     BACK MULTIPLICATION.
!
DO 130 I = LP1, P
    V(I, L) = E(I)
130 CONTINUE
140 CONTINUE
150 CONTINUE
160 CONTINUE
170 CONTINUE
!
!     SET UP THE FINAL BIDIAGONAL MATRIX OR ORDER M.
!
M = MIN(P, N + 1)

```

```

NCTP1 = NCT + 1
NRTP1 = NRT + 1
if (NCT < P) S(NCTP1) = X(NCTP1, NCTP1)
if (N < M) S(M) = 0.0D0
if (NRTP1 < M) E(NRTP1) = X(NRTP1, M)
E(M) = 0.0D0
!
!   if REQUIRED, GENERATE U.
!
if (.NOT.WANTU) go to 300
if (NCU < NCTP1) go to 200
DO 190 J = NCTP1, NCU
    DO 180 I = 1, N
        U(I, J) = 0.0D0
180  CONTINUE
        U(J, J) = 1.0D0
190 CONTINUE
200 CONTINUE
    if (NCT < 1) go to 290
    DO 280 LL = 1, NCT
        L = NCT - LL + 1
        if (S(L) == 0.0D0) go to 250
        LP1 = L + 1
        if (NCU < LP1) go to 220
        DO 210 J = LP1, NCU
            T = -DDOT(N - L + 1, U(L, L), 1, U(L, J), 1) / U(L, L)
            call DAXPY(N - L + 1, T, U(L, L), 1, U(L, J), 1)
210  CONTINUE
220  CONTINUE
            call DSCAL(N - L + 1, -1.0D0, U(L, L), 1)
            U(L, L) = 1.0D0 + U(L, L)
            LM1 = L - 1
            if (LM1 < 1) go to 240
            DO 230 I = 1, LM1
                U(I, L) = 0.0D0
230  CONTINUE
240  CONTINUE

```

```

    go to 270
250  CONTINUE
      DO 260 I = 1, N
          U(I, L) = 0.0D0
260  CONTINUE
      U(L, L) = 1.0D0
270  CONTINUE
280 CONTINUE
290 CONTINUE
300 CONTINUE
    !
    !  if IT IS REQUIRED, GENERATE V.
    !
    if (.NOT.WANTV) go to 350
    DO 340 LL = 1, P
        L = P - LL + 1
        LP1 = L + 1
        if (L > NRT) go to 320
        if (E(L) == 0.0D0) go to 320
        DO 310 J = LP1, P
            T = -DDOT(P - L, V(LP1, L), 1, V(LP1, J), 1) / V(LP1, L)
            call DAXPY(P - L, T, V(LP1, L), 1, V(LP1, J), 1)
310  CONTINUE
320  CONTINUE
        DO 330 I = 1, P
            V(I, L) = 0.0D0
330  CONTINUE
        V(L, L) = 1.0D0
340 CONTINUE
350 CONTINUE
    !
    !  MAIN ITERATION LOOP FOR THE SINGULAR VALUES.
    !
    MM = M
    ITER = 0
360 CONTINUE
    !

```

```

!   QUIT if ALL THE SINGULAR VALUES HAVE BEEN FOUND.
!
if (M == 0) go to 620
!
!   if TOO MANY ITERATIONS HAVE BEEN PERFORMED, SET
!   FLAG AND RETURN.
!
if (ITER < MAXIT) go to 370
INFO = M
go to 620
370 CONTINUE
!
!   THIS SECTION OF THE PROGRAM INSPECTS FOR
!   NEGLIGIBLE ELEMENTS IN THE S AND E ARRAYS. ON
!   COMPLETION THE VARIABLES KASE AND L ARE SET AS FOLLOWS.
!
!   KASE = 1   if S(M) AND E(L-1) ARE NEGLIGIBLE AND L < M
!   KASE = 2   if S(L) IS NEGLIGIBLE AND L < M
!   KASE = 3   if E(L-1) IS NEGLIGIBLE, L < M, AND
!               S(L), ..., S(M) ARE NOT NEGLIGIBLE (QR STEP).
!   KASE = 4   if E(M-1) IS NEGLIGIBLE (CONVERGENCE).
!
DO 390 LL = 1, M
  L = M - LL
  if (L == 0) go to 400
  TEST = ABS(S(L)) + ABS(S(L + 1))
  ZTEST = TEST + ABS(E(L))
  if (ZTEST /= TEST) go to 380
  E(L) = 0.0D0
  go to 400
380  CONTINUE
390  CONTINUE
400  CONTINUE
  if (L /= M - 1) go to 410
  KASE = 4
  go to 480
410  CONTINUE

```

```

LP1 = L + 1
MP1 = M + 1
DO 430 LLS = LP1, MP1
  LS = M - LLS + LP1
  if (LS == L) go to 440
  TEST = 0.0D0
  if (LS /= M) TEST = TEST + ABS(E(LS))
  if (LS /= L + 1) TEST = TEST + ABS(E(LS - 1))
  ZTEST = TEST + ABS(S(LS))
  if (ZTEST /= TEST) go to 420
  S(LS) = 0.0D0
  go to 440
420 CONTINUE
430 CONTINUE
440 CONTINUE
  if (LS /= L) go to 450
  KASE = 3
  go to 470
450 CONTINUE
  if (LS /= M) go to 460
  KASE = 1
  go to 470
460 CONTINUE
  KASE = 2
  L = LS
470 CONTINUE
480 CONTINUE
  L = L + 1
  !
  !   PERFORM THE TASK INDICATED BY KASE.
  !
  go to (490, 520, 540, 570), KASE
  !
  !   DEFLATE NEGLIGIBLE S(M).
  !
490 CONTINUE
  MM1 = M - 1

```

```

F = E(M - 1)
E(M - 1) = 0.0D0
DO 510 KK = L, MM1
  K = MM1 - KK + L
  T1 = S(K)
  call DROTG(T1, F, CS, SN)
  S(K) = T1
  if (K == L) go to 500
  F = -SN * E(K - 1)
  E(K - 1) = CS * E(K - 1)
500  CONTINUE
      if (WANTV) call DROT(P, V(1, K), 1, V(1, M), 1, CS, SN)
510  CONTINUE
      go to 610
      !
      !   SPLIT AT NEGLIGIBLE S(L).
      !
520  CONTINUE
      F = E(L - 1)
      E(L - 1) = 0.0D0
      DO 530 K = L, M
        T1 = S(K)
        call DROTG(T1, F, CS, SN)
        S(K) = T1
        F = -SN * E(K)
        E(K) = CS * E(K)
        if (WANTU) call DROT(N, U(1, K), 1, U(1, L - 1), 1, CS, SN)
530  CONTINUE
      go to 610
      !
      !   PERFORM ONE QR STEP.
      !
540  CONTINUE
      !
      !   CALCULATE THE SHIFT.
      !
      SCALE = MAX(ABS(S(M)), ABS(S(M - 1)), ABS(E(M - 1)), &

```

```

      ABS(S(L)), ABS(E(L)))
SM = S(M) / SCALE
SMM1 = S(M - 1) / SCALE
EMM1 = E(M - 1) / SCALE
SL = S(L) / SCALE
EL = E(L) / SCALE
B = ((SMM1 + SM) * (SMM1 - SM) + EMM1**2) / 2.0D0
C = (SM * EMM1)**2
SHIFT = 0.0D0
if (B == 0.0D0 .AND. C == 0.0D0) go to 550
SHIFT = SQRT(B**2 + C)
if (B < 0.0D0) SHIFT = -SHIFT
SHIFT = C / (B + SHIFT)
550 CONTINUE
F = (SL + SM) * (SL - SM) - SHIFT
G = SL * EL
!
!   CHASE ZEROS.
!
MM1 = M - 1
DO 560 K = L, MM1
  call DROTG(F, G, CS, SN)
  if (K /= L) E(K - 1) = F
  F = CS * S(K) + SN * E(K)
  E(K) = CS * E(K) - SN * S(K)
  G = SN * S(K + 1)
  S(K + 1) = CS * S(K + 1)
  if (WANTV) call DROT(P, V(1, K), 1, V(1, K + 1), 1, CS, SN)
  call DROTG(F, G, CS, SN)
  S(K) = F
  F = CS * E(K) + SN * S(K + 1)
  S(K + 1) = -SN * E(K) + CS * S(K + 1)
  G = SN * E(K + 1)
  E(K + 1) = CS * E(K + 1)
  if (WANTU .AND. K < N) &
    call DROT(N, U(1, K), 1, U(1, K + 1), 1, CS, SN)
560 CONTINUE

```

```

E(M - 1) = F
ITER = ITER + 1
go to 610
!
!   CONVERGENCE.
!
570 CONTINUE
!
!   MAKE THE SINGULAR VALUE POSITIVE.
!
if (S(L) >= 0.0D0) go to 580
S(L) = -S(L)
if (WANTV) call DSCAL(P, -1.0D0, V(1, L), 1)
580 CONTINUE
!
!   ORDER THE SINGULAR VALUE.
!
590 if (L == MM) go to 600
if (S(L) >= S(L + 1)) go to 600
T = S(L)
S(L) = S(L + 1)
S(L + 1) = T
if (WANTV .AND. L < P) &
    call DSWAP(P, V(1, L), 1, V(1, L + 1), 1)
if (WANTU .AND. L < N) &
    call DSWAP(N, U(1, L), 1, U(1, L + 1), 1)
L = L + 1
go to 590
600 CONTINUE
ITER = 0
M = M - 1
610 CONTINUE
go to 360
620 CONTINUE
return
end

```

```

!-----
!>No.1 DAXPY
!-----
subroutine DAXPY (N, DA, DX, INCX, DY, INCY)
!
!! DAXPY computes a constant times a vector plus a vector.
!
!***LIBRARY  SLATEC (BLAS)
!***CATEGORY  D1A7
!***TYPE     DOUBLE PRECISION (SAXPY-S, DAXPY-D, CAXPY-C)
!***KEYWORDS  BLAS, LINEAR ALGEBRA, TRIAD, VECTOR
!***AUTHOR  Lawson, C. L., (JPL)
!           Hanson, R. J., (SNLA)
!           Kincaid, D. R., (U. of Texas)
!           Krogh, F. T., (JPL)
!***DESCRIPTION
!
!           B L A S Subprogram
! Description of Parameters
!
! --Input--
!   N number of elements in input vector(s)
!   DA double precision scalar multiplier
!   DX double precision vector with N elements
!   INCX storage spacing between elements of DX
!   DY double precision vector with N elements
!   INCY storage spacing between elements of DY
!
! --Output--
!   DY double precision result (unchanged if N <= 0)
!
! Overwrite double precision DY with double precision DA*DX + DY.
! For I = 0 to N-1, replace DY(LY+I*INCY) with DA *DX(LX+I*INCX) +
!   DY(LY+I*INCY),
! where LX = 1 if INCX >= 0, else LX = 1+(1-N)*INCX, and LY is
! defined in a similar way using INCY.
!

```

```

!***REFERENCES C. L. Lawson, R. J. Hanson, D. R. Kincaid and F. T.
!           Krogh, Basic linear algebra subprograms for Fortran
!           usage, Algorithm No. 539, Transactions on Mathematical
!           Software 5, 3 (September 1979), pp. 308-323.
!***ROUTINES CALLED (NONE)
!***REVISION HISTORY (YYMMDD)
! 791001 DATE WRITTEN
! 890831 Modified array declarations. (WRB)
! 890831 REVISION DATE from Version 3.2
! 891214 Prologue converted to Version 4.0 format. (BAB)
! 920310 Corrected definition of LX in DESCRIPTION. (WRB)
! 920501 Reformatted the REFERENCES section. (WRB)
!***END PROLOGUE DAXPY
DOUBLE PRECISION DX(*), DY(*), DA
!***FIRST EXECUTABLE STATEMENT DAXPY
if(N <= 0 .OR. DA == 0.0D0) RETURN
if(INCX == INCY) IF (INCX - 1) 5, 20, 60
!
! Code for unequal or nonpositive increments.
!
5 IX = 1
  IY = 1
  if(INCX < 0) IX = (-N + 1) * INCX + 1
  if(INCY < 0) IY = (-N + 1) * INCY + 1
  DO 10 I = 1, N
    DY(IY) = DY(IY) + DA * DX(IX)
    IX = IX + INCX
    IY = IY + INCY
10 CONTINUE
  return
!
! Code for both increments equal to 1.
!
! Clean-up loop so remaining vector length is a multiple of 4.
!
20 M = MOD(N, 4)
  if(M == 0) go to 40

```

```

DO 30 I = 1, M
    DY(I) = DY(I) + DA * DX(I)
30 CONTINUE
    if(N < 4) RETURN
40 MP1 = M + 1
    DO 50 I = MP1, N, 4
        DY(I) = DY(I) + DA * DX(I)
        DY(I + 1) = DY(I + 1) + DA * DX(I + 1)
        DY(I + 2) = DY(I + 2) + DA * DX(I + 2)
        DY(I + 3) = DY(I + 3) + DA * DX(I + 3)
50 CONTINUE
    return
    !
    ! Code for equal, positive, non-unit increments.
    !
60 NS = N * INCX
    DO 70 I = 1, NS, INCX
        DY(I) = DA * DX(I) + DY(I)
70 CONTINUE
    return
end
!-----
!>No.2 DDOT
!-----
DOUBLE PRECISION FUNCTION DDOT (N, DX, INCX, DY, INCY)
!
!! DDOT computes the inner product of two vectors.
!
!***LIBRARY SLATEC (BLAS)
!***CATEGORY D1A4
!***TYPE DOUBLE PRECISION (SDOT-S, DDOT-D, CDOTU-C)
!***KEYWORDS BLAS, INNER PRODUCT, LINEAR ALGEBRA, VECTOR
!***AUTHOR Lawson, C. L., (JPL)
! Hanson, R. J., (SNLA)
! Kincaid, D. R., (U. of Texas)
! Krogh, F. T., (JPL)
!***DESCRIPTION

```

```

!
!       B L A S Subprogram
! Description of Parameters
!
! --Input--
!   N number of elements in input vector(s)
!   DX double precision vector with N elements
!   INCX storage spacing between elements of DX
!   DY double precision vector with N elements
!   INCY storage spacing between elements of DY
!
! --Output--
!   DDOT double precision dot product (zero if N <= 0)
!
! Returns the dot product of double precision DX and DY.
!   DDOT = sum for I = 0 to N-1 of DX(LX+I*INCX) * DY(LY+I*INCY),
!   where LX = 1 if INCX >= 0, else LX = 1+(1-N)*INCX, and LY is
!   defined in a similar way using INCY.
!
!***REFERENCES C. L. Lawson, R. J. Hanson, D. R. Kincaid and F. T.
!       Krogh, Basic linear algebra subprograms for Fortran
!       usage, Algorithm No. 539, Transactions on Mathematical
!       Software 5, 3 (September 1979), pp. 308-323.
!***ROUTINES CALLED (NONE)
!***REVISION HISTORY (YYMMDD)
! 791001 DATE WRITTEN
! 890831 Modified array declarations. (WRB)
! 890831 REVISION DATE from Version 3.2
! 891214 Prologue converted to Version 4.0 format. (BAB)
! 920310 Corrected definition of LX in DESCRIPTION. (WRB)
! 920501 Reformatted the REFERENCES section. (WRB)
!***END PROLOGUE DDOT
DOUBLE PRECISION DX(*), DY(*)
!***FIRST EXECUTABLE STATEMENT DDOT
DDOT = 0.0D0
if(N <= 0) RETURN
if(INCX == INCY) IF (INCX - 1) 5, 20, 60

```

```

!
! Code for unequal or nonpositive increments.
!
5 IX = 1
  IY = 1
  if( INCX < 0 ) IX = (-N + 1) * INCX + 1
  if( INCY < 0 ) IY = (-N + 1) * INCY + 1
  DO 10 I = 1, N
    DDOT = DDOT + DX(IX) * DY(IY)
    IX = IX + INCX
    IY = IY + INCY
10 CONTINUE
  return
!
! Code for both increments equal to 1.
!
! Clean-up loop so remaining vector length is a multiple of 5.
!
20 M = MOD(N, 5)
  if( M == 0 ) go to 40
  DO 30 I = 1, M
    DDOT = DDOT + DX(I) * DY(I)
30 CONTINUE
  if( N < 5 ) RETURN
40 MP1 = M + 1
  DO 50 I = MP1, N, 5
    DDOT = DDOT + DX(I) * DY(I) + DX(I + 1) * DY(I + 1) + DX(I + 2) * DY(I + 2) + &
      DX(I + 3) * DY(I + 3) + DX(I + 4) * DY(I + 4)
50 CONTINUE
  return
!
! Code for equal, positive, non-unit increments.
!
60 NS = N * INCX
  DO 70 I = 1, NS, INCX
    DDOT = DDOT + DX(I) * DY(I)
70 CONTINUE

```

```

return
end
!-----
!>No.3 DNRM2
!-----
DOUBLE PRECISION FUNCTION DNRM2 (N, DX, INCX)
!
!! DNRM2 computes the Euclidean length (L2 norm) of a vector.
!
!***LIBRARY  SLATEC (BLAS)
!***CATEGORY  D1A3B
!***TYPE    DOUBLE PRECISION (SNRM2-S, DNRM2-D, SCNRM2-C)
!***KEYWORDS  BLAS, EUCLIDEAN LENGTH, EUCLIDEAN NORM, L2,
!             LINEAR ALGEBRA, UNITARY, VECTOR
!***AUTHOR  Lawson, C. L., (JPL)
!           Hanson, R. J., (SNLA)
!           Kincaid, D. R., (U. of Texas)
!           Krogh, F. T., (JPL)
!***DESCRIPTION
!
!           B L A S Subprogram
! Description of parameters
!
! --Input--
!   N number of elements in input vector(s)
!   DX double precision vector with N elements
!   INCX storage spacing between elements of DX
!
! --Output--
! DNRM2 double precision result (zero if N <= 0)
!
! Euclidean norm of the N-vector stored in DX with storage
! increment INCX.
! If N <= 0, return with result = 0.
! If N >= 1, then INCX must be >= 1
!
! Four phase method using two built-in constants that are

```

```

! hopefully applicable to all machines.
!   CUTLO = maximum of SQRT(U/EPS) over all known machines.
!   CUTHI = minimum of SQRT(V) over all known machines.
! where
!   EPS = smallest no. such that EPS + 1. > 1.
!   U = smallest positive no. (underflow limit)
!   V = largest no. (overflow limit)
!
! Brief outline of algorithm.
!
! Phase 1 scans zero components.
! move to phase 2 when a component is nonzero and <= CUTLO
! move to phase 3 when a component is > CUTLO
! move to phase 4 when a component is >= CUTHI/M
! where M = N for X() real and M = 2*N for complex.
!
! Values for CUTLO and CUTHI.
! From the environmental parameters listed in the IMSL converter
! document the limiting values are as follows:
! CUTLO, S.P. U/EPS = 2**(-102) for Honeywell. Close seconds are
!   Univac and DEC at 2**(-103)
!   Thus CUTLO = 2**(-51) = 4.44089E-16
! CUTHI, S.P. V = 2**127 for Univac, Honeywell, and DEC.
!   Thus CUTHI = 2**(63.5) = 1.30438E19
! CUTLO, D.P. U/EPS = 2**(-67) for Honeywell and DEC.
!   Thus CUTLO = 2**(-33.5) = 8.23181D-11
! CUTHI, D.P. same as S.P. CUTHI = 1.30438D19
! DATA CUTLO, CUTHI /8.232D-11, 1.304D19/
! DATA CUTLO, CUTHI /4.441E-16, 1.304E19/
!
!***REFERENCES C. L. Lawson, R. J. Hanson, D. R. Kincaid and F. T.
!   Krogh, Basic linear algebra subprograms for Fortran
!   usage, Algorithm No. 539, Transactions on Mathematical
!   Software 5, 3 (September 1979), pp. 308-323.
!***ROUTINES CALLED (NONE)
!***REVISION HISTORY (YYMMDD)
! 791001 DATE WRITTEN

```

```

! 890531 Changed all specific intrinsics to generic. (WRB)
! 890831 Modified array declarations. (WRB)
! 890831 REVISION DATE from Version 3.2
! 891214 Prologue converted to Version 4.0 format. (BAB)
! 920501 Reformatted the REFERENCES section. (WRB)
!***END PROLOGUE DNRM2
INTEGER NEXT
DOUBLE PRECISION DX(*), CUTLO, CUTHI, HITEST, SUM, XMAX, ZERO, &
    ONE
SAVE CUTLO, CUTHI, ZERO, ONE
DATA ZERO, ONE /0.0D0, 1.0D0/
!
DATA CUTLO, CUTHI /8.232D-11, 1.304D19/
!***FIRST EXECUTABLE STATEMENT DNRM2
if(N > 0) go to 10
DNRM2 = ZERO
go to 300
!
10 ASSIGN 30 TO NEXT
SUM = ZERO
NN = N * INCX
!
!                               BEGIN MAIN LOOP
!
I = 1
20 go to NEXT, (30, 50, 70, 110)
30 if (ABS(DX(I)) > CUTLO) go to 85
ASSIGN 50 TO NEXT
XMAX = ZERO
!
!           PHASE 1. SUM IS ZERO
!
50 if (DX(I) == ZERO) go to 200
if (ABS(DX(I)) > CUTLO) go to 85
!
!           PREPARE FOR PHASE 2.
!

```

```

ASSIGN 70 TO NEXT
go to 105
!
!           PREPARE FOR PHASE 4.
!
100 I = J
    ASSIGN 110 TO NEXT
    SUM = (SUM / DX(I)) / DX(I)
105 XMAX = ABS(DX(I))
    go to 115
    !
    !           PHASE 2. SUM IS SMALL.
    !           SCALE TO AVOID DESTRUCTIVE UNDERFLOW.
    !
70 if (ABS(DX(I)) > CUTLO) go to 75
    !
    !           COMMON CODE FOR PHASES 2 AND 4.
    !           IN PHASE 4 SUM IS LARGE. SCALE TO AVOID OVERFLOW.
    !
110 if (ABS(DX(I)) <= XMAX) go to 115
    SUM = ONE + SUM * (XMAX / DX(I))**2
    XMAX = ABS(DX(I))
    go to 200
    !
115 SUM = SUM + (DX(I) / XMAX)**2
    go to 200
    !
    !           PREPARE FOR PHASE 3.
    !
75 SUM = (SUM * XMAX) * XMAX
    !
    !   FOR REAL OR D.P. SET HITEST = CUTHI/N
    !   FOR COMPLEX   SET HITEST = CUTHI/(2*N)
    !
85 HITEST = CUTHI / N
    !
    !           PHASE 3. SUM IS MID-RANGE. NO SCALING.

```

```

!
DO 95 J = I, NN, INCX
    if (ABS(DX(J)) >= HITEST) go to 100
95 SUM = SUM + DX(J)**2
    DNRM2 = SQRT(SUM)
    go to 300
!
200 CONTINUE
    I = I + INCX
    if (I <= NN) go to 20
!
!     END OF MAIN LOOP.
!
!     COMPUTE SQUARE ROOT AND ADJUST FOR SCALING.
!
    DNRM2 = XMAX * SQRT(SUM)
300 CONTINUE
    return
end
!-----
!>No.4 DROT
!-----
subroutine DROT (N, DX, INCX, DY, INCY, DC, DS)
!
!! DROT applies a plane Givens rotation.
!
!***PURPOSE  Apply a plane Givens rotation.
!***LIBRARY  SLATEC (BLAS)
!***CATEGORY D1A8
!***TYPE    DOUBLE PRECISION (SROT-S, DROT-D, CSROT-C)
!***KEYWORDS BLAS, GIVENS ROTATION, GIVENS TRANSFORMATION,
!     LINEAR ALGEBRA, PLANE ROTATION, VECTOR
!***AUTHOR  Lawson, C. L., (JPL)
!     Hanson, R. J., (SNLA)
!     Kincaid, D. R., (U. of Texas)
!     Krogh, F. T., (JPL)
!***DESCRIPTION

```

```

!
!       B L A S Subprogram
! Description of Parameters
!
! --Input--
!   N number of elements in input vector(s)
!   DX double precision vector with N elements
!   INCX storage spacing between elements of DX
!   DY double precision vector with N elements
!   INCY storage spacing between elements of DY
!   DC D.P. element of rotation matrix
!   DS D.P. element of rotation matrix
!
! --Output--
!   DX rotated vector DX (unchanged if N <= 0)
!   DY rotated vector DY (unchanged if N <= 0)
!
! Multiply the 2 x 2 matrix ( DC DS) times the 2 x N matrix (DX**T)
!           (-DS DC)           (DY**T)
! where **T indicates transpose. The elements of DX are in
! DX(LX+I*INCX), I = 0 to N-1, where LX = 1 if INCX >= 0, else
! LX = 1+(1-N)*INCX, and similarly for DY using LY and INCY.
!
!***REFERENCES C. L. Lawson, R. J. Hanson, D. R. Kincaid and F. T.
!           Krogh, Basic linear algebra subprograms for Fortran
!           usage, Algorithm No. 539, Transactions on Mathematical
!           Software 5, 3 (September 1979), pp. 308-323.
!***ROUTINES CALLED (NONE)
!***REVISION HISTORY (YYMMDD)
! 791001 DATE WRITTEN
! 861211 REVISION DATE from Version 3.2
! 891214 Prologue converted to Version 4.0 format. (BAB)
! 920310 Corrected definition of LX in DESCRIPTION. (WRB)
! 920501 Reformatted the REFERENCES section. (WRB)
!***END PROLOGUE DROT
DOUBLE PRECISION DX, DY, DC, DS, ZERO, ONE, W, Z
DIMENSION DX(*), DY(*)

```

```

SAVE ZERO, ONE
DATA ZERO, ONE /0.0D0, 1.0D0/
!***FIRST EXECUTABLE STATEMENT DROT
if(N <= 0 .OR. (DS == ZERO .AND. DC == ONE)) go to 40
if(.NOT. (INCX == INCY .AND. INCX > 0)) go to 20
!
!   Code for equal and positive increments.
!
NSTEPS = INCX * N
DO 10 I = 1, NSTEPS, INCX
    W = DX(I)
    Z = DY(I)
    DX(I) = DC * W + DS * Z
    DY(I) = -DS * W + DC * Z
10 CONTINUE
go to 40
!
!   Code for unequal or nonpositive increments.
!
20 CONTINUE
KX = 1
KY = 1
!
if(INCX < 0) KX = 1 - (N - 1) * INCX
if(INCY < 0) KY = 1 - (N - 1) * INCY
!
DO 30 I = 1, N
    W = DX(KX)
    Z = DY(KY)
    DX(KX) = DC * W + DS * Z
    DY(KY) = -DS * W + DC * Z
    KX = KX + INCX
    KY = KY + INCY
30 CONTINUE
40 CONTINUE
!
return

```

```

end
!-----
!>No.5 DROTG
!-----
subroutine DROTG (DA, DB, DC, DS)
!
!! DROTG constructs a plane Givens rotation.
!
!***PURPOSE Construct a plane Givens rotation.
!***LIBRARY SLATEC (BLAS)
!***CATEGORY D1B10
!***TYPE DOUBLE PRECISION (SROTG-S, DROTG-D, CROTG-C)
!***KEYWORDS BLAS, GIVENS ROTATION, GIVENS TRANSFORMATION,
! LINEAR ALGEBRA, VECTOR
!***AUTHOR Lawson, C. L., (JPL)
! Hanson, R. J., (SNLA)
! Kincaid, D. R., (U. of Texas)
! Krogh, F. T., (JPL)
!***DESCRIPTION
!
! B L A S Subprogram
! Description of Parameters
!
! --Input--
! DA double precision scalar
! DB double precision scalar
!
! --Output--
! DA double precision result R
! DB double precision result Z
! DC double precision result
! DS double precision result
!
! Construct the Givens transformation
!
! ( DC DS )
!  $G = \begin{pmatrix} & \\ & \end{pmatrix}$ ,  $DC^{**2} + DS^{**2} = 1$  ,

```

```

!      (-DS DC )
!
!      which zeros the second entry of the 2-vector (DA,DB)**T .
!
!      The quantity R = (+/-)SQRT(DA**2 + DB**2) overwrites DA in
!      storage. The value of DB is overwritten by a value Z which
!      allows DC and DS to be recovered by the following algorithm.
!
!      If Z=1 set DC=0.0 and DS=1.0
!      If ABS(Z) < 1 set DC=SQRT(1-Z**2) and DS=Z
!      If ABS(Z) > 1 set DC=1/Z and DS=SQRT(1-DC**2)
!
!      Normally, the subprogram DROT(N,DX,INCX,DY,INCY,DC,DS) will
!      next be called to apply the transformation to a 2 by N matrix.
!
!***REFERENCES C. L. Lawson, R. J. Hanson, D. R. Kincaid and F. T.
!      Krogh, Basic linear algebra subprograms for Fortran
!      usage, Algorithm No. 539, Transactions on Mathematical
!      Software 5, 3 (September 1979), pp. 308-323.
!***ROUTINES CALLED (NONE)
!***REVISION HISTORY (YYMMDD)
! 791001 DATE WRITTEN
! 890531 Changed all specific intrinsics to generic. (WRB)
! 890531 REVISION DATE from Version 3.2
! 891214 Prologue converted to Version 4.0 format. (BAB)
! 920501 Reformatted the REFERENCES section. (WRB)
!***END PROLOGUE DROTG
DOUBLE PRECISION DA, DB, DC, DS, U, V, R
!***FIRST EXECUTABLE STATEMENT DROTG
if (ABS(DA) <= ABS(DB)) go to 10
!
! *** HERE ABS(DA) > ABS(DB) ***
!
U = DA + DA
V = DB / U
!
! NOTE THAT U AND R HAVE THE SIGN OF DA

```

```

!
R = SQRT(0.25D0 + V**2) * U
!
! NOTE THAT DC IS POSITIVE
!
DC = DA / R
DS = V * (DC + DC)
DB = DS
DA = R
return
!
! *** HERE ABS(DA) <= ABS(DB) ***
!
10 if (DB == 0.0D0) go to 20
   U = DB + DB
   V = DA / U
   !
   ! NOTE THAT U AND R HAVE THE SIGN OF DB
   ! (R IS IMMEDIATELY STORED IN DA)
   !
   DA = SQRT(0.25D0 + V**2) * U
   !
   ! NOTE THAT DS IS POSITIVE
   !
   DS = DB / DA
   DC = V * (DS + DS)
   if (DC == 0.0D0) go to 15
   DB = 1.0D0 / DC
   return
15 DB = 1.0D0
   return
   !
   ! *** HERE DA = DB = 0.0 ***
   !
20 DC = 1.0D0
   DS = 0.0D0
   return

```

```

!
end
!-----
!>No.6 DSCAL
!-----
subroutine DSCAL (N, DA, DX, INCX)
!
!! DSCAL multiplies a vector by a constant.
!
!***LIBRARY  SLATEC (BLAS)
!***CATEGORY  D1A6
!***TYPE    DOUBLE PRECISION (SSCAL-S, DSCAL-D, CSCAL-C)
!***KEYWORDS  BLAS, LINEAR ALGEBRA, SCALE, VECTOR
!***AUTHOR  Lawson, C. L., (JPL)
!      Hanson, R. J., (SNLA)
!      Kincaid, D. R., (U. of Texas)
!      Krogh, F. T., (JPL)
!***DESCRIPTION
!
!      B L A S Subprogram
!  Description of Parameters
!
!  --Input--
!    N  number of elements in input vector(s)
!    DA  double precision scale factor
!    DX  double precision vector with N elements
!    INCX  storage spacing between elements of DX
!
!  --Output--
!    DX  double precision result (unchanged if N <= 0)
!
!  Replace double precision DX by double precision DA*DX.
!  For I = 0 to N-1, replace DX(IX+I*INCX) with DA * DX(IX+I*INCX),
!  where IX = 1 if INCX >= 0, else IX = 1+(1-N)*INCX.
!
!***REFERENCES  C. L. Lawson, R. J. Hanson, D. R. Kincaid and F. T.
!      Krogh, Basic linear algebra subprograms for Fortran

```

```

!          usage, Algorithm No. 539, Transactions on Mathematical
!          Software 5, 3 (September 1979), pp. 308-323.
!***ROUTINES CALLED (NONE)
!***REVISION HISTORY (YYMMDD)
! 791001 DATE WRITTEN
! 890831 Modified array declarations. (WRB)
! 890831 REVISION DATE from Version 3.2
! 891214 Prologue converted to Version 4.0 format. (BAB)
! 900821 Modified to correct problem with a negative increment.
!      (WRB)
! 920501 Reformatted the REFERENCES section. (WRB)
!***END PROLOGUE DSCAL
DOUBLE PRECISION DA, DX(*)
INTEGER I, INCX, IX, M, MP1, N
!***FIRST EXECUTABLE STATEMENT DSCAL
if(N <= 0) RETURN
if(INCX == 1) GOTO 20
!
!   Code for increment not equal to 1.
!
IX = 1
if(INCX < 0) IX = (-N + 1) * INCX + 1
DO 10 I = 1, N
    DX(IX) = DA * DX(IX)
    IX = IX + INCX
10 CONTINUE
return
!
!   Code for increment equal to 1.
!
!   Clean-up loop so remaining vector length is a multiple of 5.
!
20 M = MOD(N, 5)
if(M == 0) GOTO 40
DO 30 I = 1, M
    DX(I) = DA * DX(I)
30 CONTINUE

```

```

    if(N < 5) RETURN
40 MP1 = M + 1
    DO 50 I = MP1, N, 5
        DX(I) = DA * DX(I)
        DX(I + 1) = DA * DX(I + 1)
        DX(I + 2) = DA * DX(I + 2)
        DX(I + 3) = DA * DX(I + 3)
        DX(I + 4) = DA * DX(I + 4)
50 CONTINUE
    return
    end
!-----
!>No.7 DSWAP
!-----
subroutine DSWAP (N, DX, INCX, DY, INCY)
!
!! DSWAP interchanges two vectors.
!
!***LIBRARY  SLATEC (BLAS)
!***CATEGORY  D1A5
!***TYPE     DOUBLE PRECISION (SSWAP-S, DSWAP-D, CSWAP-C, ISWAP-I)
!***KEYWORDS  BLAS, INTERCHANGE, LINEAR ALGEBRA, VECTOR
!***AUTHOR  Lawson, C. L., (JPL)
!           Hanson, R. J., (SNLA)
!           Kincaid, D. R., (U. of Texas)
!           Krogh, F. T., (JPL)
!***DESCRIPTION
!
!           B L A S Subprogram
! Description of Parameters
!
! --Input--
!   N number of elements in input vector(s)
!   DX double precision vector with N elements
!   INCX storage spacing between elements of DX
!   DY double precision vector with N elements
!   INCY storage spacing between elements of DY

```

```

!
! --Output--
!   DX input vector DY (unchanged if N <= 0)
!   DY input vector DX (unchanged if N <= 0)
!
!   Interchange double precision DX and double precision DY.
!   For I = 0 to N-1, interchange DX(LX+I*INCX) and DY(LY+I*INCY),
!   where LX = 1 if INCX >= 0, else LX = 1+(1-N)*INCX, and LY is
!   defined in a similar way using INCY.
!
!***REFERENCES C. L. Lawson, R. J. Hanson, D. R. Kincaid and F. T.
!               Krogh, Basic linear algebra subprograms for Fortran
!               usage, Algorithm No. 539, Transactions on Mathematical
!               Software 5, 3 (September 1979), pp. 308-323.
!***ROUTINES CALLED (NONE)
!***REVISION HISTORY (YYMMDD)
! 791001 DATE WRITTEN
! 890831 Modified array declarations. (WRB)
! 890831 REVISION DATE from Version 3.2
! 891214 Prologue converted to Version 4.0 format. (BAB)
! 920310 Corrected definition of LX in DESCRIPTION. (WRB)
! 920501 Reformatted the REFERENCES section. (WRB)
!***END PROLOGUE DSWAP
DOUBLE PRECISION DX(*), DY(*), DTEMP1, DTEMP2, DTEMP3
!***FIRST EXECUTABLE STATEMENT DSWAP
if(N <= 0) RETURN
if(INCX == INCY) IF (INCX - 1) 5, 20, 60
!
!   Code for unequal or nonpositive increments.
!
5 IX = 1
  IY = 1
  if(INCX < 0) IX = (-N + 1) * INCX + 1
  if(INCY < 0) IY = (-N + 1) * INCY + 1
  DO 10 I = 1, N
    DTEMP1 = DX(IX)
    DX(IX) = DY(IY)

```

```

        DY(IY) = DTEMP1
        IX = IX + INCX
        IY = IY + INCY
10 CONTINUE
    return
    !
    !   Code for both increments equal to 1.
    !
    !   Clean-up loop so remaining vector length is a multiple of 3.
    !
20 M = MOD(N, 3)
    if (M == 0) go to 40
    DO 30 I = 1, M
        DTEMP1 = DX(I)
        DX(I) = DY(I)
        DY(I) = DTEMP1
30 CONTINUE
    if (N < 3) RETURN
40 MP1 = M + 1
    DO 50 I = MP1, N, 3
        DTEMP1 = DX(I)
        DTEMP2 = DX(I + 1)
        DTEMP3 = DX(I + 2)
        DX(I) = DY(I)
        DX(I + 1) = DY(I + 1)
        DX(I + 2) = DY(I + 2)
        DY(I) = DTEMP1
        DY(I + 1) = DTEMP2
        DY(I + 2) = DTEMP3
50 CONTINUE
    return
    !
    !   Code for equal, positive, non-unit increments.
    !
60 NS = N * INCX
    DO 70 I = 1, NS, INCX
        DTEMP1 = DX(I)

```

```
DX(I) = DY(I)
DY(I) = DTEMP1
70 CONTINUE
return
end
```